TESIS DOCTORAL

LINA MARÍA AGUIRRE-DÍAZ

2015

NEW ALUMINIUM, GALLIUM AND INDIUM POLYMERIC FRAMEWORKS AS HETEROGENEOUS GREEN CATALYSTS

Tesis Doctoral

Lina María Aguirre-Díaz

Memoria presentada para aspirar al grado de
Doctor en Cristalografía y Cristalización

Instituto de Ciencia de Materiales de Madrid
Universidad Internacional Menéndez Pelayo
2015

NEW ALUMINIUM, GALLIUM AND INDIUM POLYMERIC FRAMEWORKS AS HETEROGENEOUS GREEN CATALYSTS

Lina María Aguirre-Díaz

Memoria presentada para aspirar al grado de
Doctor en Cristalografía y Cristalización

Instituto de Ciencia de Materiales de Madrid
Universidad Internacional Menéndez Pelayo
2015

NEW ALUMINIUM, GALLIUM AND INDIUM POLYMERIC FRAMEWORKS AS HETEROGENEOUS GREEN CATALYSTS

Lina María Aguirre-Díaz

Memoria presentada para aspirar al grado de
Doctor en Cristalografía y Cristalización

Dirigida por:
Prof. Dra. Maria Ángeles Monge Bravo
Dra. Natalia Snejko Shalneva

Instituto de Ciencia de Materiales de Madrid
Universidad Internacional Menéndez Pelayo
2015

A mi madre y a tu sonrisa

"Que el saber nos ayude a crecer como seres humanos, llenándonos de comprensión y tolerancia con el mundo"
LMAD

Agradecimientos

Me gustaría dar gracias de corazón a mi directora y codirectora de tesis, las doctoras Ángeles Monge y Natalia Snejko por su paciencia, dedicación, motivación y criterio, que han hecho de esta experiencia doctoral un camino de aprendizaje y crecimiento profesional. Realmente ha sido un privilegio poder contar con su guía y ayuda.

Gracias Nines por tenerme el cariño de madre y aguantar por tres años que te dijera “profe” y “jefa”, tu sabes que siempre ha sido con el mayor respeto y cariño, gracias por todos las enseñanzas y por tu confianza.

Gracias Natalia por tu apoyo incondicional por darme ánimos y siempre estar pendiente de mi, siempre recordaré nuestras charlas amenas en el despacho, las risas que compartimos, los buenos y duros momentos en los cuales me apoyaste y me permitieron retomar mi camino tanto científico como personal.

Gracias a Enrique, que siempre trasmite optimismo y una manera muy dulce de ver la vida y de compartir conocimiento, ojalá todos los científicos fueran más como tú.

Gracias porque los tres junto a Felipe, Manuela, Celia, Daniel y todos los que han estado de paso por el laboratorio (Celeste, Rocío, Germán) han hecho parte de mi familia científica, la que me ha motivado a estar estos cuatro años con una sonrisa permitiéndome trabajar en una de mis pasiones que es la Cristalografía. Sepan que les quiero mucho y les llevaré por siempre en mi corazón.

Agradezco especialmente a la Dra. Marta Iglesias, quien ha compartido conmigo su amplio y valioso conocimiento de la catálisis y me enseñó a evaluar las opciones más allá de lo convencional, mil gracias por tu amabilidad y cordialidad.

Durante los 3 meses que decidí realizar mi estancia en Milán, tuve el privilegio de contar con la guía profesional del Dr. Davide Proserpio a quien agradezco sus enseñanzas, amabilidad y cariño que hicieron de mi estancia muy amena. Gracias también a la Dra. Lucia Carlucci por permitirme pasar algunas horas en su laboratorio que me ayudó a despejar la mente haciendo algo de ciencia experimental.

Ahora bien, la tesis no se desarrolla como un ente solitario y se hace necesaria de la colaboración de diferentes personas para avanzar en cada investigación, por ello estoy muy agradecida al servicio de análisis químico (Carolina, Mari Carmen y Pedro) del ICMM; así como al servicio del Sidi de la Universidad Autónoma.

Agradezco poder contar con uno de los más sabios recursos a lo largo de estos 4 años: *La amistad*, que me permitió hacer llevadero los obstáculos del día a día, llenándome de optimismo y energía para mejorar y poder alcanzar mis metas. Mil gracias Ángela, Anto, Constanza y Eva quienes me acogieron a mí llegada al instituto, con ustedes compartí momentos muy bonitos, sobre todo esas risas relajantes en las comidas.

A Sandra que más que una amiga, es una hermana, es mi heroína, te quiero muchísimo y te agradezco el que cuidases de mi y tu apoyo infinito; saber que cuentas con alguien con quien llorar y reír, eso no tiene precio, sabes que siempre contarás conmigo.

Gracias a Adolfo, que con su carácter especial me enseñó a mantener la calma, gracias por tu amistad, por esos momentos Zen, por compartir tus emociones conmigo y por aguantarme.

Luz K mi querida oveja descarriada, te quiero muchísimo gracias por esas charlas en el café, por confiar en mis conocimientos, por preocuparte siempre por mi bienestar, sabes que cuentas con mi amistad siempre.

Gracias a los chicos del grupo de magnetismo Ester Calle, Ester Palmero, Jose, Roberto, Rhimou, David, Irene, por abrirme un espacio y compartir conmigo su buen ánimo. Gracias también a Eli, Vanessa, Elena, David Serantes, y todos aquellos que con un simple hola y una sonrisa me hicieron sentir los pasillos del instituto más cálidos.

La vida no sería la misma sin aquellos que uno elige para que sean parte de su familia, esos amigos incondicionales que te llenan el corazón y están en las buenas y en las malas; gracias a mis Nenuchis Mary y Nía que son mis hermanas, mi roca, mi apoyo en todo momento. Gracias a mi incondicional Mary Dávila que a pesar de las distancias hemos conservado esta bella amistad, compartiendo nuestro gusto por la cristalografía. Gracias a mi querida Adriana, porque sin tu apoyo esto no hubiera sido posible, gracias por ser una de las mejores almas que he conocido en mi vida, por darme la mano y por tus innumerables enseñanzas, te quiero. Gracias a Claudimar, por sus cuentos, sus risas, y que sepas que te echo de menos.

Diana Jimena y Diego Javier ustedes son mi pareja favorita, les quiero montones y agradezco vuestra amistad, la cual espero que podamos seguir compartiendo siempre.

Gracias a mis chicos de la ONU Fran, Delia, Alfredo y Aline por tener el tiempo y las ganas para disfrutar de los gratos momentos que nos brinda la vida.

A mi querida Kate gracias por tantos momentos compartidos, gracias por demostrarme que la risa nunca debe perderse, que los abrazos son gratuitos y que la pasión siempre debe alimentarse. A mis queridos y siempre presentes Pablo, Miguel y María con quienes he vivido increíbles momentos y comparten mi pasión por el orden estructural, gracias por compartir vuestra vida conmigo.

Cómo no agradecer a mi querida Angelikus, a quien admiro y respeto muchísimo, tu sabes que compartimos una amistad única de esas que durarán para toda la vida, te quiero mi pichurria.

Agradezco a mi familia, que aunque lejos, sé que me apoyan y siempre me tienen presente. En especial a mi madre que siempre ha tenido fe en mí y a mis abuelos que me enseñaron que solo con esfuerzo, voluntad y dedicación se alcanzan los sueños. A Isabel, mi querida Sis, te agradezco el tiempo, la amistad, cada momento juntas, seremos hermanas por siempre.

A Cristina, Jennifer, Bibiana y Tatiana gracias por ser esas amigas que no dejan que la distancia nos separe y siempre me envían sus mejores vibras.

Finalmente, para Alejandro mi esposo, a tu sonrisa va la dedicatoria de esta tesis, pues eres el mejor compañero que he podido encontrar para compartir mi camino, me has dado tu amor y ternura para superar los obstáculos y agradezco que estés a mi lado construyendo una vida plena y feliz. Te amo.

Summary

The development of green materials and processes with easy handling and of low cost has become one of the main goals of synthetic chemistry. The manufacture of economic, easily produced and non toxic materials that can then be used as heterogeneous catalysts becomes very important in the development of processes with less environmental impact. These materials will increase efficiency, and could avoid using of contaminants - toxic solvents, release agents, etc. - and reduce waste. For this purpose, several Metal-Organic Frameworks (MOFs) have attracted great interest during the past years and a large amount of compounds have been designed and synthesized for various energy and environmentally relevant applications, such as heterogeneous catalysis as well as luminescence, magnetism, gas storage and separation, adsorption, conductivity and molecular recognition.

The catalytic interest in MOFs materials arises from the high versatility that they offer. This versatility is due to the wide range of possibilities of combining a variety of polyatomic organic linkers and inorganic units, which act as coordination centers. The control of the bond angles and restricting the number of coordination sites that can be made during the synthesis of MOFs, results in tailored solid robust materials with high thermal and mechanical stability with a wide range of morphologies and geometries, which exhibit particular properties.

Currently, MOFs built up from higher valence cations are less abundant (except lanthanide cations) than those using divalent cations. The use of trivalent metals like the *p*-elements in group 13 (Al, Ga, In) for the preparation of MOFs are even less common, in contrast to their use in other inorganic materials, such as aluminosilicates, gallium-phosphates and phosphate zeolites.

In terms of catalytic applications, MOFs are relatively new materials within the domain of heterogeneous catalysis. Yet, *p*-elements based MOFs have proved to be very effective in various catalytic processes.

The work presented in this thesis is focused on obtaining new MOFs using *p*-elements such as: **aluminum, gallium** and **indium** as metal centers. The use of *p*-metals to synthesize new MOFs remains a scientific challenge, mainly due to the inherent difficulties concerning to their formation/crystallization using environmental friendly conditions. In spite of all this, the development of these *p*-MOFs could represent a comparatively cheap, nontoxic and green alternative to conventional MOFs.

Concerning the organic ligands used in this work, the ligand functionality evaluated is focused on the carboxylate group.

With regard to carboxylate ligands, flexible dipodal linkers have been considered to obtain new *p*-MOFs. The used linker 4,4'-hexafluoroisopropylidene)*bis*(benzoic) acid (**H_2hfipbb**) has been utilized before in our research group to synthesize transition metals, alkali-earth and rare-earth elements MOFs. These previous studies have shown that this flexibility can induce interesting materials phenomena like polymorphism, as well as the formation of a wide variety of networks with unexpected topologies. Continuing in this way,

the role that play nonbinding $–CF_3$ groups present in **H_2hfipbb** in the formation of some selected frameworks has been studied, compared to its counterpart with nonbinding –H groups (diphenylmethane-4,4'-dicarboxylic acid, **H_2dpmda**). These results are presented in **Chapter 4 sections 4.1** and **4.2**.

Continuing with the flexible multicarboxylate ligands, aiming to additional topologies that could bring the increment of the number of carboxylate groups the tripodal linker 5-(4-carboxy-2-nitrophenoxy)-1,3-benzenedicarboxylic acid (**H_3popha**) was exhaustive study in order to elucidate the effect of a no symmetry V-shaped ligand in the formation of different supramolecular frameworks. These results are presented in **Chapter 4 section 4.3**.

The topology of the twenty crystal structures obtained, are studied in **Chapter 4** defining in a simplified manner the dimensional connectivity presented by these networks. To this end, it has been generated a network of nodes which represents the connectivity of atoms or clusters, through the different organic linkers employed. Furthermore, this topological characterization allows the observation and understanding of the relation between the properties exhibited by the presented materials with a simplified description of their structure in **Chapter 5**.

As the principal application of the developed MOFs materials, the study of their heterogeneous catalytic activity based on the Lewis acidic catalyzed cyanosilylation reaction together with the scope of these catalytic activities in multicomponent reactions at mild conditions are presented in **Chapter 5**.

Resumen

En la actualidad, uno de los principales objetivos de la química sintética se centra en el desarrollo de materiales y procesos amigables con el medio ambiente, que impliquen un manejo sencillo y de bajo coste. La fabricación de materiales no tóxicos, económicos, de fácil producción, que puedan emplearse como catalizadores heterogéneos se vuelve muy importante en el desarrollo de procesos con menor impacto ambiental; los cuales buscan aumentar la eficiencia del proceso, evitando el uso de contaminantes -disolventes tóxicos, agentes de liberación, entre otros- reduciendo la generación de residuos. Para conseguirlo, materiales de tipo metal-orgánico (MOF, por sus siglas en inglés) los cuales han atraído un gran interés durante los últimos años, han sido diseñados y sintetizados para diversas aplicaciones relevantes para el medio ambiente, tales como la catálisis heterogénea, así como luminiscencia, magnetismo, almacenamiento de gas y la separación, la adsorción, la conductividad y el reconocimiento molecular.

El interés catalítico que existe en los materiales tipo MOFs surge de la gran versatilidad que ofrecen. Esta versatilidad es debida a la amplia gama de posibilidades obtenidas al combinar una gran variedad de ligandos orgánicos con unidades inorgánicas, las cuales actúan como centros de coordinación. El control de los ángulos de enlace y la restricción en el número de sitios de coordinación que pueden realizarse durante la síntesis de MOF, da como resultados materiales robustos sólidos adaptados que exhiben alta estabilidad térmica y mecánica con una amplia gama de morfologías y geometrías, que presentan propiedades particulares.

Los materiales de tipo MOFs fabricados empleando cationes con valencia ≥ 3 son menos abundantes (excepto en el caso de los lantánidos) que aquellos que emplean cationes divalentes. En el caso de metales trivalentes como los elementos del grupo 13 (Al, Ga, In) en la preparación de MOFs es aún menos común, en contraste con su utilización en otros materiales inorgánicos, tales como aluminosilicatos, galio-fosfatos y zeolitas de fosfato.

Los materiales del tipo MOFs son relativamente nuevos materiales dentro del dominio de la catálisis heterogénea. No obstante, MOFs basados en elementos del tipo *p* (*p*-MOFs) han demostrado ser muy eficaz en diversos procesos catalíticos.

El trabajo presentado en esta tesis se enfoca en la obtención de nuevos MOF utilizando aluminio, galio e indio como centros metálicos. El uso de estos metales en la síntesis de nuevas estructuras sigue siendo un reto científico, principalmente debido a las dificultades inherentes en relación a su formación / cristalización usando condiciones favorables al medio ambiente. A pesar de todo esto, el desarrollo de estos *p*-MOF podría representar una alternativa no tóxica y verde frente a los MOFs convencionales.

En cuanto a los ligandos orgánicos utilizados en este trabajo, la funcionalidad ligando evaluado se centra en el grupo carboxilato; empleando diferentes estructuras flexibles que exhiben una geometría de tipo V con funcionalidades di-y tripodales, como el ácido di-benzoico-4,4-hexafluorisopropilideno (H_2hfipbb), el cual ha sido empleado antes en nuestro grupo de investigación junto a metales de transición, metales alcalinotérreos y tierras raras

para sintetizar diferentes MOFs, demostrando que la flexibilidad de este ligando puede inducir en los materiales obtenidos interesantes fenómenos como polimorfismo, así como la formación de una amplia variedad de redes con topologías inesperadas. El ácido difenilmetano-4,4'-dicarboxílico (H_2dpmda), el cual posee grupos -H no enlazantes en lugar de los grupos -CF_3 presentes en su análogo H_2hfipbb, es igualmente empleado en la formación de MOFs lo que ha permitido estudiar el efecto en la geometría de estos grupos no-enlazantes estos resultados se presentan en el **Capítulo 4 secciones 4.1** y **4.2.**

Con el objetivo de estudiar las topologías adicionales que podrían traer el incremento del número de grupos carboxilato, se empleó el ácido 5-(4-carboxi-2-nitrofenoxi)-1,3-bencenodicarboxílico (H_3popha), el cual posee tres grupos carboxilato. Adicionalmente, se estudió el efecto de un ligando flexible con geometría V de tipo no-simétrico y como afecta este en la formación de las redes supramoleculares. Estos resultados se presentan en el **capítulo 4 sección 4.3**.

Para definir de una manera simplificada la conectividad y dimensionalidad de las redes obtenidas, se realiza un estudio de la topología de cada una de las veinte estructuras cristalinas obtenidas. Esto se ha realizado a través de la generación de una red de nodos la cual representa la conectividad bien sea de átomos o grupos, unidos por los diferentes ligandos empleados. Así mismo, esta caracterización permite una mejor apreciación y comprensión entre la relación estructura-propiedad de cada material. (Capítulo 5).

El desarrollo de estos materiales tiene como principal enfoque su aplicación en catálisis heterogénea, por esta razón en el **capítulo 5** se presenta el estudio de la actividad catalítica de cada compuesto. Considerando la acidez de Lewis como la principal propiedad exhibida por los materiales desarrollados, su aplicación catalítica es evaluada a través de la cianosililación de compuestos carbonílicos, la cual permite encontrar los mejores catalizadores y poder así realizar un estudio más profundo de las aplicaciones catalíticas que exhiben los materiales enfocándolos a catalizar reacciones multicomponentes en condiciones suaves.

Contents

Page

Page

CHAPTER 1

INTRODUCTION

In the past two decades, developments in the chemistry of the Group 13 metal containing materials have often been driven by the promise of practical applications. In fact, hundreds of these materials with specific electronic, structural, thermal or chemical properties have been designed with a massive impact in our society changing the way we perceive the world nowadays. In this chapter, a brief history of the aluminium, gallium and indium chemistry is presented, together with their recent growth in the metal-organic materials and the different synthetic techniques to improve the material purity.

Materials science is nowadays one of the most important fields in our society development. Our modern culture is heavily dependent on advanced materials: lightweight composites for faster vehicles, optical fibres for telecommunications and silicon microchips for the information revolution. Being directly responsible for the study of the relations between the properties and the composition of a determined material, materials science has allowed along the years enormous breakthroughs giving rise to a massive design of new materials built chasing exclusive properties.[1]

Seeking for resources, which promote the preservation and/or the solution of the global energetic requirement, the area of metal-organic materials has been the subject of intense efforts in research development in laboratories and on the industrial scale.[2] Nevertheless, the research perspective and development in inorganic and metal-organic synthesis has been traditionally focused on the "green" and environmentally-friendly applications such as energy storage, carbon sequestration, hydrogen storage as well as heterogeneous and homogeneous catalysis, among others,[3] which leaved sometimes the synthetic process of the material itself outside the "green" scope.

The energy efficiency, toxicity and environmental impact of all chemical processes have highlighted the importance of discovering *real green* methods for the material synthesis, giving a new challenge to the material research area. These new methods would have to be able to be applied at large scale, which could favour their industrial commercialization impact with a remarkable impact in the society.[4]

1.1. Metal-Organic Frameworks

One of the most popular and rapidly developing areas of modern metal-organic materials chemistry are the Metal-Organic Frameworks (MOFs), which are built from organic bridging ligands and metal connecting points giving rise to one-dimensional (1D), two-dimensional (2D) or three-dimensional (3D) arrangements through coordination bonds (Figure 1.1).

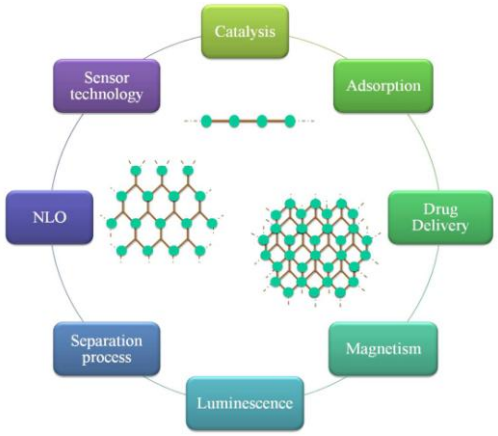

Figure 1.1 Representation of 1D, 2D and 3D Metal-Organic frameworks with several of its applications.

The history of metal-organic frameworks began with the discovery of the Prussian Blue in 1704 by Diesbach,[5] although its characterization was made 200 years later; the incredible industrial impact achieved by this material made one of the most important advances in the coordination chemistry. Since the 60's (Tomic and Biondi) a variety of coordination polymers was discovered,[6] but it wasn't until 1989 when Hoskins and Robson[7] proposed the design of open frameworks that this new kind of materials really fire up.[8] Yaghi and co-workers back in 1995 finally presented a formal MOFs concept, which guides its development as a new research field.[9] Now, within two decades of continue academic and industrial growth on this specific matter, thousands of MOFs have been developed, characterized and their potential applications explored (Figure 1.1),[10] manufacturing materials for a number of technologies, with an extensive set of properties like: adsorption,[11] separation processes,[12] drug delivery,[13] sensor technology,[14] magnetism,[15] luminescence,[16] non-linear optics (NLO, frequency doubling)[17] and heterogeneous catalysis.[18]

As a particular curiosity, the correct terminology for these material have been a point of several discussions along the years, given rise to the use of several names: Coordination Polymers (CPs), Metal-Organic Frameworks (MOFs), Coordination Networks (CNs), hybrid organic-inorganic materials, organic zeolites analogues and even combinations among them.

In 2013, the IUPAC set a series of recommendations in order to clarify the use of the correct terminology in the area of MOFs. The most general term considered was the CPs, which was defined as a coordination compound with repeating coordination entities without the requirement of being a crystalline material. As a subset of the CPs, the coordination network was defined as a coordination compound extending, through repeating coordination entities, in 1, 2 or 3 dimensions. Finally, MOFs were considered as a subset of the CNs.[19] Regarding to this thesis, the use of the term Metal-Organic Frameworks (MOFs) implies the following attributes: Crystalline material whose geometrically well-defined framework is constituted by metal ions or metal ion clusters, occupying nodal framework positions, and by multidentate organic ligands coordinated to the metal ion or clusters.

The information gathered along the years on the hundreds of designed MOFs (Figure 1.2), has allowed to the crystal engineering the search for trends in connectivity and to identify the principles that govern the design of MOFs, in order to develop and implement new structural, theoretical, topological, modelling and specific synthetic strategies for the production of specific new MOFs.[20]

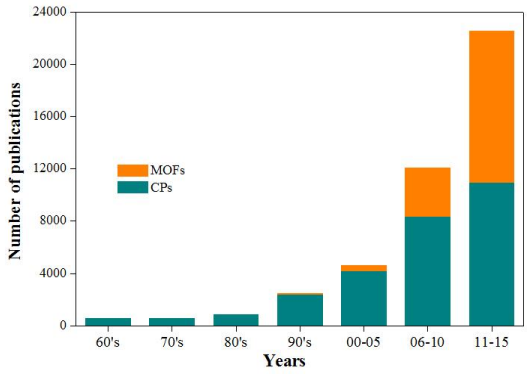

Figure 1.2 Publication number on MOFs and CPs materials along years, Scifinder®.

The principal interest in the design of this type of new materials relies on the versatility displayed by the main components that can be used for the synthesis of the MOFs. The extensive number of different possible arrangements between the metal source and the organic part promotes an increment in the quantity of structures that can be obtained and consequently the increase in the amount of the properties displayed by these materials and their posterior applications.

In order to facilitate the efficiency and pertinence of the MOFs synthesis, three important points have to be carefully evaluated: i) the metal source, ii) the linker and iii) the reaction conditions.

1.2. The Metal Source: group 13 - *Aluminium, Gallium and Indium*-

The first impression of the trivalent *p*-metal ions such as Aluminium, Gallium and Indium may be caused by the harmony of these 13th group elements coming up from the common configuration $ns^2\ np^1$ shared by the valence electrons in the ground state of each atom. The predominance of the formal oxidation state +3 and the acceptor properties that characterises the derivatives using these *p*-metals, together with the discontinuous build-up of the periodic table, which makes difficult to follow the agreement of the variation of properties dictated by the generally increasing atomic size and decreasing hold of the nucleus on the valence electrons as the atomic number increases, makes that each member of the group has its own individual character.[21]

1.2.1. Aluminium

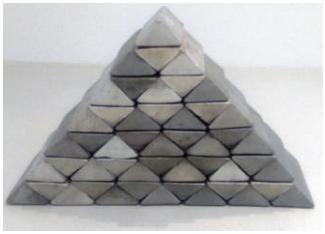

Being the most abundant metal in the biosphere and due to its environmental importance, aluminium is by far one of the most widely studied elements, with a history extended back more than 150 years. Its name derives from *Alum* [$KAl(SO_4)_2$], a salt, which was used as an astringent in ancient Greece and Rome, as a fireproofing agent for wood and also as a mordant in dyeing. Aluminium is one of the major constituents of naturally available minerals like feldspars, zeolites, and micas; it played one of the most important contributions to the revolution in the materials industry, when commercial plants started the extraction of aluminium salts back in the XV century.[22] Since then until today, materials science would be unthinkable without the use of this element. Among the principal uses of aluminium and its compounds can be described: packaging industry (cans and foil), household utensils, aviation fuel, electrical wiring, hydrogen production, electronic devices and transistors, glass and ceramics manufacture, as well as antacid tablets, water purification, papermaking, paints and manufacture of synthetic gemstones.[23]

The highly soluble aluminium complexes are ideal for solution-processed functional oxide films because their high tendency to form hydroxo-bridged network structures in aqueous solution and amorphous oxides. Enormous amount of work has been made in the field of synthetic aluminum mineral mimics, because this enables the prediction of some of the

natural processes that take place at the surface of natural minerals, such as exchange of water and/or oxygen atoms.

One of the most significant achievements in aluminum chemistry occurred with the discovery of insertion reactions of alkenes and the polymerization of ethylene and propene at low pressure in the presence of organometallic catalysts aluminum and titanium Ziegler and Natta (Nobel Prize in Chemistry in 1963).[24]

1.2.2. Gallium

Mendeleev predicted its existence around 1870, but it was in **1875** through spectroscopy that its discovery came by a French chemist *Paul Emile Lecoq de Boisbaudran* who named the new element in honour to *Gallia* (Latin for France).

Currently, gallium is obtained mainly as a by-product of aluminum or zinc industries, and is employed in a wide variety of applications in different fields. The main use of gallium is as semiconductor, where it is commonly used in microwave circuits and some infrared applications; other applications of gallium are in the LEDs manufacture in blue and violet laser diodes, as a component in some types of solar panels and even for the stabilization of the enriched plutonium in nuclear weapons.[25]

Alloys with gallium, indium and tin (*galinstan)* led to thermometers that replaced the traditional mercury thermometer; they also had been used for the production of hydrogen being used in conjunction with aluminum.[26]

In medical applications, gallium salts have been used to treat people with excess of calcium in their blood. The discovery of ^{67}Ga, led to the development of the ^{67}Ga scan methodology for detecting tumors in patients and prompted further evaluation of the potential antineoplastic activity of stable gallium salts. After several studies using gallium nitrate, different gallium-based metallodrugs have emerged as cancer therapeutic agents in the preclinical and clinical areas along the years.[27]

1.2.3. Indium

Discovered by Ferdinand Reich and Hieronymous Richter in 1863, indium was obtained as a yellow precipitate, which showed a brilliant violet line in its atomic spectroscope giving rise to the name indium, from the Latin word *indicum*, which means violet.[28]

Indium occurs only in the form of its compounds, except occasionally as rare grains of free metal. It is widely spread in nature, generally in very low concentrations. The content of indium in the earth crust is estimated to be 0.1 ppm. Indium is found as a trace element in many minerals. Sphalerite is the most important indium-containing mineral followed by lead and copper sulphides.[29]

No other metal is as versatile as indium. In its various forms it is well known for have been used as sealing in cryogenic applications (it stays malleable and ductile below -150°C), soldering or fusing applications (alloys melt at temperatures ranging from 6.5°C to 310°C), high-end device cooling (reduces operating temperatures by up to 10°C), as an absorber layer material in solar panels, in a variety of compounds of semiconductor materials (InAs, InGaAs, and InGaN) to enable electronics and electro-optic applications like integrated circuits, lasers, and LEDs.[30]

Among all indium compounds, one that is widely recognized today is the indium tin oxide (ITO), a transparent conductor, which dominates the use of indium compounds across the world today. It is use essentially for building flat panel displays and touch sensors in TVs, computer monitors, tablets and smart phones. The recent discoveries include a combination between indium, gallium and zinc oxides named IGZO as future material in the pixel switching transistors in the next-generation displays.[31]

In the nuclear medicine, radiochemistry and molecular imaging areas the use of ^{111}In radiometal had been extensively studied. Its wide utilization in these areas resulted in an extensive study of indium complexes formation with polydentate polyamino polycarboxylate ligands.[32]

1.3. The organic linker: Flexible multicarboxylate ligands

The choice of appropriate ligands is no doubt the key factor because it has an obvious influence on the topologies of the MOFs and behaviour of the molecules. At this time, most studies have so far been focused on the assembly of MOFs with rigid ligands;[33] especially those carboxylate containing ligands have attracted much attention because of the diversity of the binding modes of the carboxylate group. Up to date, extensive works have been carried out by using carboxylate-containing ligands, for instance, 1,3,5-benzenetricarboxylate acid (H_3btc),[34] 4,4′,4″-benzene-1,3,5-triyl-tribenzoic acid (H_3btb),[35] 1,4-benzenedicarboxylic acid (p-H_2bdc),[36] and 1,3-benzenedicarboxylic acid (m-H_2bdc).[37] In these cases, most of the bridging ligands used in the construction of the frameworks are rigid; frequently, porous structures with high dimensionality have been obtained. The use of the extended rigid organic linker skeleton has allowed the study of large families of materials with correlated structures and incremented pore size; the influence of such increase on the properties of the corresponding materials has been demonstrated.[29-32]

Meanwhile, multidentate flexible linkers remain infrequent in the construction of porous MOFs, possibly because of less predictability and difficulties in analyzing the topologies of the coordination architectures.[38] In contrast to the rigid ligands, the conformation of flexible ones is variable and consequently, they can meet the coordination geometrical requirement of metal ions through changing their conformation, which may provide more possibility for the construction of unprecedented high-connected frameworks.

The challenge of the use of flexible ligands to build MOFs can be summarized as follows: i) the ligand itself can adopt different conformations and possess low symmetry as a consequence of rotations about single bonds, which can lead to a loss of control in the design and assembly of the aggregates; ii) structures based on flexible ligands are more sensitive to subtle changes in reaction conditions and their synthesis are somewhat more difficult.[39] However, the flexibility of ligands is essential for forming some particular properties and structures. Some of those properties are the molecular switch derived from a conformational change, the ‘‘breathing’’ ability in the solid state, adaptive recognition property for coexisting guests or counterions, flexible molecular clips composed of coordination of discrete molecules.

Furthermore, the flexibility of the ligand allows a good opportunity to observe the details of a self-assembly process and provide more structure information for the directional synthesis possibility of a target material. In recent years, our group have been involved in the synthesis of several MOFs using multicarboxylated flexible ligands (Figure 1.3) like the 4,4’-hexafluoroisopropylidene (H_2hfipbb) and the diphenylmethane-4,4-dicarboxylic acid (H_2dpmda) reaching a wide range of material topologies, which lead to several important properties.[40]

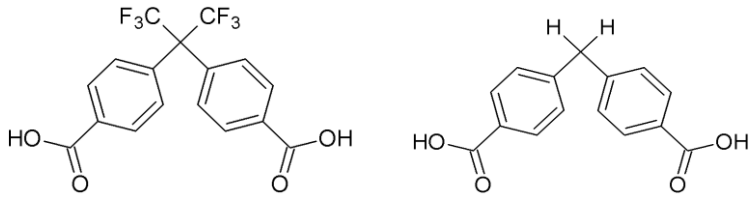

Figure 1.3 Different flexible ligands used for MOFs synthesis in our research group, from left to right: H_2hfipbb and H_2dpmda.

The use of V-shaped linkers as H_2dpmda or H_2hfipbb has been recently explored due to the interest in design and constructing of helically structured MOFs. This interest relies in part on the fact that helical structures are ubiquitous in nature and are the foundation of the genetic code; they have attracted increased interest in coordination chemistry and material chemistry owing to their importance in biological systems, asymmetric catalysis, and producing of optical devices.[41]

On the other hand, the employment of mixed ligands during the self-assembly process has gradually become an effective approach, with which it is expected to obtain frameworks with more diverse structural motifs compared to using only one type of ligands. Therefore, auxiliary ligands such as the nitrogenated ones (for example, phenanthroline or bipyridine), are frequently introduced into the reaction systems to obtain more metal coordination environment diversity, which also affects the final framework geometry and consequently the properties of the obtained material.

1.4. *p*-MOFs

A large number of the MOFs solids are prepared with divalent transition metals (Zn^{2+}, Cu^{2+},

Cd^{2+} etc.). Considerably less MOFs were obtained with trivalent transition (V^{3+}, Cr^{3+}, Fe^{3+}, Sc^{3+}…) or rare earth metals.[42] The use of trivalent *p* elements of the 13th group (Al^{3+}, Ga^{3+}, In^{3+}) for the preparation of MOFs, although tending to generate structurally stable and appealing frameworks suitable for conducting further applications,[43] are less common in contrast to their use in other inorganic materials (aluminosilicates and gallium-phosphates).

To comprehend the chemistry of MOFs formed by high-valence cations, it is necessary first to take in consideration the strong competition between two processes: the formation of the inorganic compounds (oxides and hydroxides) and the formation of metal-ligand complexes. As a tendency, the use of polar solvents together with metal precursors containing traces of water favours the inorganic precipitation during the synthesis process. In order to avoid the formation of these metal hydroxides or oxides and to maintain a sufficient concentration of metal complexes necessary for the formation of frameworks in solution, the use of slightly acidic conditions and higher temperatures are generally required.

The common pattern for trivalent derivates is to adopt structures, in which the metal atom achieves a coordination number (CN) higher than 3, either by taking up additional ligands or by establishing supplementary links to the existing ligands.

The CN and the geometry assumed by the metal atom depend only partly on the properties of the metallic centre. Unquestionably the size of the centre is a significant factor and the greater bulk of indium in front of aluminium and gallium facilitates the achievement of environments with 6-, 7- or 8- fold coordination of the metal. However, if it were, aluminium and gallium, which have similar radii, would be expected to be almost identical in their structural preferences. In fact, while having much in common with aluminium, gallium tends to 4-coordinate environments.

The trajectory of aluminium based MOFs starts in 2003 with Férey and co-workers, which first prepared, characterized and intensively studied various new structures (e.g. MIL-53, MIL-96, MIL-100, MIL-110).[44] These Aluminium-MIL series exhibit extraordinary thermal stability (>450ºC) and its members reversibly uptake/release water; the framework stability can be afford by the octahedral coordination of aluminum and the strong Al–O bonds, which provide aluminum–organic frameworks superior stability compared to highly moisture-sensitive zinc-based MOFs like MOF-5.[45] Therefore, Al-MOFs are very attractive materials for industrial applications, as demonstrated by the simultaneous BASF industry development of its own portfolio of Al-MOFs, which nowadays has reached to the optimization of commercial synthesis in water-based and organic solvent-free preparation (Basolite A520).[46]

In the last few years there has been an avalanche of data on the synthesis, structural studies and applications of 1D to 3D indium structures, which were prepared using multicarboxylate ligands. This contributions started in 2002, when several new synthesis of *p*-elements-based MOF have been reported by our research group and others, reaching up to date more than 498 references for indium MOFs (Table 1.1)[47] and 187 references for gallium MOFs (Scifinder data base).[35-48]

Table 1.1 Representative Indium MOFs and its applications

Formula	Properties/Application
[In(OH)(1,4-bdc)]	Bio-mimetic Nose
$[In(OH)(1,4\text{-}NDC)]\cdot 2H_2O$	Luminescence
$[In(btb)_{0.67}(OA)(DEF)_{1.5}$	White light emission
$[H_2tmdp][In_6(btc)_8].40H_2O$	Ion exchange
$[In_3(btc)_4]$	Gas sorption
$[InH(_D\text{-}C_{10}H_{14}O_4)_2]$	Adsorption
$[In_2(OH)_2(1,3\text{-}bdc)_2(2,2'\text{-}bipy)_2]$	Photoluminescence
[In(OH)(hfipbb)]	Catalysis

bdc=benzene dicarboxylic acid, NDC= nicotinic dicarboxylic acid, btb= benzene-1,3,5-tribenzoate, btc= benzene tricarboxylic acid, hfipbb= hexafluorisopropylidenebis(benzoic) acid, tmdp= 4,4'-trimethylenedipyridine

1.5. Synthesis of MOFs

An infinite number of metal/ligand combinations can be used in the synthesis of MOFs having as a result greater diversity in structures. For this reason the building blocks units (BBUs) should be chosen considering the looked-for properties in the final MOF material.

In contrast to most laboratory solvent-based syntheses reported, the industrial manufacturing criteria strongly advise against the use of soluble nitrate salts and metal halides as metal precursors, due to the toxicity problems, the oxidizing properties and corrosion tendency associated with these counterions. In contrast, if metal oxides and sulphates are used as precursors, the previously discussed adverse issues are not encountered; however their low solubility has to be considered when an efficient transformation is needed. So, generally speaking, the use of green metal sources has to be decisive for the final synthesis planning; this can allow an improvement on the large scale implementing of the laboratory results.

The nature of the organic component in a MOF is one of the priorities at the time of being selected, because it acts as a spacer between the metallic centers. One essential condition is that the chosen ligands need to be stable under the conditions of synthesis; otherwise the formation of byproducts of sometimes completely unexpected materials can interfere with the process. The second most important thing is to take advantage of the linker (functional groups) nature, which is crucial to the material development and the material properties. The most conventional functional groups of linkers used in MOFs synthesis are the carboxylates ($-CO_2$), which coordinate to the metal centers *via* their oxygen atoms; followed by the cyano (-CN) and amino ($-NH_2$) derivatives with nitrogen atoms coordinated to metal centers (figure X). Other functional groups as phosphate ($-PO_4$) and sulfonate ($-SO_3$) have been used as well. Nowadays, the versatility of material design has been increased due to the development of MOFs using organic linkers with mixed functional groups or employing more than one type of ligand.

The synthesis of MOFs is commonly performed using the *Solvothermal methods* employing well-soluble salts as the source for the metal component together with the selected

organic ingredient, supplied in an organic solvent under stirring; MOFs structures are formed by self-assembly at temperatures from 25ºC to 250ºC within usually hours or days, the energy is generally introduced using conventional heating (CH). Then, the processes of filtering and drying of the material also are very important, because the material may have 50 to 150 wt% of occluded solvent.[49]

Looking for fast reactions and continuous syntheses, which offer an advantage in large scale of MOFs production, different synthetic routes have been used. Focusing on the energy source and considering the closest relation of the reaction duration, and pressure and energy per molecule that are introduced into a system, different energy sources like electronic circuits, electromagnetic radiation or mechanical energy transfer, has been thought to obtain a reduction in the reaction time and temperature in order to reach higher energy-efficient processes and less demanding synthesis equipment. Some of these alternatives routes are going to be described below (Figure 1.4).[50]

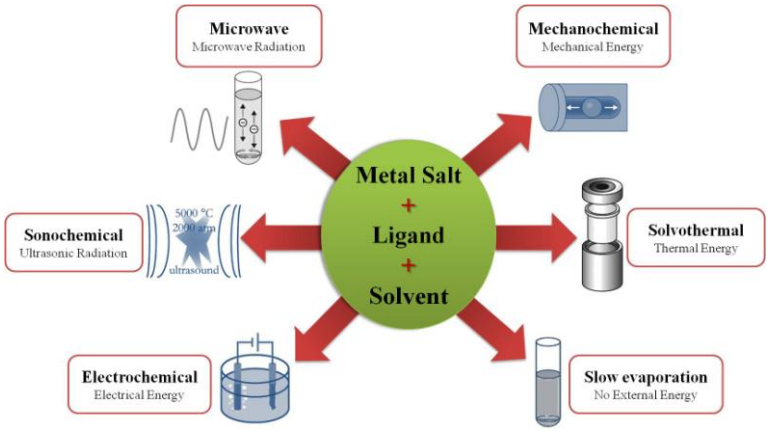

Figure 1.4 Synthesis methods commonly used for MOF preparation.

1.5.1. Microwave-Assisted Synthesis

Introduction of energy using microwave irradiation is a well established method in synthetic chemistry; it has been mainly used in organic chemistry. Currently, microwave syntheses of MOFs are performed applying the appropriate frequency to the sample allowing collisions between the molecules, which lead to an increase in the kinetic energy of the system. Due to the direct interaction of the radiation with the solution/reactants, MW-assisted heating presents a very energy efficient method of heating.[51]

1.5.2. Electrochemical Synthesis

BASF industry reported in 2005 the first electrochemical synthesis of MOFs; this process is based on the continuous introduction of metal ions through an anodic dissolution to the reaction medium, which contains the dissolved linker molecules and a conducting salt. The metal deposition on the cathode is avoided by using protic solvents, but in the process H_2 is formed. One of the industrial scopes for the electrochemical route is the possibility to run a continuous process and to increase the yield compared to a normal process. [52]

1.5.3. Mechanochemical Synthesis

With a long history in synthetic chemistry and in inorganic solid-state chemistry, this synthetic process has recently been employed in multicomponent reactions to form pharmaceutically active co-crystals. In materials science mechanochemical synthesis was introduced back in 2006, focusing on the mechanical breakage of intramolecular bonds followed by a chemical transformation. [53]

1.5.4. Sonochemical synthesis

This methodology deals with the chemistry that takes place upon application of high-energy ultrasound to a reaction mixture. Starting in 2008, this method has been applied to the investigation of MOFs but it is still largely unexplored.[54]

1.6. Prospective MOFs Applications

The highly diverse applications of MOFs have been listened in a number of comprehensive reviews. A brief summary of the most important applications for MOFs developed in our research group are presented in the following items.

1.6.1. Gas and Vapour Storage

As a new class of adsorbents due to their open and flexible frameworks, MOFs are leading to a wide application field in fuel storage, especially towards hydrogen and methane, as well as waste gases. These uses are based on physisorption, being the interaction between the gas molecules and the MOFs walls very weak; thus the storage capacities are below the targets established to make practical application possible, except at very low temperatures.

Dynamic frameworks can be used as selective organic solvent sponges, as the case of **AEPF-1**dry where the material shows a high adsorption capacity for acetonitrile and acetone, and a very low one for aromatic solvents (benzene, toluene), with no sorption observed for aliphatic organic solvents, making this material a good candidate for selective solvent adsorption in mixed liquids under mild conditions (Figure 1.5).[40b]

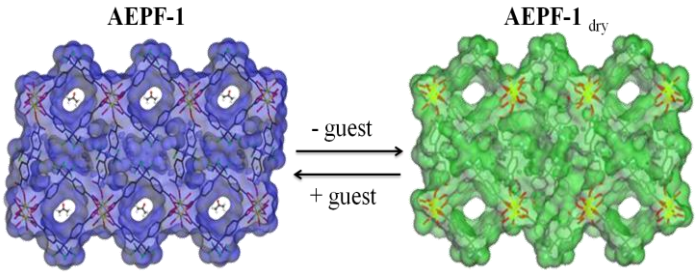

Figure 1.5 AEPF-1 sponge with the voids filled of solvent molecules and AEPF-1_{dry} with empty voids.

1.6.2. Luminescence

The properties of MOFs made them the ideal candidates to prepare luminescent materials by combining luminescent metallic centers with linkers, guest molecules, and cooperative effects among them, like charge transfer between the metal and linker. Besides, in MOFs, the active centers are at much more distances from each other than in condensate system, (i.e., oxides, etc.), and this separation can be changed as a function of the size of the organic-ligand spacers; in consequence, effects like quenching of the luminescent emissions can be minimized.

In our research group several MOFs using H_2hfipbb as a long hydrophobic linker have been synthesized. Among them, using the lanthanide series (Y, La, Ce, Pr, Nd, Sm, Eu, Gd, Tb, Dy, Ho, Er, Yb) a family of rare-earth polymeric frameworks (RPF) were obtained, and their luminescence properties explored showing that the Eu, Tb MOFs could be promising for red light emitting diodes and green luminescent material, respectively (Figure 1.6).[55]

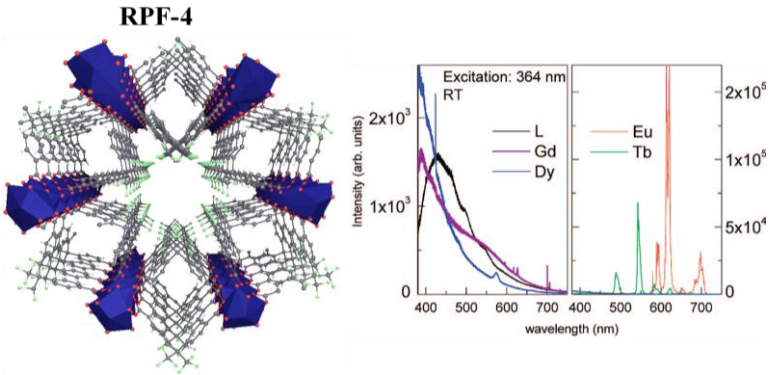

Figure 1.6 RPF-4 Emission spectra in the visible region.

1.6.3. Heterogeneous Catalysis

Catalysis is considered one of the pillars in the green chemistry philosophy, because catalysts enable slow reactions to proceed, drastically reducing the energy consumption during the process, generating energy savings and less waste production compared to the version of a process using stoichiometrical amounts of activating reagents. Looking for the new materials with catalytic properties, MOFs were proposed 25 years ago as materials with high expectations for this application,[56] but only after a substantial foundation of the MOF synthetic chemistry an extensive experimental exploration in the catalytic area has been made. Despite many recent developments (more than 6119 references up to date, Scifinder®), the area of MOF-based catalysis is in a young phase, yet there are important issues in the catalytic chemistry to exploit the remarkable features of MOFs. For example: i) useful multi-catalyst architectures that are very difficult to access otherwise, ii) metal coordination environments, and therefore reactivity, that can be achieved in no other way, and iii) reactivity-defining microenvironments that can be achieved in few other ways.[57]

Among several MOFs developed by our group, the teflon®-like channelled nanoporous Zn-MOF with formula [Zn(hfipbb)] presents a chiral structure (Figure 1.7), which showed catalytic chiral recognition properties. The study of its catalytical properties was performed using the acetalization of (*R,S*)-2-phenylpropionaldehyde, reaching high conversion and moderate enantioselectivity under mild conditions (60% yield after 24 h). The structure of this material favours the preferable formation of one of the enantiomeric acetals.[58]

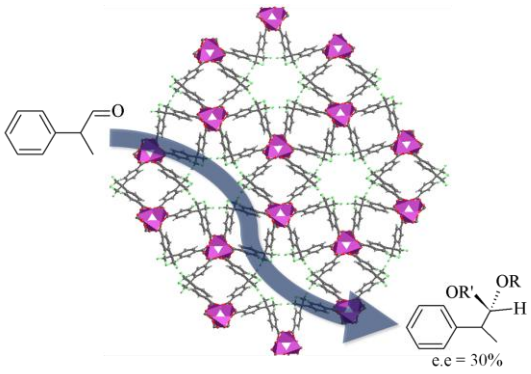

Figure 1.7 The [Zn(hfipbb)] material in the 2-phenylpropionaldehyde acetalization.

1.6.3.1. The role of MOFs in the Heterogeneous Catalysis nowadays

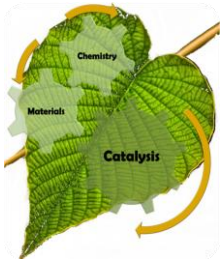

The well recognized Zeolites materials are one of the most important heterogeneous catalysts at industry level since 1960 in a large number of gas-phase reactions;[59] its excellent performance is due to the selectivity on the way to target products that can be regularly accomplished. The synthesis procedure for this type of materials involves the use of organic templates, which later are disintegrated to obtain the inorganic scaffolds with high thermal stability. However, in zeolites materials nothing, beyond the contribution to the structure of the zeolite obtained, is explored from the part of organic templates. In any case, new heterogeneous catalysts with greater reusability, efficiency, and ease of synthesis are continuously sought for environmental concerns.

On the other hand, the synthesis of MOFs allows achieving crystalline materials with high metal content and consequently, notably elevated number of uniform active metal sites in their structures; an almost complete control of the synthesis process and of the structure of the material obtained is usually possible. Moreover, because they also contain organic components, MOFs can be synthesized in much greater chemical variety than zeolites. Thus, the rational design of extended frameworks with coordinatively unsaturated metal sites and controlled pore/channel size for size-selective Lewis acidity allowed to produce MOF materials with specific characteristics, which can compete or even overwhelm the activity of the zeolites in liquid phase reactions, where the reactions can be performed under mild conditions (Figure 1.8).

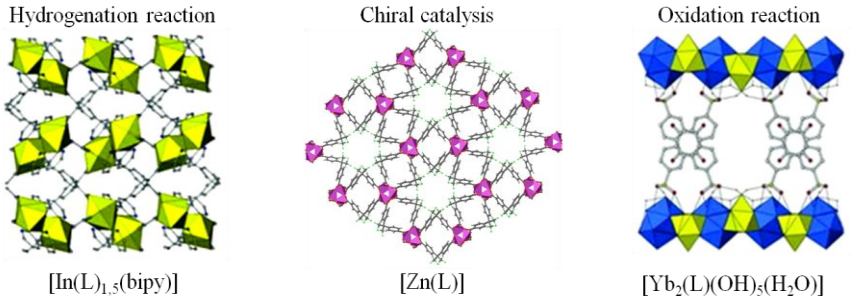

Figure 1.8 Some of the MOFs developed in our research group with good catalytic activity.

While many MOFs exhibit zeolites-like permanent porosity, others collapse when solvents are removed. The persistence of microporosity after solvent evacuation is essential for gas-phase catalysis, as well as for many other applications discussed before; however, it may not be essential for catalysis in condensed-phase reactions. As an example, the first reported MOF with catalytic application emerged in 1994, in which a 2D cadmium network was used as heterogeneous catalyst in the cyanosilylation of aldehydes;[60] very few studies had been performed before the years~2000-2005. Since then, research in this field has been devoted to probing the concept of heterogeneous catalysis in a variety of reactions, supported by the gradual progress in maturation of crystal engineering in the field.[61] Nowadays, MOF materials are moving towards the discovery of specific and distinctive catalytic applications that are not matched by MOF's conventional analogues.[62]

Usually, according to the obtained specific MOF structures, there are different ways to harness the interaction between this material and the organic reactants in a catalysis reaction, from the direct contact of the reactants with metal sites or functional moieties in the framework, to the encapsulation of catalytic nanoparticles inside the material pores. A brief description of each case can be found in the following.

1.6.3.1.1. MOFs with catalytically active metal sites

The metal sites in a MOF play the essential role in the catalyst activity of the material. The carefully made studies on catalysis by MOFs materials[52-54] showed that in catalytically active MOFs low metal coordination environments or metal-connecting points that are coordinated to labile solvent molecules or counter ions are present. So, the Lewis acidic nature of the available metal centers can activate the organic substrates and the subsequent organic transformation can take place (Figure 1.9).[63]

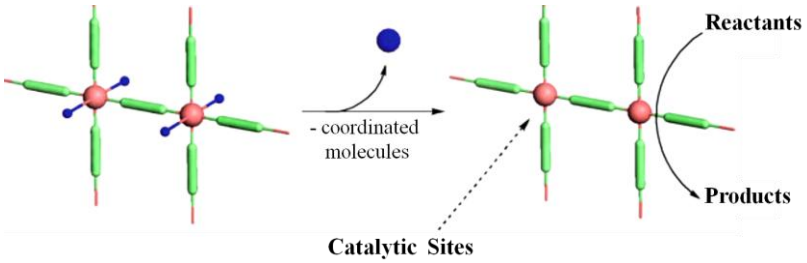

Figure 1.9 Generation of unsaturated metal connecting points as active catalytic sites.

Our research group have synthesized several indium MOFs named **InPF** (from Indium Polymeric Frameworks).[35] Among them, the **InPF-11α** material with formula [In(OH)hfipbb] (H_2hfipbb = diphenylmethane-4,4-dicarboxylic acid) is formed by -[In-O-In]- inorganic chains that connect through the organic linker to obtain thick layers-containing square-shaped channels, which allows the direct interaction of the available indium metal catalytic sites (coordination number, CN, 6) with the organic reactants. This material proved to be an efficient heterogeneous catalyst for the acetalization of aldehydes. The difference in the catalytic activity between compounds with empty or filled channels confirmed that catalytic reaction did take place inside the pores. (Figure 1.10).[40f]

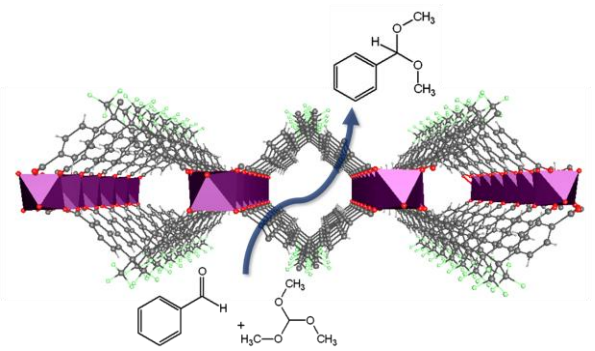

Figure 1.10 Polyhedral representation of the 2D structure of **InPF-11α** showing the acetalization catalyzed inside the material pores.

1.6.3.1.2. Functional Linkers as Catalytic Sites

Taking into consideration the wide portfolio of different organic ligands used in the development of new functional MOFs, several organic linkers besides their functional groups especially selected to coordinate to the metal ions while composing MOFs, can also possess some functional active sites that might be implicated in a determinate catalytic system (Figure x). The involving of these additional catalytically active sites into catalytic transformation is sometimes responsible of dual mechanisms, which could lead to the selective control of the reactants activation processes. Several works have demonstrated the possibility of using of MOFs as basic catalysts by introducing pyridyl, amide or amino groups in the organic linkers, and have been used in the Knoevenagel condensation and transesterification reaction.[64] However, it is sometimes difficult to demonstrate that these catalytic organic sites can be reached out by the reactants, because they need to be appropriately placed in the framework to be available in the catalytic reaction (Figure 1.11).[55]

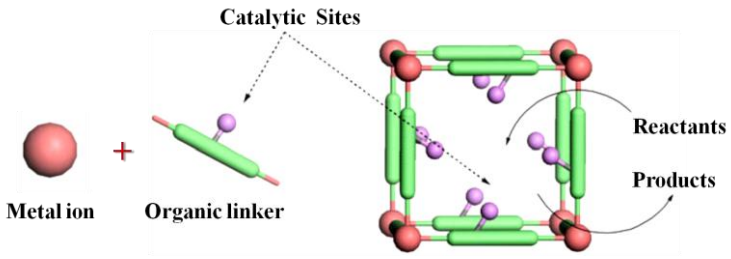

Figure 1.11 Functional groups in the bridging ligands as active catalysts.

1.6.3.1.3. Catalysis in MOFs doped with metal catalysts

The inherent host-guest chemistry of porous MOFs materials allows the implementation of desired properties by filling the framework cavities with various guest molecules and clusters. In particular, the doping of MOFs with metal nanoparticles (MNPs) is of interest for heterogeneous catalysis.[65] Several MNPs@MOFs have been employed in different heterogeneous catalytic reactions such as methanol synthesis, hydrogenation of hydrocarbons, reduction of ketones, oxidation of alcohols, CO oxidation and C-C bond formation. As an example, in Figure 1.12 the Au@ZIF-8 is present elaborated by Fischer group; [66] this material showed a high catalytic activity in the oxidation of alcohols.

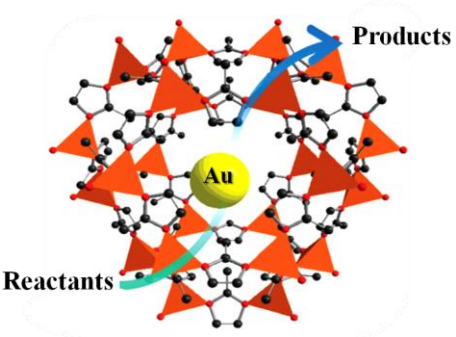

Figure 1.12 Catalytic applications of Au@ZIF-8 (Zn atoms are shown as orange octahedra).

1.6.3.2. Common Lewis acid MOFs mediated organic transformations

Among the widely explored organic transformations using Lewis acid catalyst, here some examples are presented of the most common reactions used to confirm the existence of Lewis acid catalytic activity in MOFs.

1.6.3.2.1. Cyanosilylation

Cyanohydrins are useful starting materials for the synthesis of several biologically active compounds due to the presence of hydroxyl and nitrile functionalities, which can be transformed into a wide range of building blocks.[67] Generally, a common reaction to prepare cyanohydrins goes through the cyanosilylation of carbonyl compounds in the presence of trimethylsilyl cyanide (TMSCN) promoted by moderately strong Lewis acid catalysts (scheme 1.1). The TMSCN is used instead of other cyanide sources, which are highly toxic, like HCN or alkali metal salts (NaCN or KCN); this reduces the safety issues and the handling problems, which these classical cyanation reagents usually presented, without losing the efficiency in the reaction process.[68]

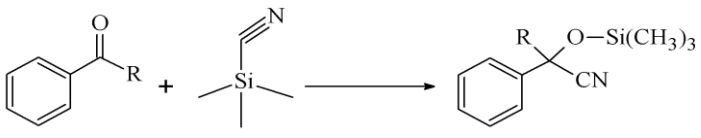

Scheme 1.1 Cyanosilylation of carbonyl compounds.

As mentioned earlier, cyanosilylation reaction was the first catalytic reaction tested using a MOF as catalyst in 1994 by Fujita and co-workers. The activity of the Cd(II) centers as Lewis acid catalysts was illustrated by cyanosilylation of aldehydes and imines, proving that the substrates can be hosted by the cavity of the first layer, and interact further with the Lewis acid Cd(II) catalytic center in the second layer. However, up to date the results achieved with MOFs for this organic transformation are still far from optimum; one of the goals should be to achieve the mildest conditions reactions.

1.6.3.2.2. Ring opening of epoxides

In the pharmaceutical industry and for natural products development the ring opening of epoxides by nucleophilic attack (using amines, alcohols, thiols, azides, and halides) is important because it allows the formation of 1,2-difunctionalized compounds (Scheme 1.2).

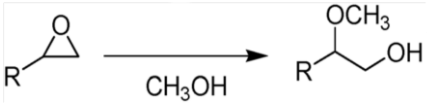

Scheme 1.2 Ring opening epoxide using methanol.

The classical approach for the nucleophilic ring opening of epoxides involves the use of homogeneous and heterogeneous Brønstead or Lewis acid as clays, alumina and zeolites, in the presence of solvents. The ultimate goal of this organic transformation is to achieve highly region-selective ring opening of epoxides by using alcohols under mild reaction conditions, leading to the design of new catalysts with high selectivity capable to raise the nucleophilicity of alcohols, which are normally lower than that of amines.

1.6.3.2.3. Acetalization of aldehydes

Formation of dimethyl acetals is frequently carried out using trimethyl orthoformate as reagent due to the incompatibility of Lewis-acid catalysts with methanol (Scheme 1.3). Formation of dimethyl acetals using trimethyl orthoformate as reagent and MOFs as catalysts has been previously reported by our research group using rare earth MOF with formula $[Yb(C_4H_4O_4)_{1.5}]$[69] as well as using the InPF-11α MOF; excellent results have been achieved.[35]

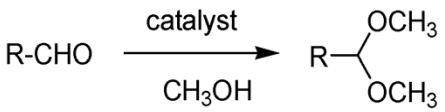

Scheme 1.3 Acetalization of aldehydes.

1.6.3.2.4. Selective hydrogenations

For the hydrogenation of apolar carbon–carbon multiple bonds, which is a general reaction in organic chemistry, it is always desirable to develop alternative hydrogenation catalysts

avoiding precious noble metals: normally, this hydrogenation reaction is performed using hydrogen (Scheme 1.4) and supported noble or transition metal catalysts such as Rh/C, Pd/C, nickel RANEY® or Adam's catalyst (PtO_2).[70] Contributing to the development of green catalysts, several AEPF catalyst (AEPF: alkaline-earth polymeric framework) were created by our group. These catalysts had been tested in several hydrogenations showing a 100% selectivity at short times with low catalytic loadings (1 mol %).[71]

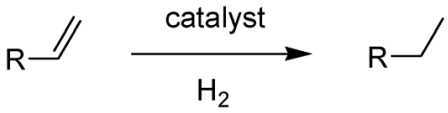

Scheme 1.4 Alkene hydrogenation with H_2.

1.6.3.3. Multi-Component Reactions: Looking for green reactions

Nowadays, the understanding of the impact that chemical industry has on the environment, has guided us to several *green* chemistry ideas in order to enable synthetic process with environmental considerations that look for waste level minimization rather than dealing with the common treatments employed in the most of industries. The Multicomponent Reactions (MCRs) usually employ simple and green synthetic procedures that allow the creation of several bonds in a single operation using three or more reactants, which offer great advantages in operational simplicity, atom economy, reduction in the time of reaction development, extraction and purification processes and consequently, in the waste minimization. For these reasons, the MCRs have attracted attention in the last decades of investigators in several areas like the pharmaceutical, the organic synthesis and even the materials science (Figure 1.13).[72]

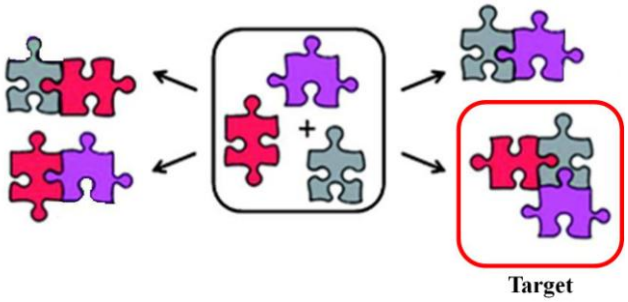

Figure 1.13 A multicomponent reaction possibilities.

One of the biggest contributors to the environment pollution is the use of volatile organic solvents in the chemical manufacturing processes, becoming an important aspect of the green chemistry the elimination or replacement of these polluting organic solvents and the search for alternatives capable of conducting the same reaction. Suitable solvent-free processes have been developed for those reactions having at least one liquid reactant. However, there are some cases where the solvent remains crucial to the process; in this sense several green unconventional solvents (water, ionic liquids, polyethylene glycol and some bio-based chemicals) have been tested in the reaction media improving the synthetic efficiency.[73]

Along the years, many MCRs have been successfully developed under solvent-free conditions or with the use of unconventional solvents in order to improve the reaction yield, to simplify isolation of products and catalyst recycling. As examples, Eli Lilly's synthesis of the anticonvulsant drug candidate LY300164 and Pfizer's Zoloft® were obtained after their synthetic process improving *via* multiple one-pot procedures; these viable green solutions gave to the both the US presidential Green Chemistry Challenge Award.[74]

There are two different approaches in the performing of MCRs (Figure 1.14). One is the one pot methodology normally used when all components can be added without a certain order, ensuring the wanted product formation with no side-products. Another methodology known as the cascade or domino reaction and is based on the synergistic use of sequential reactions for the multiple bond formation processes avoiding kinetics competitions between reactants. Several studies showing the green chemistry potential of catalytic cascade reactions in the synthesis of several compounds can be found in the literature.[75]

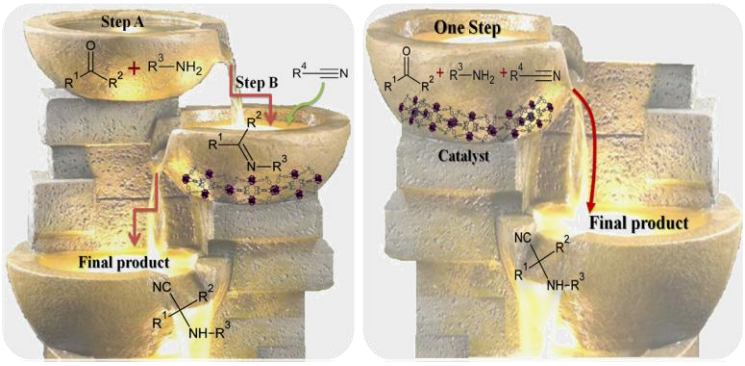

Figure 1.14 Cascade (left) and One-pot (right) multicomponent reaction methodologies.

Although some classes of MCRs can be performed under mild conditions without any use of catalyst, some other reactions found beneficial or indispensable the use of catalytic materials. For this reason the development of efficient catalytic systems represents one of the most active areas in green multicomponent chemistry research.[76] Nowadays, catalysis in MCRs diverges in multiple directions depending on the type of the catalyst used: Brønsted and Lewis acids, organocatalysts, metal complexes, heterogeneous catalysts, biocatalysts as well as nanoparticles.[77]

A general examination of the MCRs chemistry has demonstrated that these reactions have almost the perfect atom economy (≥80%). They also are capable to ensure the high incorporation of the starting materials into the final product with a minimal formation of waste by-products, making simple the isolation of the desired product by using solvents or chromatographic materials in small amounts. In table 1.2, representative examples of the MCRs employed in the course of this thesis are presented, together with their calculated atom economy and their corresponding by-product in each case.

Table 1.2 Representative MC reactions employed in this thesis

Name	Reaction scheme	Atom economy (ae) [a]	by-product	Environmental factor (Ef) [b]
Strecker 1850 [78]	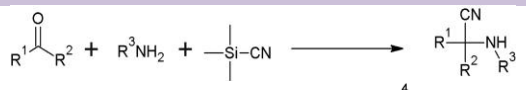	80%	H_2O	0.26
Passerini 1921 [79]	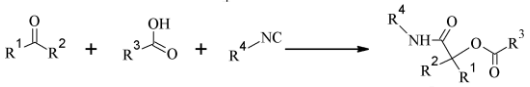	100%	none	0
Ugi 1959 [80]	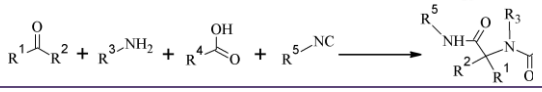	91%	H_2O	0.10

[a] Atom economy (ae) = $MW_{product}/MW_{reactants}$, calculated for R = Me. [b] Environmental factor = $MW_{by\text{-}product}/MW_{product}$

1.7. References

1. a) S. D. Hutagalung, *Materials Science and Tecnology*. Ed. InTech, Rejika, Croatia, **2012**, 324pp; b) S. W. Cranford, J. de Boer, C. Van Blitterswijk and M. J. Buehler, *Adv. Mater.* **2013**, *25*, 802.

2. a) R. M. Izatt, S. R. Izatt, R. L. Bruening, N. E. Izatt and B. A. Moyer, *Chem. Soc. Rev*. **2014**, *43*, 2451; b) H. J. Federsel, *Green Chem*. **2013**, *15*, 3105; c) P. J. Dunn, *Chem. Soc. Rev*. **2012**, *41*, 1452.

3. a) J. Lu, L. Li, J. –B. Park, Y.-K. Sun, F. Wu and K. Amine. *Chem. Rev*. **2014**, *114*, 5611; b) R. Sathre and E. Masanet, *RSC Adv*. **2013**, *3*, 4964; c) A. M. Seayad and D. M. Antonelli, *Adv. Mater*. **2004**, *16*, 765; d) J. Weitkamp, *Solid State Ionics* **2000**, *131*, 175.

4. a) A. Czaja, E. Leung, N. Trukhan and U. Müller, Industrial MOFs synthesis. *In Metal-organic Frameworks: Applications from catalysis to gas storage*, 1st ed; D. Farrusseng, Ed.; Wiley-VCH Verlag &Co: Weinheim, German, **2011**; b) P. Saravade, H. Tan and V. Polshettiwar, *ACS Sustainable Chem. Eng*. **2013**, *1*, 66.

5. H. J. Buser, D. Schwarzenbach, W. Petter and A. Ludi, *Inorg. Chem.* **1977**, *16*, 2704.

6. a) E. A. Tomic, *J. Appl. Polym. Sci*. **1965**, *9*, 3745; b) C. Biondi, M. Bonamico, L. Torelli and A. Vaciago, *Chem. Commun.* **1965**, 191.

7. a) S. R. Batten, B. F. Hoskins and R. Robson, *J. Am. Chem. Soc.* **1995**, *117*, 5385; b) B. F. Abrahams, B. F. Hoskins, D. M. Michail and R. Robson, *Nature*, **1994**, 369, 727; c) B. F. Hoskins and R. Robson, *J. Am. Chem. Soc.* **1990**, *112*, 1546; d) B. F. Hoskins and R. Robson, *J. Am. Chem. Soc.* **1989**, *111*, 5962.

8. a) S. Decurtins, H. W. Schmalle, P. Schneuwly and H. R. Oswald, *Inorg. Chem.* **1993**, *32*, 1888; b) G. De Munno, M. Julve, F. Nicolo, F. Lloret, J. Faus, R. Ruiz and E. Sinn, *Angew. Chem., Int. Ed.* **1993**, *32*, 613; c) P. Brandt, A. K. Brinah and R. D. Fischer, *Angew. Chem., Int. Ed*. **1988**, *27*, 1521.

9. O. M. Yaghi, G. Li and H. Li. *Nature* **1995**, *378*, 703.

10. a) S. L. James, *Chem. Soc. Rev*. **2003**, *32*, 276; b) N. R. Champness, *Dalton Trans*. **2006**, 877; c) A. U. Czaja, N. Trukhan and U. Müller, *Chem. Soc. Rev.* **2009**, *38*, 1284; d) G. Férey, *Dalton Trans.* **2009**, 4400; e) R. Robson, *DaltonTrans.* **2008**, 5113; f) K. M. Fromm, *Coord. Chem. Rev.* **2008**, *252*, 856.

11. a) J. L. C. Rowsell and O. M. Yaghi, *Angew. Chem., Int. Ed*. **2005**, *44*, 4670; b) J.-R. Li, R. J. Kuppler and H.-C. Zhou, *Chem. Soc. Rev.* **2009**, *38*, 1477; c) T. K. Maji and S. Kitagawa, *Pure Appl. Chem*. **2007**, *79*, 2155.

12. S. Ma, D. Sun, M. Ambrogio, J. A. Fillinger, S. Parkin and H. C. Zhou, *J. Am. Chem. Soc.* **2007**, *129*, 1858.

13. P. Horcajada, T. Chalati, C. Serre, B. Gillet, C. Sebrie, T. Baati, J. F. Eubank , D. Heurtaux, P. Clayette, C. Kreuz, J.-S. Chang, Y. K. Hwang, V. Marsaud, P.-N. Bories, L. Cynober, S. Gil, G. Férey, P. Couvreur and R. Gref, *Nature Materials*, **2010**, *9*, 172.

14. G. J. Halder, C. J. Kepert, B. Moubaraki, K. S. Murray and J. D. Cashion, *Science*, **2002**, *298*, 1762.

15. M. Kurmoo, *Chem. Soc. Rev*. **2009**, *38*, 1353.

16. M. D. Allendorf, C. A. Bauer, R. K. Bhakta and R. J. T. Houk, *Chem. Soc. Rev*. **2009**, *38*, 1330.

17. C. Janiak, T. G. Scharmann, P. Albrecht, F. Marlow and R. MacDonald, *J. Am. Chem. Soc.* **1996**, *118*, 6307.

18. a) J.-Y. Lee, O. K. Farha, J. Roberts, K. A. Scheidt, S. T. Nguyen J. T. Hupp, *Chem.Soc. Rev*. **2009**, 38, 1450; b) T. E. Gier, X. Bu, P. Feng, G. D. Stucky, *Nature* **1998**, *395*, 154.

19. S. R. Batten, N. R. Champness, X. –M. Chen, J. García-Martínez, S. Kitagawa, L. Öhrström, M. O'Keeffe. M. Park Suh and J. Reedijk, *Pure Appl. Chem*. **2013**, *85*, 1715.

20. a) C. Janiak, *Dalton Trans.* **2003**, 2781; b) S. Kitagawa, R. Kitaura and S. Noro, *Angew. Chem. Int. Ed.* **2004**, *43*, 2334; c) G. Férey, *Chem. Soc. Rev.* **2008**, *37*, 191.

21. a) P. Atkins, *The Periodic Kingdom*, Weidenfeld & Nicolson, London, UK, **1995**, 149 pp; b) A. J. Downs, *Chemistry of Aluminium, Gallium, Indium and Thallium*; Blackie Academic and Professional: Glasgow, UK, **1993**.

22. W. H. Casey, *chem. Rev*. **2006**, *106*, 1.

23. a) G. Furrer, B. L. Phillips, K. U. Ulrich, R. Pothig and W. H. Casey, *Science*, **2002**, *297*, 2245; b) T. A. Stewart, D. E. Trudell, T. M. Alam, C.A. Ohlin, C. Lawler, W. H. Casey, S. Jett and M. Nyman, *Environ. Sci. Technol.* **2009**, *43*, 5416; c) H. W. Roesky and S. Shravan Kumar, *Chem. Commun.* **2005**, 4027; d) Z. L. Mensinger, W. Wang, D. A. Keszler and D. W. Johnson, *Chem. Soc. Rev*. **2012**, *41*, 1019.

24. G.Wilke, *Angew. Chem., Int. Ed.* **2003**, *42*, 5000.

25. a) B. J. Stanbery, *Solid State and Materials Sciences*, **2002**, *27*, 73; b) D. Tsonev, C. Hyunchae, S. Rajbhandari, J. J. D. McKendry, S. Videv, E. Gu, M. Haji, S. Watson, A. E. Kelly, G. Faulkner, M. D. Dawson, H. Haas and D. O'Brien, *IEEE Photon. Technol. Lett.* **2014**, *26*, 637; c) S. S. Hecker, "Plutonium and Its Alloys". *Los Alamos Science*, **2000**, *26*.

26. T. Liu, P. Sen and C.-J. Kim, *J. Microelectromech. Syst.* **2012**, *21*, 443.

27. a) M. M. Hart and R. H. Adamson, *Proc Natl Acad Sci USA*. **1971**, *68*, 1623; b) C. R. Chitambar, *Future Med Chem.* **2012**, *4*, 1257.

28. F. Reich and T. H. Richter, *J. Prakt. Chem.* **1863**, *89*, 441.

29. Roskill: The Economics of Indium 1987, 4th ed., Roskill Information Services Ltd., London **1987**.

30. S. Nakamura, T. Mukai and M. Senoh, *Appl. Phys. Lett.* **1994**, *64*, 1687.

31. J. Emsley, Nature's Building Blocks: An A-Z Guide to the Elements, Oxford University Press, New York, 2nd Edition, **2011**.

32. T. J. Wadas, E. H. Wong, G. R. Weismann and C. J. Anderson, *Chem.Rev.* **2010**, *110*, 2858.

33. N. L. Rosi, J. Eckert, M. Eddaoudi, D. T. Vodak, J. Kim, M. O'Keeffe and O. M. Yaghi, *Science* **2003**, 1127.

34. N. L. Rosi, M. Eddaoudi, J. Kim, M. O'Keeffe and O. M. Yaghi, *Angew. Chem., Int. Ed.* **2002**, *41*, 284.

35. B. Chen, M. Eddaoudi, S. T. Hyde, M. O'Keeffe and O. M. Yaghi, *Science* **2001**, *291*, 1021.

36. C. Serre, F. Millange, J. Marrot and G. Férey, *Chem. Mater*. **2002**, *14*, 2409.

37. M. Eddaoudi, J. Kim, J. B. Wachter, H. K. Chae, M. O'Keeffe and O. M. Yaghi, *J. Am. Chem. Soc.* **2001**, *123*, 4368.

38. a) S. Neogi, G. Savitha, S. Neogi, *Inorg. Chem.* **2004**, *43*, 3771; b) B. Moulton and M. J. Zaworotko, *Chem. Rev.* **2001**, *101*, 1629; c) L. Carlucci , G. Ciani and D.M. Proserpio, *Chem. Commun.* **2004**, *4*, 380.

39. T. –F. Liu, J. Lu and R. Cao, *CrystEngComm* **2010**, *12*, 660.

40. a) M. C. Bernini, A.E. Platero-Prats, N. Snejko, E.Gutiérrez-Puebla, A. Labrador, R.Sáez-Puche, J. Romero de Paze and M. A. Monge, *CrystEngComm* **2012**, *14*, 5493; b) A. E. Platero-Prats, V. A. de la Peña-O'Shea, D. M. Proserpio, N. Snejko, E. Gutierrez-Puebla and A. Monge, *J. Am. Chem. Soc.* **2012**, *134*, 4762; c) A. E. Platero-Prats, M. C. Bernini, M. E. Medina, E. López-Torres, E. Gutiérrez-Puebla, M. A. Monge and N. Snejko *CrystEngComm*, **2011**, *13*, 4965; d) B. Gómez-Lor, E. Gutiérrez-Puebla, M. A. Monge, C. Ruiz-Valero, N. Snejko, *Inorg. Chem.* **2002**, *41*, 2429; e) B. Gomez-Lor, E. Gutierrez-Puebla, M. Iglesias, M.A. Monge, C. RuizValero, N. Snejko, *Chem. Mater.* **2005**, *17*, 2568; f) F. Gándara, B. Gomez-Lor, E. Gutierrez-Puebla, M. Iglesias, M. A. Monge, D. M. Proserpio, N. Snejko, *Chem. Mater.* **2008**, *20*, 72; g) M. E. Medina, A. E. Platero-Prats, N. Snejko, Alex Rojas, A.

Monge, F. Gándara, E. Gutiérrez-Puebla, and M. A. Camblor, *Adv. Mater.* **2011**, *23*, 5283; h) A. E. Platero-Prats, V. A. de la Peña-O'Shea, N. Snejko, A. Monge and E. Gutierrez-Puebla, *Chem. Eur. J.* **2010**, *16*, 11632.

41. a) J. –P. Zhang, Y. -Y. Lin, X. –C. Huang, and X. –M. Chen, *Chem. Commun.* **2005**, 1258; b) H. -L. Jiang, B. Liu, and Q. Xu, *Cryst. Growth Des.* **2010**, *10*, 806.

42. a) K. Barthelet, J. Marrot, G. Férey and D. Riou, *Chem. Commun.* **2004**, 520; b) T. R. Whitfield, X. Wang, L. Liu and A. Jacobson, *J. Solid State Sci*. **2005**, *7*, 1096; c) C. Volkringer, T. Loiseau, M. Haouas, F. Taulelle, D. Popov, M. Burghammer, C. Riekel, C. Zlotea, F. Cuevas, M. Latroche, D. Phanon, C. Knofelv, P. L. Llewellyn and G.Férey, G. *Chem. Mater.* **2009**, *21*, 5783.

43. a) R. Hajjar, C. Volkringer, T. Loiseau, N. Guillou, J. Marrot, G. Férey, I. Margiolaki, G. Fink, C. Morais and F. Taulelle, *Chem. Mater.* **2011**, *23*, 39 ; b) C. Volkringer, T. Loiseau, N. Guillou, G. Férey, E. Elkaim, A. Vimont, *Dalton Trans.* **2009**, 2241 ; c) G. Chaplais, A. Simon-Masseron, F. Porcher, C. Lecomte, D. Bazer-Bachi, N. Bats, J. Patarin, *Phys. Chem. Chem. Phys.* **2009**, *11*, 5241; d) Z. L. Mensinger, L. N. Zakharov, D. W. Johnson, *Inorg. Chem.* **2009**, *48*, 3505; e) C. Volkringer, T. Loiseau, N. Guillou, G. Férey, E. Elkaïm, *Solid State Sci.* **2009**, *11*, 1507; f) M. T. Wharmby, M. Snoyek, T. Rhauderwiek, K. Ritter, N. Stock, Norbert, *Cryst. Growth Des*. **2014**, *14*, 5310; g) H. Li, Y. Zhu, J. Zhang, Z. Chi, L. Chen, C-Y. Su, *RSC Adv.* **2013**, *3*, 16340; h) D. Hermann, H. Emerich, R. Lepski, D. Schaniel, U. Ruschewitz, *Inorg. Chem.* **2013**, *52*, 2744; i) C. Volkringer, T. Loiseau, N. Guillou, G. Férey, D. Popov, M. Burghammer, C. Riekel, *Solid State Sci.* **2013**, *26*, 38; j) N. Reimer, H. Reinsch, A. K. Inge, N. Stock, *Inorg. Chem.* **2015**, *54*, 492; k) C. Nanthamathee, S. Ling, B.Slater, M. P. Attfield, *Chem. Mater.* **2015**, *27*, 85.

44. a) M. Gaab, N. Trukhan, S. Maurer, R. Gummaraju, U. Müller, *Micropor. Mesopor. Mat.* **2012**, *157*, 131; b) G. Férey, M. Latroche, C. Serre, F. Millange, T. Loiseau and A. Percheron-Guegan, *Chem. Commun.* 2**003**, 2976.

45. J. J. Low, A. I. Benin, P. Jakubczak, J. F. Abrahamian, S. A. Faheem and R. R. Willis, *J. Am. Chem. Soc.* **2009**, *131*, 15834.

46. M. Schubert, U. Mueller, H. Mattenheimer and M. Tonigold, **WO2007/023119**, and other patents.

47. a) T. Lee, Z. Xin Liu and H. Lin Lee, *Cryst. Growth Des.* **2011**, *11*, 4146; b) L. Wang, L. Zhang, T. Song, C. Li, J. Xu, L. Wang, *Micropor. Mesopor. Mat.* **2012**, *155*, 281; c) D. F. Sava, L. E. S. Rohwer, M. A. Rodriguez, and T. M. Nenoff, *J. Am. Chem. Soc.* **2012**, *134*, 3983; d) Z.-Z. Lin , F.-L. Jiang, L. Chen, C.-Y. Yue, D.-Q. Yuan, A.-J. Lan and M.-C. Hong, *Cryst. Growth Des.* **2007**, *7*, 1712; e) L. Wang, T. Song, L. Huang, J. Xu, C. Li, C. Ji, L. Shan and L. Wang, *CrystEngComm* **2011**, *13*, 4005; f) *J. Mol. Struct.* **2010**, *975*, 215.

48. a) Y. Liu, V.C. Kravtsov, D.A. Beauchamp, J.F. Eubank, M. Eddaoudi, *J. Am. Chem. Soc.* **2005**, *127*, 7266; b) Y. Liu, J. F. Eubank, A.J. Cairns, J. Eckert, V.C. Kravtsov, R. Luebke, M.

Eddaoudi, *Angew. Chem., Int. Ed.* **2007**, *46*, 3278; c) Z. Lin, F. Jiang, L. Chen, D. Yuan, M. Hong, *Inorg. Chem*. **2005**, *44*, 73.

49. A. U. Czaja, N. Trukhan and U. Müller, *Chem. Soc. Rev.* **2009**, *38*, 1284.

50. a) N. Stock and S. Biswas, *Chem. Rev.* **2012**, *112*, 933; b) C. Dey, T. Kundu, B. P. Biswal, A. Mallick and R. Banerjee, *Acta Cryst.* **2014**, *B70*, 3.

51. Z. Ni and R. I. Masel, *J. Am. Chem. Soc.* **2006**, 128, 12394.

52. A. Martinez Joaristi, J. Juan-Alcañiz, P. Serra-Crespo, F. Kapteijn, and J. Gascon *Cryst. Growth Des.* **2012**, 12, 3489.

53. a) T. Friščić, *J. Mater. Chem*. **2010**, *20*, 7599; b) M. Klimakow, P. Klobes, A. F. Thünemann, K. Rademann and F. Emmerling, *Chem. Mater*. **2010**, *22*, 5216.

54. W.-J. Son, J. Kim, J. Kim and W.-S. Ahn, *Chem. Commun*. **2008**, 6336.

55. F. Gándara, A. de Andrés, B. Gómez-Lor, E. Gutiérrez-Puebla, M. Iglesias, M. A. Monge, D. M. Proserpio, and N. Snejko, *Cryst. Growth Des.* **2008**, *8*, 378.

56. B. F. Hoskins and R. Robson, *J. Am. Chem. Soc*. **1990**, *112*, 1546.

57. J. Y. Lee, O.K. Farha, J. Roberts, K. A. Scheidt, S. B. T. Nguyen and J. T. Hupp, *Chem. Soc. Rev*. **2009**, *38*, 1450.

58. A. Monge, N.Snejko , E. Gutiérrez-Puebla , M. Medina , C. Cascales , C. Ruiz-Valero , M. Iglesias and B. Gómez-Lor, *Chem. Commun.* **2005**, 1291.

59. D. W. Breck , W. G. Eversole and R. M. Milton , *J. Am. Chem. Soc*. **1956**, *78*, 2338.

60. M. Fujita, Y. J. Kwon, S. Washizu and K. Ogura, *J. Am. Chem. Soc.* **1994**, *116*, 1151.

61. M. O'Keeffe, *Chem. Soc. Rev.* **2009**, *38*, 1215.

62. a) P. García -García, M. Müller and A. Corma, *Chem. Sci.* **2014**, *5*, 2979 and references cited therein; b) A. Corma, H. García and F. X. Llabrés i Xamena, *Chem. Rev.* **2010**, *110*, 4606; c) L. Ma, C. Abney and W. Lin, *Chem. Soc. Rev*. **2009**, *38*, 1248.

63. L. Ma and W. Lin, *Top Curr Chem*, **2009**, *20*, 1.

64. a) S. Hasegawa, S. Horike, R. Matsuda, S. Furukawa, K. Mochizuki, Y. Kinoshita and S. Kitagawa, *J. Am. Chem. Soc.* **2007**, *129*, 2607; b) J. S. Seo, D. Whang, H. Lee, S. I. Jun, J. Oh, Y. J. Jeon and K. Kim, *Nature* **2000**, *404*, 982; c) P. Serra-Crespo, E. V. Ramos-Fernandez, J. Gascon and F. Kapteijin, *Chem. Mater*. **2011**, *23*, 2565.

65. H. Li, M. Eddaoudi, M. O'Keeffe and O. M. Yaghi, *Nature* **1999**, *402*, 276; b) T. Ishida, M. Nagaoka, T. Akita and M. Haruta, *Chem. Eur. J.* **2008**, *14*, 8456; c) J. Liu, L. Chen, H. Cui, J. Zhang, L. Zhang and C.-Y. Su. *Chem. Soc. Rev.* **2014**, *43*, 6011.

66. D. Esken, S. Turner, O. I. Lebedev, G. Van Tendeloo and R. A. Fischer, *Chem. Mater.* **2010**, *22*, 6393.

67. M. North, D. L. Usanov and C. Young, *Chem. Rev.* **2008**, *108*, 5146.

68. a) B. Y. Park, K. Y. Ryu, J. H. Park and S.-G. Lee, *Green Chem.* **2009**, *11*, 946; b) J. Gawronski, N. Wascinska and J. Gajewy, *Chem. Rev.* **2008**, *108*, 5227.

69. M. C. Bernini, F. Gándara, M Iglesias, N. Snejko,E. Gutiérrez-Puebla, E. V. Brusau, G. E. Narda and M. A. Monge, *Chem. Eur. J.* **2009**, *15*, 4896.

70. a) A. A. Pavlic and H. Adkins, *J. Am. Chem. Soc.*, **1946**, *68*, 1471; b) R. Adams, V. Voorhees, R. L Shriner, *Organic Syntheses*, Wiley & Sons: New York, **1941**; Collect. Vol. 1, p 463.

71. A. E. Platero-Prats, V. A. de la Peña-O'Shea, M. Iglesias, N. Snejko, A. Monge and E. Gutierrez-Puebla, *ChemCatChem*, **2010**, *2*, 147.

72. a) D. M. D'Souza and T. J. J. Mueller, *Chem Soc. Rev.* **2007**, *36*, 1095; b) C. Grondal, M. Jeanty and D. Enders, *Nat. Chem.* **2010**, *2*, 167.

73. Y. Gu, *Green Chem.* **2012**, *14*, 2091.

74. R. C. Cioc, E. Ruijter and R. V. A. Orru, *Green Chem.* **2014**, *16*, 2958.

75. W. Wang and P. –F. Xu, *catalytic cascade reactions*, John Wiley and Sons Inc., Hoboken, New Jersey, **2013**.

76. M. J. Climent, A. Corma and S. iborra, *RSC Adv.* **2012**, *2*, 16.

77. a) S. C. Pan and B. List, *Angew. Chem., Int. Ed.* **2008**, *47*, 3622; b) A. Shaabani, S. Keshipour, S. Shaabani and M. Mahyari, *Tetrahedron Lett.* **2012**, *53*, 1641; c) S. Ghandi and B. List, *Angew. Chem., Int. Ed.* **2013**, *52*, 2573; d) G. Villaverde, A. Corma, M. Iglesias and F. Sanchez, *ACS Catal.* **2012**, *2*, 399; e) J. R. Avalani, D. S. Patel and D. K. Rava, *J. Mol. Catal. B: Enzym.* **2013**, *90*, 70; f) A. Maleki, *Tetrahedron Lett.* **2013**, *54*, 2055.

78. A. Strecker, *Justus Liebigs Ann. Chem.* **1850**, *75*, 27.

79. M. Passerini, *Gazz. Chim. Ital.* **1921**, *51*, 126.

80. I. Ugi, R. Meyr, U. Fetzer and C. Steinbrückner, *Angew. Chem.* **1959**, *71*, 386.

CHAPTER 2

OBJECTIVES AND APPROACH

2.1. General Objectives

The main objective of this thesis is to design, synthesize, purify and perform the spectroscopic and structural characterization of new metal-organic materials (MOFs) with 1D, 2D and 3D frameworks, to be used as heterogeneous catalysts in different organic transformations. In order to do so, the following steps have to be performed:

i) To design, to synthesize and to characterize new green materials.
ii) To study the catalytic activity for all obtained materials.

2.2. Specific Objectives

Taking in to account the previously mentioned, in this thesis the following specific objectives are proposed:

i) Adequate selection of the building blocks in order to allow the synthesis of materials with several dimensionalities (1 to 3) with the certain catalytic properties.
ii) Synthesis conditions screening to evaluate their influence on the synthesis result, where the purity and high yield of the material are the main goals.
iii) Single crystal growth promotion of the materials in order to perform the study of the structural features of the obtained compounds using the single crystal X-ray diffraction technique.
iv) Structural data treatment implementation in order to obtain the crystalline structure for each new material.
v) Accomplishment of the crystallographic description and the topological analysis for each network obtained.
vi) Adequate selection of the organic transformations in order to test the heterogeneous catalytic activity of each obtained material.
vii) Evaluation of the results of the studies on the catalytic activity of the obtained materials in order to establish appropriate goals for the future progress in the area.

2.3. Approach

2.3.1 Choosing the adequate Building Blocks Units (BBUs)

We have already discussed the incredible amount of MOFs synthesized along the years using transition metals and lanthanides linked by all kind of ligands from simple inorganic molecules to large and bulky poly-aromatic hydrocarbons. The choice of the right building blocks units will focus the MOFs production to obtain new architectures with the specific desired functional properties.

In this work we selected as BBUs Indium, Gallium, Aluminum, together with multicarboxylate bending V-shaped ligands 4,4'-hexafluoroisopropylidene (**H_2hfipbb**), diphenylmethane-4,4-dicarboxylic acid (**H_2dpmda**), 5-(4-carboxy-2-nitrophenoxy)-1,3-benzenedicarboxylic acid (**H_3popha**) and also additional nitrogenated ligands as 1,10-phenantroline (1,10-phen), 1,7-phenantroline (1,7-phen), 2,2'-bipyridine (2,2'-bipy) and 4,4'-bipyridine (4,4'-bipy).

2.3.2. Multi-carboxylate bending linkers as BBUs

The geometry of organic ligands influences greatly the final structures of metal organic materials. The carboxylate unit is one of the most widely used in the synthesis of MOFs;[1] MOFs constructed on the base of dicarboxylates have received a lot of attention and their materials exhibit useful properties.[2]

In case of materials with multicarboxylic entities, the position of the coordinating group in the linker often plays a major role in directing the corresponding MOF dimensionality.[3] Considering the general positions of the coordinating groups in a simple phenyl ring (*ortho*, *meta*-, and *para*-), the angle between the positions of the coordinating groups in the linker, which is known as linker coordination angle (LCA), varies according to the geometry of the spacer; as a result, the overall coordination geometry of the concerned linker in the resulting material is adjusted. In case of materials containing rigid ligands (Figure 2.1), these ones have been widely studied exploiting their LCAs due to their regular and well defined coordination modes.[4]

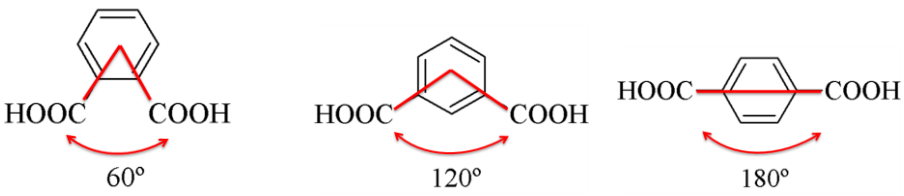

Figure 2.1 Linker Coordination Angle (LCA) for different substituent positions in a phenyl ring

In contrast, MOFs constructed with bending and flexible ligands are still limited due probably to the unpredictable nature of such systems arising from the flexible nature of spacers that

allows more of degrees of freedom. For this reason using these types of multicarboxylate ligands would supply diverse conformations to control over the stereochemistry of the metallic centers, and could create different frameworks.[5]

In this work, flexible V-shaped dicarboxylate linkers as H_2hfipbb and H_2dpmda were used; these ligands exhibit different type of coordination modes, which could allow a wide range of new compounds with new structures and a great potential in several properties. The geometry of both ligands is given by the central carbon atom having a sp3 hybridization, which generates a tetrahedral geometry (Figure 2.2).

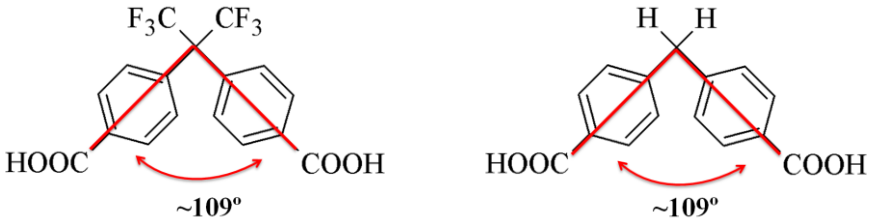

Figure 2.2 The V-shaped linkers **H_2hfipbb** and **H_2dpmda** showing their LCA

From 2005 until now, several MOFs have been reported using the H_2hfipbb as a connector demonstrating the high stability of these MOFs frameworks, which is due to the less-free rotation of the sp^3-carbon because of the presence of the voluminous -CF_3 groups. On the other hand, with the H_2dpmda linker there are only eight MOFs and CPs materials reported,[6] which makes it interesting in order to explore the challenges in the synthetic procedures of the corresponding MOF materials and the studies of the influences of the geometrical features of the ligand (compared with those of H_2hfipbb) on the structure and properties of the materials obtained.

In addition, the tricarboxylate linker H_3popha was utilized in this work. This ligand has an oxygen sp^3 as central atom and also this ether derivate presents a nitro group breaking the molecule symmetry. Despite interesting geometry (V-shaped with a tendency to obtain helical chains) and several biological applications of this ligand, up to date only a few studies of MOFs with this ligand are reported.[7]

Although the geometry of H_3popha remains V-shaped, the raise in the number of the possible coordinated entities generates an increment of the number of LCAs. So, the H_3popha linker with three carboxylate entities shows three different LCA values, being the most important LCA values those that describe the geometry angles between two carboxylate entities of different phenyl rings (Figure 2.3).

Even though the oxygen central atom as well as the nitro group could be considered as functional groups for catalytic systems, in our case the substitution positions in the phenyl ring make it difficult their interaction with the reactants, and for this instance we do not considered them as possible catalytic sites in the organic transformations performed with the materials developed using H_3popha as organic linker.

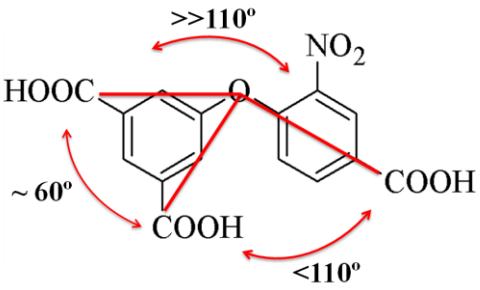

Figure 2.3 V-shaped tripodal **H_3popha** linker showing its LCA values.

2.3.3. Metal BBUs Selection.

MOFs with high valence cations are not very frequent, excluding Ln^{3+} ions. Their chemical reactivity seems to be in essential discrepancy with those materials with lower valence metals; this can lead to less control over the crystallization process, which decreases the possibility to obtain single crystals in order to perform their structure determination.[8] Still there are advantages to consider when developing higher valence metal containing materials; one of the interesting features of such MOFs is the chemical stability that they offer and the possibilities of developing new architectures with new and interesting properties.

In view of the previously mentioned, trivalent Group 13 *p*-metals ions Indium, Gallium and Aluminum have been selected in order to provide new polymeric frameworks.

The most common geometry observed for the M^{3+} ions in MOFs is the octahedra (CN=6) produced usually by an environment of oxygen and nitrogen atoms; chains of M-O-M are typical for this kind of materials and no particular dimensionality seems to be preferred exclusively. Among the properties of the materials containing the selected metals BBUs, their good chemical stability makes them suitable candidates for heterogeneous catalysis, which is based on their Lewis acidity. Previous works in our research group demonstrated that group 13 materials showed interesting catalytic properties in the acetalization of carbonyl compounds.[9]

According to previous works of our research group in this area and the results found in the literature, Indium, Gallium and Aluminum were selected as metallic sources because these metals are great candidates for catalytic purpose; as principal organic entities this work is focused on bending V-shaped multicarboxylate linkers, which according to previously mentioned could contribute to obtaining of different materials with interesting topologies and required properties.

Our main goal is a part of a larger project that aims to understand and gain more control on the synthesis methods, making good structural characterization of materials (MOFs) and their corresponding chemical and physical properties.

2.4. References

1. a) C. N. R. Rao, S. Natarajan and R. Vaidhyanathan, *Angew. Chem., Int. Ed*. **2004**, *43*, 1466; b) Z. B. Han, B. Y. Li, J. W. Ji, Y. E. Du, H. Y. An and M. H. Zeng, *Dalton Trans*. **2011**, *40*, 9154.

2. a) H. Furukawa, N. Ko, Y. B. Go, N. Aratani, S. B. Choi, E. Choi, A. O. Yazaydin, R. Q. Snurr, M. O'Keeffe, J. Kim and O. M. Yaghi, *Science*, **2010**, *329*, 424; b) J. Tao, R. J. Wei, R. B. Huang and L. S. Zheng, *Chem. Soc. Rev.*, **2012**, *41*, 703; c) M. Kurmoo, *Chem. Soc. Rev*. **2009**, *38*, 1353.

3. a) A. Schaate, S. Klingelhofer, P. Behrens and M. Wiebcke, *Cryst. Growth Des*. **2008**, *8*, 3200; b) Y. Liu, Y. Qi, Y. Y. Lv, Y. X. Che and J. M. Zheng, *Cryst. Growth Des*. **2009**, *9*, 4797; c) Z. X. Li, T. L. Hu, H. Ma, Y. F. Zeng, C. J. Li, M. L. Tong and X. H. Bu, *Cryst. Growth Des.* **2010**, *10*, 1138; d) J. Yang, J. F. Ma, S. R. Battern and Z. M. Su, *Chem. Commun.* **2008**, 2223.

4. a) A. J. Blake, N. R. Champness, S. S. M. Chung, W. S. Li and M. Schröder, *Chem. Commun.* **1997**, 1005; b) M. Maekawa, H. Konaka, Y. Suenaga, T. K. Sowa and M. Munakata, *J. Chem. Soc*. **2000**, 4160; c) H. C. Wu, P. Thanasekaran, C. H. Tsai, J. Y. Wu, S. M. Huang, Y. S. Wen and K. L. Lu, *Inorg. Chem*. **2006**, *45*, 295; d) B. Y. Cho, D. Min and S. W. Lee, *Cryst. Growth Des*. **2006**, *6*, 342.

5. a) A. J. Blake, N. R. Brooks, N. R. Champness, M. Crew, A. Deveson, D. Fenske, D. H. Gregory, L. R. Hanton, P. Hubberstey and M. Schroder, *Chem. Commun.* **2001**, 1432; b) S. Sanda, S. Parshamoni, A. Adhikary and S. Konar, *Cryst. Growth Des.* **2013**, *13*, 5442; c) S. Sanda , S. Biswas , and S. Konar, *Inorg. Chem.* **2015**, *54*, 1218.

6. a) A. E. Platero-Prats, N. Snejko, M. Iglesias, M. A. Monge and E. Gutierrez-Puebla, *Chem. Eur. J.* **2013**, *19*, 15572; b) G. – X. Liu, X. – C. Cha, X.- L. Li, C. – Y. Zhang, Y. Wang, S. Nishihara and X. – M. Ren, *Inorg. Chem. Commun.* **2011**, *14*, 867; c) J.-Q. Liu, J. Wu, Z.-B. Jia, H.-L. Chen, Q.-L. Li, H. Sakiyama, T. Soares, R. Fei, C. Daiguebonne, O. Guillou and S. W. Ng, *Dalton Trans*. **2014**, *43*, 17265; d) Y.- H. Liao, W. Hsu, C. - C.Yang, C. – Y Wu, J. – D. Chen and J. – C. Wang, *CrystEngComm.* **2013**, *15*, 3974; e) L. Guang-Xiang, W. Xiao-Feng and Z. Hong, *J. Sol. State Chem.* **2013**, *199*, 305.

7. a) C. Qin, X. L. Wang, E. B. Wang, Y. F. Q, H. Jin, S. Chang and L. Xu, *J. Mol. Struct.* **2005**, *749*, 138; b) H.L. Wang, D. P. Zhang, D. F. Sun, Y. T. Chen, L. F. Zhang, L. J. Tian, J. Z. Jiang and Z. H. Ni, *Cryst. Growth Des.* **2009**, *9*, 5273; c) C. Y. Kong, *J. Inorg. Organomet. Polym.* **2011**, *21*, 189; d) J. K. Sun, Q. X. Yao, Z. F. Ju and J. Zhang, *Cryst. Eng. Commun*. **2010**, *12*, 1709; e) H. L. Wang, D. P. Zhang, D. F. Sun, Y. T. Chen, K. Wang, Z. H. Ni, L. J. Tian and J. Z. Jiang, *Cryst. Eng. Commun*. **2010**, *12*, 1096; f) X. L. Zhang, M. F. Jin, Y. E. Qiu and F. Guo, *J. Inor.g Organomet. Polym*. **2011**, *21*, 498; g) L. – L. Yu, *J. Inorg. Organomet. Polym*. **2012**, *22*, 278.

8. T. Devid and C. Serre, *Chem.Soc. Rev.* **2014**, *43*, 6097.

9. a) F. Gándara, B. Gomez-Lor, E. Gutiérrez-Puebla, M. Iglesias, M. A. Monge, D. M. Proserpio and N. Snejko. *Chem. Mater*. **2008**, *20*, 72; b) B. Gómez-Lor, E. Gutiérrez-Puebla, M. Iglesias, M. A. Monge, C. Ruiz-Valero and N. Snejko. *Chem. Mater*. **2005**, *17*, 2568.

CHAPTER 3

MANUFACTURING PROCEDURES AND EXPERIMENTAL TECHNIQUES

From an environmental and economical point of view, the use of methodologies, which employ mild conditions and nontoxic solvents for material manufacture, is the most important scope nowadays. Herein, using two different energy sources, conventional and microwave, a cleaner and faster fabrication of new metal-organic materials is allowed, reaching purity and high yields for these materials whose catalytic activity are then tested.

In this chapter, the description of the synthesis conditions and the corresponding characterization of each material are presented as well as the details of the catalytic procedures performed. Finally, a brief apparatus description for each experimental technique employed in the curse of this thesis is given.

3.1. Manufacture Procedures of MOFs: Synthesis and Spectroscopy Characterization of New Indium, Gallium and Aluminium Materials

In this section the synthesis is described of fifteen new MOFs using different V-shaped multicarboxylate ligands together with different auxiliary ligands. All the syntheses were performed under conventional hydrothermal conditions and the primary characterization of the materials was carried out using elemental analysis, infrared spectroscopy and thermogravimetric analysis.

3.1.1. Synthesis of New MOFs using H_2hfipbb linker

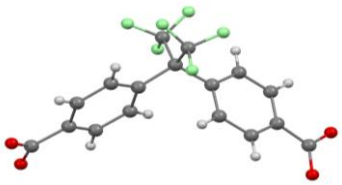

The synthesis of the following indium MOFs was performed using H_2hfipbb as organic linker and additional nitrogenated auxiliary ligands. All materials were obtained under conventional hydrothermal conditions.

[Al(OH)(hfipbb)] (AlPF-1)

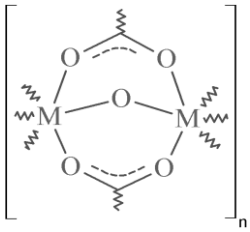

The mixture of H_2hfipbb (0.105g, 0.260 mmol) and $Al(NO_3)_3.9H_2O$ (0.100 g, 0.260 mmol) in ethanol/water (3mL/12mL), was stirred and then transferred to a Teflon-lined stainless steel autoclave and heated at 160 ºC for 72 hours. After cooling to room temperature, colourless crystals formed were filtered off and washed with distilled water, ethanol and acetone. Yield: 0.106g, 94%.

Elemental analysis, weight% found (calculated): C, 47.36 (47.02); H, 2.24 (2.09).

IR (KBr, cm^{-1}): 3700 and 3510 ν(μ-OH), 3430 ν(O-H $_{H2O}$), 3066 ν(C-H), 1603 $\nu(C=O)_{as}$, 1558 ν(C=C), 1518 $\nu(C-C)_{as}$, 1441 and 1259 $\nu(C-O)_s$, 1214 $\nu(C-C)_s$, 1174ν(C-F), 789, 748 and 731 $\delta_{oop}(C-H)_L$.

TG (air, 10ºC/min): the framework is stable up to 550ºC; under further heating the loss of 81% material content is observed, corresponding to the organic part of the material. The final residue at ~1000ºC corresponds to a 16% of material converted into Al_2O_3 (ICSD_151589).

[Ga(OH)(hfipbb)] (GaPF-1)

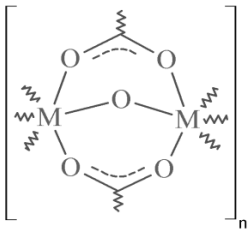

The mixture of H_2hfipbb (0.158g, 0.391 mmol) and $Ga(NO_3)_3{\cdot}3H_2O$ (0.100 g, 0.391 mmol) in water (12mL) was stirred and then transferred to a Teflon-lined stainless steel autoclave and heated at 170 ºC for 72 hours. After cooling to room temperature, colourless crystals formed were filtered off and washed with distilled water, ethanol and acetone.

Yield: 0.056g, 30%.

Elemental analysis, weight% found (calculated): C, 41.63 (42.81); H, 2.07 (1.90).

IR (KBr, cm^{-1}): 3664 ν(μ-OH), 3426 ν(O-H $_{H2O}$), 3068 ν(C-H), 1640 $\nu(C=O)_{as}$, 1598 $\nu(C=C)_{as}$, 1552 $\nu(C-C)_{as}$, 1424 and 1259 $\nu(C-O)_{s}$, 1211 $\nu(C-C)_{s}$, 1174 ν(C-F), 784 and 730 δ_{oop}(C-H).

TG (air, 10ºC/min): the framework is stable up to 480ºC; under further heating the loss of 67% of material content is observed follow by a loss of and 9% of material content at ~515ºC, which corresponds to the organic part of the material. The final residue at ~1000ºC corresponds to a 20% of material converted into Ga_2O_3 (ICSD_83645).

$[In(O_2C_2H_4)_{0.5}$(hfipbb)] (InPF-11β)

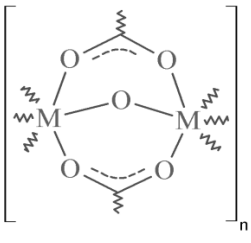

The mixture of H_2hfipbb (0.134 g, 0.342mmol) and $In(OAc)_3 \cdot H_2O$ (0.100g, 0.342 mmol) in ethyleneglycol/water (6mL/6mL) was stirred and then transferred to a Teflon-lined stainless steel autoclave and heated at 160 ºC for 72 hours. After cooling to room temperature, colourless crystals formed were filtered off and washed with distilled water, ethanol and acetone. Yield: 0.095g, 53%.

Elemental analysis, weight% found (calculated): C, 39.98 (40.45); H, 1.65 (1.87).

IR (KBr, cm^{-1}): 3432$\nu(O\text{-}H_{H_2O})$, 3078 ν(C-H) 2939 and 2864 $\nu(C\text{-}H)C_2H_4$, 1619 $\nu(C=O)_{as}$, 1591 $\nu(C=C)_{as}$, 1542 ν(O-C $_{ethyleneglycoxide}$)s, 1417 and 1255 ν(C-O)s, 1214 ν(C-C)s, 1172 ν(C-F), 779, 749 and 726 δ_{oop}(C-H).

TG (air, 10ºC/min): the framework is stable up to 500ºC, and then the loss of 72% of material content is observed that corresponds to the organic part of the material. The final residue at ~1000ºC corresponds to a 28% of material converted into In_2O_3 (ICSD_6040179).

$[In_2(hfipbb)_3(1,10\text{-}phen)_2]\cdot 2H_2O$ (InPF-12)

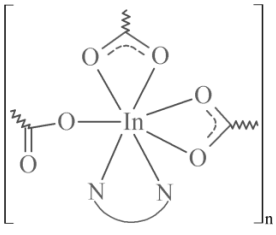

The mixture of H_2hfipbb (0.201 g, 0.513mmol), 1,10-phen (0.067g, 0.342 mmol) and $In(OAc)_3 \cdot H_2O$ (0.100 g, 0.342 mmol) in 8 mL of water, was transferred after stirring to a Teflon-lined stainless steel autoclave and heated at 170ºC for 18 hours, then cooled to room temperature. Colourless crystals formed were filtered off and washed with distilled water, ethanol and acetone, yielding 0.223g of the product (73%).

Elemental analysis, weight% found (calculated): C, 49.69 (49.64); H, 2.65 (2.55); N, 3.04 (3.09).

IR (KBr, cm^{-1}): 3543$\nu(O\text{-}H_{H_2O})$, 3432 ν(C-H $_{phen}$), 3079 ν(C-H), 1720 $\nu(\eta^1\text{-}C=O)_{as}$, 1600 $\nu(\eta^2\text{-}C=O)_{as}$, 1549 ν(C=N $_{phen}$), 1432 $\nu(C=C)_{as}$, 1421 and 1254 $\nu(C-O)_{s}$, 1212 $\nu(C-C)_{s}$, 1176 ν(C-F), 872, 857 δ_{oop}(C-H $_{phen}$), 785, 750 and 724 δ_{oop}(C-H).

TG (air, 100mL/min): Initial weight loss starts at ~100ºC: the loss of 3% is attributed to

hydration water molecules departure. At ~410ºC the loss of 56% of material content and at ~460ºC the loss of 21% content occur. The final residue at ~800ºC corresponds to a 20% of material converted into In_2O_3 (ICSD_640179).

$[In_2(hfipbb)_3(2,2'\text{-bipy})_2]\cdot 2H_2O$ (InPF-13)

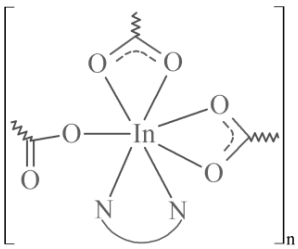

The mixture of H_2hfipbb (0.201 g, 0.513mmol), 2,2'-bipy (0.047 g, 0.342 mmol) and $In(OAc)_3\cdot H_2O$ (0.100 g, 0.342 mmol) in 8 mL of distilled water was heated in a Teflon-lined stainless steel autoclave at 170 ºC for 72 hours. After cooling to room temperature, colourless crystals formed were filtered off and washed with distilled water, ethanol and acetone. Yield: 0.230g, 77%.

Elemental analysis, weight% found (calculated): C, 48.36 (48.76); H, 2.17 (2.54); N, 3.11 (3.20).

IR (KBr, cm^{-1}): 3593ν(O-H_{H2O}), 3532 ν(C-$H_{2,2'\text{-bipy}}$), 3120 and 3064 ν(C-H), 1717 $\nu(\eta^1$-C=O)$_{as}$, 1604 $\nu(\eta^2$-C=O)$_{as}$, 1541 ν(C=$N_{2,2'\text{-bipy}}$), 1445 ν(C=C)$_{as}$, 1424, 1375 and 1250ν(C-O)$_s$, 1212 ν(C-C)$_s$, 1176 ν(C-F), 874, 860 δ_{oop}(C-$H_{2,2'\text{-bipy}}$), 781, 775 and 724 δ_{oop}(C-H).

TG (air, 100mL/min): Initial weight loss starts at ~100ºC (the 2% loss is attributed to hydration water molecules departure). The loss at ~300ºC of 18% of material content corresponds to the 2,2-bipy molecules, and after ~440ºC the loss of 60% of content can be attributed to breakdown of the $hfipbb^{-2}$ linker. The final residue at ~800ºC corresponds to a 20% of material converted into In_2O_3 (ICSD_640179).

$[In_2(hfipbb)_3(4,4'\text{-bipy})]$ (InPF-14)

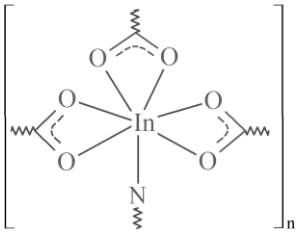

The mixture of H_2hfipbb (0.201 g, 0.513mmol), 4,4'-bipy (0.024 g, 0.171 mmol) and $In(OAc)_3\cdot H_2O$ (0.100 g, 0.342 mmol) in 8 mL of distilled water was heated in a Teflon-lined stainless steel autoclave at 170 ºC for 72 hours. After cooling to room temperature, colourless crystals formed were filtered off and washed with distilled water, ethanol and acetone. Yield: 0.210g, 79%.

Elemental analysis, weight% found (calculated): C, 46.68 (47.07); H, 2.2(2.07); N, 1.61(1.80).

IR (KBr, cm^{-1}): 3421 ν(C-$H_{4,4'\text{-bipy}}$), 3246 and 3117 ν(C-H), 1614 ν(C=O)$_{as}$, 1597 (C=C)$_{as}$, 1543 ν(C=$N_{4,4'\text{-bipy}}$), 1426 and 1298 ν(C-O)$_s$, 1255 and 1242 ν(C-C)$_s$, 1177 ν(C-F), 878, 859 δ_{oop}(C-$H_{4,4'\text{-bipy}}$), 781, 752 and 726 δ_{oop}(C-H).

TG (air, 100mL/min): Initial weight loss starts at ~470ºC (79% of material content). The final residue at ~800ºC corresponds to a 21% of material converted into In_2O_3 (ICSD_640179).

[$In_4(OH)_4(hfipbb)_4(4,4'\text{-bipy})$] (InPF-15)

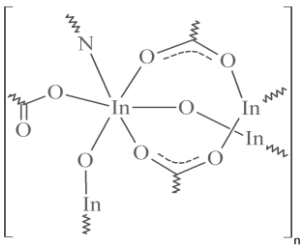

The mixture of H_2hfipbb (0.132 g, 0.336 mmol), 4,4'-bipy (0.048 g, 0.307 mmol) and $In(OAc)_3 \cdot H_2O$ (0.100 g, 0.342 mmol) in 6 mL of distilled water was heated in a Teflon-lined stainless steel autoclave at 200 ºC for 72 hours. After cooling to room temperature, colourless crystals were filtered off and washed with distilled water, ethanol and acetone. Yield: 0.568g, 82%

Elemental analysis, weight% found (calculated): C, 41.22 (41.82); H, 1.91(1.80); N, 1.23(1.25).

IR (KBr, cm^{-1}): 3632ν(μ-OH), 3430 ν(C-$H_{4,4'\text{-bipy}}$), 1700 $\nu(\eta^1\text{-C=O})_{as}$, 1619 $\nu(\eta^2\mu\text{-C=O})$, 1588 $\nu(C=C)_{as}$, 1531 $\nu(C=N_{4,4'\text{-bipy}})$, 1406 and 1269$\nu(C\text{-O})_s$, 1255 and 1238 $\nu(C\text{-C})_s$, 1173 ν(C-F), 863, 846 $\delta_{oop}(C\text{-}H_{4,4'\text{-bipy}})$, 769, 736 and 711 δ_{oop}(C-H).

TG (air, 100mL/min): Initial weight loss starts at ~470ºC (77% of material content). The final residue at ~800ºC corresponds to a 23% of material converted into In_2O_3 (ICSD_640179).

3.1.2. Synthesis of New MOFs with H_2dpmda linker

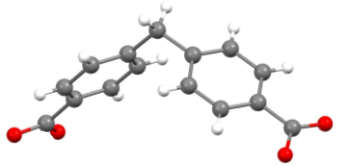

The synthesis of the following indium MOFs was performed using H_2dpmda as organic linker together with different nitrogenated auxiliary ligands.

[In(OH)(dpmda)(H_2O)] (InPF-22)

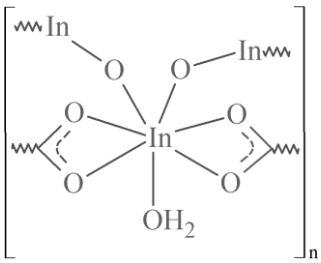

The mixture of H_2dpmda (0.085 g, 0.332mmol) and $In(NO_3)_3$ (0.100 g, 0.332 mmol) in 8 mL of distilled water was heated in a Teflon-lined stainless steel autoclave at 180ºC for 96 hours. After cooling to room temperature, yellow crystalline powder was filtered off and washed with distilled water, ethanol and acetone. Yield: 0.067g, 50%.

Elemental analysis, weight% found (calculated): C, 44.34 (44.58); H, 2.75(3.24).

IR (KBr, cm^{-1}): 3385 $\nu(O\text{-H}_{\text{coordinated } H_2O})$, 3071 and 3052 $\nu(C_{sp^2}\text{-H})$, 2924 and 2854 $\nu(C_{sp^3}\text{-H})$, 1648 ν(C=O), 1585 $(C=C)_{as}$, 1530 and 1501$\nu(C\text{-C})_{as}$, 1419 and 1302 $\nu(C\text{-O})_s$ 1282 and 1180 $\nu(C\text{-C})_s$, 728 δ_{oop}(C-H).

TG (air, 100mL/min): Initial weight loss starts at ~260ºC (5% attributed to coordinated water molecule); at ~450ºC the material experiments second weight loss of 60% of material content. The final residue at ~800ºC corresponds to a 35% of material converted into In_2O_3 (ICSD_640179).

$[In_2(dpmda)_3(1,10\text{-}phen)_2]\cdot 2H_2O$ (InPF-9)

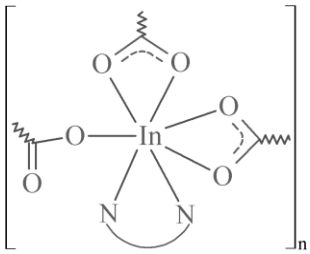

The mixture of H_2dpmda (0.132 g, 0.513mmol), phen (0.068 g, 0.342 mmol) and $In(OAc)_3\cdot H_2O$ (0.100 g, 0.342 mmol) in 6 mL of distilled water was heated in a Teflon-lined stainless steel autoclave at 200 ºC for 72 hours. After cooling to room temperature, light yellow crystals formed were filtered off and washed with distilled water, ethanol and acetone. Yield: 0.130g, 55%.

Elemental analysis, weight% found (calculated): C, 60.04 (60.45); H, 3.56(3.53); N, 3.88(4.09).

IR (KBr, cm^{-1}): 3430 $\nu(OH_{H2O})$, 3119 ν(C-H $_{phen}$), 3062 $\nu(C_{sp^2}\text{-H})$, 3040 $\nu(C_{sp^3}\text{-H})$, 1702 $\nu(\eta^1\text{-C=O})_{as}$, 1605 $\nu(\eta^2\text{-C=O})_{as}$, 1586 ν(C=N $_{phen}$), 1415 and 1402 $\nu(\text{C-O})_s$, 1181 $\nu(\text{C-C})_{as}$, 1107 and 1021 $\nu(\text{C-C})_s$, 876 δ_{oop}(C-H $_{phen}$), 769 and 717 δ_{oop}(C-H).

TG (air, 100mL/min): Initial weight loss starts at ~100ºC (the loss of 2% is attributed to hydration water molecules). Then the material experiences losses at ~300ºC, ~380ºC and ~460ºC (losses of 8%, 41% and 30% of material content, respectively). The final residue at ~800ºC corresponds to a 19% of material converted into In_2O_3 (ICSD_640179).

[$In_2(dpmda)_3(2,2'\text{-}bipy)_2]\cdot 2H_2O$ (InPF-10)

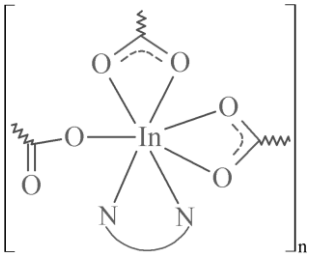

The mixture of H_2dpmda (0.132 g, 0.513mmol), 2,2'-bipy (0.047 g, 0.342 mmol) and $In(OAc)_3\cdot H_2O$ (0.100 g, 0.342 mmol) in a mixed solution of 5mL of distilled water with 1mL ethanol was heated in a Teflon-lined stainless steel autoclave at 180ºC for 72 hours. After cooling to room temperature, colourless crystals were filtered off and washed with distilled water, ethanol and acetone. Yield: 0.170g, 74%.

Elemental analysis, weight% found (calculated): C, 57.82 (58.32); H, 3.63 (3.61); N, 4.22 (4.19).

IR (KBr, cm^{-1}): 3418ν(O-H $_{H2O}$), 3118 ν(C-$H_{2,2'\text{-bipy}}$), 3061 $\nu(C_{sp^2}\text{-H})$, 2924 $\nu(C_{sp^3}\text{-H})$, 1710 $\nu(\eta^1\text{-C=O})_{as}$, 1621 $\nu(\eta^2\text{-C=O})_{as}$, 1586 $\nu(\text{C=C})_{as}$, 1567 $\nu(\text{C=}N_{2,2'\text{-bipy}})$, 1444 $\nu(\text{C-}N_{2,2'\text{-bipy}})$, 1420 and 1350 $\nu(\text{C-O})_s$, 1179 and 1107 $\nu(\text{C-C})_s$, 875 δ_{oop}(C-$H_{2,2'\text{-bipy}}$), 769 δ_{oop}(C-H).

TG (air, 100mL/min): Initial weight loss starts at ~100ºC (4%, attributed to hydration water molecules). Then the material undergoes losses at ~360ºC and ~470ºC (losses of 32% and 25% of material content, respectively). The final residue at ~800ºC corresponds to a 23% of material converted into In_2O_3 (ICSD_640179).

[In(OH)(dpmda)].0.5(4,4'-bipy) (InPF-23)

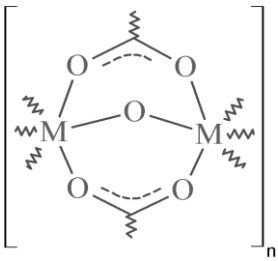

The mixture of H_2dpmda (0.092 g, 0.343mmol), 4,4'-bipy (0.048 g, 0.342 mmol) and $In(OAc)_3 \cdot H_2O$ (0.100 g, 0.343 mmol) in 6 mL of distilled water was heated in a Teflon-lined stainless steel autoclave at 200 ºC for 120 hours. After cooling to room temperature, brown crystalline powder was filtered off and washed with distilled water, ethanol and acetone. Yield: 0.150g, 94%.

Elemental analysis, weight% found (calculated): C, 52.36 (51.75); H, 3.42 (3.25); N, 2.35(3.01).

IR (KBr, cm^{-1}): 3217 ν(μ-OH), 3119 $\nu(C_{sp^2}$-H), 3059, 3036 and 3001 ν(C-$H_{4,4'\text{-bipy}}$), 2943 and 2920 $\nu(C_{sp^3}$-H), 1621 and 1605 $\nu(C{=}O)_{as}$, 1588 $\nu(C{=}C)_{as}$, 1544 $\nu(C{=}N_{4,4'\text{-bipy}})$, 1417 $\nu(C\text{-}N_{4,4'\text{-bipy}})$, 1403 and 1350 ν(C-O)s, 1179 and 1107 $\nu(C\text{-}C)_s$, 854 δ_{oop}(C-$H_{4,4'\text{-bipy}}$), 770 δ_{oop}(C-H).

TG (air, 100mL/min): Initial weight loss starts at ~300ºC (19%, attributed to the half of bipyridine molecule) and then undergoes a loss 46% of material content at ~450ºC. The final residue at ~800ºC corresponds to a 35% of material converted into In_2O_3 (ICSD_640179).

3.1.3. Synthesis of New MOFs using H_3popha linker

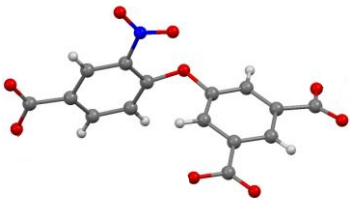

The synthesis of the following indium MOFs was performed using H_3popha as organic linker with and without different nitrogenated auxiliary ligands. All materials were obtained using conventional hydrothermal conditions as well as through microwave assisted synthesis.

$[In_8(OH)_6(popha)_6(H_2O)_4]\cdot 3H_2O$ (InPF-16)

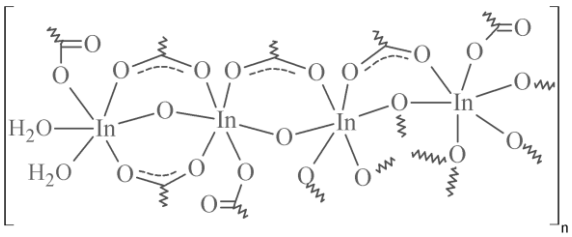

The mixture of H_3popha (0.089g, 0.256mmol) and $In(OAc)_3 \cdot H_2O$ (0.100 g, 0.343 mmol) in 6 mL of water was transferred to a Teflon-lined stainless steel autoclave and heated at 170ºC for 72 hours. After cooling to room temperature, colorless crystals formed were filtered off and washed with distilled water, ethanol and acetone. Yield: 0.781g, 95%.

Elemental analysis of the product: weight% found (calculated): C, 33.68 (33.65); H, 1.72 (1.76); N, 2.68(2.62).

MW synthesis: 0.030g (0.085mmol) of H_3popha, 0.033g (0.114mmol) of $In(OAc)_3$ and 2 mL of water were placed in a glass vial, and submitted to MW radiation with a dynamic method at 170ºC with high stirring (30min, 200W, 10 bar). Yield: 0.265g, 97%.

Elemental analysis of the product: weight% found (calculated): C, 33.55 (33.65); H, 1.99

(1.76); N, 2.45(2.62).

IR (KBr, cm^{-1}): 3636 ν(μ-OH), 3539 ν(O-H, $_{coordinated\ H2O}$), 3231 ν(O-H $_{H2O}$), 3078 and 3088 ν(C_{sp^2}-H), 1633 ν(η^1-C=O)$_{as}$, 1613 ν(η^2μ-C=O)$_{as}$, 1586 ν(C=C)$_{as}$, 1562 ν(N-O)$_{as}$, 1458, 1419 and 1410 ν(C-O)$_s$, 1351 and 1313 ν(N-O)$_s$, 1259 and 1229 ν(O_{sp^3}-C), 1143 ν(C-C)s, 777, 767 and 712 δ_{oop}(C-H).

TG (air, 100mL/min): Initial weight loss (of ~5%) starts at ~100ºC, which is attributed to the loss of coordinated and the physisorbed water molecules; then at ~420ºC loss 60% of material content occurs. The final residue at ~800ºC corresponds to a 35% of material converted into In_2O_3 (ICSD_640179).

[In(popha)(2,2'-bipy)]·3H_2O (InPF-17)

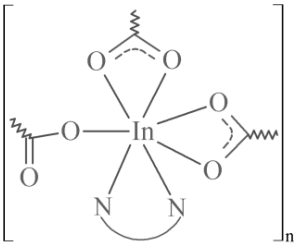

The mixture of H_3popha (0.119 g, 0.343 mmol), 2,2'-bipy (0.047 g, 0.343 mmol) and In(OAc)$_3$·H_2O (0.100 g, 0.343 mmol) in 12 mL of distilled water was heated in a Teflon-lined stainless steel autoclave at 150ºC for 24 hours. After cooling to room temperature, light violet crystals formed were filtered off and washed with distilled water, ethanol and acetone. Yield: 0.177g, 79%.

Elemental analysis, weight% found (calculated): C, 43.56 (43.69); H, 3.10 (3.22); N, 5.90 (6.11).

MW synthesis: 0.040 g (0.114mmol) of H_3popha, 0.016 g (0.114 mmol) of 2,2'-bipy, 0.033g (0.114mmol) of In(OAc)$_3$ and 2 mL of water were placed in a glass vial, and submitted to MW radiation with a dynamic method at 160ºC with high stirring (30min, 200W, 9bar). Yield: 0.067g, 90%.

Elemental analysis, weight% found (calculated): C, 43.12 (43.69); H, 3.28 (3.22); N, 5.85 (6.11).

IR (KBr, cm^{-1}): 3620, 3559 ν(O-H $_{H2O}$), 3449 ν(C-H $_{bipy}$), 3115 and 3083 ν(C_{sp^2}-H), 1619 ν(η^1-C=O)$_{as}$ and 1602 ν(η^2-C=O)$_{as}$, 1579 ν(C=C), 1562 ν(N-O)$_{as}$, 1530 ν(C=N $_{bipy}$), 1496, 1477, 1458 and 1444 ν(C-O)$_s$, 1382 ν(C-C)$_{as}$, 1349 and 1319 ν(N-O)$_s$, 1264 and 1253 ν(O_{sp^3}-C_{ether}), 1176 and 1164 ν(C-C)$_s$, 921 and 836 δ_{oop}(C-H $_{bipy}$), 779, 771 and 759 δ_{oop}(C-H).

TG (air, 100mL/min): Initial weight loss starts at temperatures below 100ºC, when the water molecules physisorbed inside the framework are lost (total loss ~8%); at ~430ºC the loss of 70% material content is observed. The final residue at ~800ºC corresponds to a 22% of material converted into In_2O_3 (ICSD_640179).

[$In_3(OH)_3(popha)_2$(4,4'-bipy)]·4H_2O (InPF-18)

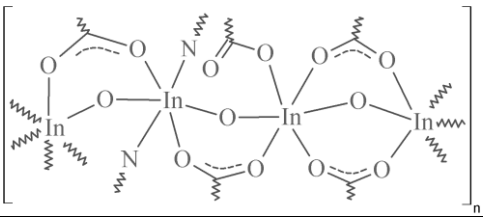

The mixture of H_3popha (0.119 g, 0.343mmol), 4,4'-bipy (0.047 g, 0.343 mmol) and In(OAc)$_3$·H_2O (0.100 g, 0.343 mmol) in 10 mL of distilled water was heated in a Teflon-lined stainless steel autoclave

at 180 ºC for 18 hours. After cooling to room temperature, colorless crystals formed were filtered off and washed with distilled water, ethanol and acetone. Yield: 0.350g, 81%.

Elemental analysis, weight% found (calculated): C, 36.87 (37.86); H, 1.66(1.59); N, 4.22 (4.41).

MW synthesis: 0.040g (0.114mmol) of H_3popha, 0.016 g (0.114 mmol) of 4,4'-bipy, 0.033g (0.114mmol) of $In(OAc)_3$ and 2 mL of water were placed in a glass vial, and submitted to MW radiation with a dynamic method at 180ºC with high stirring (30min, 200W, 11bar). Yield: 0.096g, 96%.

Elemental analysis, weight% found (calculated): C, 36.98 (37.86); H, 2.12(1.59); N, 4.34 (4.41).

IR (KBr, cm^{-1}): 3610 ν(μ-OH), 3447 ν(O-H $_{H2O}$), 3076 ν(C_{sp^2}-H), 1645 ν(η^1-C=O)$_{as}$, 1625 ν(η^2μ-C=O)$_{as}$, 1590 ν(C=C)$_{as}$, 1576 ν(N-O)$_{as}$, 1532 ν(C=N $_{bipy}$), 1499, 1451 and 1417 ν(C-O)$_s$, 1390 ν(C-C)$_{as}$, 1353 and 1307 ν(N-O)$_s$, 1271 and 1255 ν(O_{sp^3}-C $_{ether}$), 1224 and 1142 ν(C-C)s, 905 and 856 δ_{oop}(C-H $_{bipy}$), 777, 759 and 716 δ_{oop}(C-H).

TG (air, 100mL/min): Initial weight loss starts at temperatures below 100ºC, when the water molecules physisorbed inside the framework are lost (total loss ~7%); at ~250ºC loss of 3% of material corresponding to the hydroxyl groups in the framework is observed; finally at ~450ºC the 60% of material loss occurs. The final residue at ~800ºC corresponds to a 30% of material converted into In_2O_3 (ICSD_640179).

$[In_2(popha)_2(4,4'\text{-bipy})_2]\cdot 3H_2O$ (InPF-19)

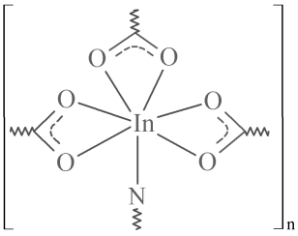

The mixture of H_3popha (0.119 g, 0.343 mmol), 4,4'-bipy (0.047 g, 0.343 mmol) and $In(OAc)_3\cdot H_2O$ (0.100 g, 0.343 mmol) in a mixed solution of EtOH/H_2O (6 mL/5 mL) was heated in a Teflon-lined stainless steel autoclave at 165ºC for 18 hours. After cooling to room temperature, colorless crystals formed were filtered off and washed with distilled water, ethanol and acetone. Yield: 0.308g, 73%.

Elemental analysis, weight% found (calculated): C, 48.22 (48.80); H, 1.91(2.29); N, 6.23(6.83).

MW synthesis: 0.040g (0.114mmol) of H_3popha, 0.016 g (0.114 mmol) of 4,4'-bipy, 0.033g (0.114mmol) of $In(OAc)_3$ and 2 mL of water were placed in a glass vial, and submitted to MW radiation with a dynamic method at 155ºC with high stirring (10min, 200W, 9bar). Yield: 0.119g, 85%.

Elemental analysis, weight% found (calculated): C, 48.08 (48.80); H, 2.79 (2.29); N, 5.20 (6.83).

IR (KBr, cm^{-1}): 3414 ν(O-H $_{H2O}$), 3243 ν(C-H $_{bipy}$), 3121 and 3097 ν(C_{sp^2}-H), 1614 ν(C=O)$_{as}$, 1600 ν(C=C)$_{as}$, 1564 ν(N-O)$_{as}$, 1537 ν(C=N $_{bipy}$), 1466 and 1420 ν(C-O)$_s$, 1407 and 1385 ν(C-C)$_{as}$, 1347 and 1321 ν(N-O)$_s$, 1258 and 1225 ν(O_{sp^3}-C $_{ether}$), 1163 and 1122 ν(C-C)$_s$, 977 and 928 δ_{oop}(C-H $_{bipy}$), 778, 750 and 727 δ_{oop}(C-H).

TG (air, 100mL/min): Initial weight loss starts at ~100ºC when the water molecules physisorbed inside the framework are lost (total loss ~5%); at ~420ºC the loss of 66% material content is observed. The final residue at ~800ºC corresponds to a 29% of material converted into In_2O_3 (ICSD_640179).

[In(OH)(Hpopha)]·0.5(1,7-phen) (InPF-20)

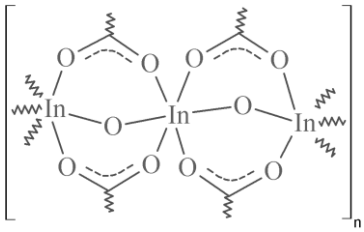

The mixture of H_3popha (0.119 g, 0.343 mmol), 1,7-phen (0.061 g, 0.343 mmol) and $In(OAc)_3·H_2O$ (0.100 g, 0.343 mmol) in 10 mL of distilled water was heated in a Teflon-lined stainless steel autoclave at 175ºC for 48 hours. After cooling to room temperature, colorless crystals formed were filtered off and washed with distilled water, ethanol and acetone. Yield: 0.095g, 58%.

Elemental analysis, weight% found (calculated): C, 43.50 (44.47); H, 2.47(2.13); N, 4.83(4.94).

MW synthesis: 0.040 g (0.114mmol) of H_3popha, 0.017 g (0.057 mmol) of 1,7-phen, 0.033g (0.114mmol) of $In(OAc)_3$ and 2 mL of water were placed in a glass vial, and submitted to MW radiation with a dynamic method at 175ºC with high stirring (90 min, 200 W, 9 bar). Yield: 0.038g, 70%.

Elemental analysis, weight% found (calculated): C, 44.81 (44.47); H, 2.79 (2.13); N, 5.23 (4.94).

IR (KBr, cm^{-1}): 3637 ν(μ-OH), 3608 ν(O-H $_{acid}$), 3389 ν(C-H $_{phen}$), 3232 and 3103 ν(C_{sp^2}-H), 1688 ν(C=O $_{acid}$)$_{as}$, 1619 ν(η^2μ-C=O)$_{as}$, 1598 ν(C=C)$_{as}$, 1567 ν(N-O)as, 1552 ν(C=N $_{phen}$), 1493 ν(C-O $_{acid}$), 1459 and 1417 ν(C-O)$_s$, 1394 and 1304 ν(N-O)$_s$, 1267 and 1257 ν(O_{sp^3}-C $_{ether}$), 1143 and 1111 ν(C-C)$_s$, 1078 and 976 δ_{oop}(C-H $_{phen}$), 777, 759 and 707 δ_{oop}(C-H).

TG (air, 100mL/min): Initial weight loss starts at ~200ºC; the final residue at ~800ºC corresponds to a 31% of material converted into In_2O_3 (ICSD_640179).

[In(popha)(1,10-phen)]·4H_2O (InPF-21α)

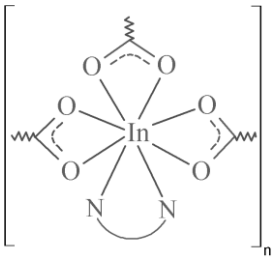

The mixture of H_3popha (0.119 g, 0.343 mmol), 1,10-phen (0.061 g, 0.343 mmol) and $In(OAc)_3·H_2O$ (0.100 g, 0.343 mmol) in 8 mL of distilled water was heated in a Teflon-lined stainless steel autoclave at 160ºC for 72 hours. After cooling to room temperature, yellow crystals formed were filtered off and washed with distilled water, ethanol and acetone. Yield: 0.220g, 91%.

Elemental analysis, weight% found (calculated): C, 45.86 (45.59); H, 2.86 (3.12); N, 5.79 (5.91).

MW synthesis: 0.040g (0.114mmol) of H_3popha, 0.034 g (0.114 mmol) of 1,10-phen, 0.033g (0.114mmol) of $In(OAc)_3$ and 2 mL of water were placed in a MW glass vial, and submitted

to MW radiation with a dynamic method adjusted at 160ºC with high stirring during 60min using 200W and 7bar. Yield: 0.072g, 96%.
Elemental analysis, weight% found (calculated): C, 45.05 (45.59); H, 3.10 (3.12); N, 5.69 (5.91).
IR (KBr, cm^{-1}): 3455 ν(O-H $_{H2O}$), 3248 ν(C-H $_{phen}$), 3081 ν(C_{sp^2}-H), 1621 ν(C=O)$_{as}$, 1590 ν(C=C)$_{as}$, 1563 ν(N-O)$_{as}$, 1527 ν(C=N $_{phen}$), 1432 and 1403 ν(C-O)$_{as}$, 1383 ν(C-C)$_{as}$, 1348 and 1311 ν(N-O)$_{s}$, 1263 and 1252 ν(O_{sp^3}-C $_{ether}$), 1150 and 1107 ν(C-C)$_{s}$, 1074 and 982 δ_{oop}(C-H $_{phen}$), 779, 748 and 724 δ_{oop}(C-H).
TG (air, 100mL/min): Initial weight loss starts at ~100ºC when the water molecules physisorbed inside the framework are lost (total loss ~7%), and at ~450ºC the loss of 68% material content is observed. The final residue at ~800ºC corresponds to a 25% of material converted into In_2O_3 (ICSD_640179).

3.1.4. Synthesis of Multi-metallic MOFs using H_2hfipbb linker

This procedure involved solvothermal synthetic strategy based on the reaction of H_2hfipbb organic linker and different mixtures of group XIII metal salts ($In(OAc)_3$, $Ga(NO_3)_3$, $Al(NO_3)_3$).

3.1.4.1. InGaPF materials

$[In_{0.72}Ga_{0.28}(O_2C_2H_4)_{0.5}$(hfipbb)] (InGaPF-1)
The mixture of H_2hfipbb (0.134g, 0.343mmol), $In(OAc)_3{\cdot}H_2O$ (0.100g, 0.343 mmol) and $Ga(NO_3)_3{\cdot}3H_2O$ (0.088g, 0.343 mmol) in ethyleneglycol/water (6mL/6mL) was heated in a Teflon-lined stainless steel autoclave at 170 ºC for 72 hours. After cooling to room temperature, the white solid was filtered off and washed with distilled water, ethanol and acetone. Yield: 0.180g, 75%.
Elemental analysis, weight% found (calculated): C, 39.92 (41.00); H, 2.00 (1.91).
ICP: 221 ppm In, 52 ppm Ga (2.5In: 1Ga).
TXRF: 365.13umr In, 100.00umr Ga (69% In: 31%Ga).
IR (KBr, cm^{-1}): 3430ν(O-H $_{H2O}$), 3075 ν(C_{sp^2}-H), 2940 ν(C-H $_{C2H4O2}$), 1614 ν(C=O)$_{as}$, 1590 ν(C=C)$_{as}$, 1538 ν(C-O $_{C2H4O2}$)$_{as}$, 1416 and 1254ν(C-O)$_{s}$, 1212 ν(C-C)s, 1174 ν(C-F), 781 and 730 δ_{oop}(C-H).
TG (air, 10ºC/min): the framework is stable up to 460ºC; above this temperature the loss of 65% of material is observed, corresponding to the organic part of the product. The final residue at ~1000ºC corresponds to a 33% of material converted into $InGaO_3$ (ICSD_184330).

$[In_{0.55}Ga_{0.45}(O_2C_2H_4)_{0.5}$(hfipbb)] (InGaPF-2)
The mixture of H_2hfipbb (0.268g, 0.684mmol), $In(OAc)_3{\cdot}H_2O$ (0.050g, 0.171 mmol) and $Ga(NO_3)_3{\cdot}3H_2O$ (0.088g, 0.343 mmol) in ethyleneglycol/water (6mL/6mL), was heated in a Teflon-lined stainless steel autoclave at 170 ºC for 72 hours. After cooling to room

temperature, the white powder was filtered off and washed with distilled water, ethanol and acetone. Yield: 0.086g, 59%.
Elemental analysis, weight% found (calculated): C, 40.38 (42.02); H, 1.76 (1.94).
ICP: 121 ppm In, 60 ppm Ga (1,2In:1Ga).
TXRF: 179.37umr In, 100.00umr Ga (52%In:48%Ga).
IR (KBr, cm^{-1}): 3430ν(O-H_{H2O}), 3068 ν(C_{sp^2}-H), 2932 and 2864 ν(C-H_{C2H4O2}), 1615 ν(C=O)$_{as}$, 1591 ν(C=C)$_{as}$, 1542 ν(C-O $_{C2H4O2}$), 1422 and 1256 ν(C-O)$_s$, 1211 ν(C-C)$_s$, 1175 ν(C-F), 776 and 726 δ_{oop}(C-H).
TG (air, 10ºC/min): the framework is stable up to 490ºC; above this temperature the loss of 74% of material is observed, corresponding to the organic part of the product. The final residue at ~1000ºC matches to a 26% of material converted into a mixture of two $InGaO_3$ polymorphs (ICSD_184328 and ICSD_184330).

[$In_{0.28}Ga_{0.72}(O_2C_2H_4)_{0.5}$(hfipbb)] (InGaPF-3)
The mixture of H_2hfipbb (0.134g, 0.343mmol), $In(OAc)_3{\cdot}H_2O$ (0.050g, 0.171mmol) and $Ga(NO_3)_3{\cdot}3H_2O$ (0.088g, 0.343mmol) in ethyleneglycol/water (6mL/6mL), was heated in a Teflon-lined stainless steel autoclave at 170 ºC for 72 hours. After cooling to room temperature, the white solid was filtered off and washed with distilled water, ethanol and acetone. Yield: 0.105g, 72%.
Elemental analysis, weight% found (calculated): C, 41.29 (42.98); H, 1.86 (1.79).
ICP: 52 ppm In, 221ppm Ga (1In:2.5Ga)
TXRF: 64.5umr In, 100.00umr Ga (28%In:72%Ga).
IR (KBr, cm^{-1}): 3430ν(O-H_{H2O}), 3070 ν(C_{sp^2}-H), 2936 and 2864 ν(C-H_{C2H4O2}), 1615 ν(C=O)$_{as}$, 1587 ν(C=C)$_{as}$, 1542 ν(C-O $_{C2H4O2}$), 1417 and 1256 ν(C-O)$_s$, 1207(C-C)$_s$, 1175 ν(C-F), 779 and 730 δ_{oop}(C-H).
TG (air, 10ºC/min): the framework is stable up to 400ºC; above this temperature the loss of half of ethyleneglycoxide molecule is observed (2% of material); then, at ~520ºC the loss of 64% of material content occurs, which corresponds to the organic part of the material. The final residue at ~1000ºC corresponds to a 24% of material converted into a mixture of two $InGaO_3$ polymorphs (ICSD_184328 and ICSD_184330).

3.2. Heterogeneous catalytic procedures

3.2.1. Material preparation

In order to test the heterogeneous catalytic activity of the previous synthesized materials, it is necessary to work with pure uniform crystalline samples; in case of materials obtained by solvothermal synthesis, those materials need to be grinded in order to obtain crystalline powders; in case of materials prepared using MW synthesis they are used as synthesized without further treatment.

The new material is heated overnight to 130ºC in order to remove physisorbed molecules of solvents which may affect the material performance. Then, the material is weighted and placed inside the container (glass vials, schlenk or flasks) where the catalytic transformations will be carried out. After the catalytic reaction is concluded, the solid catalyst has to be separated from the reaction crude usually made by centrifugation, and then the preservation of the material's purity and crystallinity is confirmed by PXRD.

In cases when the catalytic activity is remarkable, recycling tests were carried out in order to study the recyclability of the material (reflected in the product yield). Also leaching tests were performed for each catalytic reaction in order to demonstrate the heterogeneous nature of the catalytic activity of the material.

3.2.2 Catalytic reaction procedure

Considering the nature of the new materials, among all possible organic transformations, only those, which require a Lewis acid as catalyst, were taken into account. From that extensive list, the standard organic transformations that were chosen in order to evaluate the catalytic activity of the developed materials are: the cyanosilylation reaction, the Strecker 3-component reaction (S3-CR), the Passerini 3-component reaction (P3-CR) and the Ugi 4-components reaction (U4-CR). The procedure for each catalytic reaction is presented below (Figure 3.1).

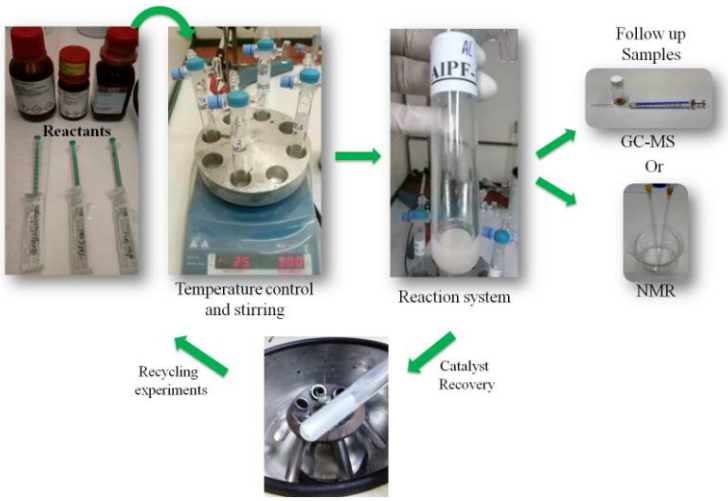

Figure 3.1 Representation of the different steps of the catalytic procedure.

3.2.2.1. Cyanosilylation of carbonyl compounds

Catalytic amounts of the selected material (1mol %, 2,5mol%, 5mol% and 10mol%) is placed in a Schlenk tube under nitrogen atmosphere without solvents, together with the corresponding carbonyl compound (1 equivalent); trimethylsilyl cyanide (1.5 equivalent) is then added dropwise by syringe. The mixture was stirred until disappearance of the carbonyl compound; the kinetics of the reaction and its yield are checked by GC-MS.

3.2.2.2. Danishefsky reaction

Catalytic amounts of the selected material (1mol %) is placed in glass vial together with a mixture of benzoic acid (1 equivalent) and cyclohexyl isocyanide (1 equivalent) is stirred in a sealed tube at room temperature for an appropriate time in solvent-free condition. After the completion of the reaction, the mixture is diluted with DCM and the catalyst is separated by centrifugation and the reaction is followed by ^{1}H, NMR and GC-MS.

3.2.2.3. Strecker 3-Component reaction

Catalytic amounts of the selected material (0.01mol%, 0.1mol%, 1mol %, 2,5mol%, 5mol% and 10mol%) is placed in a glass vial together with a mixture of carbonyl compound (1 mmol), amine (1 mmol), trimethylsilyl cyanide (1.1 mmol), then the mixture is stirred at room temperature for an appropriate time in solvent-free condition. The progress and completion of the reaction was monitored by CG-MS until disappearance of the substrates and the white solid product is analyzed by ^{1}H, ^{13}C NMR, MS and IR without further purification.

3.2.2.4. Passerini 3-Component reaction

Catalytic amounts of the selected material (1mol %) is placed in glass vial together with a mixture of carbonyl compound (1 equivalent), benzoic acid (1 equivalent), cyclohexyl isocyanide (1 equivalent); the mixture is stirred in a sealed tube at room temperature for an appropriate time in solvent-free condition. After the completion of the reaction, the mixture is diluted with DCM and the catalyst is separated by centrifugation and the white solid product is weighted and analyzed by ^{1}H, ^{13}C NMR, MS and IR without further purification.

3.2.2.5. Ugi 4-Component reaction

Catalytic amounts of the selected material (1mol %) is placed in glass vial together with a mixture of carbonyl compound (1 equivalent), benzoic acid (1 equivalent), cyclohexyl isocyanide (1 equivalent) and aniline (1 equivalent); the mixture is stirred in a sealed tube at room temperature for an appropriate time, using different solvents (H_2O and EtOH) as well as in solvent-free condition. After the completion of the reaction, the mixture is diluted with DCM and the catalyst is separated by centrifugation and the product is weighted and analyzed by ^{1}H, ^{13}C NMR, MS and IR without further purification.

3.3. Characterization Techniques

The characterization process conducted for each material covers a range of techniques that aims to determine the chemical composition, crystal structure, morphology, particle size, thermal stability and purity of the material.

3.3.1. General Physical Techniques

3.3.1.1. Elemental Analysis (EA)

In order to verify the purity of the material obtained after filtration and air dried, a sample is send to the Sidi services at the UAM university, where it is weighted using a micro-scale **Mettler-Toledo XP6** and then put in to an **ECO CHNS-932** analyzer, where the carbon, hydrogen and nitrogen content of the sample is obtained. Then calculated and experimental values are compared and if the difference between both values is under 1 unit, the material is considered for the further use.

3.3.1.2. Infrared Spectroscopy (IR)

The characteristic Infrared spectra for each material were recorded from KBr pellets in a 4000-300 cm^{-1} range using a **Nicolet FT-IR 20SXC** spectrometer placed in one of the ICMM laboratories.

3.3.1.3. Thermogravimetric Analysis (TA)

The thermal stability for each MOM was determinate using a **TG/ATD/DSC simultaneous model SDT Q600** from **TA Instruments** apparatus. The measurements were performed in a range of 25-800ºC in open air with a flow of 10mL/min. All measurements were collected by the analysis service laboratories at the ICMM.

3.3.1.4. Inductively Coupled Plasma Mass Spectrometry (ICP-MS)

ICP-MS is an analytical technique used in order to determine the metal content for those multi-metallic MOFs developed in this thesis; the measurements were performed by the Sidi services at the UAM University, using a **Perkin Elmer Optima 2100 DV** apparatus.

3.3.1.5. Total Reflection X-ray Fluorescence (TXRF)

In TXRF an incident beam impinges upon a sample at angles below the critical angle of external total reflection for X-rays resulting in reflection of almost 100% of the excitation beam photons, which exhibits a characteristic energy of the atom that generates an intensity that depends directly on the concentration of the atoms in the sample. Using a **S2 PICOFOX BRUKER** apparatus at the Sidi service from UAM university, the analysis of the elements present in the sample (qualitative analysis) was performed, by integrating each of the elementary profiles of their mass ratios (mass ratios analysis). This technique was used to determine the metal mass ratios for multi-metallic MOFs.

3.3.1.6. Scanning Electron Microscope (SEM)

The SEM technique was employed to compare the particle sizes from samples of different synthesis types and also to confirm the metal ratios of the multimetallic materials. The metal quantification and distribution in the sample can be determinate, as well as the morphology

and an approximately average particle size, by employing a **XL30 Philips** apparatus for the scanning electron microscope at the ICMM laboratories.

3.3.1.7. Gas Chromatography (GC-MS)

This technique was employed in order to follow and analyze the evolution and conversion of several catalytic reactions by using a **KONIK HRGC 40000B** chromatograph equipped with a **KONIK Quadrupole MSQ12** mass detector and an **Agilent J&W GC DB-5**column with 30m x 0.25mm id, 0.25 μm specifications.

The first step consists in taking a sample from the crude of the catalytic reaction. Then, using a common solvent, the second step is to dilute the sample and inject it in the liner in order to be vaporized and then analyzed by separating the components of the mixture, which are carried through a stationary phase (chromatographic column) by a mobile phase using Helium gas. The components are then separated depending on their interaction with the stationary phase which lead to different elutes timing (retention time).

3.3.1.8. Nuclear Magnetic Resonance (NMR)

This technique was employed in order to follow and analyze the evolution and product yield of heterogeneous catalytic reactions in the cases, when the final product was a solid with high molecular weight (>280g/mol). An approximately 10 mg of crude sample dissolved using deuterated solvent is poured into a NMR tube, then placed in a **BRUKER AC-200Hz** at the ICMM laboratories or in a **AVIII-HD Nanobay AMX-300** equipment in the Sidi service of the UAM university. Then, using the ^{1}H and/or ^{13}C NMR spectra all hydrogen and carbon atoms respectively can be identified in the sample according to their interaction with the electromagnetic radiation.

3.3.1.9. Dynamic Light Scattering (DLS)

To obtain the average particle size of the materials obtained by MW technique, a horizontal dynamic light scattering analysis was performed to a material suspension, previously prepared using water as a solvent at 25 ºC (10mg of each material /4mL H_2O). A drop of the suspension was placed in the **Vasco2 Particle Size Analyzer,** which used the thermal motions of particles in suspension (Brownian motion) to determine their size. Here the sample suspension was irradiated by a laser and the light scattered in a certain direction detected with high time resolution. From the fluctuation of the intensity of the scattered light, the mobility of the particles can be calculated and then again via the Stokes-Einstein formula, their size can be calculated.[1]

3.3.2. Structural Determination Techniques

The life indeed would be different without all the technology developed up to now. So, in order to understand how everything evolved as we know it, first we have to look back in 1895

when **Wilhelm Conrad Röntgen**, professor in physics, was the first person to discover the possibility of using electromagnetic radiation to create what we know nowadays as the X-ray, producing an amazing step forward in the history.[2] In the medicine field, this radiation allows the body be visible without having to cut into the flesh. In the material science area, some important studies had been made by the physicist **Charles Glover Barkla.** Starting in 1902 with the studies on the quality of this radiation by measuring their absorption in different materials, he found some fundamental properties of the X-rays, when they were scattered by different elements.[3] But the real breakthrough was made when the interaction of X-rays with ZnS crystals was studied by the physicist **Max von Laue** in 1912, demonstrating the X-rays ondulatory behavior and the periodic nature of crystals, which led to the creation of the Crystallography world, to new techniques development, based on the X-ray diffraction phenomena and transforming the X-ray spectroscopy.[4]

The first X-ray structure solving was made in 1913 using NaCl crystals by father and son: **William Henry Bragg** and **William Lawrence Bragg**. They were able to explain the phenomenon of the X-ray diffraction in crystals through crystallographic planes acting as special mirrors for X-rays, known as the **Bragg's Law**.[5]

$$\mathbf{n\,\lambda = 2d\sin\theta} \qquad (3.1)$$

As a result, the use of the X-ray Diffraction changed the world to an era where this technique is commonly used to determine the arrangement of atoms in solid compounds allowing the measure of bond lengths and structures, based on the diffraction phenomena. The Bragg's Law (Figure 3.2) can be explained in the way that the penetrating X-rays travels down to the internal layer, reflects, and travels back over the same distance before being back at the surface. The distance travelled depends on the separation of the layers (**d**) and the angle (**θ**) at which the X-ray entered the material. For this wave to be in phase with the wave which reflected from the surface it needs to have travelled a whole number of wavelengths while inside the material. When **n** is an integer (1, 2, 3 etc.) the reflected waves from different layers are perfectly in phase with each other and produce a bright point. Otherwise the waves are not in phase, and will either be missing or feint as can be observed in Figure 3.2.

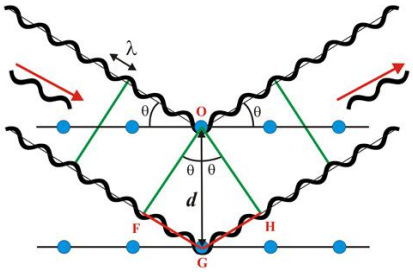

Figure 3.2. Graphic representation of Bragg's Law.

The first three decades of X-ray crystallography were essential; extremely brilliant scientists were required to come up with an inspired supposition in order to finding a trial structure, to obtain a structure by a systematic procedure that many more crystallographers could apply.

This last work began with **Arthur Lindo Patterson,** which in 1934 developed one of the most important functions to determine small-molecule structures.[6] It can be said than the glory days of the Patterson methods ran from 1936 to 1970. After this period, thanks to David **Harker** who found the first inequalities among crystal structure factors and related them with their magnitudes, and imposed a limitation on their values, lead to the Direct methods development, since then, the use of direct methods for solving standard organic structures was irresistible. His scientific breakthroughs contributed directly to current knowledge of the molecular structure of drugs, hormones, proteins and antibiotics, and the molecular basis for chemical and biological processes.[7]

The structural characterization of most of the MOFs obtained in this thesis was performed using the **single crystal X-Ray diffraction** technique, which allows the determination of the precise spatial arrangement of the atoms in the crystalline state of the material, through its simplest repeating pattern. This minimum repeating volume of the lattice known as the **unit cell**, is characterized by three lattice constants ***a, b, c*** (the lengths of the basis vectors) and three angles **(α, β, γ)**, which separate these vectors from one another.

3.3.2.1 The Single-Crystal X-Ray Diffraction Technique

Nowadays, when the X-Ray diffraction is a well-know and accessible technique, the success of a diffraction experiment depends almost entirely on the quality of the studied substance. This means that obtaining of single crystals of the developed material is one of the most important goals for its structure characterization (Figure 3.3). In case of MOFs, the crystal growth takes place during the synthesis process, and for this reason the synthetic conditions must be optimized not only for purification purposes, also in order to obtain the best quality crystals possible. Due to the fact that ideal conditions for the growth of suitable crystals cannot previously be predicted when a new material is being designed, it has to be considered that crystal development depends on the relative rates of nucleation and growth in each particular system, for instance: i) large nucleation rate compared to the rate of growth, favors formations of agglomerates of small crystallites. ii) Increasing the rate of growth, favors the inclusion of defects in crystals.

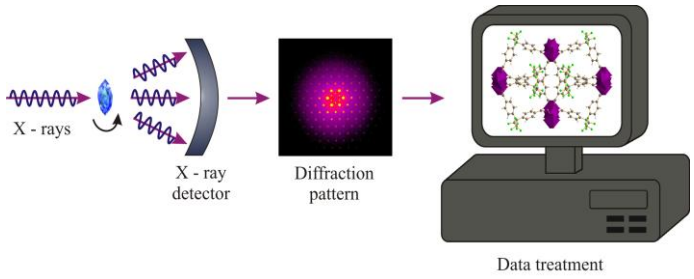

Figure 3.3 Representation of Single Crystal diffraction procedure.

Considering the previously mentioned and in order to determinate the structure of the new crystalline materials, several steps have to be carried out:

3.3.2.1.1. Single crystal selection and handling

When single crystals are obtained, the use of a polarized microscope (figure 3.4) in which different crystalline planes can be appreciated; will help to confirm the uniformity of the entire crystalline sample to avoid any crystalline sub-products that could contaminate the sample. Then the morphology study of the crystal is made in order to carefully select a flawless (free of defects, faces and edges defined), right sized crystal.

Figure 3.4 Polarize microscope and a crystal sample under the objective.

After the best crystal is selected, it has to be mounted and incorporated into the X-ray diffractometer goniometric head. The crystal assembly can be done in several ways (Figure 3.5). One of the most commonly tools used is a glass fiber employing epoxy resin to attach the crystal; in case of low temperatures experiments are necessary, the single crystal is mounted on a loop of polyimide using mineral perfluoropolyether oil.

The chosen crystal is placed in the goniometric head which allows centering the crystal respect to the beam using a video camera installed near to the goniometric head.

Figure 3.5 Different ways to mount crystals, goniometric head and a 4 angle Kappa Diffractometer.

3.3.2.1.2. Unit cell determination and crystal system

To verify that crystal diffracts and to know the ideal time for the beam exposure, a quick test is performed. First, the detector distance is adjust and then, considering the type of elements present in the crystal and its size, the angles and the exposure time is selected and the response is collected by the detector, showing the diffraction results. If the image shows good diffraction spots, the reciprocal space study is performed and the unit cell parameters and their orientation will be obtained. This process is set by the diffractometer program, which made a random search for reflections at different zones in the reciprocal space and high values of 2θ; in this way the orientation matrix is determinate from the reflection positions,

and their indexing is developed.

Based on the unit cell data and the equivalence of the reflexions intensity from the sample, the crystal system is calculated. Then, other parameters has to be define such as the speed of data collection, resolution, detector distance, maximum angle and minimum measurement sweep type and whether to consider the equivalent reflections depending on the type of unit cell and crystal system. Finally, using the reduced cell obtained, the corresponding orientation matrix is determined and the complete data collection is carried out.

3.3.2.1.3. Data treatment

Following the data collection, a software program is used to perform the integration of the intensities for the observed reflexions in the volume of the observed reciprocal space. This step is a feedback process, and the orientation matrix and the geometrical parameters of the diffractometer have to be also refined while the process is been carried out. Subsequently, the semi-empirical absorption and scale correction based on equivalent reflection is performed.
The final output consists in the cell parameters and the intensities in terms of structure factors F(*hkl*), which are used later to solve and refine the structure. For a determinate *hkl* reflection its F(*hkl*) can be described as:

$$F(HKL) = \sum_{j=1}^{atomos} f_j \exp\left[2\pi \bullet i\left(hx_j + ky_j + lz_j\right)\right] \tag{3.2}$$

This formula shows the relation between the structure of a molecule and the structure factors. The fj term refers to the spreading factor of the j atom which depends on the atom type and the diffraction angle of the corresponding reflection. The magnitude of the measured intensities are related to the module structure factors but the phase of these vectors is indeterminate and may be determined routinely, but not directly, the structure of a target molecule from the intensities of the reflections of a sample. Structure factors F(*hkl*) are related to the intensities I(*hkl*) reflection for each follows:

$$I_{hkl} = \left|F\left(hkl\right)\right|^2 \bullet LP \bullet A \tag{3.3}$$

Lp are geometry factors (Lorentz) and polarization, which depend on the particular experimental arrangement. A is a correction factor for absorption and its use depends on the material characteristics. Since the electron density of each atom is related to the structure factors and intensities, the diffraction pattern can be transformed into real space since it is known that this is a reciprocal space image. Knowing the structure factors with module and phase can obtain the actual structure of the molecule.

Once the structure is through the development of a model, this is confirmed by the index of disagreement between the values of factors observed and calculated structure.

3.3.2.1.4. Structure solution

The space group determination was carried out using XPREP software. Then, the first structure model is solved by direct methods, where the initial phase is assigned, followed by a refinement, which gives the electronic density map in which atoms are situated. Posterior cycles of refinement are carried out by full-matrix least-squares analyses, first using isotropic thermal factors in order to locate all the non-hydrogen atoms, followed by a refinement considering the anisotropic thermal parameters of all non-hydrogen atoms. In case of hydrogen atoms, they sometimes can be located in the Fourier map, but in most of the times their positions are calculated geometrically.

Finally, after the solving of the crystal structure and when the positions of all atoms are known, several graphical representations can be made using different software.

3.3.2.2. Single crystal study of p-MOFs materials

For single crystal X-ray diffraction, the equipment for the collection data used in this work was a **Bruker four circle kappa-diffractometer** equipped with a Cu INCOATEC microsource operated at 30W power (45kV, 0.60 mA) to generate Cu Kα radiation (λ= 1.54178 Å), and a Bruker VANTEC 500 (microgap technology) area detector.

Single crystals were obtained for all MPF materials, and each crystal was placed in the goniometric head using a glass fiber and an epoxy resin. The data collection variables for each crystal are showed in Table 3.1.

Table 3.1 Single crystal variables in data collection of *p*-MOF materials.

Material	Crystal size	time/ frame	Measure type	Width
AlPF-1	0.10x0.04x0.04	60	φ /ω	1.0
GaPF-1	0.10x0.04x0.02	45	φ /ω	1.0
InPF-9	0.08x0.06x0.02	30	φ /ω	1.0
InPF-10	0.10x0.06x0.04	30	φ /ω	1.0
InPF-11β	0.04x0.02x0.02	40	φ /ω	1.0
InPF-12	0.40x0.30x0.20	20	φ /ω	1.0
InPF-13	0.10x0.10x0.04	40	φ /ω	1.0
InPF-14	0.25x0.08x0.04	20	φ /ω	1.0
InPF-15	0.08x0.06x0.02	40	φ /ω	1.0
InPF-16	0.20x0.10x0.08	20	φ /ω	1.0
InPF-17	0.10x0.10x0.04	20	φ /ω	1.0
InPF-18	0.08x0.06x0.06	40	φ /ω	1.0
InPF-19	0.20x0.08x0.08	20	φ /ω	1.0
InPF-20	0.10x0.06x0.04	20	φ /ω	1.0
InPF-21α	0.20x0.16x0.06	25-40	φ /ω	1.0
InPF-21β	0.04x0.04x0.01	30	φ /ω	1.0
InPF-22	0.20x0.06x0.02	20	φ /ω	1.0
InPF-23	0.18x0.04x0.04	20	φ /ω	1.0

3.3.2.3. The Powder X-Ray Diffraction Technique

The most commonly used X-ray methodology is powder diffraction, in which fine powder of the material is used. This method relies on the fact that the array of tiny crystals randomly arranged will present all possible lattice planes for reflection of the incident monochromatic x-ray beam.

Over the past three decades powder diffraction has played a central role in structural physics, chemistry and material science. Important advances in structural studies of materials ranging from high temperature superconductors and fullerenes to zeolites and high-pressure research have relied heavily on this technique.

Unfortunately, structure determination from powder diffraction data is much more difficult than form single crystal data. The essential difference between single-crystal and powder diffraction is the loss of information that results from the rotational projection of the three-dimensional grid of reciprocal lattice points on to the one dimension of a powder diffraction pattern, aggravated by the structural imperfections. Still, with improvements in instrumentation and algorithm developments coupled with greater computing power, complex crystal structures can be solved, and actually, have been solved from power diffraction data alone.[8]

Through powder diffraction experiment of the material, there are a multitude of analyses that can be performed; these include the qualitative and quantitative phase analysis of a multiphase mixture, determination of unit-cell dimensions through pattern indexing, the solution of an unknown crystal structure or the refinement of a partially known structure using the Rietveld method. The powder pattern obtained for a particular material serves as a signature and can be used for identification, chemical composition and determination of degree of material crystallinity.

In the present work, powder X-ray diffraction technique was used to confirm the purity of all materials obtained as well as for the confirmation of the crystallinity preservation of the material after its use in catalytic transformation.

In case of the **InGaPF** materials, their full pattern profile refinements (Pawley refinements) were carried out using the Reflex module of Materials Studio v.7.0. Pseudo-Voigt function was used to define the profile, with a 12-coefficient polynomial background function.

3.4. References

1. http://www.cordouan-tech.com/en/products/physical-chemistry-analysis/particles-characterization/particle-size-analyzer-vasco

2. P.B. Riesz, *AJR* **1995**, *165*, 533.

3. R. J. Stephenson, *Am. J. Phys.* **1967**, *35*, 140.

4. M. Eckert , *Ann. Phys*. **2012**, *524*, A83.

5. M. F. Perutz, *Acta Cryst.* **1990**, *A46*, 633.

6. C. H. Schwalbe, *Crystallography Reviews* **2014**, *20*, 295.

7. M. Montoya, *Nature Milestones* **2014**, *7*, 1.

8. W. I. F. David, K. Shankland, L. B. McCusker and Christian Baerlocher, *Structure Determination from powder diffraction data*, IUCr Monographs on Crystallography 13. Oxford Science publications. 2006.

CHAPTER 4

STRUCTURAL AND TOPOLOGICAL CHARACTERIZATION

The conformational variations of the chosen flexible linkers combined with different coordination preferences of metal ions result in the structural diversity of the materials developed in this work. In the following chapter, the structural description of twenty new p-MOFs is presented, showing different linker coordination types and their possible relation with the geometry adopted by the group 13 metals, giving rise to 1D, 2D and 3D polymeric frameworks with versatile topologies.

The fact that the design of MOFs based on flexible carboxylate ligands have been less explored compared to their rigid analogues could be related to the different conformations that the flexible linkers can adopt leading to several symmetries during the self-assembly process, making the production of these types of MOFs even more susceptible to any changes in the reaction parameters including temperature, time, type of solvent used, pH, among others. The challenge of controlling the ideal synthetic conditions for an intended material led us to explore the use of bending V-shaped organic linkers and their influence in the final compound structure.

Multicarboxylic linkers with bend angles are chosen because their ability to induce the assembly of different metal-rings.[1] The chelate nitrogenated ligands are chosen to increase the metal coordination number (CN) generating 1D and 2D architectures. In case of the auxiliary nitrogenated ligand like the 4,4'-bipyridine, is used to provide additional cross-links in the framework to generate an overall 3D architecture. In this work, three different V-shaped multicarboxylated ligands have been chosen as study objects (Figure 4.1): i) The 4,4′-(hexafluoroisopropylidene)-bis(benzoic acid) named H_2hfipbb, ii) the diphenylmethane-4,4-dicarboxylic acid named H_2dpmda and iii) the 5-(4-carboxy-2-nitrophenoxy)isophthalic acid named H_3popha, that together with aluminium, gallium and indium salts as metal sources, give rise to twenty new polymeric frameworks synthesized through the use of hydrothermal synthesis allows high yield, the material purity guarantee and no use of toxic solvents.

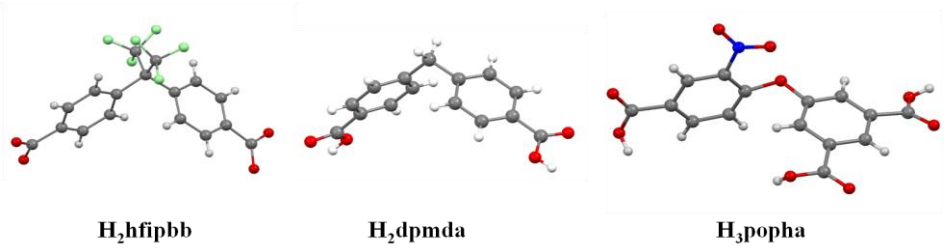

Figure 4.1 V-shaped multicarboxylated ligands chosen as object of study.

Now on, considering the diverse coordination modes that can be adopted by the carboxylate entities to the metal ions and in order to understand such behaviour a simple way of description is needed. Figure 4.2 shows the corresponding nomenclature for the most common cases.

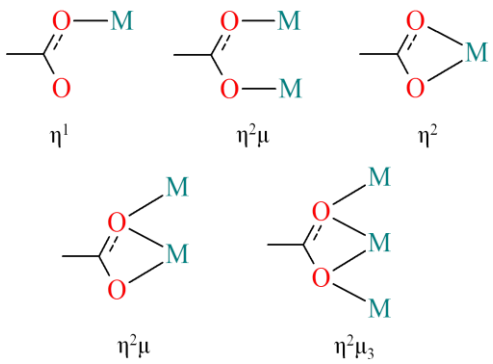

Figure 4.2 Characteristic coordination modes for the carboxylate group.

The following sections present each MOF family obtained with the use of the different organic ligands.

4.1. New Polymeric Frameworks with the H_2hfipbb linker

In order to analyze the V-shaped ligand conformation when a certain coordination mode is adopted, several geometrical parameters have to be considered. In figure 4.3, the principal parameters for the hfipbb^{2-} organic linker are presented.

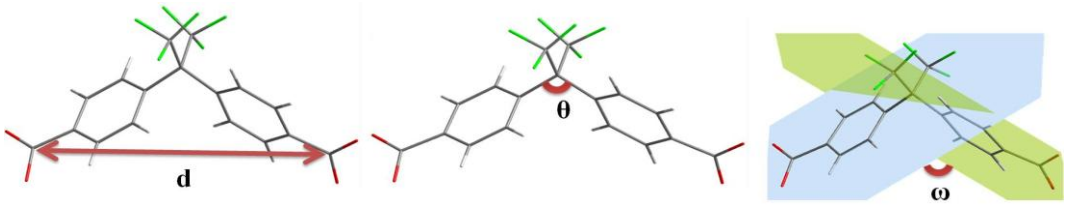

Figure 4.3 Definition of **d** distance, **θ** angle, and **ω** dihedral angle of the hfipbb^{2-} linker.

Theoretically, a tetrahedral configuration is expected for the central sp^3-carbon, (θ =109º) of the H_2hfipbb molecule. However, it is interesting to know the actual geometrical parameters of the organic linker before it is linked to any metal atom, as well as to have an idea of its initial configuration.

The reported H_2hfipbb organic molecule crystallizes in two different monoclinic space groups: *P2$_1$/c* and *P2/c*. In table x, some of the crystallographic parameters of each H_2hfipbb polymorph described in the CSD data base [2] and their calculated geometrical data are given in Table 4.1.

Table 4.1 Crystallographic information and Geometry data for **H_2hfipbb**

Polymorph	**H_2hfipbb TUPNOI** [3]	**H_2hfipbb TUPNOI01**
Formula	$C_{17}H_{10}F_6O_4$	$C_{17}H_{10}F_6O_4$
Crystal System	Monoclinic	Monoclinic
Space Group	$P2_1/c$	P2/c
Unit cell dimensions	a = 7.7523(16) Å b = 13.381(3) Å c = 16.134(3) Å α = 90° β = 102.294(4)° γ = 90°	a = 30.257(3) Å b = 7.5419(6) Å c = 15.2513(13) Å α = 90° β = 104.405(2)° γ = 90°
Volume	1634.26(2) Å^3	3370.86(2) Å^3
Z	4	8
Geometrical parameters		
d	9.519Å	9.152 Å and 9.213 Å
θ	111.55º	110.46º and 110.62º
ω	67.43º	60.23º and 61.21º
LCA	110.17º	103.70º and 104.62º

The geometry observed in the organic H_2hfipbb molecule results slightly different to our ideal presumption of a 109º for the tetrahedral central carbon; instead an average value of 110.9º is assumed and this although small distortion could be due supramolecular interactions between adjacent molecules (synthon between the carboxylic entities O-H···O and weak F···F interactions).

After analyzing these three geometrical parameters, the concept of the LCA (linker coordination angle) takes more meaning, because match up the previous geometrical parameters giving an only value that can be easier to analyze and correlated with the material characteristics (Figure 4.4).

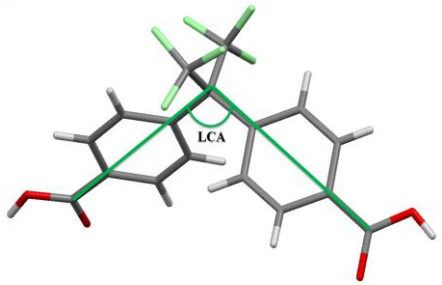

Figure 4.4 Definition of **LCA** in H_2hfipbb organic ligand.

In this section it is presented the structural determination of seven new *p*-metal containing MOFs (**MPF** from now on) bearing the H_2hfipbb as principal organic linker (Scheme 4.1).

The spectroscopic characterization was performed by IR and the thermal stability of the frameworks was determinate by TG analysis. Finally, the crystal structures for all materials were determinate using single crystal X-ray diffraction.

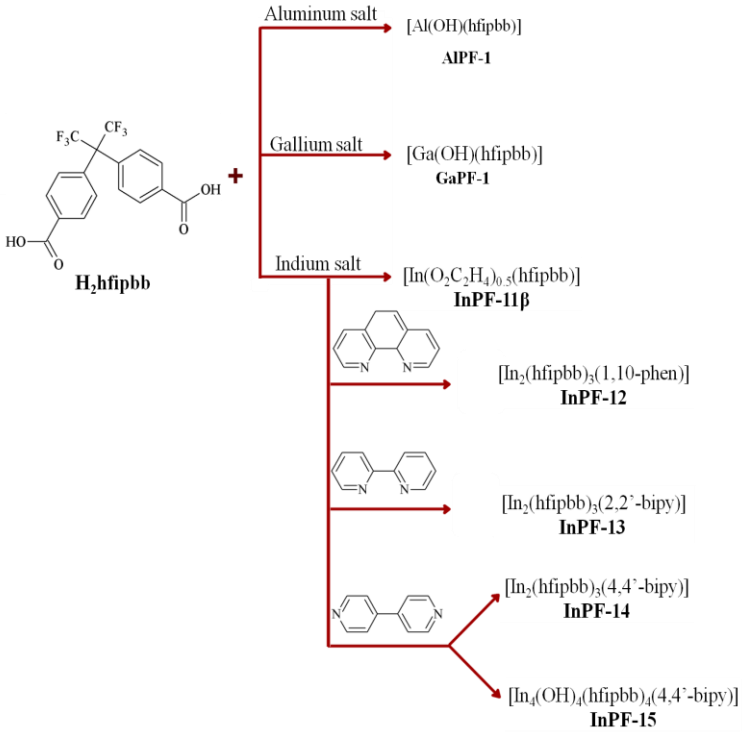

Scheme 4.1 New **MPF** materials with H_2hfipbb linker and additional nitrogenated ligands.

4.1.1. General Characterization

The H_2hfipbb organic ligand in the polymeric frameworks described presents predominantly three different coordination modes to the metal ions when it is fully deprotonated (Figure 4.5). The L_1 type exhibits the monodentate mode exhibit for both carboxylate entities, L_2 represents the chelate coordination mode to the metal ion for both carboxylate entities and finally the L_3 type describes a bridge mode connecting two metal ions for each carboxylate moiety.

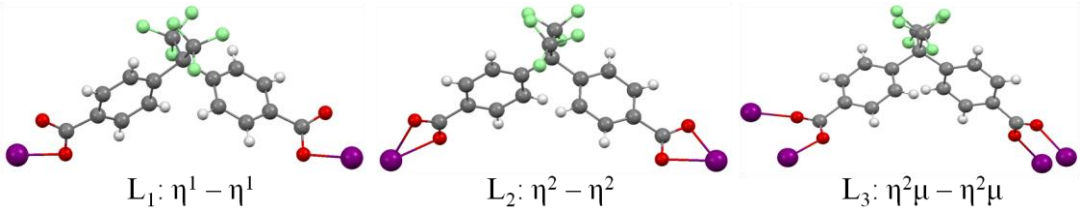

Figure 4.5 The L_1, L_2 and L_3 coordination modes for $hfipbb^{-2}$ organic linker.

For all **MPF** materials, the infrared spectra show absorption in regions between 1720 – 1600 cm^{-1} and 1441 – 1255 cm^{-1}, which corresponds to the bound carboxylate group $\nu_{asym}(CO_2M)$ and ν_{sym} (CO_2M), respectively (Table 4.2). In case of materials with two different coordination modes of the organic linker like **InPF-12**, **InPF-13** and **InPF-15**, two different C=O bands can be appreciated. The absence in all cases of the characteristic bands the range 1713–1702 cm^{-1} attributed to the protonated carboxylate groups indicates the complete deprotonation of H_2hfipbb.

Table 4.2 Characteristic COO^- stretching frequencies of **MPF** materials

Material	C=O ν_{as} cm^{-1}	C-O ν_s cm^{-1}	Linker coordination mode
AlPF-1	1603	1441, 1259	$\eta^2\mu - L_3$
GaPF-1	1640	1424, 1259	$\eta^2\mu - L_3$
InPF-11β	1619	1417, 1255	$\eta^2\mu - L_3$
InPF-12	1720 1600	1421, 1254	$\eta^1 - L_1$ $\eta^2 - L_2$
InPF-13	1717 1604	1424, 1375	$\eta^1 - L_1$ $\eta^2 - L_2$
InPF-14	1614	1416, 1298	$\eta^2 - L_2$
InPF-15	1700 1619	1406, 1269	$\eta^1 - L_1$ $\eta^2\mu - L_3$
H_2hfipbb	1713-1702	929	acid

The stability of each material was studied through thermogravimetric analysis (TGA), showing that materials with $hfipbb^{2-}$ as unique organic part in the framework are stable in a range between 480 and 550ºC. Materials containing additional nitrogenated ligand like the 4,4'-bipy (**InPF-14** and **InPF-15**) are stable up to 470ºC. In case of materials with 1,10-phen and 2,2'-bipy (**InPF-12** and **InPF-13,** respectively) the corresponding frameworks undergo

three-step weight loss: i) the first step corresponds to a weight loss under the 100°C attributed to the loss of the physisorbed solvent molecules inside the frameworks. ii) Then, the structures remain intact between 300-400°C. iii) Finally, impressive loss of weight occurs (440 to 460°C), where all the organic parts are removed from the frameworks. For all seven materials the destruction of the framework (between 800 and 1000°C) ends with the formation of the corresponding M_2O_3 as a main product.

4.1.2. Aluminium, Gallium and Indium isostructural MOFs

Three isostructural materials with formula [M(OR)(hfipbb)], (M= Al, Ga, In; R= H or CH_2) were synthesized by reaction between H_2hfipbb and different aluminium, gallium and indium salts. Their crystal structures were obtained through single crystal XRD.

In the aluminium and gallium compounds, the formula corresponds to [M(OH)(hfipbb)], but for the indium material the formula changes to $[M(O_2C_2H_4)_{0,5}(hfipbb)]$ due to the coordination of the ethyleneglycoxide used in the synthesis medium. The use of ethyleneglycol is necessary in order to obtain the isostructural material, because if water or different solvent mixtures are employed, the **InPF-11α** polymorph with a 2D network is obtained.[4] Analysis of the X-ray powder diffraction of these materials (Figure 4.6) confirmed the isostructural nature of **AlPF-1**, **GaPF-1** and **InPF-11β**; slight differences in the cell parameters found are due to the size of the metal cation (Al < Ga < In) (Table 4.3).

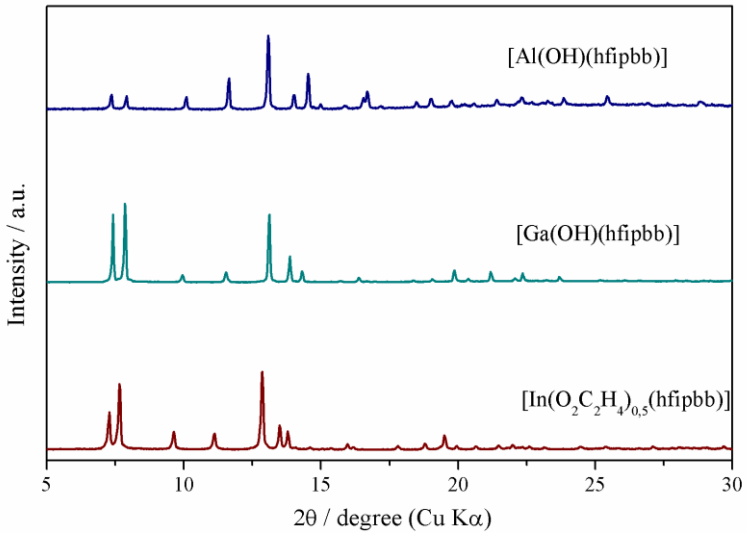

Figure 4.6 Powder diffraction pattern for the **MPF** materials showing their isostructural behavior.

All **MPF** compounds crystallize in the monoclinic system, *C2/c* space group (Table 4.3). The asymmetric unit consists of two half crystallographic independent M^{3+} ions (each cation is placed in a symmetry element: M_1 is placed on a 2 fold axis and M_2 is onto an inversion center), one μ-O and one molecule of completely deprotonated $hfipbb^{2-}$ ligand (Figure 4.7).

Table 4.3 Main crystallographic data for **MPF** materials

Identification Code	**AlPF-1**	**GaPF-1**	**InPF-11β**
Formula	$C_{17}H_9F_6O_5Al$	$C_{17}H_9F_6O_5Ga$	$C_{18}H_{10}F_6O_5In$
Molecular Weight	434.22 g/mol	476.96 g/mol	535.08 g/mol
Temperature	293(2) K	293(2) K	296(2) K
Wavelength	Cu Kα 1.54178Å	Cu Kα 1.54178Å	Cu Kα 1.54178Å
Crystal System	Monoclinic	Monoclinic	Monoclinic
Space Group	*C2/c*	*C2/c*	*C2/c*
Unit cell dimensions	a =24.988(3) b =12.695(2) c =12.395(2) α = 90° β = 108.173(12)º γ = 90°	a =25.097(6) b =12.774(4) c =12.636(3) α = 90° β = 108.232(11)º γ = 90°	a = 25.375(1) Å b = 13.1271(6) Å c = 13.1893(6) Å α = 90° β = 107.305(3)° γ = 90°
Volume	3736.0(9)Å^3	3847.6(18) Å^3	4194.5(4) Å^3
Z	8	8	8
Dx	1.544 g.cm^{-3}	1.643 g.cm^{-3}	1.695 g.cm^{-3}
Absorption coefficient (μ)	1.769 mm^{-1}	2.751 mm^{-1}	9.752 mm^{-1}
F(000)	1744	1880	2088
Theta range for data collection	[5.49 – 63.79]º	[5.49 – 63.79]º	[5.49 – 63.79]º
Index ranges	-38<*h*<23, -14<*k*<15, -25<*l*<25	-38<*h*<23, -14<*k*<15, -25<*l*<25	-38<*h*<23, -14<*k*<15, -25<*l*<25
Reflections collected	13466	13466	13466
Completeness	96.4%	96.4%	96.4%
Absorption correction	Multi – scan	Multi – scan	Multi – scan
Max. and min. Transmission	0.194, 0.376	0.194, 0.376	0.194, 0.376
Refinement method	Fsqd	Fsqd	Fsqd
Data / restrains / parameters	5766/0/549	5766/0/549	5766/0/549
Goodness of fit on F^2	0.874	0.908	1.025
Final R indices [I>2σ(I)]	R1=0.1056 wR2=0.2579	R1=0.0661 wR2=0.1583	R1=0.0761 wR2=0.1879
R indices (all data)	R1=0.2836 wR2=0.3543	R1=0.1474 wR2=0.1913	R1=0.1263 wR2=0.2552

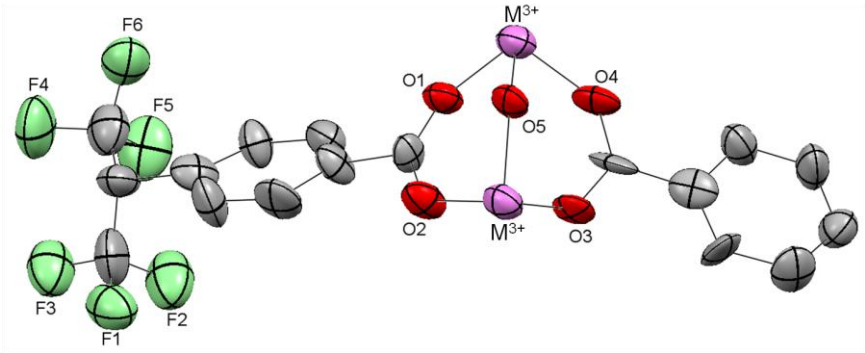

Figure 4.7 ORTEP representation of the asymmetric unit for **MPF.** Ellipsoids are displayed at the 50% probability level. Symmetry codes: i) x, y, z; ii) -x, y, ½-z; iii)1/2+x, ½+y, ½-z; iv)1/2-x, ½+y, ½-z ; v) -x, -y, -z; vi) x, -y, ½+z; vii) ½-x, ½-y, -z; viii) ½+x, ½-y, ½+z.

The M^{3+} ions are six coordinated with a MO_6 environment showing an octahedral (OC-6) geometry for each cation. Two of the M-O bonds come from the hydroxyl group acting as bridge between both cations; these bonds are slightly shorter than the four M-O bonds from the two carboxylic groups of the $hfipbb^{2-}$ organic linker which also acts as bridge between metal cations (Table 4.4).

Table 4.4 Relevant distances and angles for **MPF** compounds.

Distances (Å)	**AlPF-1**	**GaPF-1**	**InPF-11β**
M1-O5 (μ-OH)	1.848(9)	1.909(5)	2.135(11)
M2-O5 (μ-OH)	1.844(9)	1.902(5)	2.130(12)
M1 – O1	1.914(10)	1.944(5)	2.201(11)
M2 – O2	1.914(8)	1.982(7)	2.148(11)
M1 – O3	1.925(10)	1.999(5)	2.108(12)
M2 – O4	1.897(9)	1.982(5)	2.174(12)
M1··· M2	3.320(3)	3.3844(9)	3.5953(8)
d L_3	9.37(2)	9.27(1)	9.24(2)
Angles (º)			
M1-O5-M2	128.1(4)	125.3(3)	114.8(4)
θ L_3	108 (1)	109.3(8)	109 (2)
ω L_3	72.4(4)	72.7(3)	69.9(6)
LCA	105.7(4)	105.3(2)	104.5

Chains of sharing vertex -[MO_6]- octahedra run along the *c* direction via μ-OH and bridging carboxylate groups. The fully deprotonated linker $hfipbb^{2-}$ connects these inorganic chains giving rise to a 3D arrangement with a 4-connected uninodal network showing a **dia** topology (Figure 4.8).[5]

The M-O distances are longer when the cation size is bigger: the M-O bonds decrease their strength depending on the cation size, this phenomenon is reflected in the distance between cations M···M in the inorganic chains formed (Table 4.4).

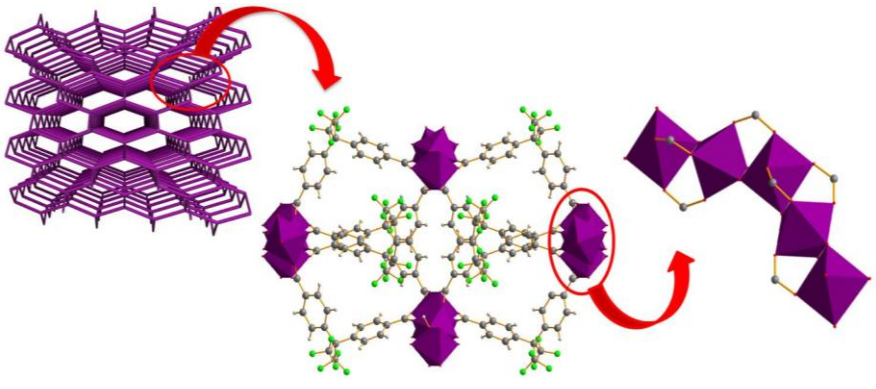

Figure 4.8 The **AlPF-1**, **GaPF-1** and **InPF-11β** 3D framework. Left: **dia** topological representation. Right: inorganic chain SBUs and complete structure.

In terms of geometry (Table 4.4), the organic linker plays a key role in the preservation of the same spatial arrangement; distance values between C1···C17 (carbon – carbon distance between the two carboxyl groups of the linker) are similar for all three compounds showing

that this geometry is the most preferred for the organic linker, so that it is the hfipbb^{2-} linker that directs the spatial arrangement in the unit cell. The values of M-O-M angles do change with the cation size, being more obtuse at small cation size.

4.1.3. Indium MOFs with H_2hfipbb linker and nitrogenated ligands

The important role that auxiliary chelating ligands, such as 1,10-phenanthroline (phen) or 2,2´-bipyridine (bipy), play as coordination blocking molecules, allows the MOF dimensionality control, and in many cases the specific material catalytic activity. In this part we have also included the no-chelating 4,4´-bipyridine linker for comparative purposes. The result is a series of four new indium MOFs $[In_2(hfipbb)_3(1,10\text{-phen})_2]\cdot 2H_2O$ (**InPF-12**), $[In_2(hfipbb)_3(2,2'\text{-bipy})_2]\cdot 2H_2O$ (**InPF-13**), and with the no chelating $[In_2(hfipbb)_3(4,4'\text{-bipy})]$ (**InPF-14**) and $[In_4(OH)_4(hfipbb)_4(4,4'\text{-bipy})]$ (**InPF-15**) (Scheme 4.1).

*4.1.3.1. The **InPF-12** material, $[In_2(hfipbb)_3(1,10\text{-phen})_2]\cdot 2H_2O$*

The **InPF-12** material crystallizes in the monoclinic *C2/c* space group (Table 4.5).

Table 4.5 Main crystallographic data for **InPF-12**

Identification Code	**InPF-12**
Formula	$C_{75}H_{44}F_{18}N_4O_{14}In_2$
Molecular Weight	1796.78 g/mol
Temperature	296(2) K
Wavelength	Cu Kα 1.54178Å
Crystal System	Monoclinic
Space Group	*C2/c*
Unit cell dimensions	a = 33.0893(4) Å b = 12.9108(2) Å c = 22.2089(3) Å α = 90° β = 129.956(1)° γ = 90°
Volume	7272.8(2) Å^3
Z	4
Dx	1.641 g.cm^{-3}
Absorption coefficient (μ)	6.088 mm^{-1}
F(000)	3576
Theta range for data collection	[5.49 – 63.79]º
Index ranges	-38<*h*<23, -14<*k*<15, -25<*l*<25
Reflections collected	13466
Completeness	96.4%
Absorption correction	Multi – scan
Max. and min. Transmission	0.194, 0.376
Refinement method	Fsqd
Data / restrains / parameters	5766/0/549
Goodness of fit on F^2	0.995
Final R indices [I>2σ(I)]	R1=0.0336 wR2=0.0888
R indices (all data)	R1=0.0422 wR2=0.0953

The asymmetric unit consists of one In^{3+} ion, one phenantroline molecule, one and a half molecules of the $hfipbb^{2-}$ linker, and one hydration water molecule (Figure 4.9). A positional disorder is observed for one of the three crystallographically independent CF_3 groups (C_{26}, F_7, F_8 and F_9).

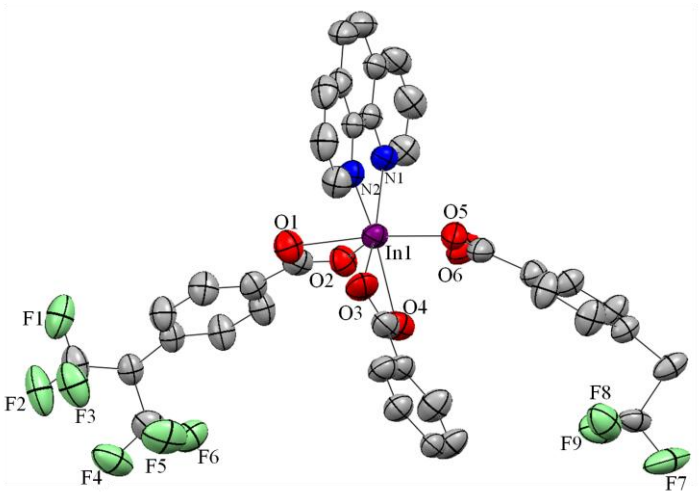

Figure 4.9 ORTEP representation of the asymmetric unit for **InPF-12**. Ellipsoids are displayed at the 50% probability level. Hydrogen atoms and water molecules were omitted for clarity. Symmetry codes: i) x, y, z; ii) -x, y, ½-z; iii)1/2+x, ½+y, ½-z; iv)1/2-x, ½+y, ½-z ; v) -x, -y, -z; vi) x, -y, ½+z; vii) ½-x, ½-y, -z; viii) ½+x, ½-y, ½+z.

The In^{3+} cation is heptacoordinated in a -[InO_5N_2]- monocapped octahedron OCF-7, where the two In-N bonds come from the chelating ancillary ligand and the five In-O bonds from the fully deprotonated $hfipbb^{2-}$ linker. The linker bonds the indium cations through L_1 and L_2 coordination modes, giving rise to helical chains that run along the [101] direction with a ladder-shaped topology (Figure 4.10).

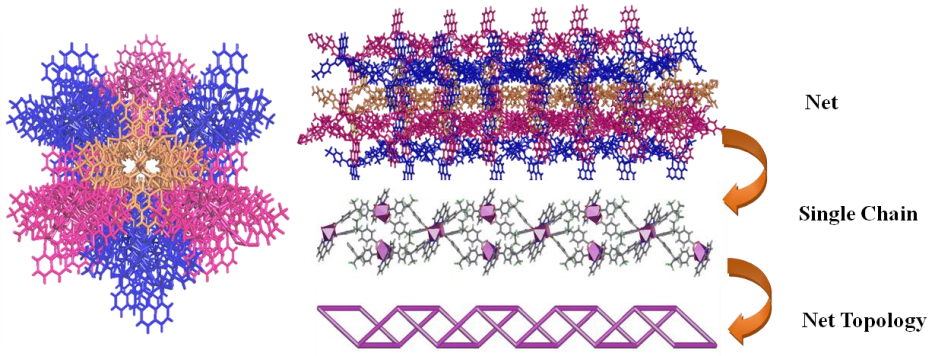

Figure 4.10 View of the chain 1D framework of **InPF-12** and its topology representation.

For **InPF-12**, the two different coordination modes of $hfipbb^{2-}$ are described based on the geometrical parameters illustrated previously in Figure 4.3. The distance between the carboxylate groups in L_1 is larger than in L_2; the dihedral angle (ω) in L_1 is higher than the value for L_2, and the θ angle, which according to the sp^3 coordination of the central carbon

atom should be near to 109º, seems to suffer an increment in both cases. So, in order to describe numerically the distortion, the LCA was calculated for both cases, reflecting a broad distortion in the geometry for L_1 with a value of 119º against the 113º value found for L_2 (Table 4.6).

Table 4.6 Relevant distances and angles for **InPF-12** material

Parameter	value	Parameter	value
In1 – O1	2.247(4)Å	In1··· $In1^{ii}$	14.199Å
In1 – O2	2.319(2)Å	d L_1	9.989(6)Å
In1 – O3	2.253(3)Å	d L_2	9.774(5)Å
In1 – O4	2.407(2)Å	θ L_1	112.06º
In1 – O5	2.137(4)Å	θ L_2	111.83º
In1 ··· O6	2.679 Å	ω L_1	79.8(5)º
In1 – N1	2.280(3)Å	ω L_2	77.8(1)º
In1 – N2	2.310(3)Å	LCA (L_1)	119.21º
In1··· $In1^{i}$	14.387Å	LCA (L_2)	113.85º

After topological simplification of the chains a network of three-connected nodes is described (Figure 4.10). This uninodal net exhibits a SP1 topology with point symbol (4^2.6). Taking into account the inter-chain interactions, the net connectivity increases and a 4,6T40 three dimensional supramolecular net is described (Figure 4.11). This connectivity is supported mainly by two weak interactions. The first interaction corresponds to a π···π stacking between the 1,10-phenantroline rings from parallel chains with distance between centroids ≈ 3.68Å in both compounds and an offset between rings of 21.04º; the second one is a F···F interaction C26-F9···F1-C9 (d: 2.725 Å, φ: 26.32º, θ_1: 153.41º and θ_2: 117.96º) between the -CF_3 groups.

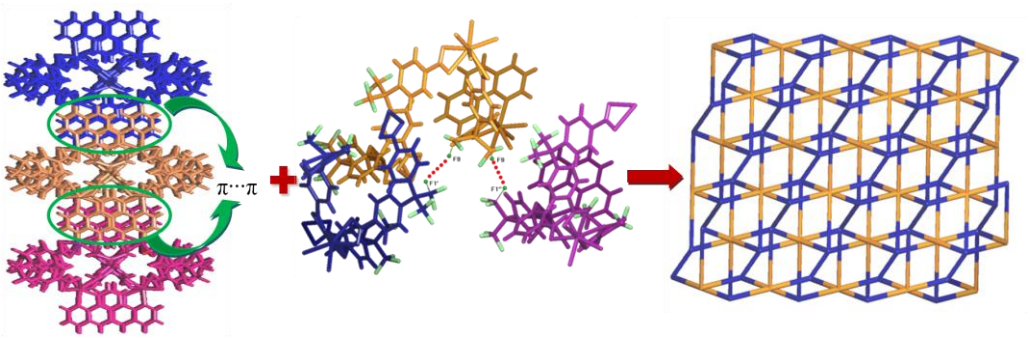

Figure 4.11 View of the 2D and 3D supramolecular frameworks of **InPF-12.**

Hydration water molecules are located in the supramolecular channels forming hydrogen bonds with carboxylate oxygen atoms and C-H groups from phenantroline ligand: i) O7-$H7b_{(water)}$···$O8_{(water)}$ distance H···O is 1.781 Å and distance O-H···O is 2.422 Å; ii) C36-$H36_{(phen)}$···$O8_{(water)}$, distance H···O is 2.616 Å, and distance C-H···O is 3.270 Å. These interactions do not participate in the connectivity of the supramolecular structure.

*4.1.3.2. The **InPF-13** material, $[In_2(hfipbb)_3(2,2'\text{-bipy})_2]\cdot 2H_2O$*

The **InPF-13** material crystallizes in the monoclinic *C2/c* space group (Table 4.7). The asymmetric unit consists of one In^{3+} ion, one 2,2'-bipy molecule, one and a half molecules of the $hfipbb^{2-}$ linker, and one hydration water molecule (Figure 4.12).

Table 4.7 Main crystallographic data for **InPF-13**

Identification Code	**InPF-13**
Formula	$C_{71}H_{44}F_{18}N_4O_{14}In_2$
Molecular Weight	1748.74 g/mol
Temperature	293(2) K
Wavelength	Cu Kα 1.54178Å
Crystal System	Monoclinic
Space Group	*C2/c*
Unit cell dimensions	a = 32.6149(5) Å b = 12.4824(2) Å c = 21.4240(3) Å α = 90° β = 129.055(1)° γ = 90°
Volume	6772.97(2) $Å^3$
Z	4
Dx	1.715 $g.cm^{-.3}$
Absorption coefficient (μ)	6.516 mm^{-1}
F(000)	3480
Theta range for data collection	[3.49 – 64.36]º
Index ranges	-24<*h*<38, -14<*k*<14, -24<*l*<18
Reflections collected	8316
Completeness	96.5%
Absorption correction	Multi – scan
Max. and min. Transmission	0.7806, 0.5619
Refinement method	Fsqd
Data / restrains / parameters	5474/0/482
Goodness of fit on F^2	1.056
Final R indices [I>2σ(I)]	R1=0.0382 wR2=0.0913
R indices (all data)	R1=0.0494 wR2=0.0969

As well as for **InPF-12**, here the In^{3+} environment is an InO_5N_2 monocapped octahedron, in which two In-N bonds come from the chelating ancillary ligand and the five In-O bonds from the fully deprotonated $hfipbb^{2-}$ ligand. The linker acts in the same way that in **InPF-12** (one L_1 and one L_2), which also gives rise to ladder-shaped chains that run along the [101] direction (Figure 4.10).

In L_1, the distance between carboxylate groups is larger than the distance found for L_2 (Table 4.8); the same tendency was observed for the angle values (ω and θ): the values of L_1 are higher than those found in case of the L_2 coordination type. The wide distortion of the L_1 monodentate coordination mode is supported by a higher LCA value in front of the one calculated for the L_2 chelate form.

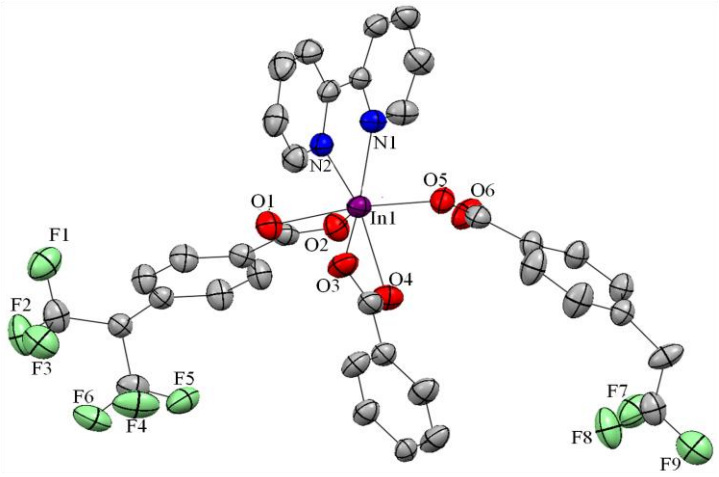

Figure 4.12 ORTEP representation of the asymmetric unit for **InPF-13.** Ellipsoids are displayed at the 50% probability level. Hydrogen atoms and water molecules were omitted for clarity. Symmetry codes: i) x, y, z; ii) -x, y, ½-z; iii)1/2+x, ½+y, ½-z; iv)1/2-x, ½+y, ½-z ; v) -x, -y, -z; vi) x, -y, ½+z; vii) ½-x, ½-y, -z; viii) ½+x, ½-y, ½+z.

After topological simplification of the chains, a network of three-connected nodes is described. This uninodal net exhibits a SP1 topology with point symbol $\{4^2.6\}$. Considering the inter-chain interactions the net connectivity increases and a 4,6T40 three-dimensional supramolecular net is found.

Table 4.8 Relevant distances and angles for **InPF-13** material

Parameter	Value	Parameter	Value
In1 – O1	2.237(5)Å	In1··· In1B	14.330 Å
In1 – O2	2.310(3)Å	d L_1	9.989(6)Å
In1 – O3	2.296(3)Å	d L_2	9.774(5)Å
In1 – O4	2.321(3)Å	θ L_1	113.91º
In1 – O5	2.150(5)Å	θ L_2	112.51º
In1 ··· O6	2.773 Å	ω L_1	79.8(5)º
In1 – N1	2.278(4)Å	ω L_2	77.8(1)º
In1 – N2	2.283(4)Å	LCA (L_1)	121.73º
In1··· In1A	14.354 Å	LCA (L_2)	115.18º

In **InPF-13** several weak interactions contribute to the change of a 1D covalent structure to the 3D supramolecular one; layers are formed through π···π stacking contacts, but interlayer joints are made via C-H···F interactions.

The π···π stacking between the 2,2'-bypiridine rings from parallel chains presents a distance between centroids ≈ 3.68Å and an offset between rings of 21.61º. Two C-H···F interactions are present in the framework (Figure 4.13): i) C20-H20···F4 with the values $d_{F4\cdots H20'}$= 2.744Å; $d_{C20'-H20'\cdots F4}$= 3.574Å; θ_1: 95.32º; θ_2: 148.94º and φ: 72.71º, ii) C22-H22···F6 with the values $d_{F6\cdots H22'}$ =2.706Å; $d_{C22'-H22'\cdots F6}$ = 3.378Å; θ1: 112.78º; θ2: 129.79º and φ: -76.11º.

Hydration water molecules are located into the supramolecular channels forming hydrogen bonds to carboxylate oxygen atoms and C-H groups from bipyridine ligand: i) O7-

$H7a_{(water)}\cdots O4_{(Linker)}$ distance is H···O 2.384 Å and distance O-H···O is 2.966 Å; ii) $O7\text{-}H7b_{(water)}\cdots O6_{(Linker)}$ distance H···O is 2.575 Å and distance O-H···O is 3.142 Å iii) $C34\text{-}H34_{(phen)}\cdots O7_{(water)}$, distance H···O is 2.421 Å and distance C-H···O is 3.266 Å. These interactions do not participate in the connectivity of the supramolecular structure.

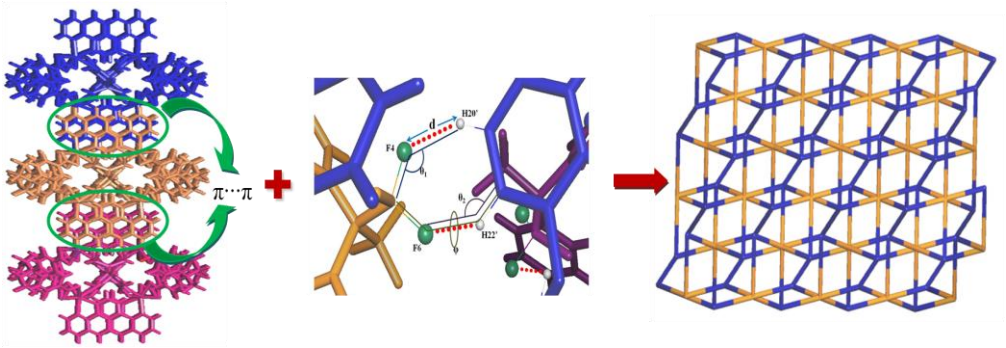

Figure 4.13 View of the 2D and 3D supramolecular frameworks of **InPF-13.**

Two different compounds (**InPF-14** and **InPF-15**) were obtained using the H_2hfipbb and 4,4'-bipyridine linkers, and indium as metal source. After adjusting the reaction conditions both compounds were obtained as pure phases, finding that for a particular stoichiometry and temperature, the main factor to manage the synthesis conditions in order to obtain either **InPF-14** or **InPF-15** is the reaction time (Figure 4.14).

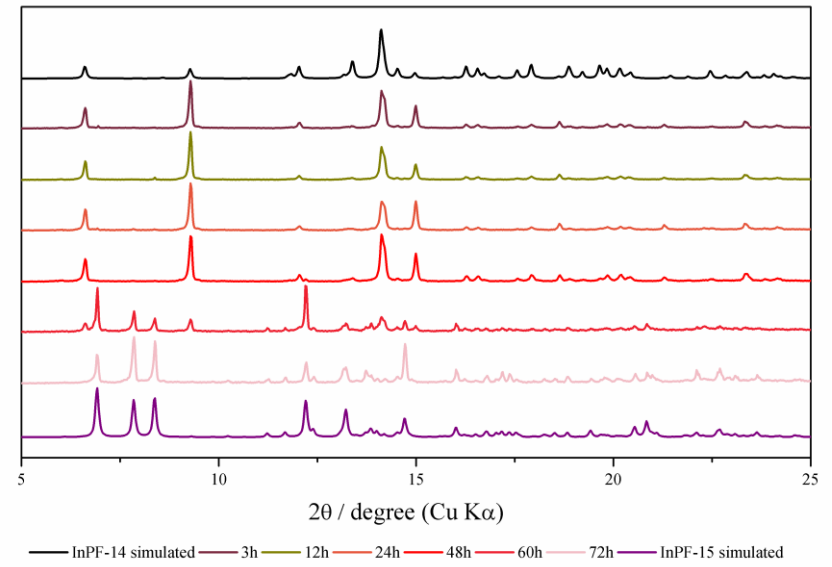

Figure 4.14 PXRD screening of the synthesis time at 200ºC and 1:1:1 stoichiometry.

The fact that two different compounds were obtained using the same starting reagents, gave the opportunity to correlate the linker coordination mode present in each structure with the metal center coordination index. The **InPF-14** material presents exclusively a L_2 coordination of the $hfipbb^{2-}$ linker and the observed metal coordination environment is a monocapped octahedra. However, in case of **InPF-15** material there are two different coordination modes (L_1 and L_3) for the $hfipbb^{2-}$ linker and two different environments for octahedra indium PBUs.

*4.1.3.3. The **InPF-14** material, [$In_2(hfipbb)_3(4,4'\text{-bipy})$]*

The **InPF-14** material crystallizes in the monoclinic *C2/c* space group (Table 4.9). The asymmetric unit consists in one In^{3+} ion, half of the 4,4'-bipyridine molecule and one and a half molecules of fully deprotonated hfipbb^{2-} organic linker. A positional disorder was found in the 4,4'-bipy phenyl rings; that was treated with PART parameters allowing the two simultaneous positions (only one position is shown in the ORTEP representation in Figure 4.15).

Table 4.9 Main crystallographic data for **InPF-14**

Identification Code	**InPF-14**
Formula	$C_{61}H_{32}F_{18}N_2O_{12}In_2$
Molecular Weight	1556.53 g/mol
Temperature	293(2) K
Wavelength	Cu Kα 1.54178Å
Crystal System	Monoclinic
Space Group	*C2/c*
Unit cell dimensions	a = 38.2784(11) Å b = 7.7778(2) Å c = 26.8178(8) Å α = 90° β = 129.831(1)° γ = 90°
Volume	6131.4(3) Å^3
Z	4
Dx	1.686 g.cm$^{-.3}$
Absorption coefficient (μ)	7.076 mm^{-1}
F(000)	3072
Theta range for data collection	[6.02 – 64.01]º
Index ranges	-43<*h*<44, -3<*k*<8, -29<*l*<30
Reflections collected	18184
Completeness	97.0%
Absorption correction	Multi – scan
Max. and min. Transmission	0.7650, 0.2707
Refinement method	Fsqd
Data / restrains / parameters	4937/0/454
Goodness of fit on F^2	1.040
Final R indices [I>2σ(I)]	R1=0.0484 wR2=0.1165
R indices (all data)	R1=0.0707 wR2=0.1308

The In^{3+} ion is hepta-coordinated to six oxygen atoms coming from three chelate carboxylate groups and one 4,4'-bipy nitrogen atom, in a monocapped octahedron [$InNO_6$], with an average In-O distance of ~2.235 Å and In-N distance of 2.282(6) Å. The hfipbb^{-2} linkers acting in a L_2 mode connects the indium PBUs along *b* and *c*, which together with the 4,4'-bipy extension of the net along *a* gives rise to a 3D structure (Figure 4.16).

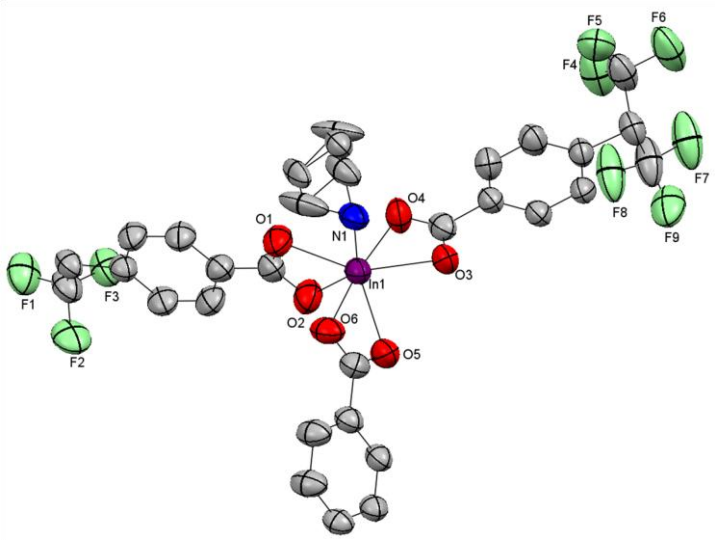

Figure 4.15 ORTEP representation of the asymmetric unit for **InPF-14**. Ellipsoids are displayed at the 50% probability level. Hydrogen atoms and water molecules were omitted for clarity. Symmetry codes: i) x, y, z; ii) -x, y, ½-z; iii)1/2+x, ½+y, ½-z; iv)1/2-x, ½+y, ½-z ; v) -x, -y, -z; vi) x, -y, ½+z; vii) ½-x, ½-y, -z; viii) ½+x, ½-y, ½+z.

It is interesting that there are two different L_2 coordinated modes of the hfipbb^{-2} linker in **InPF-14** (Table 4.10): one with a LCA value of 104.29º with linker connected the metal PBUs in a distance of 13.315Å and another with a 113.03º LCA value, where the indium PBUs are connected to the linker at longer distance (14.021Å). The distance between the indium PBUs connected through the 4,4'-bipy linker is 8.423Å shorter than expected, explaining probably the need of expansion of the hfipbb^{2-} moiety to compliment the connectivity along *a*.

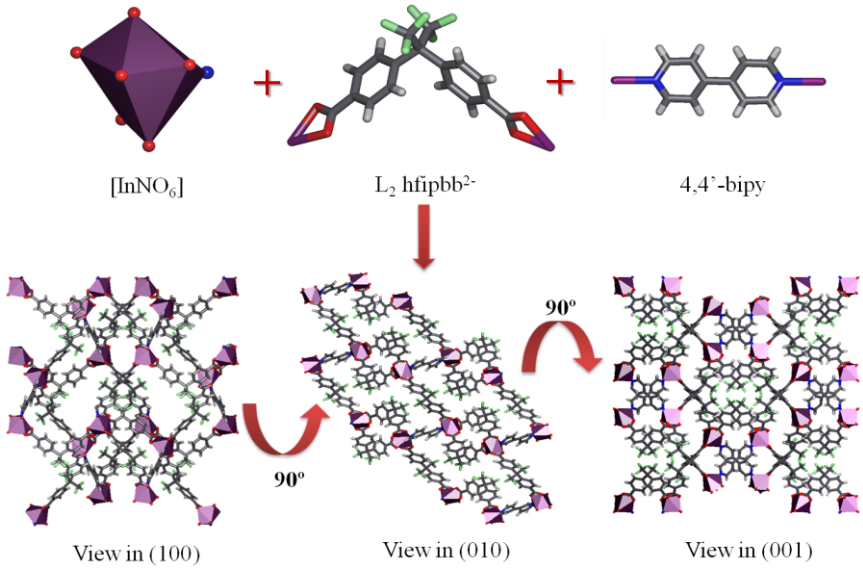

Figure 4.16 The 3D framework of **InPF-14.**

Table 4.10 Relevant distances and angles for **InPF-14** material

Parameter	Value	Parameter	Value
In1 – O1	2.225(4)Å	In1···In1^{iii}	8.423 Å
In1 – O2	2.259(5)Å	d L_2	9.188 Å
In1 – O3	2.269(3)Å	d $L_{2'}$	9.700 Å
In1 – O4	2.188(6)Å	θ L_2	110.36º
In1 – O5	2.261(4)Å	θ $L_{2'}$	112.43º
In1 – O6	2.208(6)Å	ω L_2	64.32º
In1 – N1	2.282(6)Å	ω $L_{2'}$	59.88º
In1···In1^{i}	13.315 Å	LCA (L_2)	104.29º
In1···In1^{ii}	14.021 Å	LCA ($L_{2'}$)	113.03º

The 3D framework of **InPF-14** consists of three interpenetrated **dia** networks (interpenetration class Ia). The main simplification points, as well as the final simplified net, are shown in Figure 4.17.

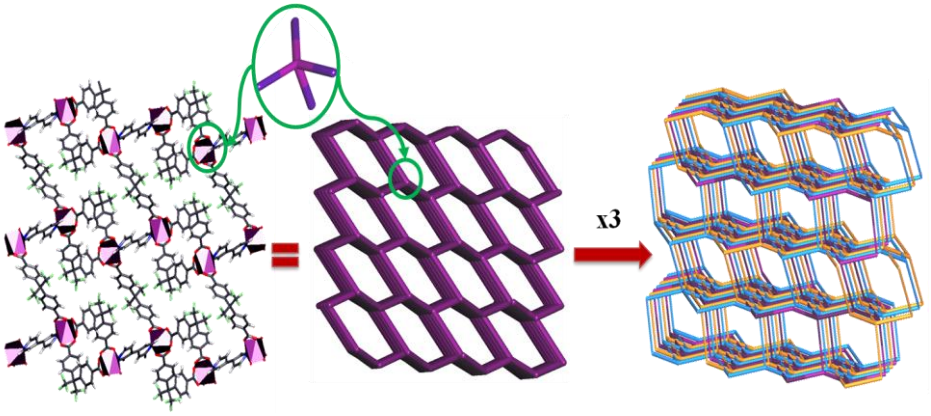

Figure 4.17 Perspective view of compound **InPF-14** along (010) and its corresponding **dia** topological representation with a class Ia interpenetration.

The -CF_3 groups show a tendency to direct the crystallization by intramolecular F2···F8 interactions between the two hfipbb^{2-} linkers with different coordination mode showing a distance of 2.914Å, which makes three linkers to form partial hydrophobic regions in the material.

*4.1.3.4. The **InPF-15** material, [$In_4(OH)_4$(hfipbb)$_4$(4,4'-bipy)]*

The **InPF-15** material crystallizes in the monoclinic system, *P2/n* space group (Table 4.11). The asymmetric unit consists of four crystallographically different In^{3+} ions, one 4,4'-bipyridine molecule, four fully deprotonated hfipbb^{2-} linkers and four hydroxyl groups (Figure 4.18).

Table 4.11 Main crystallographic data for **InPF-15**

Identification Code	**InPF-15**
Formula	$C_{78}H_{44}F_{24}N_2O_{20.35}In_4$
Molecular Weight	2252.43 g/mol
Temperature	296(2) K
Wavelength	Cu Kα 1.54178Å
Crystal System	Monoclinic
Space Group	*P2/n*
Unit cell dimensions	a = 24.165(2) Å b = 13.4565(12) Å c = 27.388(3) Å α = 90° β = 111.227(6)° γ = 90°
Volume	8301.6(13) $Å^3$
Z	4
Dx	1.802 $g.cm^{-.3}$
Absorption coefficient (μ)	9.905 mm^{-1}
F(000)	4408
Theta range for data collection	[2.09 – 63.35]º
Index ranges	-27<*h*<27, -12<*k*<15, -31<*l*<30
Reflections collected	104810
Completeness	96.7%
Absorption correction	Multi – scan
Max. and min. Transmission	0.8265, 0.5046
Refinement method	Fsqd
Data / restrains / parameters	13117/1/1226
Goodness of fit on F^2	1.014
Final R indices [I>2σ(I)]	R1=0.0532 wR2=0.1014
R indices (all data)	R1=0.0927 wR2=0.1210

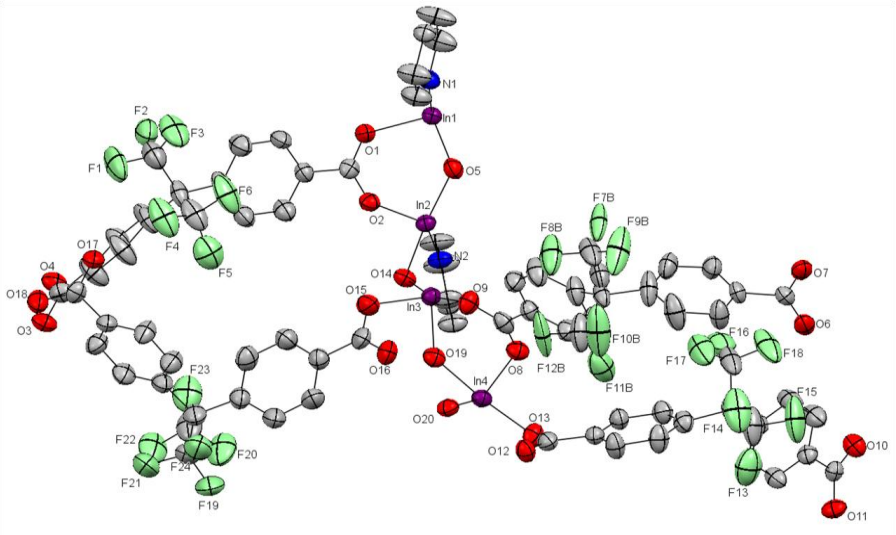

Figure 4.18 ORTEP representation of the asymmetric unit for **InPF-15.** Ellipsoids are displayed at the 50% probability level. Hydrogen atoms and water molecules were omitted for clarity. Symmetry codes: i) x, y, z; ii)1/2-x, y, ½-z ; iii) -x, -y, -z; iv) ½+x, -y, ½+z.

There are two different octahedral coordination environments for the metal centres (Table 4.12): for In1 and In2, each cation presents three In-O bonds (~2.209(7)Å for In1-O and ~2.156(7)Å for In2-O) coming from chelating carboxylate groups, two In-O from the μ-OH hydroxyl bridge and one In-N bond due to the 4,4'-bipyridine, in an $InNO_5$ octahedral PBUs.

Table 4.12 Relevant distances and angles for **InPF-15** material

Distance	value	Distance	value	Angle	value
In1 – O1	2.231(5)Å	In3 – O14	2.138(5)Å	θ L_1	109.18º
In1 – O4	2.159(6)Å	In3 – O10	2.198(5)Å	θ L_3	112.89º
In1 – O13	2.250(5)Å	In3 – O19	2.087(5)Å	θ $L_{3'}$	108.80º
In2 – O2	2.159(5)Å	In3 – O7	2.184(5)Å	θ $L_{3''}$	111.84º
In2 – O6	2.138(5)Å	In4 – O17	2.124(4)Å	ω L_1	68.13º
In2 – O11	2.189(5)Å	In4 – O8	2.231(6)Å	ω L_3	73.46º
In1 – O5	2.082(5)Å	In4 – O12	2.136(5)Å	ω $L_{3'}$	73.48º
In2 – O5	2.083(5)Å	In4 – O3	2.186(6)Å	ω $L_{3''}$	76.40º
In1 – O20	2.059(5)Å	In4 – O19	2.103(5)Å	LCA (L_1)	102.74º
In2 – O14	2.091(4)Å	In4 – O20	2.112(5)Å	LCA (L_3)	116.41º
In1 – N1	2.258(8)Å	d L_1	9.090 Å	LCA ($L_{3'}$)	112.00º
In2 – N2	2.264(5)Å	d L_3	9.878 Å	LCA ($L_{3''}$)	112.84º
In3 – O15	2.091(5)Å	d $L_{3'}$	9.639 Å		
In3 – O9	2.120(6)Å	d $L_{3''}$	9.741 Å		

In case of In3 and In4 polyhedra there are only In-O bonds for each cation, one In-O of L_1 type coordination of $hfipbb^{2-}$ linker (In3-O15 and In4-O17), three In-O bonds coming from carboxylate L_2 type groups (~2.166(7)Å for In3-O and ~2.184(7)Å for In4-O), and finally two In-O bonds of the hydroxyl bridge forming InO_6 octahedra (Figure 4.19).

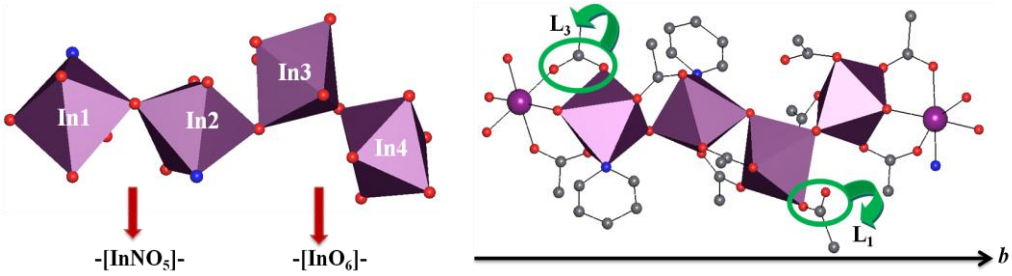

Figure 4.19 Four Indium PBUs sharing vertex forming an infinite chain SBU along *b* of **InPF-15.**

By sharing vertex octahedron infinite chains are formed that run along the [010] direction. These chains are connected along [001] direction through the complete $hfipbb^{2-}$ linkers, which present two different coordination types, one L_1 and three L_3. The LCA varies depending on the linker coordination type. It is worth mentioning that this value is higher than expected for the case of L_1 type.

A careful study of supramolecular interactions in the structure showed that the L_1 free carboxylate oxygen atoms show intramolecular hydrogen bonds with the corresponding adjacent hydroxyl bridge group (d=1.710Å for O20-H20···O16 and 2.001Å for O19-H19···O18). In such a way that L_1 in this compound is an intermediate situation between L_1 (η^1) and L_3 ($\eta^2\mu$) with In3···O16 = 3.18Å and In4···O16=3.91Å and In4···O18= 3.13Å and In3···O18=4.42Å.

The presence of the bipyridine linker distorts the indium coordination environment, incrementing the L_3 LCA value, which is considerably higher than those of the equivalent linker compared to the values obtained for **InPF-11β** polymorph with values more suitable of a L_2 coordination type.

Finally, the connection of the inorganic chains in the [100] direction is made through the 4,4'-bipyridine and as a result a 3D framework is obtained. The topology of the network was performed using a SBU of four indium octahedra with 8 connecting points, which gives rise to an 8-connected uninodal net with a **hex** topology (Figure 4.20).

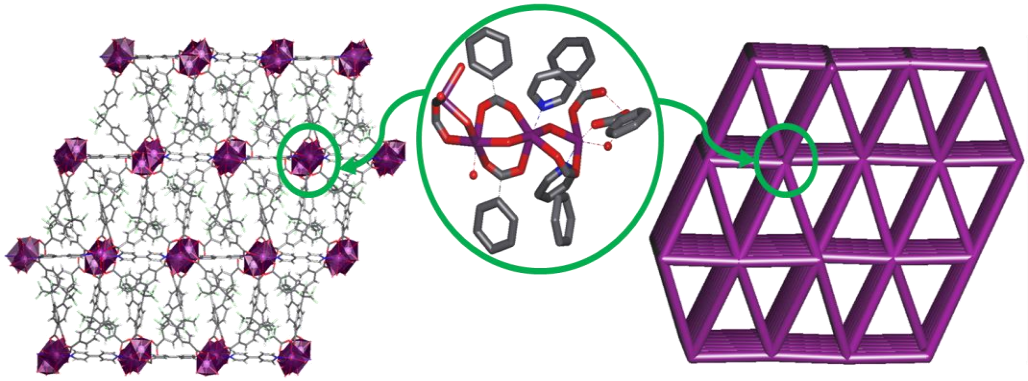

Figure 4.20 Perspective view of 3D framework of **InPF-15** in (010) and the simplification of the real framework into an 8-connected net with a **hex** topology.

4.2. New Indium MOFs with the H_2dpmda linker

To continue with the studies on the MOFs with the flexible V-shaped linkers, a new family of indium MOFs with the diphenylmethane-4,4-dicarboxylic acid ($C_{15}H_{12}O_4$) as organic linker was obtained in order to learn the differences in the framework produced by the bulky trifluoromethyl (-CF_3) group in hfipbb^{2-} -linker-contained MOFs compared to more compact dpmda^2 linker. As it can be seen in Figure 4.21, this linker is analogue to the H_2hfipbb, but without the presence of the –CF_3 groups in the central sp^3-carbon.

$C_{15}H_{12}O_4$ named **H_2dpmda** crystallizes in the monoclinic *C2/c* space group (Table 4.13). The asymmetric unit consists of half of H_2dpmda molecule. The supramolecular net for this organic compound is formed by the presence of the O-H···O synthon (distance O···H: 1.815Å) building organic chains along [100] direction (Figure 4.21).

Table 4.13 Main crystallographic data for **H_2dpmda**

Polymorph	**H_2dpmda**
Formula	$C_{15}H_{12}O_4$
Crystal System	Monoclinic
Space Group	C2/c
Unit cell dimensions	a = 19.5086(3) Å b = 4.6384(1) Å c = 13.7617(2) Å α = 90° β = 95.374(1)° γ = 90°
Volume	1239.81(4) $Å^3$
Z	4
Geometrical parameters	
d	9.473Å
θ	111.97º
ω	78.83º
LCA	110.05º

Comparison between both organic linkers can be made using the geometrical parameters described earlier in page 4, with emphasis in the LCA values.

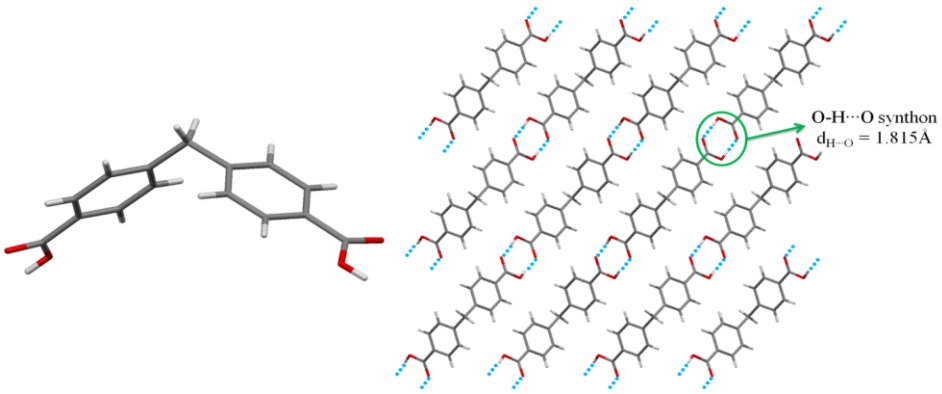

Figure 4.21 H_2dpmda structure and the O-H···O synthon formed along *c*.

The geometrical parameters of H_2dpmda are summarized in Table 4.13. Similar values of d, θ and LCA were obtained compared to the ones reported for the H_2hfipbb molecule in TUPNOI. In this case, the presence of supramolecular interactions between adjacent molecules (synthon formed between two adjacent carboxylic entities O-H···O) also influences in the final geometry configuration, leading to a distorted tetrahedral geometry of the central carbon atom. The absence of bulky substituents allows for the increasing of the ω-angle between the phenyl rings.

By means of this organic linker and additional nitrogenated ligands, four new Indium-MOFs were obtained (Scheme 4.2).

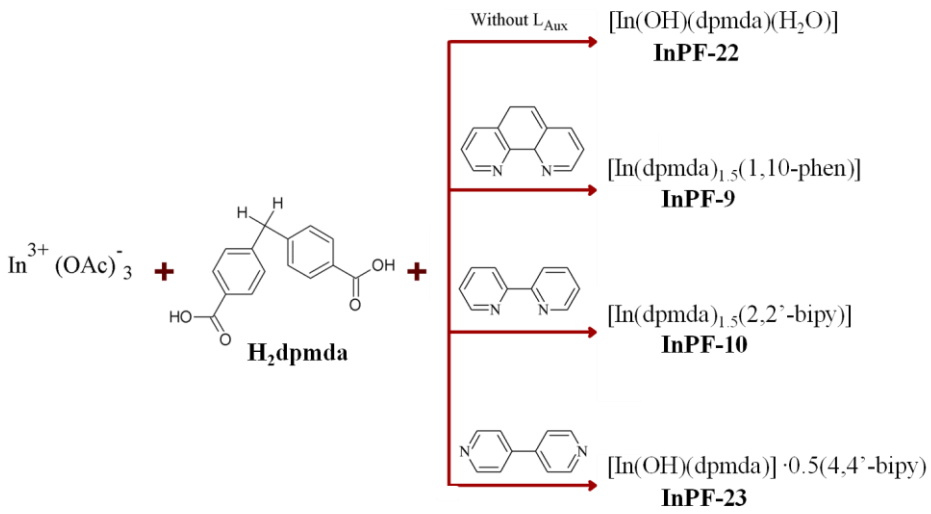

Scheme 4.2 Indium MOFs bearing H_2dpmda organic linker and nitrogenated ligands.

4.2.1. General Characterization

The dpmda^{2-} bears the same three different coordination modes (L_1 monodentate, L_2 chelate and L_3 bridge) that are previously described for the fluor counterpart (Figure 4.5).

The infrared spectra for all the InPF components of this family, show absorption in regions between [1710-1605]cm^{-1} and [1403-1302]cm^{-1}, which correspond to the bound carboxylate group ν_{asym}(C=O-M) and ν_{sym}(C-O-M), respectively. The absence of the characteristic carboxylic acid bands at 3429cm^{-1}(OH), 1705cm^{-1} (C=O)ν_{asym} and 933cm^{-1} (C-O)ν_{sym} of the H_2dpmda indicates complete deprotonation of the organic linker. Different carboxylate bands are appreciated when different coordination types are present in the material (Table 4.14).

Table 4.14 Characteristic COO$^-$ stretching frequencies of **InPF** materials

Material	C=O ν_{as} cm^{-1}	C-O ν_s cm^{-1}	Linker coordination mode
InPF-9	1702 1605	1415, 1402	$\eta^1 - L_1$ $\eta^2 - L_2$
InPF-10	1710 1621	1420, 1350	$\eta^1 - L_1$ $\eta^2 - L_2$
InPF-22	1648	1419, 1302	$\eta^2 - L_2$
InPF-23	1605	1403, 1350	$\eta^2\mu - L_3$
H_2dpmda	1705	933	acid

Thermogravimetric analyses (TGA) shows that materials containing dpmda^{2-} as unique organic part in the framework **InPF-22** and **InPF-23** are stable in a range between 300 and 450ºC. For **InPF-9** and **InPF-10** MOFs, which contains additional chelating nitrogenated ligands, after losing their physisorbed water molecules inside the framework at ~100ºC, their frameworks are stable up to ~300ºC and ~360ºC, respectively. For all four materials, the final residue is mainly In_2O_3 between 800 and 1000°C.

*4.2.1.1. The **InPF-22** material, [In(OH)(dpmda)(H_2O)]*

The **InPF-22** MOF, composed of only indium and dpmda^{2-} linker, without additional ligands, crystallizes in the orthorhombic system, *Ima2* space group (Table 4.15). The asymmetric unit consists of one In^{3+} ion, one hydroxyl molecule, half molecule of dpmda^{-2} linker and a water molecule coordinated to the metal center (Figure 4.22).

Table 4.15 Main crystallographic data for **InPF-22**

Identification Code	**InPF-22**
Formula	$C_{15}H_{13}O_6In$
Molecular Weight	404.07 g/mol
Temperature	293(2) K
Wavelength	Cu Kα 1.54178Å
Crystal System	Orthorhombic
Space Group	*Ima2*
Unit cell dimensions	a = 30.626(2) Å b = 7.5193(5) Å c = 6.0056(3) Å α = 90° β = 90° γ = 90°
Volume	1383.01(15) Å^3
Z	4
Dx	1.941 g.cm$^{-.3}$
Absorption coefficient (μ)	13.935 mm^{-1}
F(000)	1404
Theta range for data collection	[2.09 – 63.35]º
Index ranges	-27<*h*<27, -12<*k*<15, -31<*l*<30
Reflections collected	104810
Completeness	96.7%
Absorption correction	Multi – scan
Max. and min. Transmission	0.8265, 0.5046
Refinement method	Fsqd
Data / restrains / parameters	13117/1/1226
Goodness of fit on F^2	1.001
Final R indices [I>2σ(I)]	R1=0.0578 wR2=0.1544
R indices (all data)	R1=0.0978 wR2=0.1814

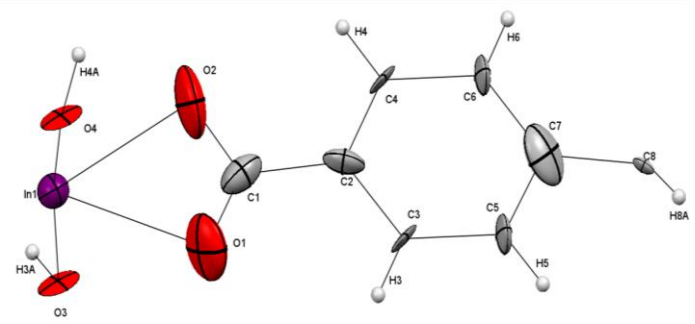

Figure 4.22 ORTEP representation of the asymmetric unit for **InPF-22.** Ellipsoids are displayed at the 50% probability level. Symmetry codes: i) x, y, z; ii) -x, -y, z; iii) ½-x, y, z; iv) ½+x, -y, z; v) ½+x, ½+y, ½+z; vi) ½-x, ½-y, ½+z; vii) -x, ½+y, ½+z; viii) x, ½-y, ½+z.

The In^{3+}environment is an InO_7 monocapped octahedron, in which the metal center shows two In-O bonds coming from the bridging hydroxyl group, four In-O bonds from the L_2-linker of ligand showing an average In-O distance of ~2.31(1)Å, and one In-O bond from the water molecule.

Regarding the $dpmda^{2-}$ linker, a L_2 coordination mode with the longest d value among the geometries is observed for materials synthesized; in contrast, a low value of the ω angle between the phenyl rings is observed. Also, high LCA value is observed (Table 4.16).

Table 4.16 Relevant distances and angles for **InPF-22** material

Parameter	**value**	**Parameter**	**value**
In1 – O1	2.32(1)Å	In1···In1^{ii}	3.87Å
In1 – O2	2.30(1)Å	d L_2	10.50Å
In1 – O3	2.08(2)Å	θ L_2	118.92º
In1 – O4	2.19(1)Å	ω L_2	51.64º
In1···In1^{i}	15.37Å	LCA (L_2)	129.51º
Hydrogen bond	**d $_{D\cdots A}$**	**d $_{D-H\cdots A}$**	
O4-H4$_A$···O1^{iii}	2.705	1.775	
Weak interactions	**d $_{D-H\cdots A}$ (Å)**	**angle (º)**	**Offset (º)**
C6-H6···C8-H8	2.879	127.36	
C4-H4... π	2.897	131.70	29.31
C5-H5... π	2.927	136.46	

This huge distortion of the tetrahedral geometry of the sp^3-carbon is supported by the presence of two different weak interactions (C-H···π and C-H···C-H) between adjacent organic moieties (Table 4.16).

Polymeric chains along the [001] direction are formed due to the sharing vertex polyhedra with an In···In distance of 3.87Å. These chains are connected through the L_2-type $dpmda^{2-}$ linker with In···In distance of 15.37Å. As a consequence of this rearrangement a 3D structure with a **dia** topology of a 4-connected uninodal net is generated. The topological analysis was performed considering the simplification of the points of extension (Figure 4.23).

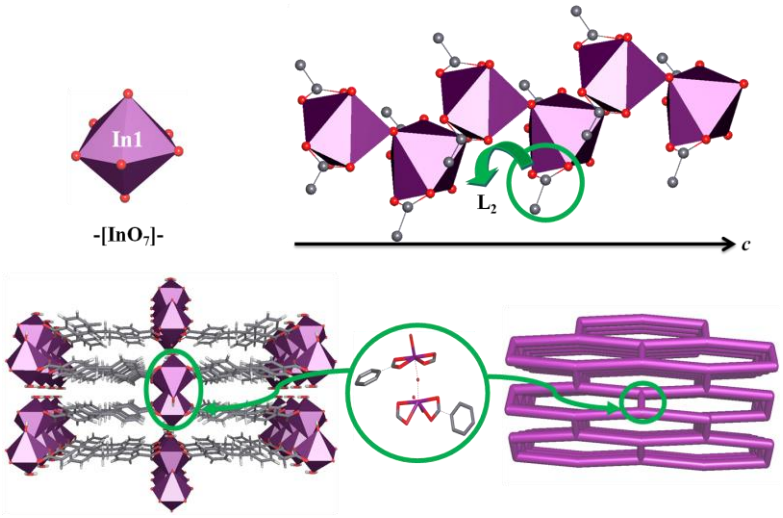

Figure 4.23 Above: polyhedral representation of the metal environment for **InPF-22** and its inorganic SBU. Down: 3D framework and its topological representation.

In the 3D structure of **InPF-22**, channels with 5.904Å x 30.626Å dimension are formed of inorganic chains. Inside these channels, there exist hydrogen bonds between the coordinated water molecule and adjacent carboxylate oxygen atoms (Table 4.16). Considering the hydrogen bonds present inside the channels, supramolecular inorganic 2D layers, which are connected through the $dpmda^{2-}$ generate a supramolecular 3D structure of InPF-22 with **pcu** topology of a 6-connected uninodal net (figure 4.24).

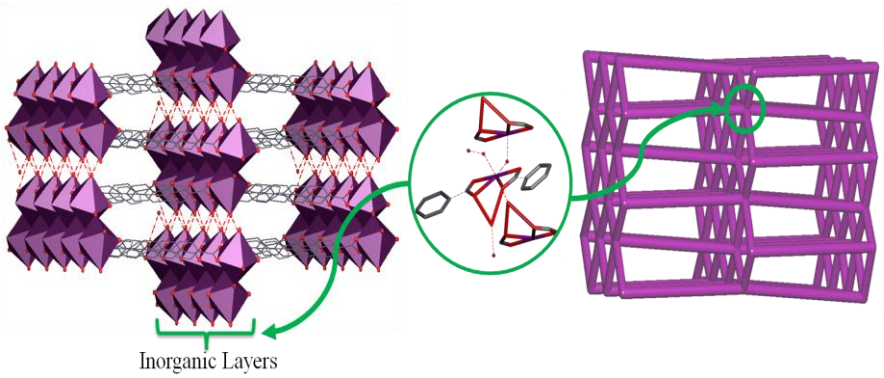

Figure 4.24 View of **InPF-22** supramolecular 3D structure and its topological **pcu** representation.

*4.2.1.2. The **InPF-9** material, $[In_2(dpmda)_3(1,10\text{-}phen)_2]\cdot 2H_2O$*

The **InPF-9** MOF crystallizes in the orthorhombic system, with *Pnn2* space group (Table 4.17). The asymmetric unit consists of one In^{3+} ion, one phenantroline molecule, one and a half molecules of $dpmda^{2-}$ linkers, and one hydration water molecule (Figure 4.25).

The metal centre environment of **InPF-9** is an InN_2O_5 monocapped octahedra, in which the indium cation is linked to five oxygen atoms coming from three ($dpmda^{2-}$) carboxylate groups with an average In-O distance of ~2.238(3)Å (Table 4.18), and two nitrogen atoms coming from the 1,10-phenantroline.

In **InPF-9**, the presence of the blocking phenantroline contributes to the increment of the coordination index if the indium center. The $dpmda^{2-}$ linkers act in L_1 and L_2 modes having thus, different geometrical characteristics that are also reflected in In···In distances.

L_1-linker displays a geometry that allows a closer interaction between the phenyl rings, which means shorter distance (d) and closer angles (θ and ω) compared to the ones of the organic ligand. As a result L_1 has a LCA value <100 and a In···In distance of 12.820(1) Å. In case of the L_2-linker, two different geometries are observed with LCA values of 111.51º and 104.09º for L_2 and $L_{2'}$ and In···In distances of 13.636(1)Å and 12.819(1)Å respectively. The distortion in the two different geometries of L_2-linker could be to the extra electron density donated by the phenantroline to the metal ion. As a consequence of this arrangement, together with the presence of the phenantroline blocking ligand, a 2D structure is generated.

The topological study performed for the structure of **InPF-9**, gave a 2D-net described as a **hcb** uninodal 3-connected net with point symbol {6·3} (Figure 4.26), constructed of layers perpendicular to the [001] direction.

Table 4.17 Main crystallographic data for **InPF-9**

Identification Code	**InPF-9**
Formula	$C_{69}H_{50}N_4O_{14}In_2$
Molecular Weight	1388.77 g/mol
Temperature	296(2) K
Wavelength	Cu Kα 1.54178Å
Crystal System	Orthorhombic
Space Group	*Pnn2*
Unit cell dimensions	a = 13.0268(4) Å b = 23.2550(6) Å c = 10.1923(3) Å α = 90° β = 90° γ = 90°
Volume	3087.64(15) $Å^3$
Z	2
Dx	1.494 $g.cm^{-3}$
Absorption coefficient (μ)	6.554 mm^{-1}
F(000)	1404
Theta range for data collection	[2.09 – 63.35]º
Index ranges	-27<*h*<27, -12<*k*<15, -31<*l*<30
Reflections collected	104810
Completeness	96.7%
Absorption correction	Multi – scan
Max. and min. Transmission	0.8265, 0.5046
Refinement method	Fsqd
Data / restrains / parameters	13117/1/1226
Goodness of fit on F^2	1.001
Final R indices [I>2σ(I)]	R1=0.0578 wR2=0.1544
R indices (all data)	R1=0.0978 wR2=0.1814

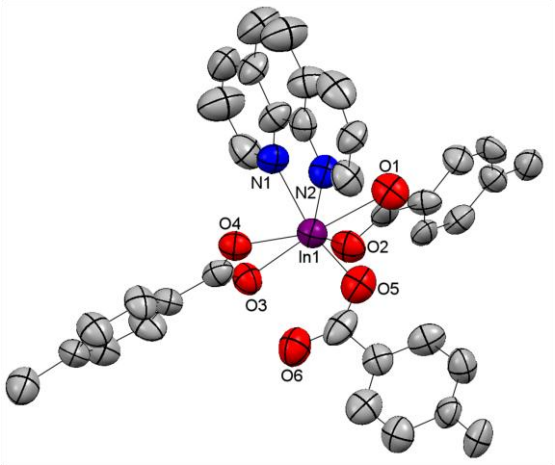

Figure 4.25 ORTEP representation of the asymmetric unit for **InPF-9**. Ellipsoids are displayed at the 50% probability level. Hydrogen atoms and water molecules were omitted for clarity. Symmetry codes: i) x, y, z; ii) -x, -y, z; iii) ½+x, ½-y, ½ +z; iv) ½-x, ½+y, ½+z.

Table 4.18 Relevant distances and angles for **InPF-9** material

Parameter	Value	Parameter	Value
In1 – O1	2.37(1)Å	d $L_{2'}$	9.102 Å
In1 – O2	2.233(9)Å	θ L_1	108.76º
In1 – O3	2.220(8)Å	θ L_2	116.23º
In1 – O4	2.29(1)Å	θ $L_{2'}$	108.77º
In1 – O5	2.08(1)Å	ω L_1	75.47º
In1 ··· O6	3.269Å	ω L_2	68.41º
In1 – N1	2.26(1)Å	ω $L_{2'}$	83.82º
In1 – N2	2.311(9)Å	LCA (L_1)	92.14º
d L_1	8.394Å	LCA (L_2)	111.51º
d L_2	9.519Å	LCA ($L_{2'}$)	104.09º

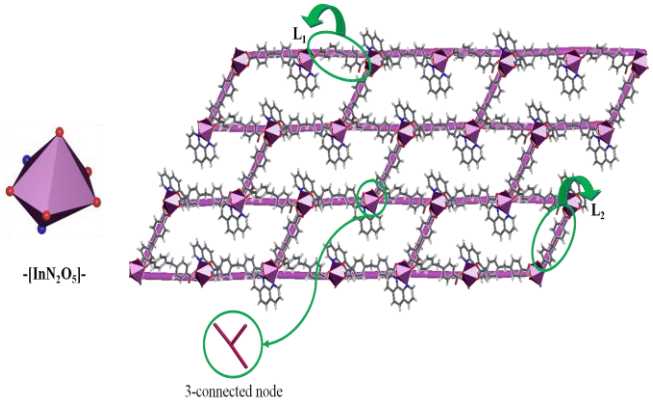

Figure 4.26 Left: Polyhedra representation of the metal environment for **InPF-9**. Right: Topological representation of **InPF-9** as a 3-connected Shubnikov hexagonal plane.

In the **InPF-9** layers, which are parallel to the (110) plane, the metallic centers are forming 6 metal rings (6R) with 26.655Å x 12.819Å dimensions. Among them, three different weak interlayer interactions are appreciated: i) C-H···π interactions between one $dpmda^{2-}$ ring centroid and an adjacent sp^3-CH ($d_{C\text{-}H\cdots\pi}$: 2.88(1)Å). ii) Csp^3-H···Csp^2 interactions between the sp^3-CH and the CH from one of the linker rings in a neighbour layer $d_{C\text{-}H\cdots C}$: 2.95(1)Å). iii) C_{32}-H_{32}···O_6 interaction was found, in which O_6 corresponds to the free oxygen from the L_1 type linker ($d_{H32\cdots O6}$: 2.48(1)Å, and $d_{C32\text{-}H32\cdots O6}$: 3.32(2)Å) giving rise to a 3D supramolecular structure with a **lvt** topology of a 4-connected net with point symbol $\{4^2.8^4\}$ (Figure 4.27).

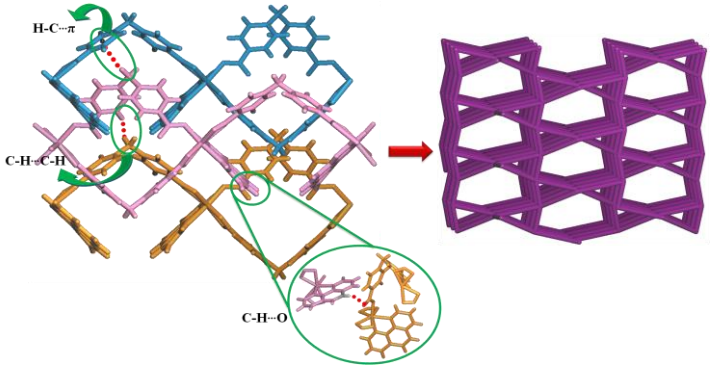

Figure 4.27 Left: Weak interactions between the layers of **InPF-9**. Right: Topological representation of the 3D supramolecular arrangement.

*4.2.1.3. The **InPF-10** material, $[In_2(dpmda)_3(2,2'\text{-bipy})_2]\cdot 2H_2O$*

The **InPF-10** MOF crystallizes in the orthorhombic system, *Pnn2* space group (Table 4.19). The asymmetric unit consists of one In^{3+} ion, one and a half molecules of $dpmda^{2-}$ linker, one 2,2'-bipyridine molecule, and one hydration water molecule (Figure 4.28).

Table 4.19 Main crystallographic data for **InPF-10**

Identification Code	**InPF-10**
Formula	$C_{65}H_{50}N_4O_{14}In_2$
Molecular Weight	1340.73 g/mol
Temperature	296(2) K
Wavelength	Cu Kα 1.54178Å
Crystal System	Orthorhombic
Space Group	*Pnn2*
Unit cell dimensions	a = 12.4606(3) Å b = 23.6079(7) Å c = 10.0948(3) Å α = 90° β = 90° γ = 90°
Volume	2969.57(14) $Å^3$
Z	2
Dx	1.499 $g.cm^{-.3}$
Absorption coefficient (μ)	6.790 mm^{-1}
F(000)	1356
Theta range for data collection	[2.09 – 63.35]º
Index ranges	-27<*h*<27, -12<*k*<15, -31<*l*<30
Reflections collected	104810
Completeness	96.7%
Absorption correction	Multi – scan
Max. and min. Transmission	0.8265, 0.5046
Refinement method	Fsqd
Data / restrains / parameters	13117/1/1226
Goodness of fit on F^2	1.038
Final R indices [I>2σ(I)]	R1=0.0717 wR2=0.2095
R indices (all data)	R1=0.1326 wR2=0.2542

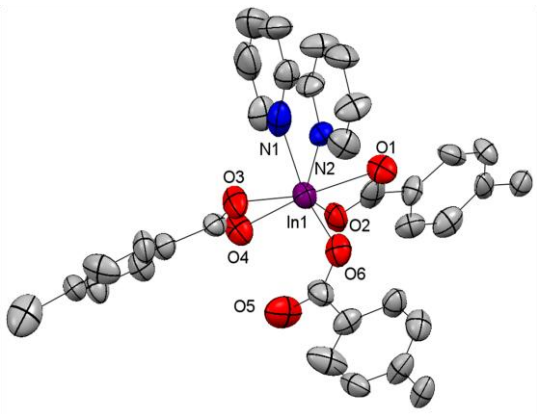

Figure 4.28 ORTEP representation of the asymmetric unit for **InPF-10.** Ellipsoids are displayed at the 50% probability level. Hydrogen atoms and water molecules were omitted for clarity. Symmetry codes: x, y, z; -x, -y, z; x+1/2, -y+1/2, z+1/2; -x+1/2, y+1/2, z+1/2.

The metal center environment is an InN_2O_5 monocapped octahedron, in which the indium cation is linked to one oxygen atom coming from the L_1-linker, four oxygen atoms coming from the L_2-linkers with average In-O distances of ~2.24(1) Å, and two In-N bonds from the chelating 2,2'-bipy (Table 4.20).

Regarding the dpmda2- geometry, the L_1 mode shows similar d value, but with higher θ and ω angles than the L_1-linker of InPF-9, again a value of LCA < 100 is obtained (Table 4.20). Comparing the two different L2-linkers that are found in the InPF-9 structure, similar d, θ and ω parameters values are observed, with LCA values >100. In···In distances of the L_1, L_2 and L_2' correspond to: 13.118 (1)Å, 13.579(1)Å and 13.056(1)Å, respectively.

The described arrangement between the indium cation and the $dpmda^{2-}$ linker together with the presence of the 2,2'-bipy blocking ligand, gives rise to a 2D framework structure constructed of layers parallel to the (110) plane. The metallic centers form rectangular 6 metal rings (6R) with 26.694 Å x 13.056 Å dimensions.

Table 4.20 Relevant distances and angles for **InPF-10** material

Parameter	value	Parameter	value
In1 – O1	2.37(2)Å	d $L_{2'}$	9.484Å
In1 – O2	2.27(1)Å	θ L_1	111.67º
In1 – O3	2.24(2)Å	θ L_2	113.12º
In1 – O4	2.23(1)Å	θ $L_{2'}$	111.16º
In1 – O5	2.10(2)Å	ω L_1	83.26º
In1 ··· O6	3.307Å	ω L_2	74.25º
In1 – N1	2.25(2)Å	ω $L_{2'}$	71.85º
In1 – N2	2.30(1)Å	LCA (L_1)	98.76º
d L_1	8.732Å	LCA (L_2)	106.55º
d L_2	9.303Å	LCA ($L_{2'}$)	108.04º

The topological study performed for **InPF-10** shows a **hcb** topology of a 3-connected uninodal net with $\{6^3\}$ point symbol (Figure 4.29).

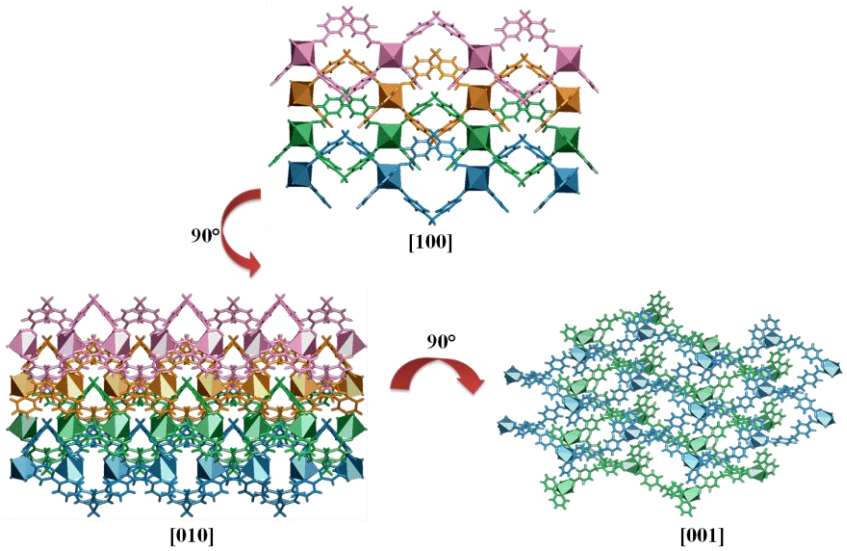

Figure 4.29 Different views of the **hcb** layers along [100], [010] and [001] for **InPF-10.**

The **InPF-10** supramolecular net is built up through the following weak interlayer interactions: i) C-H···O ($d_{H27\cdots O6}$ 2.54(2) Å and $d_{C27\cdots O6}$ 3.41(1)Å), ii) π···π interaction between one of the 2,2'-bipy rings and one $dpmda^{2-}$ ring (d π···π 3.68 Å) and iii) C-H···π interaction between two neighbour 2,2'-bipy rings ($d_{C\text{-}H\cdots\pi}$ 3.67Å) giving rise to a final 3D supramolecular structure with a **4,6T8** topology of a 4,6-connected binodal net with point symbol $\{4^2.6^4\}\{4^6.6^7.8^2\}2$ (Figure 4.30).

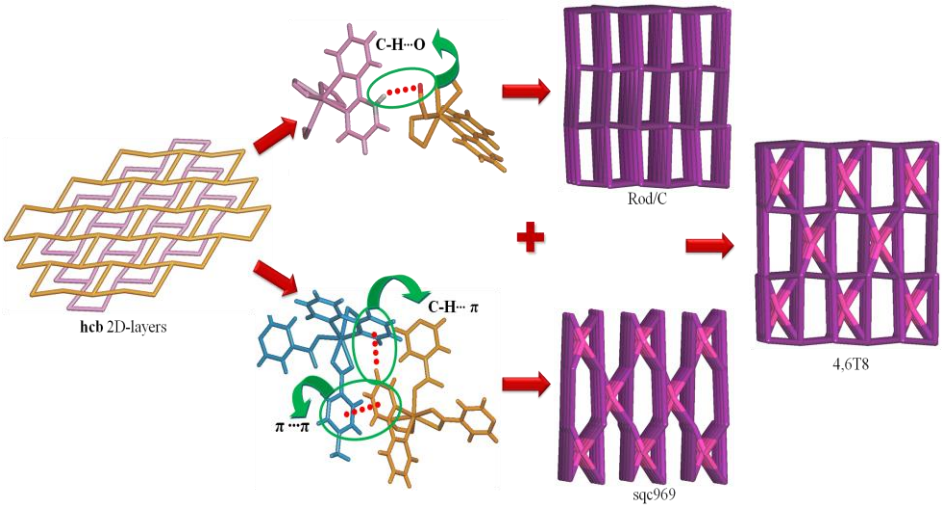

Figure 4.30 Weak interactions between the layers of **InPF-10** and the topological representation of different 3D supramolecular arrangement.

*4.2.1.4. The **InPF-23** material, [In(OH)(dpmda)]·0.5(4,4'-bipy)*

The **InPF-23** MOF crystallizes in the monoclinic system, *C2/c* space group (Table 4.21). The asymmetric unit consists of two halve of crystallographically independent In^{3+} ions, one bridging hydroxyl molecule, one $dpmda^{2-}$ linker and half of 4,4'-bipyridine molecule, which is non bonded to the indium center (Figure 4.31).

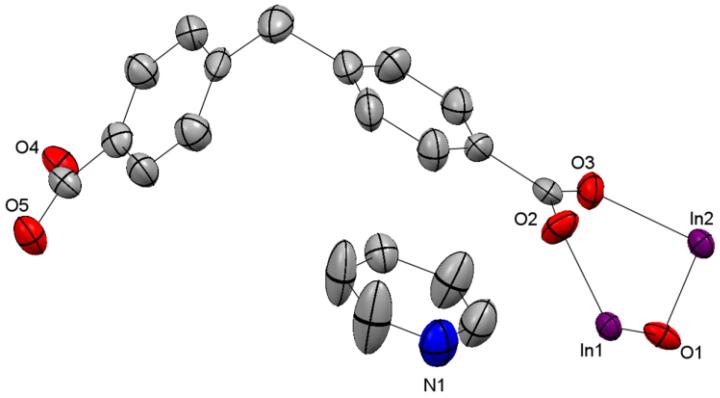

Figure 4.31 ORTEP representation of the asymmetric unit for **InPF-23.** Ellipsoids are displayed at the 50% probability level. Hydrogen atoms and water molecules were omitted for clarity. Symmetry codes: x, y, z; -x, -y, z; x+1/2, -y+1/2, z+1/2; -x+1/2, y+1/2, z+1/2.

Table 4.21 Main crystallographic data for **InPF-23**

Identification Code	InPF-23
Formula	$C_{20}H_{15}NO_5In$
Molecular Weight	464.15 g/mol
Temperature	296(2) K
Wavelength	Cu Kα 1.54178Å
Crystal System	Monoclinic
Space Group	*C2/c*
Unit cell dimensions	a = 23.0526(13) Å b = 12.8465(8) Å c = 13.4755(8) Å α = 90° β = 109.794(4)° γ = 90°
Volume	3754.9(4) $Å^3$
Z	8
Dx	1.642 $g.cm^{-3}$
Absorption coefficient (μ)	10.333 mm^{-1}
F(000)	1848
Theta range for data collection	[4.08 – 63.76]º
Index ranges	-26<*h*<19, -14<*k*<14, -15<*l*<15
Reflections collected	4758
Completeness	97.7%
Absorption correction	Multi – scan
Max. and min. Transmission	0.6827, 0.2578
Refinement method	Fsqd
Data / restrains / parameters	3029/0/250
Goodness of fit on F^2	1.010
Final R indices [I>2σ(I)]	R1=0.0618 wR2=0.1699
R indices (all data)	R1=0.0766 wR2=0.1751

The organic linker connects the inorganic chains building cages of 11.104Åx12.752Åx13.195Å dimensions settling inside the 4,4'-bipyridine that is supported by a hydrogen bond between O1-$H_{hydroxyl}$···N1 (Figure 4.32).

The In^{3+} environment is InO_6 octahedra, in which the metal center is coordinated to four oxygen atoms coming from the L_3-linker with average In-O distance of ~2.17Å, and two oxygen atoms from the bridging hydroxyl groups (Table 4.22). These indium octahedra are sharing vertex, which form chains along [001] direction.

Table 4.22 Relevant distances and angles for **InPF-23** material

Parameter	Value	Parameter	Value
In1 – O1	2.067(6) Å	$In2\cdots In2^{i}$ building cage	13.195 Å
In1 – O2	2.115(6) Å	$C_{sp^3}\cdots C_{sp^{3'}}$ building cage	11.104Å
In1 – O5	2.159(7) Å	$\mu\text{-}O\cdots\mu\text{-}O^{i}$ building cage	12.752Å
In2 – O1	2.063(5) Å	d L_3	9.311º
In2 – O3	2.227(7) Å	θ L_3	109.72º
In2 – O4	2.173(6) Å	ω L_3	81.39º
$In1\cdots In2_{sharing\ vertex}$	3.589 Å	LCA (L_3)	106.96º

In **InPF-23**, the L_3–linker presents a ω value of 81.39º indicating a distortion between the phenyl rings, which allows the cage formation and a tetrahedral geometry of the sp^3-carbon (θ=109.72º, Table 4.22).

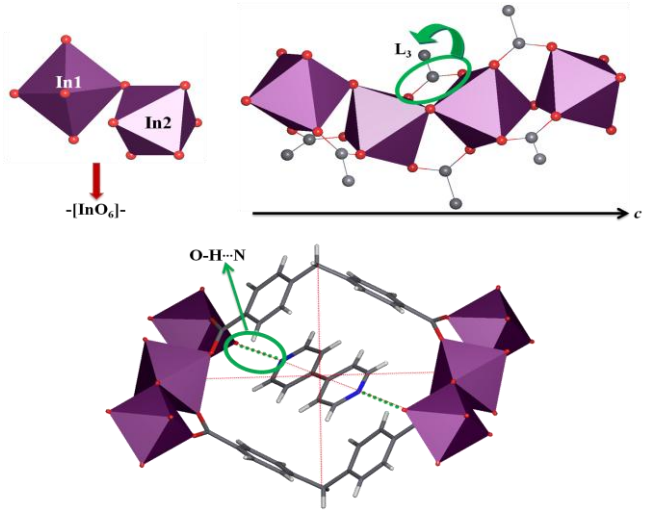

Figure 4.32 Above: polyhedral representation of the metal environment for **InPF-23** material and the inorganic chain formed. Down: cage representation with the bipy molecule inside.

The **InPF-23** structure shows a three dimensional framework with a **pcu** topology of a 6-connected uninodal net (Figure 4.33).

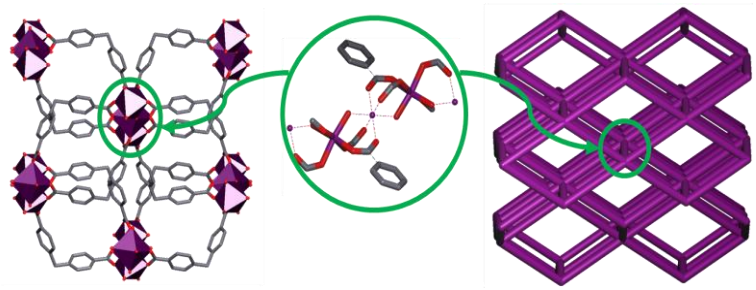

Figure 4.33 Representation of **InPF-23** 3D framework with the corresponding simplification of the SBU leading to a **pcu** topology.

4.3. New Indium MOFs with H_3popha linker

This new family of MOFs was obtained with the 5-(4-carboxy-2-nitrophenoxy)isophthalic acid ($C_{15}H_9O_9N$) as organic linker.

The less explored H_3popha linker was chosen for its capability to coordinate to the metals through three carboxylate groups in several different modes, and for the nitro group, which brakes not only the symmetry but also the electronic aromatic ring likeness, being able to assemble MOF materials with topologically very appealing structures.

H_3popha crystallizes in the Triclinic *P-1* space group. The asymmetric unit consists of one H_3popha molecule (Figure 4.34). The most important crystallographic parameters for the H_3popha crystal are described in table 4.23

Table 4.23 Main crystallographic data and geometrical parameters of **H_3popha**

Compound	H_3popha	Geometrical parameters	Value
Formula	$C_{15}H_9O_9N$	d_{1-2}	7.837 Å
Crystal System	Triclinic	d_{1-3}	10.260 Å
Space Group	*P-1*	d_{2-3}	4.968 Å
Unit cell dimensions	a = 7.8731(11)Å b = 10.3829(15)Å c = 10.7128(15)Å α = 110.397(3)º β = 102.205(3)º γ = 105.475(3)º	θ	115.33º
		ω	87.90º
		LCA_{1-2}	94.92º
		LCA_{1-3}	152.13º
		LCA_{2-3}	60.79º
Volume	744.79(18)$Å^3$		
Z	2		

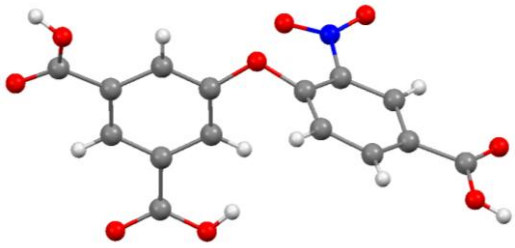

Figure 4.34 H_3popha asymmetric unit.

The increase in the number of coordinative carboxylate groups in the linker leads to an increment of the geometrical parameters to consider (distances and LCA angles). The corresponding d and LCA values are those illustrated in Figure 4.35.

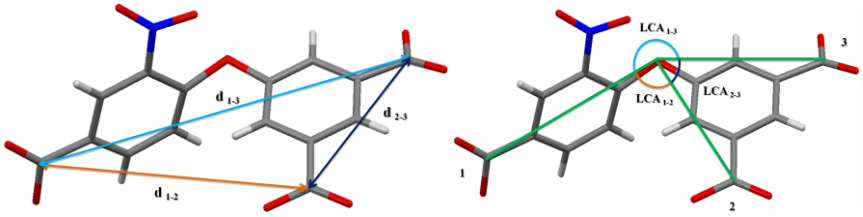

Figure 4.35 Additional $popha^{3-}$ geometrical parameters.

Theoretically, the central sp^3-oxygen of ether derivate presents a distorted tetrahedral configuration considering its two electron pairs as part of the described geometry. So, in theory the θ angle value of the H_3popha molecule is expected to be ~110º. The experimental values showed slightly higher θ that the usually value of an ether compound (Table 4.23). It is interesting to know the geometrical parameters of the organic linker before it is linked to any metal atom, as well as to have an idea of its initial configuration, so it could be a ground for comparison of the ligand's changed geometry when introducing metal cation.

Six new Indium MOFs are presented with the H_3popha as ligand, four of which contain additional nitrogenated ligands (Scheme 4.3). Their structural characterization and topological analysis are presented in the following section.

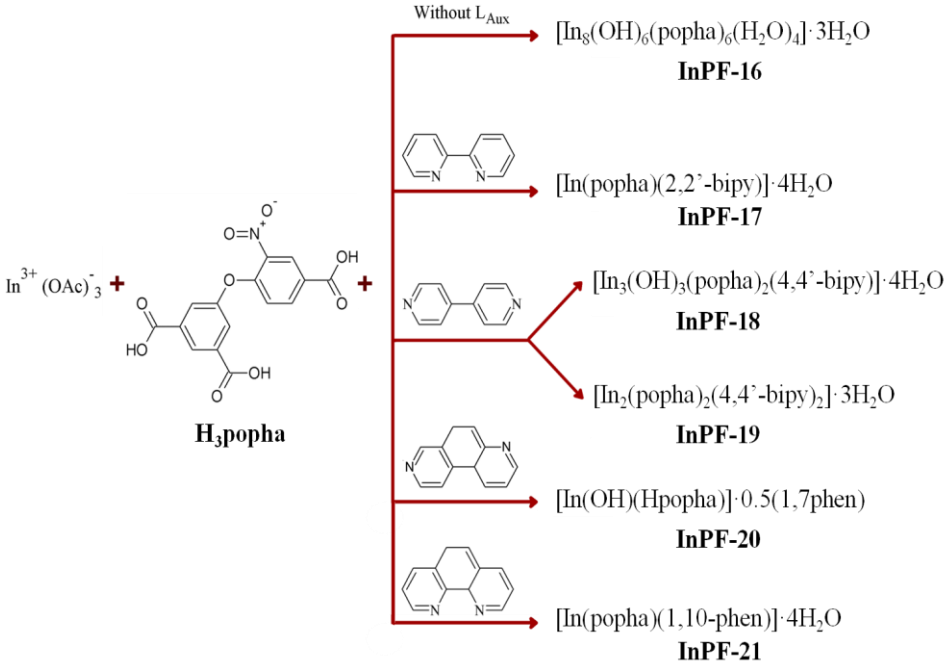

Scheme 4.3 New Indium MOFs with the tripodal V-shaped H_3popha linker and additional nitrogenated ligands.

4.3.1. General Characterization

In the InPF compounds the H_3popha linker presents seven different coordination modes to the metal ion; in six of them the H_3popha linker is fully deprotonated, and in the seventh, the linker is monoprotonated Hpopha^{2-} (Table 4.24). The NO_2 group is not involved in metal coordination for none of the presented MOFs.

The infrared spectra of every InPF material containing the popha linker, show absorption in regions between [1645-1602]cm^{-1} and [1459-1410]cm^{-1}, which correspond to the bound carboxylate group ν_{asym}(C=O-M) and ν_{sym}(C-O-M) respectively. The absence of characteristic carboxylic acid bands at 3433cm^{-1}(OH), 1692cm^{-1} (C=O)ν_{asym} and 916cm^{-1} (C-O)ν_{sym} of the H_3popha indicates complete deprotonation of the organic linker in cases of **InPF-16**, **InPF-17**, **InPF-18**, **InPF-19** and **InPF-21** materials. Different carboxylate bands are appreciated when different coordination types are present in the material (Table 4.25).

Table 4.24 Seven coordination modes of the H_3popha linker

Mode	Coordination type	Representation
L_1	η^1-$\eta^2\mu$-$\eta^2\mu$	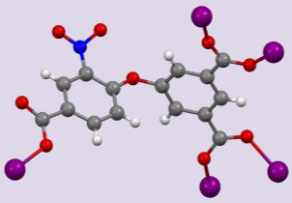
L_2	$\eta^2\mu$-η^1-η^1	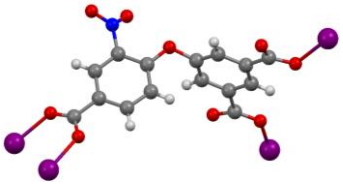
L_3	$\eta^2\mu$-$\eta^2\mu$-$\eta^2\mu$	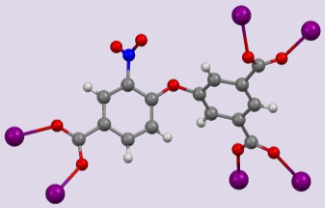
L_4	η^1-η^2-η^2	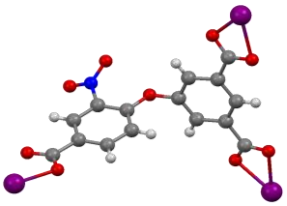
L_5	$\eta^2\mu$-$\eta^2\mu$-η^1	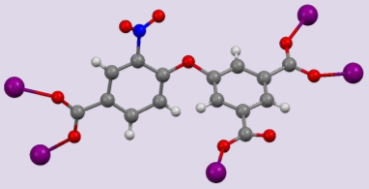
L_6	η^2-η^2-η^2	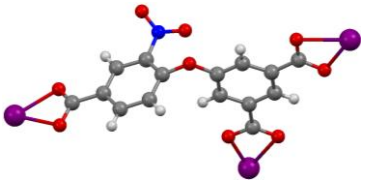
L_7	$\eta^2\mu$-$\eta^2\mu$-COOH	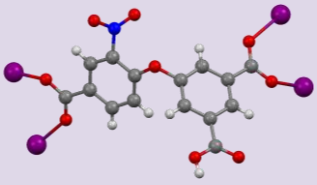

Colour codes: red-O, blue-N, gray-C, white-H and purple-In.

Table 4.25 Characteristic COO^- stretching frequencies of **InPF** materials

Material	C=O ν_{as} cm^{-1}	C-O ν_s cm^{-1}	Linker Coordination mode
InPF-16	1633, 1613	1419, 1410	η^1 and $\eta^2\mu$
InPF-17	1619, 1602	1458, 1444	$\eta^1$and η^2
InPF-18	1645, 1625	1451, 1417	$\eta^1$and $\eta^2\mu$
InPF-19	1614	1420	η^2
InPF-20	1688, 1619	1459	COOH and η^2
InPF-21	1621	1432	η^2
H_3popha	1692	916	none

Thermogravimetric analyses (TGA) show that the material containing popha^{3-} as unique organic part in the framework **InPF-16** is stable at ~420ºC. **InPF-17** and **InPF-21α** materials, which presented chelating nitrogenated ligands in their frameworks are stable at ~430ºC and ~450ºC, respectively. A large difference in thermal stability between **InPF-18** and **InPF-19** materials, which are built using the additional 4,4-bipy, is found; in case of **InPF-18** the framework is stable only up to ~250ºC but in case of **InPF-19** the framework stability is preserved up to ~420ºC. For **InPF-20** framework a low thermal stability is observed with initial weight loss at ~200ºC. For all six materials, the final residue is mainly In_2O_3.

*4.3.1.1. The **InPF-16** material, $[In_4(OH)_3(popha)_3(H_2O)_2]\cdot 2H_2O$*

The **InPF-16** material composed of only indium and popha^{3-} linker, without additional ligands, crystallizes in the triclinic *P-1* space group (Table 4.26). The asymmetric unit consists of four crystallographically different In^{3+} ions, three molecules of the fully deprotonated popha^{3-} linker, three hydroxyl groups and two coordinated water molecules (Figure 4.36).

The molecules of popha^{3-} linker show three different coordination modes: i) **L_1** with η^1-$\eta^2\mu$-$\eta^2\mu$, ii) **L_2** with $\eta^2\mu$-η^1-$\eta^1$and iii) **L_3** with $\eta^2\mu$- $\eta^2\mu$-$\eta^2\mu$ (Table 4.25). There are four crystallographically independent indium metal centers, all of them in **InO_6**-octahedral coordination environments. The relevant In-O bonds values are in Table 4.27.

The environment of the indium metallic center (In1) is built by two In-O bonds coming from two hydroxyl bridge groups, one In-O bond from the monodentate part of the L_1 popha^{3-} linker type and three In-O bonds from the chelate popha^{3-} linker (two L_1 and one L_3). The environment of the second indium metallic center (In2), is formed by two In-O bonds from bridging hydroxyl groups and four In-O bonds from the chelating linker (two L_1 and two L_3). The third indium (In3) environment consists of two In-O bonds from bridging hydroxyl groups, one In-O bond from the monodentate part of the L_2 linker and three In-O bonds from the chelating linker (one L_2 and two L_3). The fourth indium (In4) environment exhibits one In-O bond from bridging hydroxyl group, one In-O bond from monodentate part of L_2 coordination mode, two In-O bonds from chelating linker (one L_2 and one L_3) and two In-O bonds from coordinated water molecules.

Table 4.26 Main crystallographic data for **InPF-16**

Identification Code	**InPF-16**
Formula	$C_{45}H_{28}N_3O_{34}In_4$
Molecular Weight	1613.99 g/mol
Temperature	296(2) K
Wavelength	Cu Kα 1.54178Å
Crystal System	Triclinic
Space Group	*P-1*
Unit cell dimensions	a = 11.2976(3) Å b = 12.8826(4) Å c = 18.5044(5) Å α = 76.122(2)° β = 88.327(2)° γ = 78.218(2)°
Volume	2558.92(13) $Å^3$
Z	2
Dx	2.095 $g.cm^{-.3}$
Absorption coefficient (μ)	15.234 mm^{-1}
F(000)	1574
Theta range for data collection	[3.61 – 62.44]º
Index ranges	-12<*h*<8, -14<*k*<14, -20<*l*<20
Reflections collected	10041
Completeness	98.7%
Absorption correction	Multi – scan
Max. and min. Transmission	0.3753, 0.1506
Refinement method	Fsqd
Data / restrains / parameters	7256/0/786
Goodness of fit on F^2	0.967
Final R indices [I>2σ(I)]	R1=0.0574 wR2=0.1547
R indices (all data)	R1=0.0739 wR2=0.1644

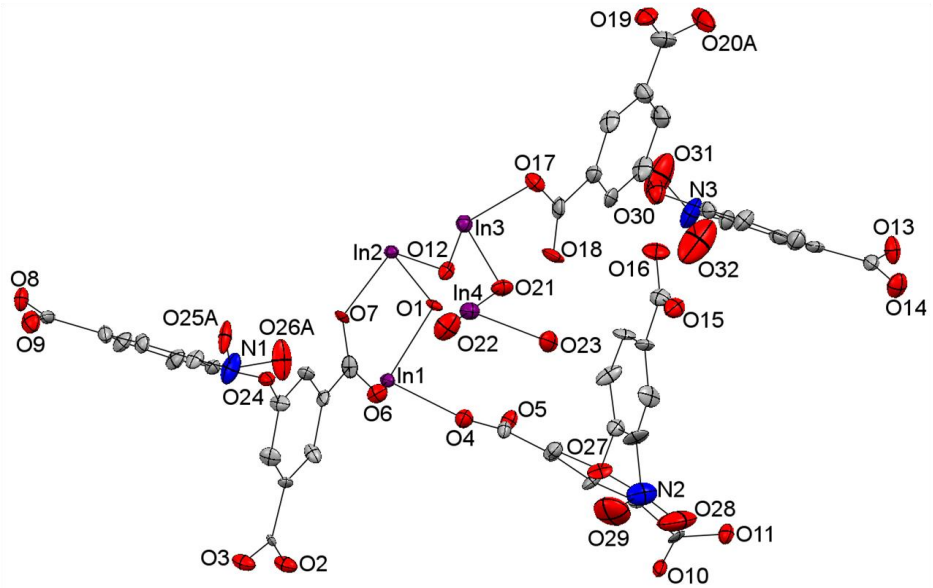

Figure 4.36 ORTEP representation of the asymmetric unit for **InPF-16**. Ellipsoids are displayed at the 50% probability level. Hydrogen atoms and water molecules were omitted for clarity. Symmetry codes: i) x, y, z; ii) -x, -y, z.

Table 4.27 Relevant distances for **InPF-16** material

Parameter	Value	Parameter	Value
In1 – O1	2.291(8)Å	In4 – O21	2.078(8)Å
In1 – O4	2.108(8)Å	In4 – O22	2.200(1)Å
In1 – O6	2.106(8)Å	In4 – O23	2.162(9)Å
In2 – O1	2.189(8)Å	In1 ··· In2	3.798 Å
In2 – O7	2.162(7)Å	In2 ··· In3	3.730 Å
In2 – O12	2.072(7)Å	In3 ··· In4	3.558 Å
In3 – O12	2.110(8)Å	In4 ··· $In1^{i}$	8.500 Å
In3 – O17	2.176(7)Å	In1 ··· $In1^{ii}$	3.518 Å
In3 – O21	2.091(8)Å		

With the different coordination modes showed by the $popha^{3-}$ linker, the acute ω angles is found between the phenyl rings as a bridging coordination is displayed. In fact, increasing the presence of bridging coordination modes seems to influence in the LCA_{1-2} and LCA_{1-3} values, showing higher LCA values in case of L_3, which presented all three carboxylate groups in $\eta^2\mu$ mode, compared to the similar LCA values of L_1 and L_2, which have mixed monodentate and bridge coordination modes (Table 4.28).

Table 4.28 Relevant geometry parameters of $popha^{3-}$ linkers in **InPF-16**

Parameter	Coordination type		
	L_1	L_2	L_3
d_{1-2}	8.691Å	8.541Å	9.043Å
d_{1-3}	9.339Å	9.331Å	9.547Å
d_{2-3}	5.010Å	5.032Å	4.993Å
θ	116.16º	118.56º	118.07º
ω	88.65º	84.17º	62.03º
LCA_{1-2}	110.67º	108.23º	121.27º
LCA_{1-3}	123.57º	125.73º	131.65º
LCA_{2-3}	61.83º	62.24º	62.12º

At a first glance, the ω value for L_2 linker ($\eta^2\mu$- η^1- η^1) should be higher than that of L_1 (η^1-$\eta^2\mu$-$\eta^2\mu$); however, as it can be seen in table 4.28, this value is lower than expected. By careful examination of the complete structure of **InPF-16**, we found that supramolecular interaction would justify this small deviation. If we take into account the strong intra hydrogen bond between the carboxylate free oxygen and the neighbor μ-hydroxyl oxygen atom (O12-H12···O18 with $d_{D\text{-}H\cdots A}$ 1.884Å and $d_{D\cdots A}$ 2.665Å, respectively), we can consider a certain level of a η^2 pseudo-coordination of this carboxylate ($d_{In1\cdots O18}$= 3.090Å, average In-O distance ~2.145).

In **InPF-16**, a SBU is formed by four sharing vertex octahedra (In1 to In4) joined through an inversion center to other four indium centers to form eight octahedra clusters in the [001] direction. In1 and In1' octahedra share a face, forming a corrugated geometry. These clusters can be described as rods (defined as a 1-periodic three-dimensional structure with a linear axis that is determined by specifying a point on the axis and its direction),[6] that are connected through the organic units in all directions. The result is a 3D structure with a 3-periodic **3,12-llj** topology of a 3,12-connected binodal net with stoichiometry (3-c)4(12-c) (Figure 4.37).

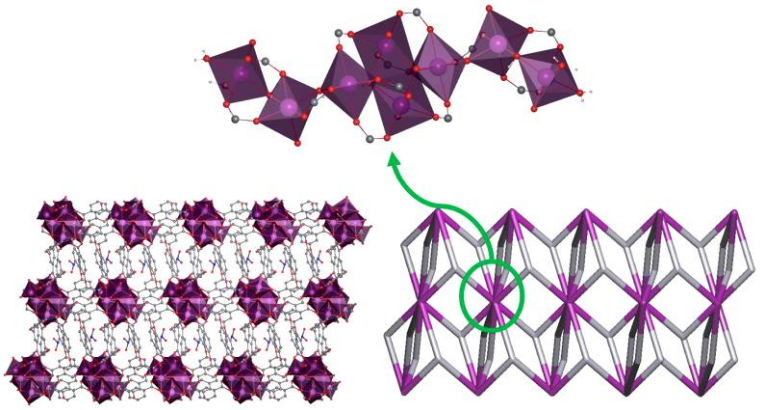

Figure 4.37 Above: Secondary Building Unit (**SBU**) cluster of **InPF-16** material. Down: polyhedral and topological **llj** representation of **InPF-16** 3D structure.

*4.3.1.2. The **InPF-17** material, [In(popha)(2,2'-bipy)]·4H$_2$O*

The **InPF-17** material crystallizes in the triclinic *P-1* space group (Table 4.29). The asymmetric unit consists of one In^{3+} ion, one fully deprotonated popha^{3-} linker, one 2,2'-bipyridine molecule and four hydration water molecules (Figure 4.38).

Table 4.29 Main crystallographic data for **InPF-17**

Identification Code	**InPF-17**
Formula	$C_{25}H_{18}N_3O_{11}In$
Molecular Weight	651.24 g/mol
Temperature	293(2) K
Wavelength	Mo Kα 0.71073Å
Crystal System	Triclinic
Space Group	*P-1*
Unit cell dimensions	a = 9.9939(6) Å b = 12.3477(8) Å c = 13.1271(8) Å α = 98.2560(10)° β = 110.7860(10)° γ = 110.3110(10)°
Volume	1352.96(15) Å^3
Z	2
Dx	1.599 g.cm^{-3}
Absorption coefficient (μ)	0.938 mm^{-1}
F(000)	652
Theta range for data collection	[2.12 – 26.37]º
Index ranges	-12<*h*<12, -15<*k*<15, -16<*l*<16
Reflections collected	12400
Completeness	99.7%
Absorption correction	Multi – scan
Max. and min. Transmission	0.9634, 0.9120
Refinement method	Fsqd
Data / restrains / parameters	5521/3/380
Goodness of fit on F^2	1.034
Final R indices [I>2σ(I)]	R1=0.0707 wR2=0.1640
R indices (all data)	R1=0.1241 wR2=0.1985

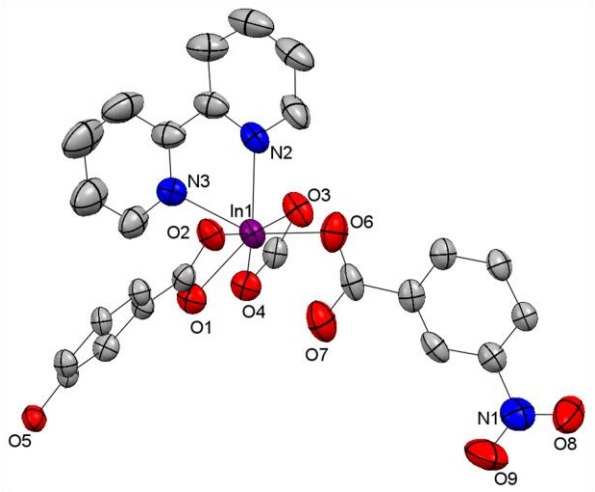

Figure 4.38 ORTEP representation of the asymmetric unit for **InPF-17.** Ellipsoids are displayed at the 50% probability level. Hydrogen atoms and water molecules were omitted for clarity. Symmetry codes: i) x, y, z; ii) -x, -y, z.

The indium environment is heptacoordinated, built with five In–O bonds from the carboxylate part of the popha^{3-} linker with average distance of ~2.273(7)Å and two In-N bonds from the 2,2'-bipyridine. Despite the fact that the distance of ~2.6Å is considered a habitual In-O distance value in the CSD histograms, the In1···O7 is presented as a weak interaction, due to the high distance deviation obtained in front of the other In-O bonds distances observed (Table 4.30).

Table 4.30 Relevant distances and angles for **InPF-17** material

Parameter	**Value**	**Parameter**	**Value**
In1 – O1	2.197(4)Å	In1 ··· O7	2.645(9)Å
In1 – O2	2.413(7)Å	In1 – N2	2.283(7)Å
In1 – O3	2.410(7)Å	In1 – N3	2.310(8)Å
In1 – O4	2.215(7)Å	In1··· In1^{ii}	9.994Å
In1 – O6	2.128(8)Å	In1···centroid	9.916Å
weak interactions	**$d_{D-x\cdots A}$**	**$d_{D\cdots A}$**	**angle $_{D-x\cdots A}$**
N1-O8···O5	2.669Å	2.805Å	82.73º
$\pi_{bipy}\cdots\pi_{bipy}^{i}$		3.832 Å	20.79˚offset
C4-H4···π_{popha}^{i}	3.314Å	3.406Å	87.70º
C24-H24...O9^{ii}	2.685Å	3.614Å	176.69º

In **InPF-17**, the popha^{3-} linker exhibits L_4 coordination geometry, in which one of the carboxylate groups is monodentate to the metal center and two carboxylate groups are bonded in a chelate mode. The geometrical parameters showed a more acute angle between the phenyl rings (ω) compared to that of the non-coordinated ligand molecule, and longer distances between the carboxylate groups. The LCA (for the carboxylates 1 and 3) value corresponds to the geometrical changes of the ligand **InPF-17** with an angle lower than the theoretical expected (Table 4.31).

Table 4.31 Geometrical parameters of L_4 popha^{3-} linker of **InPF-17**

Parameter	Value
d_{1-2}	8.820 Å
d_{1-3}	10.937Å
d_{2-3}	5.048 Å
θ	117.07º
ω	79.49º
LCA_{1-2}	113.34º
LCA_{1-3}	120.11º
LCA_{2-3}	62.43º

The InN_2O_5 polyhedra are connected through the L_4 linker to built square 3-metal containing rings of 9.994Å x 9.916Å dimensions. The presence of the blocking bipyridine together with the square shaped rings give rise to 2D layers perpendicular to the (001) direction, with **hcb** topology of a 3-connected uninodal net (Figure 4.39).

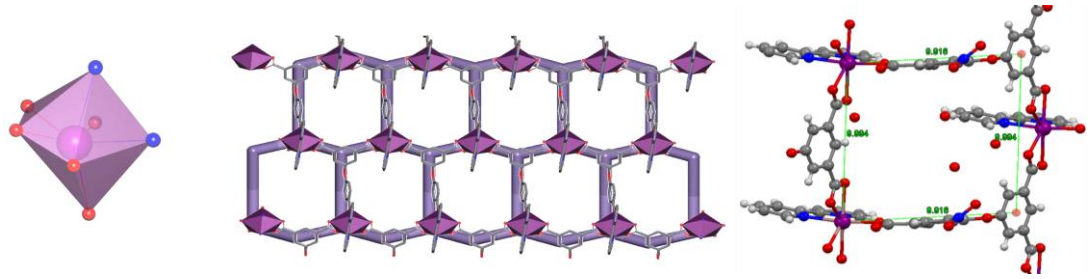

Figure 4.39 View of **InPF-17** 2D layer with the **hcb** topological representation and the square shaped 3-metal ring

The supramolecular network is built up through two types of weak interactions, which increase the dimensionality of the framework, connecting the 2D layers along *a* and *c* axis: i) π···π interactions from two neighbour molecules of 2,2'-bipyridine with a distance of 3.832 Å between centroids, displaying an offset of 20.79˚; ii) C-H···π (d_{D-A}: 3.403Å) interactions, which extend the network along (001) direction. The final 3D structure shows a **dia** topology with a 4-connected uninodal network (Figure 4.40).

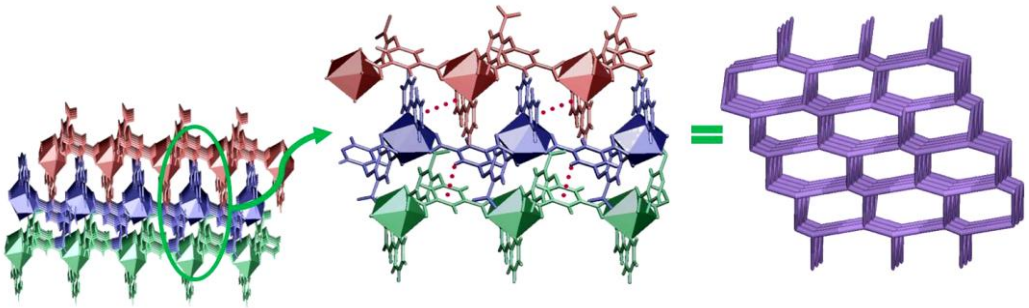

Figure 4.40 2D layers of **InPF-17** showing the π··· π interaction and the C-H··· π along *c* axis and the corresponding 3D supramolecular framework with **dia** topology.

Two different compounds named **InPF-18** and **InPF-19** were obtained using H_3popha and 4,4'-bipyridine linkers with indium as metal source. Both compounds were obtained as pure phases after adjusting the reaction conditions. The results showed the solvent nature as the decisive synthetic factor (Figure 4.41).

MOF **InPF-19** was obtained with shorter reaction times at lower synthesis temperatures, while **InPF-18** material is only obtained at temperatures above 180ºC.

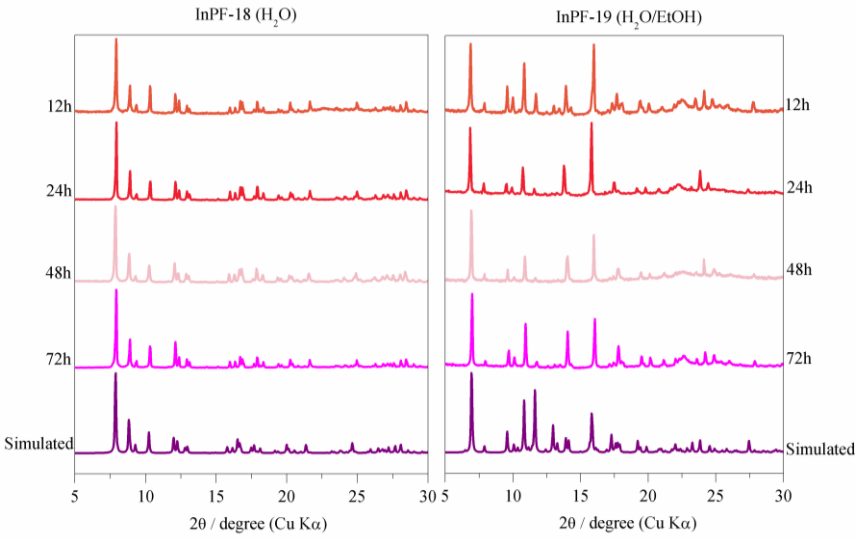

Figure 4.41 PXRD screening of the time at 180ºC with 1:1:1 stoichiometry synthesis conditions for **InPF-18** and **InPF-19** materials.

*4.3.1.3. The **InPF-18** material, $[In_3(OH)_3(popha)_2(4,4'\text{-bipy})]\cdot 4H_2O$*

The **InPF-18** material crystallizes in the monoclinic *C2/c* space group (Table 4.31). The asymmetric unit consists of one and a half crystallographically independent In^{3+} ions, one fully deprotonated $popha^{3-}$ linker, one and a half hydroxyl groups and half of 4,4'-bipyridine molecule (Figure 4.42).

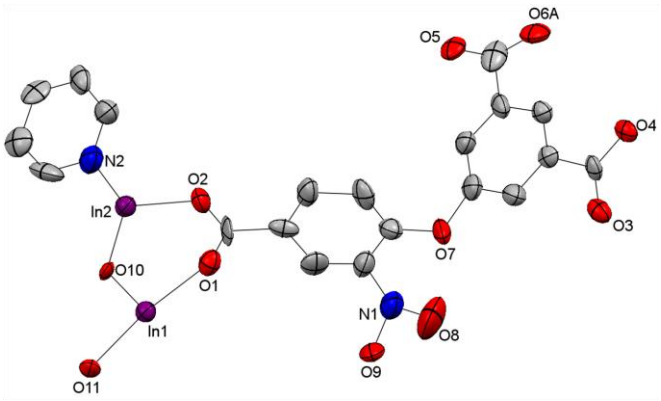

Figure 4.42 ORTEP representation of the asymmetric unit for **InPF-18.** Ellipsoids are displayed at the 50% probability level. Hydrogen atoms and water molecules were omitted for clarity. Symmetry codes: i) x, y, z; ii) -x, y, ½-z; iii)1/2+x, ½+y, ½-z; iv)1/2-x, ½+y, ½-z ; v) -x, -y, -z; vi) x, -y, ½+z; vii) ½-x, ½-y, -z; viii) ½+x, ½-y, ½+z.

Table 4.31 Main crystallographic data for **InPF-18**

Identification Code	**InPF-18**
Formula	$C_{40}H_{22}N_4O_{21.75}In_3$
Molecular Weight	1251.08 g/mol
Temperature	296(2) K
Wavelength	Cu Kα 1.54178Å
Crystal System	Monoclinic
Space Group	C2/c
Unit cell dimensions	a = 17.3631(13) Å b = 14.7586(11) Å c = 19.8896(15) Å α = 90° β = 95.180(6)° γ = 90°
Volume	5076.0(7) $Å^3$
Z	4
Dx	1.637 $g.cm^{-3}$
Absorption coefficient (μ)	11.498 mm^{-1}
F(000)	2444
Theta range for data collection	[3.94 – 39.84]º
Index ranges	-20<*h*<19, -17<*k*<17, -20<*l*<23
Reflections collected	7364
Completeness	99.6%
Absorption correction	Multi – scan
Max. and min. Transmission	0.5454, 0.4598
Refinement method	Fsqd
Data / restrains / parameters	4185/0/323
Goodness of fit on F^2	0.975
Final R indices [I>2σ(I)]	R1=0.0823 wR2=0.2011
R indices (all data)	R1=0.1671 wR2=0.2383

There are two different environments in InO_6 and InN_2O_4 octahedra PBUs. The InO_6 PBU is built by two In-O bonds from μ–OH groups connecting In1···In2 and In1...In1' respectively, and four In–O bonds from carboxylate groups, three of them having a $\eta^2\mu$ coordination and only one with η^1 mode. The InN_2O_4 PBU, has two In–N bonds from the 4,4'-bipyridine, two In–O bonds from μ–OH and two In–O bonds from carboxylate groups with $\eta^2\mu$ coordination type (Table 4.32).

Table 4.32 Relevant distances and angles for **InPF-18** material

Parameter	**Value**	**Parameter**	**Value**
In1 – O1	2.113(12)Å	In2 – O2	2.165(12)Å
In1 – O3	2.211(12)Å	In2 – O10	2.056(9)Å
In1 – O4	2.163(10)Å	In2 – N2	2.159(18)Å
In1 – O5	2.117(11)Å	In1 ··· $In1^i$	3.661Å
In1 – O10	2.140(9)Å	In1 ··· In2	3.830Å
In1 – O11	2.083(6)Å	In2 ··· $In2^{ii}$	11.394Å

In **InPF-18**, the popha^{3-} linker exhibits L_5 coordination geometry, with one monodentate carboxylate group and two carboxylate groups in bridge mode connecting two different metal centers. The geometrical parameters of L_5 show similarities with the parameters of H_3popha as a single molecule previously described in page 94. This "natural" geometry of the linker could be related to the presence of the bipyridine molecule setting a distance of 11.394Å between In2···In2' along *a* direction, which allows the location of the popha^{3-} linker without the need of its additional distortion (Table 4.33).

Table 4.33 Geometrical parameters of L_5 popha^{3-} linker of **InPF-18**

Parameter	Value
d_{1-2}	8.387 Å
d_{1-3}	10.119Å
d_{2-3}	5.041 Å
θ	121.30º
ω	63.57º
LCA_{1-2}	104.46º
LCA_{1-3}	150.82º
LCA_{2-3}	62.64º

Inorganic chains along *c* axis are built from the PBUs sharing vertex through the μ–OH groups (In···In distances in table 4.32). These chains are connected along the *a* axis through the 4,4'-bipy linker and through the popha^{3-} linker along *b* direction, generating small triangle channels of 10.675Å x 10.094Å x 6.660Å dimensions between 2 inorganic chains(Figure 4.43). Inside the framework channels of **InPF-18**, hydration water molecules are supported by hydrogen bonds with the free C=O and the NO_2 groups of the popha^{3-} linker ($d_{D\cdots A}$ = 2.729Å and 2.879Å respectively).

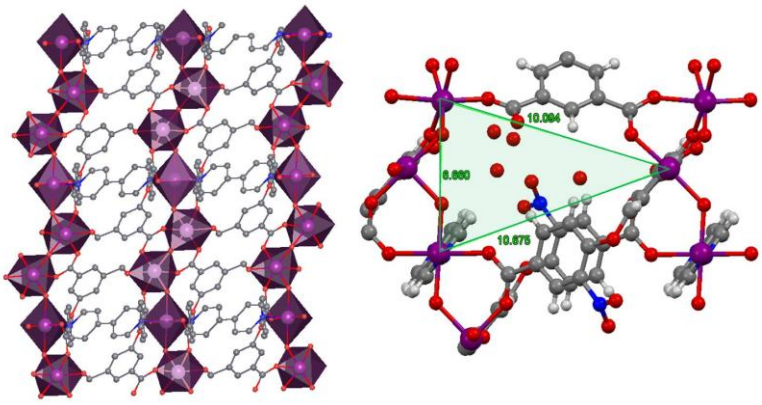

Figure 4.43 Right: (010) view of the polyhedral representation of **InPF-18** 3D structure, and Left: view of **InPF-18** triangular channels.

The SBUs generated can be described as infinite (-OH-In-)$_\infty$ rods with carboxylate O atoms and bipyridine N atoms completing the octahedral coordination around indium to result in infinite rods of InO_6 and InN_2O_4 octahedra sharing corners (Figure 4.43). These rods are connected in all direction through the $–C_{10}H_8–$and the $–C_{14}NO_3H_6–$ linkers, giving rise to a 3-dimentional framework. These rods are set in hexagonal packing going down (001) allowing

that **InPF-18** 3D arrangement could be described as a rod packing stacking/pillared 2D layers[7] with a **3,8L18** topology derivated net of a 3,10-connected binodal net with new topology (Figure 4.44).

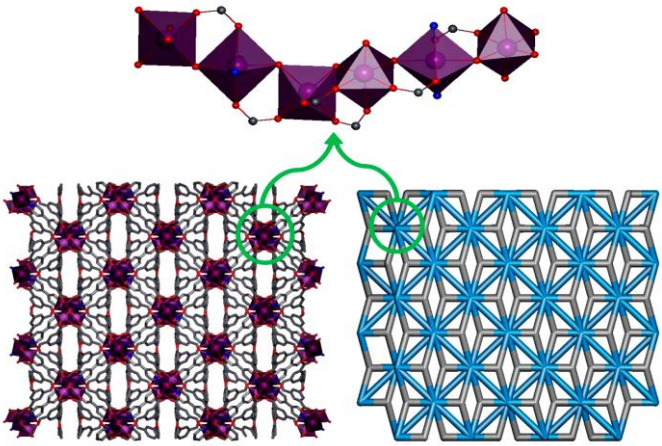

Figure 4.44 View of **InPF-18** 3D network and the corresponding rod packing topological representation (view in the (001) direction).

*4.3.1.4. The **InPF-19** material, $[In_2(popha)_2(4,4'\text{-bipy})_2]\cdot 3H_2O$*

The **InPF-19** material crystallizes in the monoclinic $P2_1/n$ space group (Table 4.34). The asymmetric unit consists of two different crystallographic In^{3+} ions, two fully deprotonated $popha^{3-}$ linkers, and two 4,4'-bipyridine molecules (Figure 4.45).

As a result, the formation of two InN_2O_6 PBUs of eight-coordinated indium centers is observed. They are built by two In-N bonds from the 4,4'-bipyridine ligands and six In-O bonds from the $popha^{3-}$ linker (Table 4.35), which display a L_6 (η^2-η^2-η^2) full chelating coordination mode for both indium metal centers.

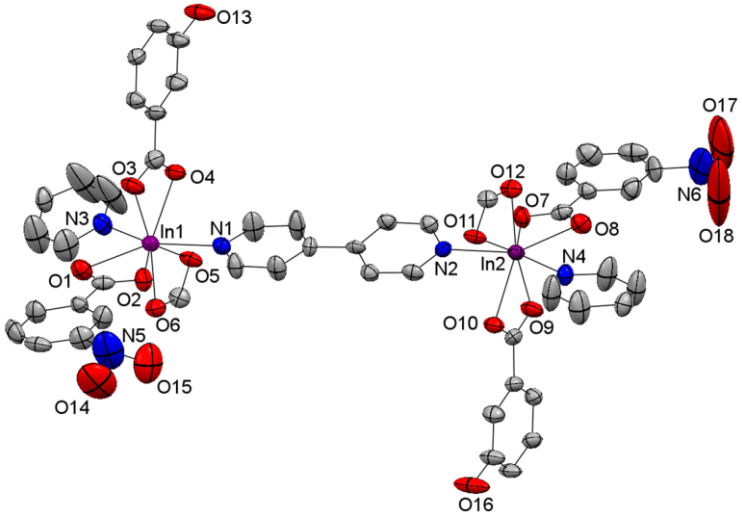

Figure 4.45 ORTEP representation of the asymmetric unit for **InPF-19**. Ellipsoids are displayed at the 50% probability level. Hydrogen atoms and water molecules were omitted for clarity. Symmetry codes: i) x, y, z; ii) ½ -x, ½+y, ½-z; x+1/2; iii) –x, -y, -z; iv) ½+x, ½-y, ½+z.

Table 4.34 Main crystallographic data for **InPF-19**

Identification Code	**InPF-19**
Formula	$C_{50}H_{28}N_6O_{18.25}In_2$
Molecular Weight	1234.42 g/mol
Temperature	296(2) K
Wavelength	Cu Kα 1.54178Å
Crystal System	Monoclinic
Space Group	$P2_1/n$
Unit cell dimensions	a = 17.4113(11) Å b = 18.4523(13) Å c = 17.9028(11) Å α = 90° β = 101.309(5)° γ = 90°
Volume	5640.1(6) $Å^3$
Z	4
Dx	1.454 $g.cm^{-.3}$
Absorption coefficient (μ)	7.170 mm^{-1}
F(000)	2456
Theta range for data collection	[3.24 – 58.92]º
Index ranges	-10<*h*<18, -20<*k*<20, -19<*l*<19
Reflections collected	26076
Completeness	97.9%
Absorption correction	Multi – scan
Max. and min. Transmission	0.5980, 0.3283
Refinement method	Fsqd
Data / restrains / parameters	7768/0/693
Goodness of fit on F^2	1.043
Final R indices [I>2σ(I)]	R1=0.0565wR2=0.1602
R indices (all data)	R1=0.0856 wR2=0.1839

Table 4.35 Relevant distances and angles for **InPF-19** material

Parameter	value	Parameter	value
In1 – O1	2.249(5)Å	In2 – O9	2.517(6)Å
In1 – O2	2.456(5)Å	In2 – O12	2.205(5)Å
In1 – O6	2.208(5)Å	In2 – O13	2.374(5)Å
In1 – O7	2.352(5)Å	In2 – O17	2.317(5)Å
In1 – O10	2.471(6)Å	In2 – O18	2.361(5)Å
In1 – N3	2.295(7)Å	In2 – N4	2.319(6)Å
In1 – N5	2.310(6)Å	In2 – N6	2.324(6)Å
In2 – O8	2.168(5)Å		

Along the *c* direction the InN_2O_6 PBUs are connected through the two 4,4-bipyridine molecules with In1····In2 distances of 11.695(1)Å and 11.746(1)Å. Connections along the *a* and *b* directions are made through the $popha^{3-}$ linker: In1····In1, In2····In2 and two In1····In2

PBUs at distances 15.554Å, 15.553Å, 9.693Å and 9.695Å, respectively, giving rise to a tridimensional structure. The structure of **InPF-19** presents semi-squared shaped open-window channels with 9.69Å x 11.69Å dimension in the *bc* plane (A); two different windows in *ab* plane are appreciated, one with 15.55 x 9.69Å dimension (B) and a small one with 8.33Å x 7.29Å dimension (C); the window in the *ac* plane has 10.83Å x 11.75Å dimension (D) (Figure 4.46).

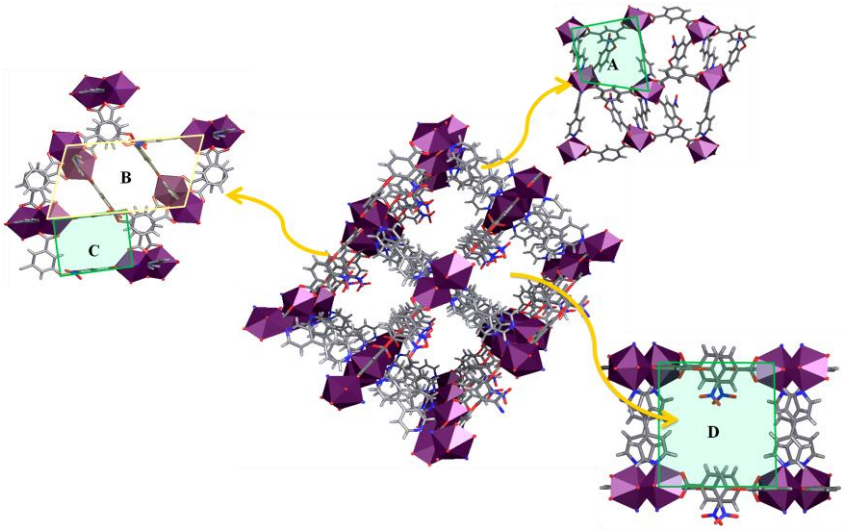

Figure 4.46 Representation of **InPF-19** 3D structure showing the semi-squared shaped open windows channels

In **InPF-19** the geometrical parameters of popha^{3-} present a θ distortion, which, as a consequence, produces the increment of the LCA_{1-3} values. The fact that two different In···In distances are determinate by the presence of two crystallographically different bipyridine molecules could explain the small distortion of the linker geometry (Table 4.36).

Table 4.36 Geometrical parameters of L_6 popha^{3-} linker of **InPF-19**

Parameter	Value	
	L6A	**L6B**
d_{1-2}	8.061Å	8.109Å
d_{1-3}	10.294Å	10.296Å
d_{2-3}	4.992Å	4.965 Å
θ	121.59º	121.55º
ω	84.55º	88.36º
LCA_{1-2}	98.91º	99.47º
LCA_{1-3}	160.32º	160.24º
LCA_{2-3}	61.42º	61.11º

The topological study shows a 3D interpenetrated (Class IIa) framework with a **dmc**, 3,4-connected binodal net, which also could be described as the derivated **fsc**-3,5-*Cmce-1* of a 3,5-connected binodal net [8] with point symbol {4.6.8}{$4.6^4.8^5$} when considering the double connectivity showed by the two crystallographically different 4,4-bipyridine along the *c* axis (Figure 4.47).

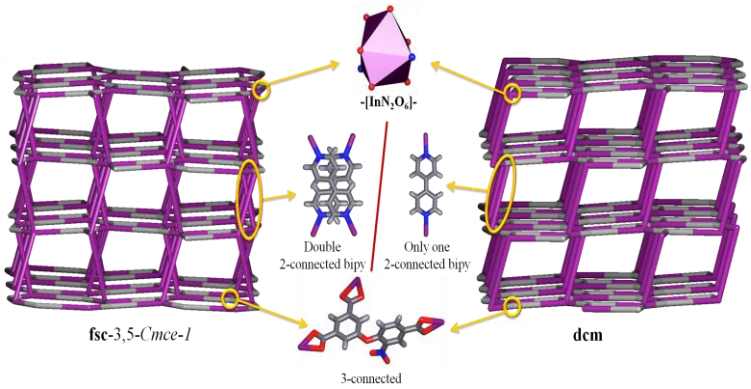

Figure 4.47 Two different topological representations of **InPF-19**.

*4.3.1.5. The **InPF-20** material, [In(OH)(Hpopha)]·x(1,7phen)·x(H_2O)*

The **InPF-20** material crystallizes in the monoclinic $P2_1/n$ space group (Table 4.37). The asymmetric unit consists of two crystallographically different In^{3+} ions, both of them placed at inversion centers, one partially deprotonated $Hpopha^{2-}$ linker, and one μ–OH group (Figure 4.48). A disordered 1,7-phenantroline molecule is placed inside the pores.

Table 4.37 Main crystallographic data for **InPF-20**

Identification Code	**InPF-20**
Formula	$C_{18}H_8N_{1.5}O_{10.3}In$
Molecular Weight	524.08 g/mol
Temperature	296(2) K
Wavelength	Cu Kα 1.54178Å
Crystal System	Monoclinic
Space Group	$P2_1/n$
Unit cell dimensions	a = 7.2776(7) Å b = 22.060(2) Å c = 15.0234(16) Å α = 90° β = 98.687(6)° γ = 90°
Volume	2384.3(4) $Å^3$
Z	4
Dx	1.460 $g.cm^{-3}$
Absorption coefficient (μ)	8.388 mm^{-1}
F(000)	1030
Theta range for data collection	[3.59 – 60.85]º
Index ranges	-7<*h*<7, -23<*k*<23, -15<*l*<14
Reflections collected	18527
Completeness	99.2%
Absorption correction	Multi – scan
Max. and min. Transmission	0.7302, 0.4876
Refinement method	Fsqd
Data / restrains / parameters	3682/0/272
Goodness of fit on F^2	1.126
Final R indices [I>2σ(I)]	R1=0.0816 wR2=0.2733
R indices (all data)	R1=0.1177 wR2=0.34302

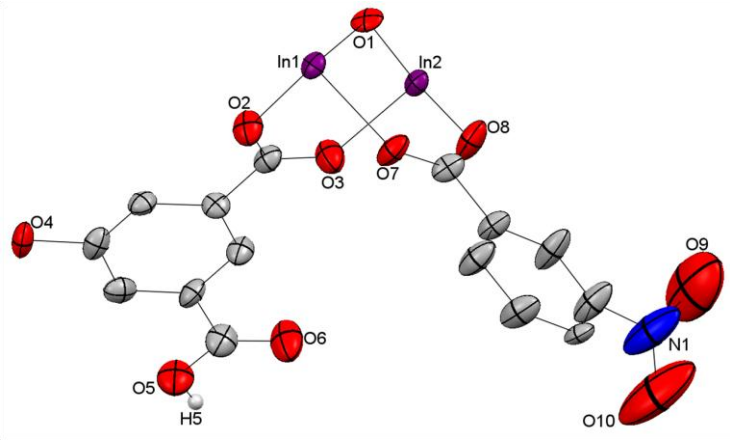

Figure 4.48 ORTEP representation of the asymmetric unit for **InPF-20.** Ellipsoids are displayed at the 50% probability level. Hydrogen atoms, 1,7-phen and water molecules were omitted for clarity. Symmetry codes: i) x, y, z; ii) ½-x, ½+y, ½-z; iii) -x, -y, z; iv) ½+x, ½-y, ½+z.

Both indium cations are InO_6 octahedral with the following bonds: two In-O bonds from the μ-hydroxyl group and four In-O bonds from the carboxylate groups (Table 4.38).

Table 4.38 Relevant distances and angles for **InPF-20** material

Parameter	Value	Parameter	Value
In1 – O1	2.078(6)Å	In1 ··· In2	3.639Å
In1 – O2	2.202(7)Å	In2 ··· In2^{ii}	14.127Å
In1 – O7	2.185(7)Å	In1··· In2^{iii}	13.345Å
In2 – O1	2.100(6)Å	d	9.281 Å
In2 – O3	2.147(9)Å	θ	117.06º
In2 – O8	2.132(7)Å	ω	68.77º
In1 ··· In1^{i}	13.530Å	LCA	123.13º

The L_7 linker configuration in the **InPF-20** material shows a similar geometry to the compounds bearing V-shaped dicarboxylates linkers (hfipbb^{2-} and dpmda^{2-}) despite the differences in the central sp^3 atom. The θ angle distortion could be related to the presence of an O-H···O synthon formed between the carboxylic parts of the neighbour linkers ($d_{H\cdots O}$ = 2,614 Å) (Table 4.38 and Figure 4.49).

The PBUs share vertices forming infinite -[In-O-In]- chains along *a* direction, the linker connects these chains by the two carboxylate bridging parts in *b* and *c* directions to built a 3-dimentional network, which can be described as a 4-connected uninodal net with a **cds** topology (Figure 4.49).

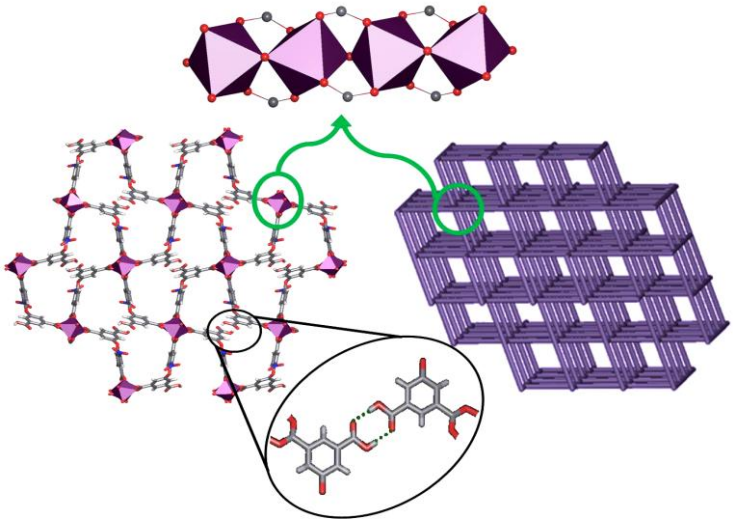

Figure 4.49 polyhedral representation of **InPF-20** and the corresponding **cds** topology of the 3D net.

*4.3.1.6. **InPF-21** materials, [In(popha)(1,10-phen)].xH$_2$O*

Two different polymorphs of [In(popha)(1,10-phen)] are presented; material **InPF-21α** was obtained as pure phase after adjustment of the reaction conditions. **InPF-21β** was obtained only as a by-product in the search of the ideal conditions for pure **InPF-21α** synthesis.

The **InPF-21α** material crystallizes in the triclinic *P-1* space group (Table 4.39). The asymmetric unit consists of one In^{3+} ion, one fully deprotonated $popha^{3-}$ linker and one 1,10-phenantroline molecule (Figure 4.50).

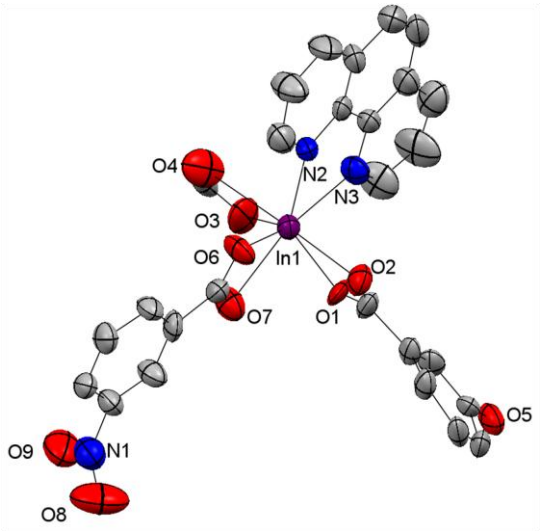

Figure 4.50 ORTEP representation of the asymmetric unit for **InPF-21α**. Ellipsoids are displayed at the 50% probability level. Hydrogen atoms and water molecules were omitted for clarity. Symmetry codes: i) x, y, z; ii) -x, -y, z.

Table 4.39 Main crystallographic data for **InPF-21** polymorphs

Identification Code	**InPF-21alpha**	**InPF-21beta**
Formula	$C_{27}H_{14}N_3O_{10}In$	$C_{27}H_{14}N_3O_9In$
Molecular Weight	655.23 g/mol	639.23 g/mol
Temperature	293(2) K	296(2) K
Wavelength	Cu Kα 1.54178Å	Cu Kα 1.54178Å
Crystal System	Triclinic	Monoclinic
Space Group	*P-1*	*C2/c*
Unit cell dimensions	a = 10.0013(5) Å b = 12.5596(6) Å c = 13.5491(7) Å α = 90° β = 105.631(3)° γ = 90°	a = 16.9620(14) Å b = 18.7428(13) Å c = 18.6539(14) Å α = 90° β = 113.558(5)° γ = 90°
Volume	1420.6(1) $Å^3$	5436.1(7) $Å^3$
Z	2	8
Dx	1.532 $g.cm^{-.3}$	1.562$g.cm^{-.3}$
Absorption coefficient (μ)	7.180 mm^{-1}	7.460 mm^{-1}
F(000)	652	2544
Theta range for data collection	[3.59 – 59.03]º	[3.69 – 63.14]º
Index ranges	-11<*h*<10, -13<*k*<13, -14<*l*<14	-16<*h*<16, -18<*k*<18, -17<*l*<18
Reflections collected	9980	11137
Completeness	95.8%	99.2%
Absorption correction	Multi – scan	Multi – scan
Max. and min. Transmission	0.6726, 0.3277	0.9291, 0.7546
Refinement method	Fsqd	Fsqd
Data / restrains / parameters	3890/0/378	2836/0/361
Goodness of fit on F^2	1.029	1.041
Final R indices [I>2σ(I)]	R1=0.0874 wR2=0.0955	R1=0.0555 wR2=0.1586
R indices (all data)	R1=0.2585 wR2=0.2722	R1=0.0709 wR2=0.1778

The indium environment is built with six In–O bonds from the carboxylate part of the $popha^{3-}$ linker with an average In-O distance of ~2.32Å and two In-N bonds from the 1,10-phen (Table 4.40).

Table 4.40 Relevant distances and angles for **InPF-21α** material

Parameter	Value	Parameter	Value
In1 – O1	2.384(10)Å	In1 – O6	2.157(11)Å
In1 – O2	2.226(10)Å	In1 – O7	2.569(15)Å
In1 – O3	2.452(11)Å	In1 – N2	2.292(13)Å
In1 – O4	2.212(10)Å	In1 – N3	2.324(13)Å

The InN_2O_6 polyhedra are connected through the L_6 linker type to built square 3 metal containing rings of 10.001 x 9.884 dimensions. The presence of the blocking phen molecule together with the square shaped rings give rise to 2D layers perpendicular to the (001) direction, with **hcb** topology of a 3-connected uninodal net (Figure 4.51).

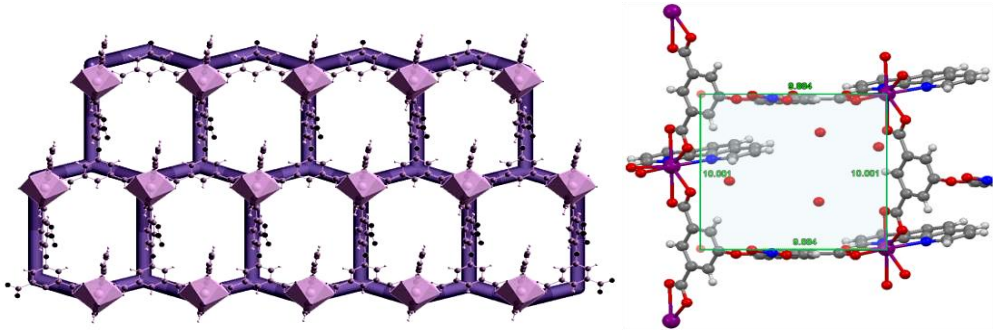

Figure 4.51 View of **InPF-21α** 2D layer with the **hcb** topological representation and the square shaped 3-metal ring.

The popha^{3-} linker with a L_6 mode (Table 4.41) supports the idea of higher distortion of the geometry when chelate ligands are used. When the θ and LCA angles of **InPF-21α** were compared to those obtained for **InPF-17** material (even though popha^{3-} linker showed different coordination modes), their geometrical parameters show similar values. In case of comparison between **InPF-21α** and **InPF-19**, in which popha^{3-} has the same L_6 coordination type, their geometrical parameters are very different.

Table 4.41 Geometrical parameters of L_6 popha^{3-} linker of **InPF-21α**

Parameter	Value
d_{1-2}	8.883 Å
d_{1-3}	8.907Å
d_{2-3}	5.039 Å
θ	117.22º
ω	86.89º
LCA_{1-2}	115.01º
LCA_{1-3}	115.80º
LCA_{2-3}	62.30º

The supramolecular network of **InPF-21α** is built through two weak interactions, which increase the dimensionality of the framework, connecting the 2D layers along *a* and *c* axis: i) $C\text{-}H_{phen}\cdots\pi_{phen}$ interaction of two neighbour 1,10-phenanthroline molecules at 3.575 Å distance between the middle of phenanthroline ring centroids and the hydrogen atom of one of the carbons from the phenanthroline molecule. ii) $C\text{-}H_L\cdots\pi_L$ ($d_{D\text{-}A}$: 3.388Å) interaction, which extend the network along (001) direction. The final 3D structure shows a **dia** topology with a 4-connected uninodal network (Figure 4.51).

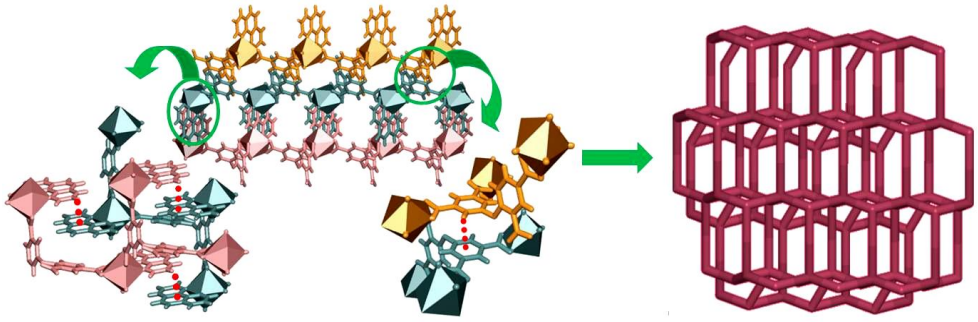

Figure 4.51 2D layers showing the C-H··· π interactions and the corresponding supramolecular 3D framework with **dia** topology of **InPF-21α**.

The Polymorph **InPF-21β** crystallizes in the monoclinic *C2/c* space group (Table 4.40). In this case, the In–O bonds have an average distance of ~2.32Å and the InN_2O_6 polyhedra are connected through the L_6 linker type building a 3D structure with rectangular 5 metal containing windows of 19.564 x 10.093 dimensions. This 3-connected uninodal net exhibits a **ths** topology with a class IIa interpenetration (Figure 4.52).

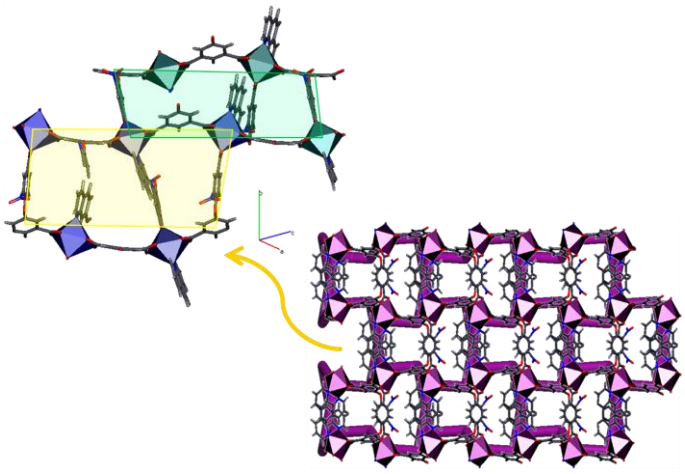

Figure 4.52 View of **InPF-21β** 3D structure and its **ths** topological representation showing the rectangular shaped 5-metal windows.

The increment in the framework dimensionality of **InPF-21β** is reflected in the geometrical parameters shown by the linker (Table 4.42), which presents a lower ω value and longer d_{1-3} distance than in the **InPF-21α** polymorph.

Table 4.42 Geometrical parameters of L_6 $popha^{3-}$ linker of **InPF-21β**

Parameter	Value
d_{1-2}	8.794Å
d_{1-3}	9.436 Å
d_{2-3}	5.011 Å
θ	117.90º
ω	72.44º
LCA_{1-2}	113.17º
LCA_{1-3}	126.46º
LCA_{2-3}	61.55º

4.4. New Bimetallic MOFs with H_2hfipbb linker

The aim of this part of the research is to find out if metal-organic frameworks (MOFs) composed of more than one metal in equivalent crystallographic sites (solid solution MOFs) can exhibit catalytic activity tunable by virtue of the metal ions ratio. Three new MOFs with general formula $[In_xGa_{1-x}(O_2C_4H_4)_{0.5}(hfipbb)]$, where x = 0.72, 0.55, and 0.28 named: **InGaPF-1**, **InGaPF-2** and **InGaPF-3**, were prepared. They are isostructural with their mono-metal counterparts, (4.1.section), which were synthesized with only Ga or In.

4.4.1. General Characterization

The infrared spectra for all the **InGaPF** components of this family show absorption in the regions 1615-1614cm^{-1} and 1422-1416cm^{-1}, which correspond to the bound carboxylate group ν_{asym}(C=O-M) and ν_{sym}(C-O-M), respectively. The absence of characteristic carboxylic acid bands at 3412cm^{-1}(OH), 1713-1702 cm^{-1} (C=O)ν_{asym} and 929cm^{-1} (C-O)ν_{sym} of the H_2hfipbb indicates complete deprotonation of the organic linker. Different carboxylate bands are appreciated when different coordination types are present in the material (Table 4.43).

Table 4.43 Characteristic COO^- stretching frequencies of **InGaPF** materials

Material	C=O ν_{as} cm^{-1}	C-O ν_s cm^{-1}	Linker coordination mode
InGaPF-1	1614	1416	$\eta^2\mu - L_3$
InGaPF-2	1615	1422	$\eta^2\mu - L_3$
InGaPF-3	1615	1417	$\eta^2\mu - L_3$
H_2hfipbb	1713-1702	929	acid

Thermogravimetric analyses (TGA) show that **InGaPF** materials are thermally stable up to 450-490ºC. The final residue for all three bimetallic MOFs is mainly is $InGaO_3$.
Furthermore, a full pattern profile refinement carried out for each one of the three compounds demonstrates that their unit cell parameters values are ranging between those of **InPF-11β** and **GaPF-1** (Table 4.44 and Figures 4.55-4.57).

The metal content in these compounds was determined with ICP and total X-ray fluorescence (TXRF) spectroscopy. The PXRD patterns of the solid solution MOFs indicate that the three compounds maintain the parent structure. The absence of peaks' splitting in the PXRD patterns of **InGaPF-1**, **InGaPF-2** and **InGaPF-3** rules out the possibility of having a mixture of two separate phases (Figure 4.54).

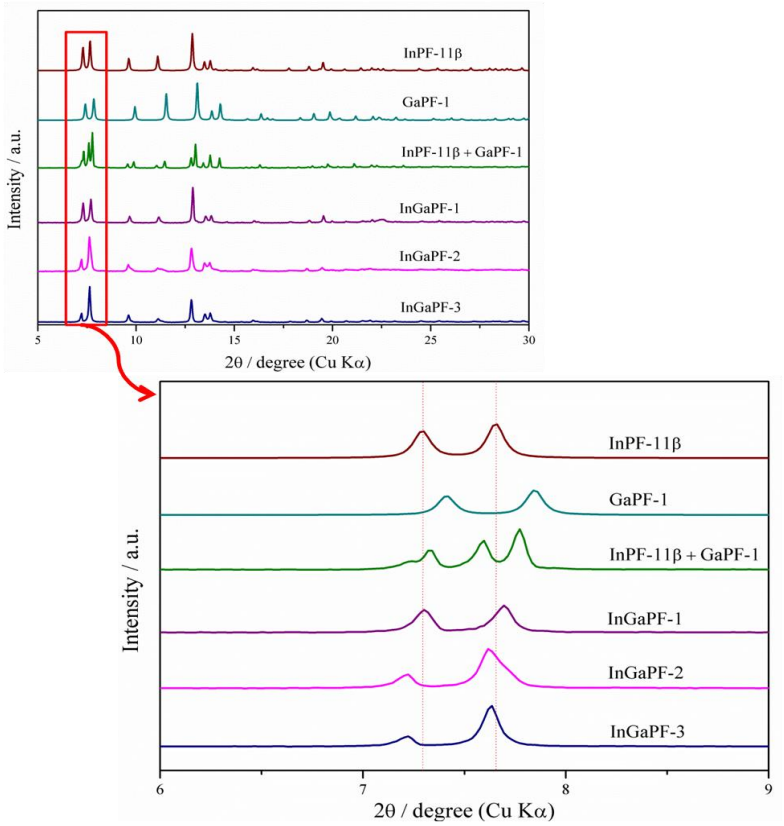

Figure 4.54 Powder diffraction pattern for the **InGaPF** materials showing the 2θ offset from their mono-metal counterparts

Table 4.44 Refined lattice parameters and refinement indicators for **InGaPF** materials [a]

Parameters	InGaPF-1	InGaPF-2	InGaPF-3
a (Å)	25.484 (1)	25.531 (2)	25.485 (2)
b (Å)	13.0993 (7)	12.902 (1)	13.022 (1)
c (Å)	13.1409 (7)	12.872 (1)	13.0592 (9)
β (°)	107.502 (4)	108.169 (8)	107.745 (5)
R_{wp} (%)	7.81	12.90	9.47
R_p (%)	6.07	9.49	7.16

[a] Full pattern profile refinements (Pawley refinements) were carried out using the Reflex module of Materials Studio v.7.0. A pseudo-Voigt function was used to define the profile, with a 12-coefficient polynomial background function.

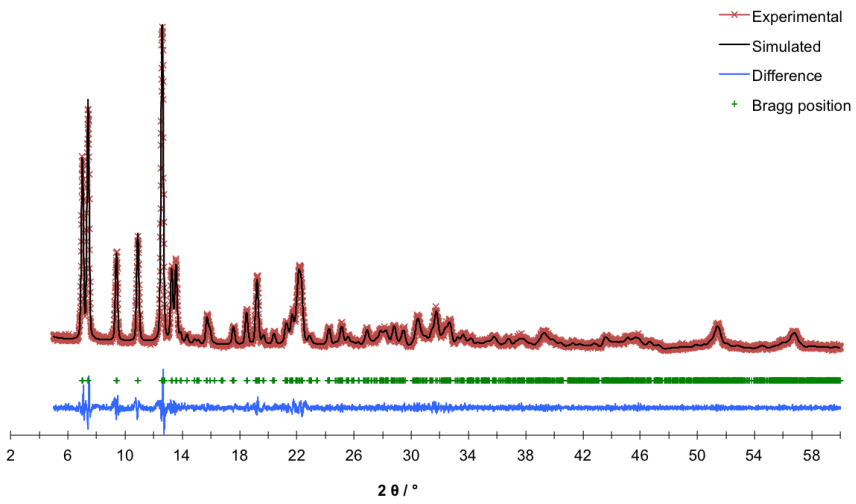

Figure 4.55 Full pattern profile refinement plot for **InGaPF-1**, showing experimental (red), refined (black) and difference (blue) patterns. Bragg positions are marked as green crosses.

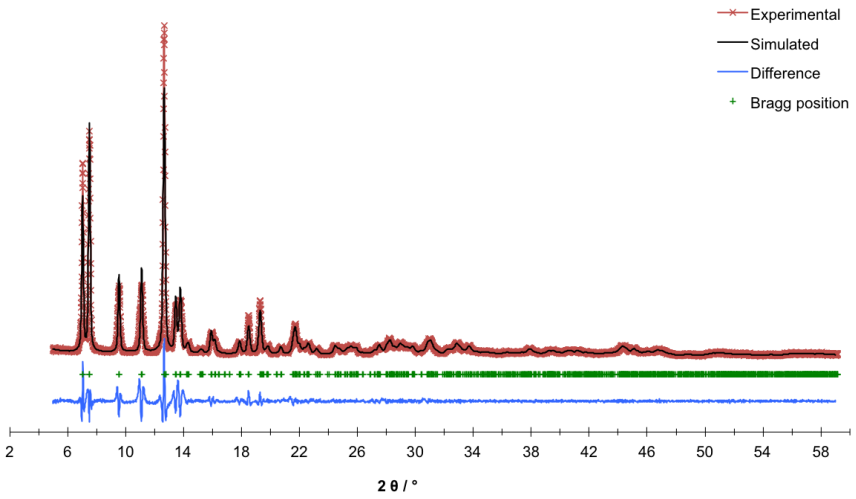

Figure 4.56 Full pattern profile refinement plot for **InGaPF-2**, showing experimental (red), refined (black) and difference (blue) patterns. Bragg positions are marked as green crosses.

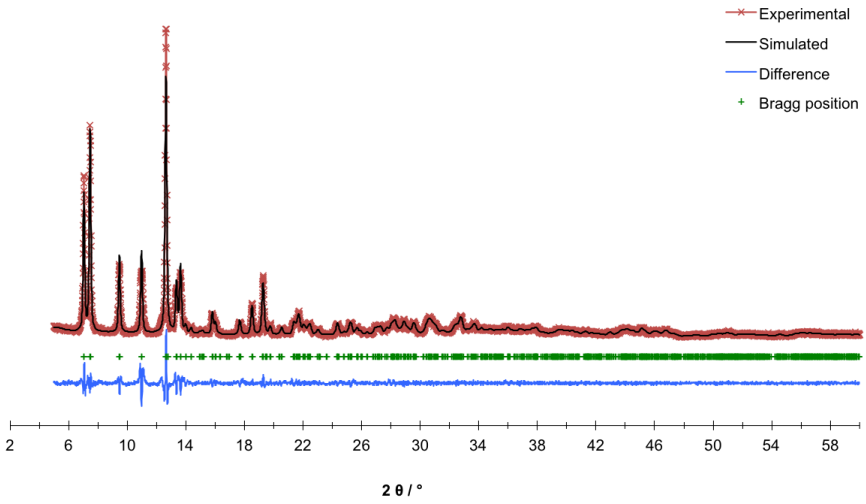

Figure 4.57 Full pattern profile refinement plot for **InGaPF-3**, showing experimental (red), refined (black) and difference (blue) patterns. Bragg positions are marked as green crosses.

4.5. References

1. S.-T. Zheng, F. Zuo, T. Wu, B. Irfanoglu, C. Chou, R. A. Nieto, P. Feng and X. Bu, *Angew. Chem. Int. Ed.* **2011**, *50*, 1849.

2. I. J. Bruno, J. C. Cole, P. R. Edgington, M. Kessler, C. F. Macrae, P. McCabe, J. Pearson and R. Taylor, *Acta Cryst.* **2002**, *B58*, 389.

3. L. Tang, Y.-P. Wu, F. Fu, Z.-L. Zhang and D. Zheng, *Acta crystallogr. Sect. E: Struct. Rep.* **2010**, *66*, 1390.

4. F. Gándara, B. Gómez-Lor, E. Gutiérrez-Puebla, M. Iglesias, M. A. Monge, D. M. Proserpio, N. Snejko, *Chem. Mater.* **2008**, *20*, 72.

5. V. A. Blatov, *TOPOS*, Samara State University, Russia. **2004**.

6. M. O'Keeffe and S. Andersson, *Acta Crystallogr.* **1977**, *A33*, 914.

7. T. G. Mitina and V. A. Blatov, *Cryst. Growth Des.* **2013**, *13*, 1655.

8. V. A. Blatov, D. M. Proserpio, *Acta Cryst.* **2009**, *A65*, 202.

CHAPTER 5

HETEROGENEOUS CATALYTIC ACTIVITY

Heterogeneous catalysis is one of the key elements of our industrialized society; with nine out of ten chemical processes linked to a catalytic process, it could be said that catalysis has an enormous impact in the global economy. Inside the heterogeneous catalysis domain, MOF materials are relatively new, but the concept of easy recovery and recycling that they can offer makes them appealing for industry processes. With this in mind, this chapter presents the heterogeneous catalytic activity study of twenty p-metal based MOFs, focusing in processes with low environmental impact, atom economy and waste reduction. The results presented have been published in several scientific journals and also gave rise to an international patent.

- L. M. Aguirre-Díaz, M. Iglesias, N. Snejko, E. Gutiérrez-Puebla and M. A. Monge. "*Send to Chemistry - European Journal*" **2015**.
- L. M. Aguirre-Díaz, F. Gándara, M. Iglesias, N. Snejko, E. Gutiérrez-Puebla and M. A. Monge**.** *J. Am. Chem. Soc.* **2015**, *137*, 6132.
- L. M. Aguirre-Díaz, M. Iglesias, N. Snejko, E. Gutiérrez-Puebla and M. A. Monge. *RSC Adv.* **2015**, *5*, 7058.
- L. M. Aguirre-Díaz, M. Iglesias, N. Snejko, E. Gutiérrez-Puebla and M. A. Monge. *CrystEngComm* **2013**, *15*, 9562.
- L. M. Aguirre-Díaz, M. Iglesias, N. Snejko, E. Gutiérrez-Puebla and M. A. Monge, PCT/ES2015/070572: "Material órgano-inorgánico cristalino basado en cationes del grupo XIII de la tabla periódica, procedimiento de preparación y uso" CSIC

Currently, *p*-metals are widely used in the industry, which has resulted in a six-fold increase in the amount of natural resources consumption over the past three decades. This rapidly rising demand for *p*-metal-containing materials has led to a dramatic increase in cost and it is estimated that there is only a several decades' supply of indium and gallium left at current consumption rates. Therefore, the development of economical and ecological procedures for material recycling is highly desired in all the synthetic fields.

Looking for recyclable catalytic systems with high reactivity that furthermore could present economic and environmental sustainability, a large number of *p*-metal compounds have been studied in catalysis because of their low environmental impact.[1]

MOFs materials offer a great potential as heterogeneous catalysts since they can have active sites in their frameworks, both in the organic linkers and in the metal centers.[2] Among them, *p*-MOFs have proved to be very effective as heterogeneous catalysts for reduction of alkenes, alkynes and α, β-unsaturated esters and nitroaromatic compounds, Knoevenagel condensation, methanolysis of epoxides, among others.[3]

Now, with the purpose to perform the catalytic activity study of the developed materials, some course of actions and terms has to be considered.

Considering the thermal stability of the framework for each material (TG and PXRD analysis), the selection of a standard catalytic reaction has to be done taking into account the nature of the material (in our case, the Lewis nature of both components, metal and organic part), only electronic interactions between the possible catalytic active sites of the material with the reactants are considered. With this in mind, the cyanosilylation of carbonyl compounds was selected as the organic transformation suitable for the catalytic activity test of the seventeen compounds developed in this thesis work.

The reaction conditions such as reactants stoichiometry, temperature, solvent and catalyst loading in the selected catalytic process had to be adjusted. In order to do it so, several Indium MOFs built with rigid organic linkers (bdc: 1,4-benzenedicarboxylic acid, btc: 1,3,5-benzenetricarboxylic acid and dpa: diphenic acid) previously obtained by our research group were explored using different reaction temperatures, solvents and catalysts loadings. Finally, the selected standard conditions for the cyanosilylation reaction were 2,5mol% of catalyst loading at 50ºC without solvent (Table 5.1).

The kinetic reaction study (Figure 5.1) performed with those catalysts described in Table 5.1, permitted to understand the activation time needed by each material, and to calculate the turnover frequency value (TOF), which allows the comparison between the evaluated catalysts and then the selection of the best material among all catalysts in the study.

Among the all employed measures in catalysis, one of the most commonly used is the yield (Y), which is the fraction of the desired product respective to the initial reactant (or the theoretical maximum) and is time dependent. Sometimes it is misused and confused with the conversion term (χ), which is not affected by the selectivity because measures the reactant consumption, regardless to the final product composition.

Table 5.1 Catalytic activity screening of InPF materials built with rigid ligands [a]

Catalyst	Formula	In_{CN}, Dimensionality	Cyanosilylation of benzaldehyde		
			Yield /% (h) [b]	TON	TOF
InPF-1	$[In_2(OH)_3(bdc)_{1,5}]$	6, 3D	97 (4)[c]	40	11
InPF-2	$[In(bdc)_{1,5}(2,2'\text{-bipy})]$	8, 2D	20 (1)	8	8
InPF-3	$[In_2(OH)_2(bdc)_2(1,10\text{-phen})_2]$	6, 2D	79 (0.33)[c]	40	271
InPF-4	$[In(btc)(H_2O)(2,2'\text{-bipy})]$	6, 2D	80 (4)[c]	40	73
InPF-5	$[In(btc)(H_2O)(1,10\text{-phen})]$	6, 2D	77 (1)[c]	40	82
InPF-6	$[In_2(dpa)_3(1,10\text{-phen})_2]\cdot H_2O$	8 y 7, 1D	98 (0.33)	40	391
InPF-7	$[In_2(OH)_2(dpa)_2(4,4'\text{-bipy})]\cdot 0.25H_2O$	7, 2D	53 (0.33)[c]	40	152
InPF-8	$[In_2(dpa)(Hdpa)(2,2'\text{-bipy})]\cdot 0.5H_2O$	8, 1D	90 (1.5)[c]	40	146

[a] Reaction conditions: solvent free, 50ºC, 2.5 mol% of catalyst under inert atmosphere (N_2) [b] Isolated yields (GC-MS). [c] After 6h the reaction was complete.

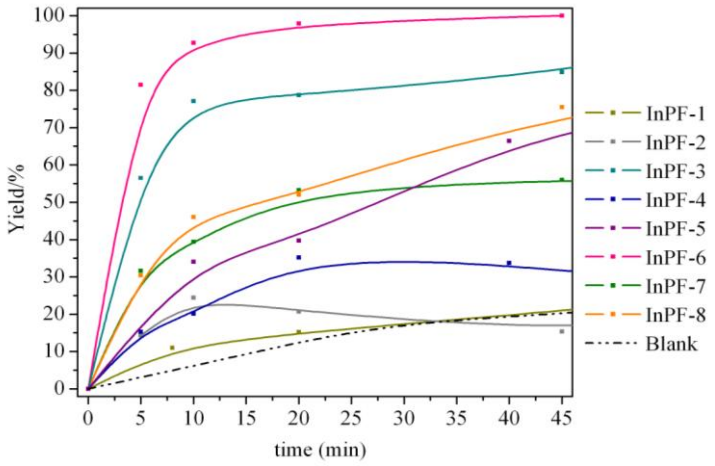

Figure 5.1 Kinetic profiles of indium MOFs built with rigid ligands acting as catalysts in the cyanosilylation reaction.

Another measure of efficiency of the catalytic reaction is the selectivity (S), which refers to the ratio between the desired and the total product of the catalytic reaction and depends on the temperature and the initial concentrations in the catalytic system; for this reason it should be presented as a standard quantity.[4]

Now, in order to focus on the catalyst role in the reaction and to be able to estimate and compare the catalytic activities of the materials under evaluation, their corresponding TON (turnover number) and TOF (turnover frequency) values had to be reported. A big debate in different catalytic areas is still generated when the concept for both terms has to be defined, which sometimes leads to a confusion and the use of the same concept for TON and TOF.

So, emphasizing the role of the catalyst, the TON value deals with the lifetime robustness of the material, and typically corresponds to the total number of turnovers the catalyst can achieve until its decays totally, regardless of time and being directly related to the final conversion reached by the catalytic sites of the material. However, due to the difficulties in

estimation of the half-life time of the tested catalysts, in this work the TON was calculated following the Boudart's concept[5] and considering the formula (5.1)

$$TON: (\chi / \text{mol catalyst}) \quad \textbf{5.1}$$

The TOF value represents the instantaneous efficiency of the catalyst, expressed as a frequency with units of [time^{-1}]. In this work, the TOF is a function of the catalyst loading (TOF_{mass})[6], which together with the conversion rate ($\Delta\chi$) deduced from the slope of the conversion curve, gives the final formula (5.2)

$$TOF_{mass}: \Delta\chi \text{ x [mol of reactant / mol catalyst]}/ \Delta t) \quad \textbf{5.2}$$

Following the proving that the crystalline structure of the catalytic material was not changed after one catalytic cycle (using the PXRD technique), the sample has to be reused several times [4-10] in order to evaluate the recyclability and the reproducibility of the catalytic system.

In case of the material with the highest catalytic activity in each following sections, a leaching test was performed verifying the heterogeneous behavior of the catalytic system.

5.1. Study of the Catalytic Activity of the developed MOFs using the Cyanosilylation reaction

The catalytic activity of seventeen MOFs materials developed in this thesis was determined by using the fundamental Lewis acid-catalyzed carbon-carbon bond forming reaction, known as cyanosilylation of carbonyl compounds (Scheme 5.1). MOFs materials catalyze the well-known reaction between the trimethylsilyl cyanide (TMSCN) and a carbonyl compound (benzaldehyde or acetophenone) to yield a cyanohydrin derivative.

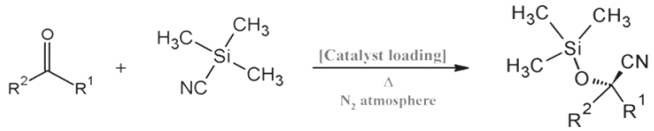

Scheme 5.1 Cyanosilylation reaction of carbonyl compounds

5.1.1 Catalytic activity of MOFs built with the hfipbb^{2-} linker

Cyanosilylation reactions were performed under standard conditions (2.5% mol of catalyst loading, without solvent at 50ºC). The initial tests showed that all compounds (Scheme 5.2) exhibit good catalytic behavior in the cyanosilylation of benzaldehyde and acetophenone (Table 5.2).

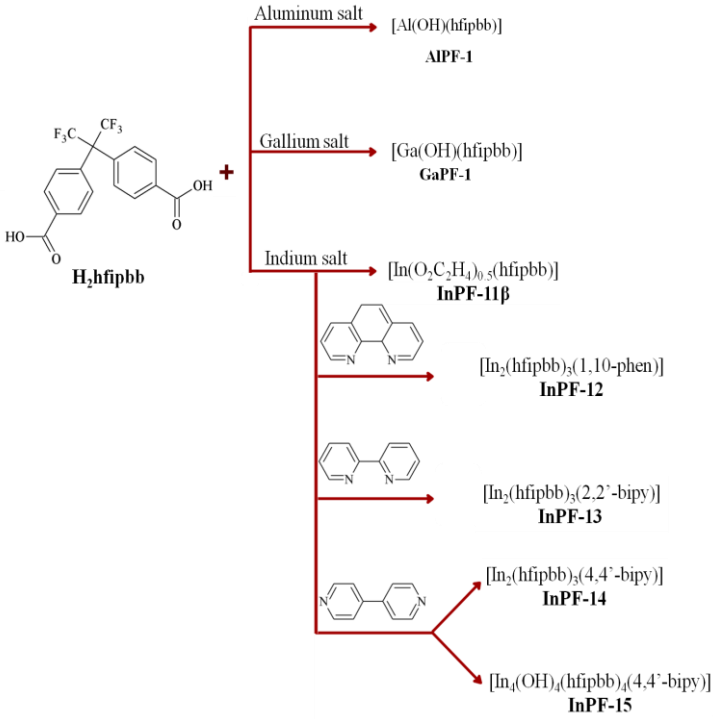

Scheme 5.2 New **MPF** materials with H_2hfipbb organic linker and additional nitrogenated ligands.

Table 5.2 Screening of **MPF** materials as catalysts for cyanosilylation reaction [a]

Material	In_{CN}, Dimensionality	Topology	Benzaldehyde		Acetophenone	
			Yield/% [b] (h)	TON	Yield /% [b] (h)	TON
AlPF-1	6, 3D	**dia**	94 (1)	38	55 (4) [c]	22
GaPF-1	6, 3D	**dia**	99 (0.08)	40	80 (2) [c]	32
InPF-11α	6, 2D		99 (0.67)	40	65 (4)	26
InPF-11β	6, 3D	**dia**	99 (0.25)	40	70(4) [c]	28
InPF-12	7, 1D	**SP1**	99 (2)	40	24 (4)	10
InPF-13	7, 1D	**SP1**	93 (2)	37	41 (2)	16
InPF-14	7, 3D	**dia**	99 (0.75)	40	45 (1)	18
InPF-15	6, 3D	**hex**	80 (1.5)	32	77 (4)	31

[a] Reaction conditions: 2.5 mol% of catalyst under N_2 atmosphere and 50ºC (benzaldehyde) or 80ºC (acetophenone), without solvent. [b] Yields (GC-MS). [c] Reactions performed at 70ºC

*5.1.1.1. The **AlPF-1**, **GaPF-1** and **InPF-11β** isostructural catalysts*

The three of them showed good catalytic activity for the cyanosilylation reaction being gallium the fastest with conversion ≥ 99% in 5 minutes (benzaldehyde) and 80% in 2 hours (acetophenone).

In case of the indium MOFs, the 3D network of **InPF-11β** is more efficient compared with its 2D counterpart **InPF-11α**[7] (Table 5.2).

The crystal structures of the three evaluated materials remain unchanged after the end of the catalytic process as shown in Figure 5.2.

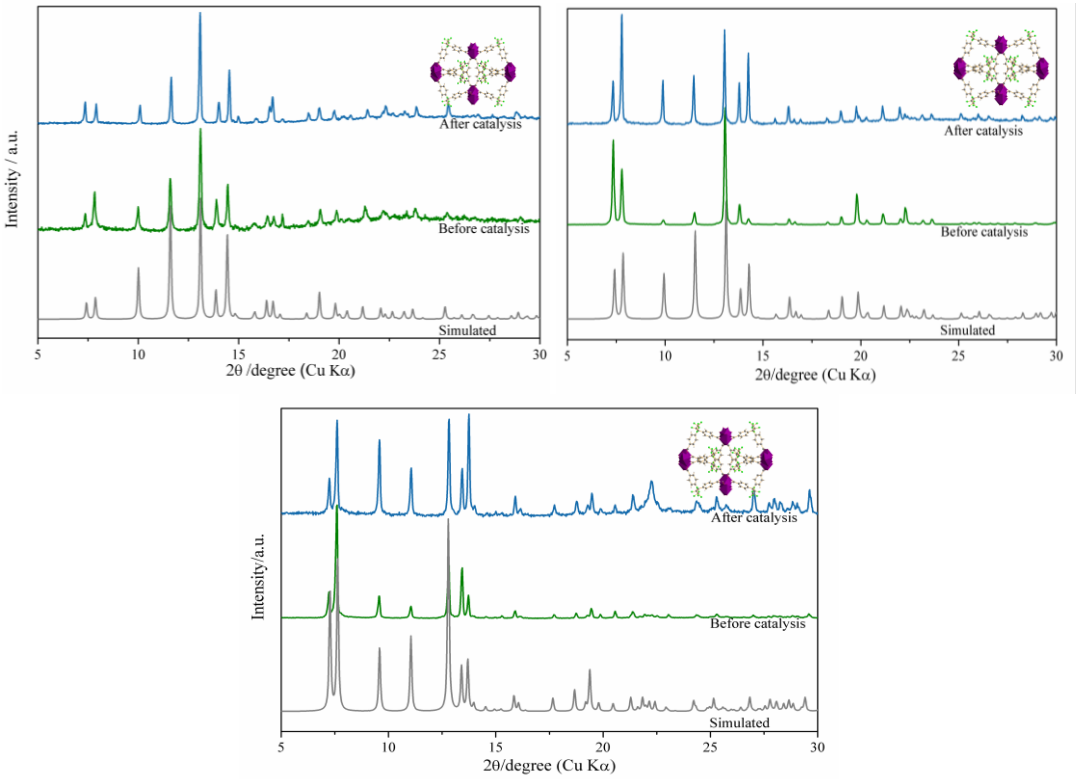

Figure 5.2 Simulated, experimental and after first catalytic reaction PXRD patterns of **AlPF-1** (Above: left), **GaPF-1** (Above: right) and **InPF-11β** (Down).

The cyanosilylation reaction was also performed at different temperatures and different loadings % of **GaPF-1** catalyst; the results in Table 5.3 show that high yields can be obtained even when temperature decreases. Thus, the use of 1% mol catalyst loading at room temperature (25ºC) is the best work conditions.

Table 5.3 Screening of different **GaPF-1** loadings and reaction temperatures. [a]

Cat. loading [mol%]	Temperature [ºC]	time h	Yield [b] %	TON
10	40	2	>99	10
10	25	0.08	>99	10
5	25	0.08	>99	20
2.5	25	0.08	>99	40
1.0	40	0.75	>99	99
1.0	25	2	>99	99

[a] Reaction conditions: without solvent, under N_2 atmosphere. [b] Yields (GC-MS)

*5.1.1.2. **InPF-12** to **InPF-15** catalysts*

The **InPF-n** (n = 12-15) materials were tested for the cyanosilylation of benzaldehyde and acetophenone (Table 5.2). It was found that the reactivity changes as a function of the carbonyl compound nature. A study of the reaction kinetics (Figure 5.3) was performed, to understand the catalytic performance of each material; their TOFs values were determined.

The different catalysts behavior observed when carbonyl source changes from benzaldehyde to acetophenone, is due to the steric hindrance introduced by the $–CH_3$ group present in the acetophenone, which makes it difficult the access to the active site on the metallic center in those catalysts with coordination number 7.

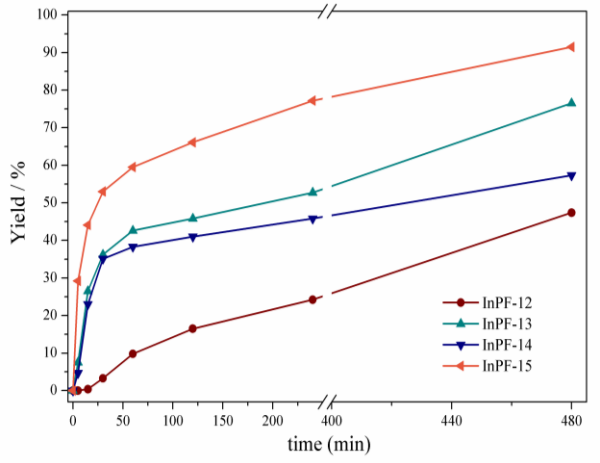

Figure 5.3 Kinetic profiles of **InPF-12** to **InPF-15** catalysts in the cyanosilylation of acetophenone.

The PXRD patterns of the recovered **InPF-14** and **InPF-15** after the catalytic reactions indicate that these materials do not suffer any structural change. However, **InPF-12** and **InPF-13** do not maintain structural integrity after the catalytic reaction, as shown in their PXRD patterns (Figure 5.4).

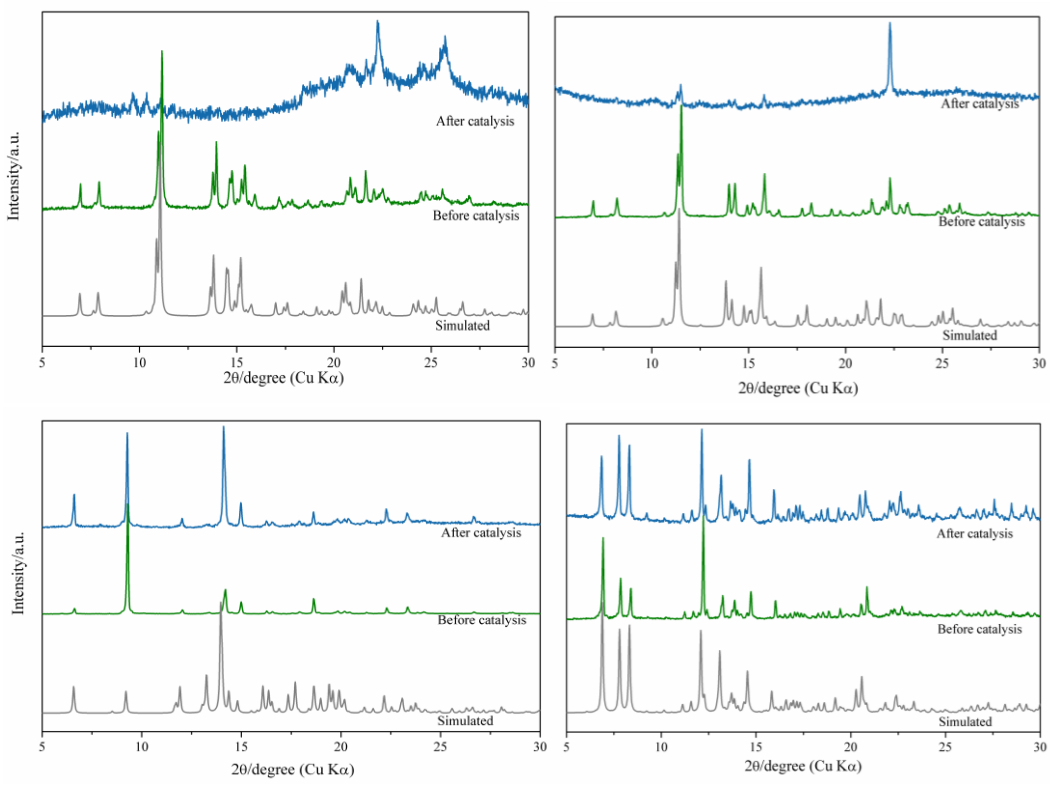

Figure 5.4 Simulated, experimental and after first catalytic reaction, PXRD patterns of **InPF-14** (left) and **InPF-15** (right).

From the data of the Table 5.2 it is evident that exits a structure/catalytic ability relationship. In-MOFs with blocking chelate ligands (1,10-phen and 2,2'-bipy) show lower conversion and higher reaction times than those without any auxiliary ligand or with a non-chelate second linker (4,4'-bipy) in their structure. **InPF-15**, with coordination number 6, and μ-OH groups, shows the best catalytic performance since it owns more available active sites around the metallic center. Besides the Lewis acid sites of the indium cation, **InPF-15** possesses in its structure two Lewis base moieties (μ-OH and C=O groups not coordinated to indium cation); due to the presence of this feature, the catalytic system can be considered of a two-component type; a mechanism based on the "dual activation" phenomenon[8] is proposed (Figure 5.5), in which the carbonyl compound is activated by the interaction with the Lewis acid site on the metallic center of our catalyst and the silyl group is activated simultaneously by the Lewis base moieties being **InPF-15** the best catalyst, even for the most sterically hindered substrates.

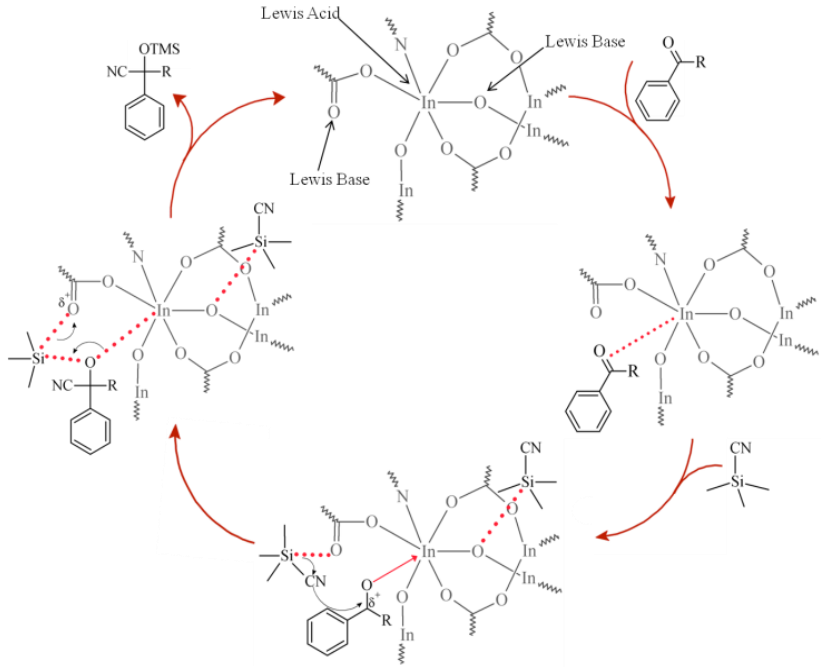

Figure 5.5 Mechanism proposed for the Indium mediated cyanosilylation of carbonyl compounds for **InPF-15** catalyst.

Another important point was the study of the catalyst loading influence (Table 5.4). In order to do it, previous works showing several indium salts with catalytic activity in the ketone cyanosilylation reaction were considered. Among them, $InBr_3$ (TON: 90, using 1mol %) and $InCl_3$ (TON: 9, using 10mol %) showed good yields at mild conditions.[1,9]

The screening of different catalytic loadings of **InPF-15** material allows to determinate the ideal catalyst amount to reach high yields (TON: 990, using 0.1mol %) with the advantage of a solvent free reaction, without side products and an easy recovery and reuse of the catalyst (Table 5.4). The cyanosilylation reaction was also performed at different temperatures using 0.1mol% of **InPF-15** as catalyst showing that faster reaction times and higher yields can be obtained when temperature rises. Thus, we decided to use 0.1% mol as catalyst loading and

80ºC for the subsequent reactions.

Table 5.4 Cyanosilylation reaction yields using acetophenone as substrate in the presence of different **InPF-15** loadings and temperatures. [a]

Cat. loading [mol%]	Temperature ºC	Yield %	time h	TON	TOF h^{-1}
2.5	80	>99	48	40	140
1.0	80	89	18	89	172
0.1	80	>99	7	990	2158
0.1	50	90	96	900	-
0.1	25	79	120	790	-

[a] Reaction conditions: Without solvent, under N_2 atmosphere. [b] Yields (GC-MS)

The scope of the cyanosilylation of ketones using **InPF-15** as catalyst is presented in Table 5.5; the results reveal that higher yields are obtained in case of non-aromatic ketones compared to the aromatic ones. Reactions with linear aliphatic ketones proceeded efficiently and gave the corresponding product in yields higher than 96%. Yields were even higher in case of the cyclic ketones (>99%). Less reactive but still with good yields, aromatic ketones gave the corresponding cyanohydrin trimethylsilyl ethers yields between 87-95%.

Table 5.5 Scope of the **InPF-15**-catalyzed cyanosilylation of ketones [a]

Ketone 1	Product 2	time h	Yield [b] %	TOF h^{-1}
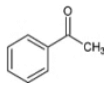 **1a**	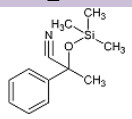 **2a**	3	87	2158
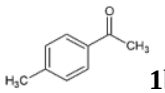 **1b**	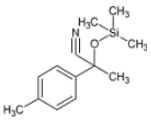 **2b**	3	89	2406
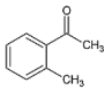 **1c**	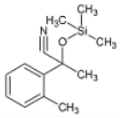 **2c**	3	95	5424
 **1d**	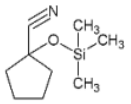 **2d**	2	98	10951
 **1e**	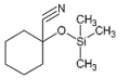 **2e**	2	>99	12048
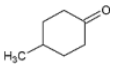 **1f**	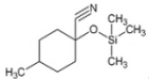 **2f**	4	>99	11686
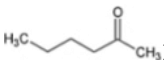 **1g**	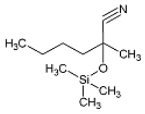 **2g**	2	>99	11400
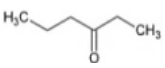 **1h**	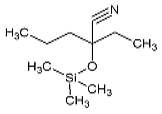 **2h**	2	96	10560

[a] Reaction conditions: 0.1 mol% of catalyst under N_2 atmosphere at 80ºC, without solvent. [b] Yields (GC-MS)

The results of the reactions carried out with acetophenone derivatives with electron-donating substituents show that with the *o*-methylacetophenone higher yields are reached (95%) while the *p*-methylacetophenone only reaches 89%.

The recyclability of the **InPF-15** material was also tested; the catalyst was recovered after centrifugation and washed several times with acetone, then dried at 130ºC and reused. This experiment showed that material maintains its crystallinity even after seven catalytic cycles, with only a small decrease of its catalytic activity, probably due to the losses during the recovery of the catalyst (Figure 5.6).

Hot filtration experiments reveal that **InPF-15** is a truly heterogeneous catalyst.

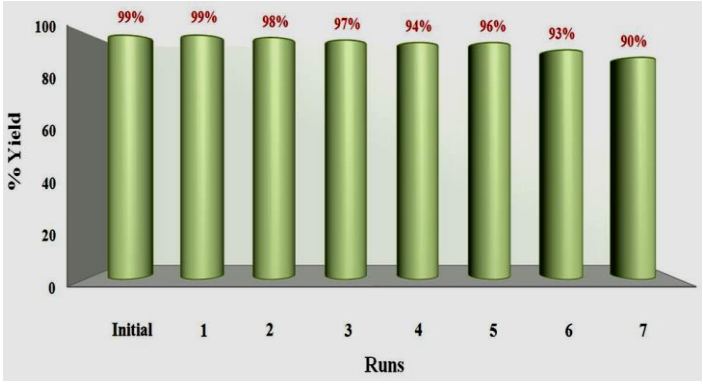

Figure 5.6 Recycling experiments using **InPF-15** as catalyst

5.1.2 Catalytic activity of MOFs built with the dpmda^{2-} linker

Reactions were performed with 2.5% mol of catalyst loading, without solvent at 50ºC temperature. The initial tests showed that all compounds (Scheme 5.3) exhibit good catalytic behavior in the cyanosilylation of carbonyl compounds (Table 5.6).

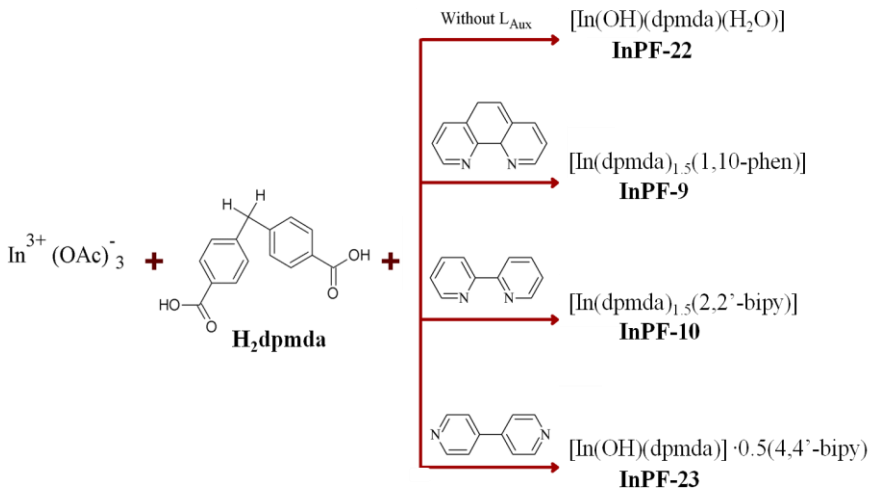

Scheme 5.3 Indium MOFs with dpmda^{2-} linker and nitrogenated ligands.

Table 5.6 Catalytic activities of InPF materials bearing the $dpmda^{2-}$ linker [a]

Catalyst	In_{CN}, Dimensionality	Topology	Cyanosilylation of benzaldehyde		
			Yield [b] % (h)	TON	TOF h^{-1}
InPF-9	7, 2D	**hcb**	81 (1)	32	183
InPF-10	7, 2D	**hcb**	82 (1)	33	222
InPF-22	7, 3D	**dia**	99 (0.08)	40	500
InPF-23	6, 3D	**pcu**	99 (0.08)	40	500
Blank	-	-	64 (6)	-	-

[a] Reaction conditions: 2.5 mol% of catalyst under inert atmosphere (N_2) at 50ºC, without solvent. [b] Isolated yields (GC-MS). After 4h all catalytic reactions were complete.

According to the obtained results the catalytic activity of the InPF materials in cyanosilylation reaction decreases in the order **InPF-23 = InPF-22 > InPF10 > InPF-9**. To explain this behavior, we analyzed the compounds structural characteristics. Some observations of these four catalysts for cyanosilylation reaction can be made: i) MOFs without additional nitrogenated linkers **InPF-22** and **InPF-23** are more catalytically active than those with chelate linker in their structures. ii) The MOF **InPF-10** with 1,10-phen in its structure, shows a faster activation time compared to the MOF **InPF-9**, with 2,2'-bipy. Both **InPF10** and **InPF-9** materials own isorreticular nets; **InPF-9** shows a slightly larger 6R dimensions, which could explain to some extent the close TOF values for this two catalysts and the trend reverse. ii) The network dimensionality seems to be a decisive factor, since **InPF-23** and **InPF-22** with 3D structures are more active in cyanosilylation reaction than **InPF-10** and **InPF-9** with 2D structures**.**

All in all, a mechanism of two-component catalytic system, based on the "dual activation" phenomenon,[8] could be proposed in case of materials **InPF-10** and **InPF-9**, which possess Lewis acid / Lewis base moieties capable to activate simultaneously both electrophile and nucleophile groups.

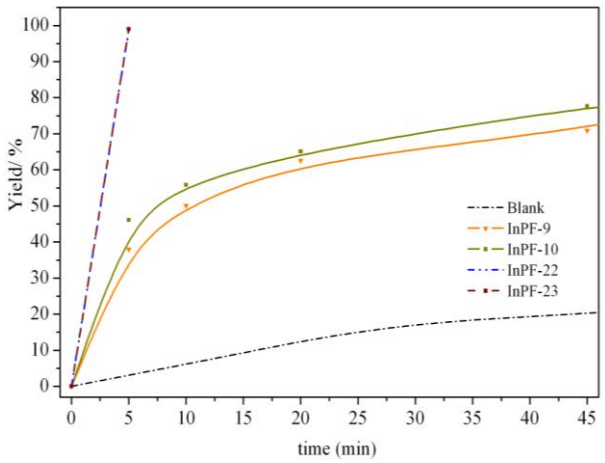

Figure 5.7 Kinetic profiles for the cyanosilylation of benzaldehyde showing InPF materials.

In case of materials **InPF-22** and **InPF-23**, their catalytic mechanism is through their Lewis acid metal active sites (7 and 6, respectively), where the reactants can access inside the channels of these 3D MOFs offering a faster electronic interaction between the carbonyl derivates and the catalyst active sites than those with 2D frameworks.

The inorganic 2D layers present in the supramolecular net of **InPF-22 (**Chapter 4, section 4.2.2.1) could explain the similarity in the catalytic activity with the **InPF-23** material despite their differences in the coordination environment (7 and 6 respectively); these 2D layers in **InPF-22** carry a large Lewis acid catalytically active surface, which compensates the higher CN (7) compared to that of **InPF-23** (6).

The 3D framework of **InPF-23**, which contains the 4,4'-bipyridine molecule inside the pores, has low CN and despite the blocking access to those, the catalytic activity seems to depend only on the interaction between the MOF's inorganic chains and the organic reagents. Also, in order to confirm this theory, several trials were performed with the aim of removing the bipyridine molecule with no success achieved: after the **InPF-23** material was recovered from the catalytic reaction, and washed several times, elemental analysis confirmed the presence of the bipyridine molecule.

The PXRD patterns of the recovered MOFs after the catalytic reactions indicate that these materials do not suffer any structural change (Figure 5.8).

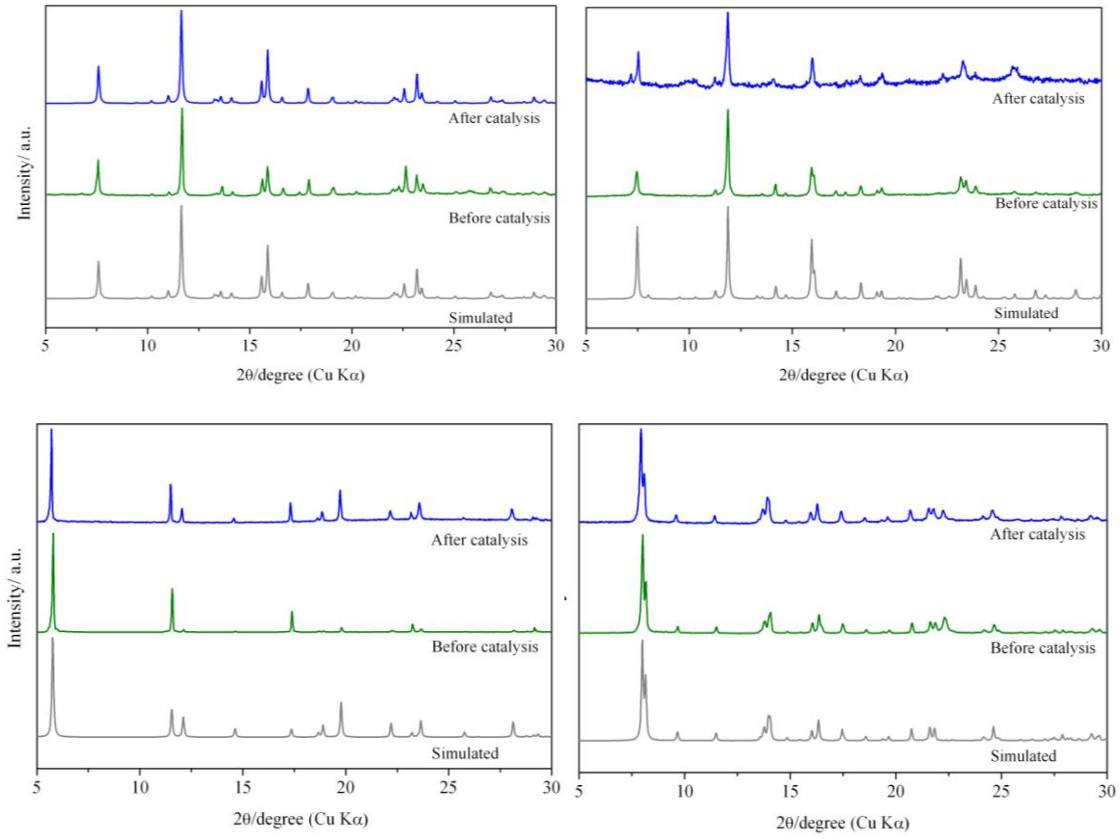

Figure 5.8 Simulated, experimental and after the first catalytic reaction, PXRD patterns of **InPF-9** (Above: left), **InPF-10** (Above: right), **InPF-22** (Down: left) and **InPF-23** (Down: right).

5.1.3. Catalytic activity of MOFs built with the popha^{3-} linker

In this section, the cyanosilylation reaction was performed using low catalytic amounts (1-5mol%) of MOFs bearing popha^{3-} linker (scheme 5.4), under inert atmosphere, without solvent and at room temperature (25ºC). The results (Table 5.7 and Figure 5.9) showed that catalysts, which posses indium atoms with coordination number (CN) six and seven (**InPF-16**, **InPF-17**, **InPF-18** and **InPF-20**), gave good yields in short reaction times, while those with CN 8, showed no catalytic activity, evidencing once again the important role that the metallic center -Lewis acid active site- plays in the reactants activation. Thus, **InPF-19** and **InPF-21** materials, which do not present available Lewis acid sites or any other groups suitable to interact with the substrates, were not considered as catalysts in the subsequent studies.

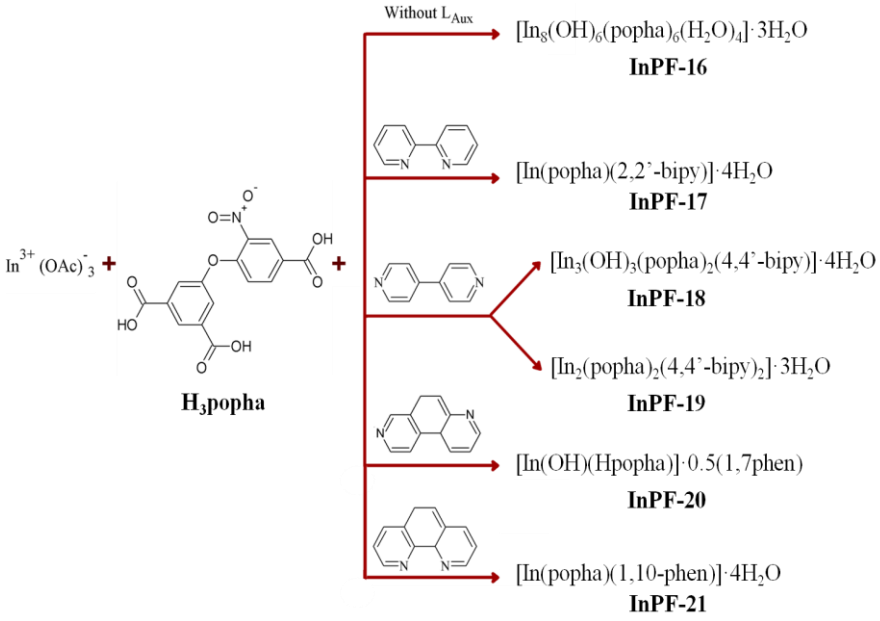

Scheme 5.4 In-MOFs with the tripodal V-shaped H_3popha linker and additional nitrogenated ligands.

Table 5.7 Screening of Indium MOFs as catalysts in the cyanosilylation reaction. [a]

Material	In_{CN}, Dimensionality	Topology	Benzaldehyde		Acetophenone	
			Yield [b] % (h)	TON	Yield [b] % (h)	TON
InPF-16	6, 3D	**llj**	99 (0.17)	99	99 (16)	20
InPF-17	7, 2D	**hcb**	67 (18)	68	53 (24)	11
InPF-18	6, 3D	**3,8L18**	85 (18)	83	80 (24)	16
InPF-19	8, 3D	**dmc**	10 (12)	10	15 (12)	6
InPF-20	6, 3D	**cds**	71 (12)	87	76 (24)	15
InPF-21	8, 2D	**hcb**	27 (12)	27	5 (12)	2
Blank	-	-	28 (24)	-	No reaction	

[a] Reaction conditions: carbonyl compound (0.001mol), TMSCN (0.001mol), catalyst: 1 mol% for benzaldehyde, 5mol% (acetophenone), without solvent, N_2 atmosphere at 25ºC. [b] Yields by GC-MS.

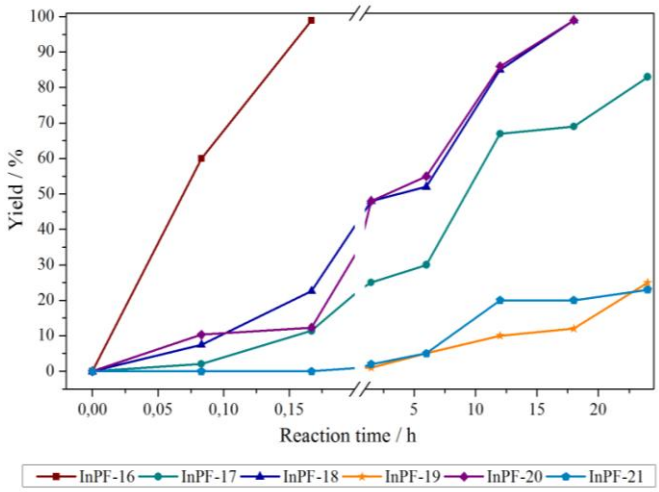

Figure 5.9 Kinetic profiles for InPF materials in the cyanosilylation of benzaldehyde

InPF-16, **InPF-17**, **InPF-18** and **InPF-20** materials own, besides indium Lewis acid sites, Lewis base moieties such as bridging hydroxyl groups (μ-OH) and/or non coordinated carbonyl groups (free C=O). This permits for two-component type catalytic systems, which follow a mechanism based on the "dual activation" phenomenon.[8] According to it, the carbonyl compound is activated by the interaction with the metallic center Lewis acid site, while the silyl group is activated simultaneously by the Lewis base moieties (Figure 5.10).

Although the presence of a central oxygen atom between the phenyl rings in the H_3popha organic ligand could be considered as a Lewis base moiety, the presence of the nitro group at the *orto* position in one of the phenyl rings withdraws the charge density of this central oxygen delocalizing the electron charge. Consequently, the basic character of this moiety decreases, not showing any influence on the catalytic behavior of the **InPF** materials. No differences between the two **InPF** catalyst series (CH and MW) behavior were found.

By increasing the number of active sites in the catalyst (acid and basic moieties) higher product yields at shorter reaction times are expected. **InPF-16** contains eight-indium clusters, μ-OH- and non-coordinated C=O groups (as possible Lewis base sites) along its framework with a M/CO/OH ratio: 4/3/3, and two easily displaceable coordinated water molecules. Consequently, it exhibits an outstanding catalytic activity reaching the 99% of yield in 10 minutes. **InPF-16**, being the best one of these MOFs in cyanosilylation reaction, was also tested with more hindered reactant like acetophenone. Although, as expected, the catalyst loading had to be increased for this latter, the yield became 67% for 2.5 mol% of catalyst loading, at room temperature in only 4h. For reaction completion a 5mol% of catalysts loading was necessary to obtain 99% of product yield in 16 hours at room temperature without any solvent (Table 5.7).

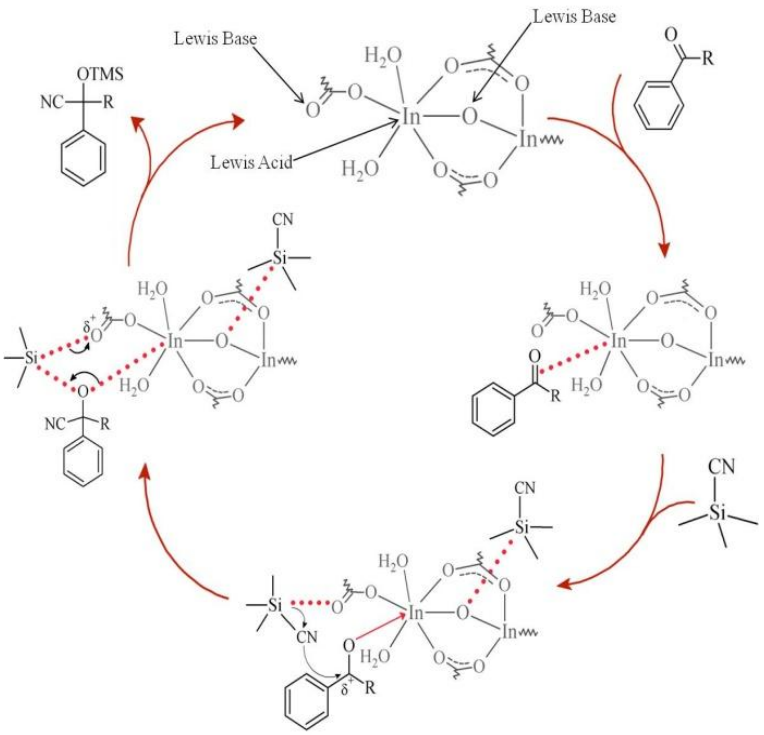

Figure 5.10 Proposed mechanism for the **InPF-16**-catalyzed cyanosilylation of carbonyl compounds.

The differences in indium coordination numbers and the presence or absence of bridging hydroxyl groups in the structures make the distinction between the catalytic activity of **InPF-17** and **InPF-18** materials. In **InPF-17**, the higher indium CN (7) together with the absence of μ-OH groups makes it a slower catalyst with moderate yields at longer times (TON: 68), compared to a more active **InPF-18** catalyst (Table 5.7). This latter contains inorganic chains -[In-O-In]- of six-connected indium cations, bridging hydroxyl groups and the free C=O groups (M/C=O/OH ratio: 3/2/3 for **InPF-18** and M/C=O ratio: 1 for **InPF-17**) along its framework.

On the other hand, the PXRD patterns (Figure 5.11) of the recovered **InPF-16, InPF-17 to InPF-19** and **InPF-21** after the catalytic reactions indicate that these materials do not suffer any structural change. However, after the first catalytic reaction the **InPF-20** crystalline structure was not preserved, meaning that interaction between the reactants and the catalyst affects its framework. Therefore, this material was not considered for subsequent studies, as structure activity relations cannot be established.

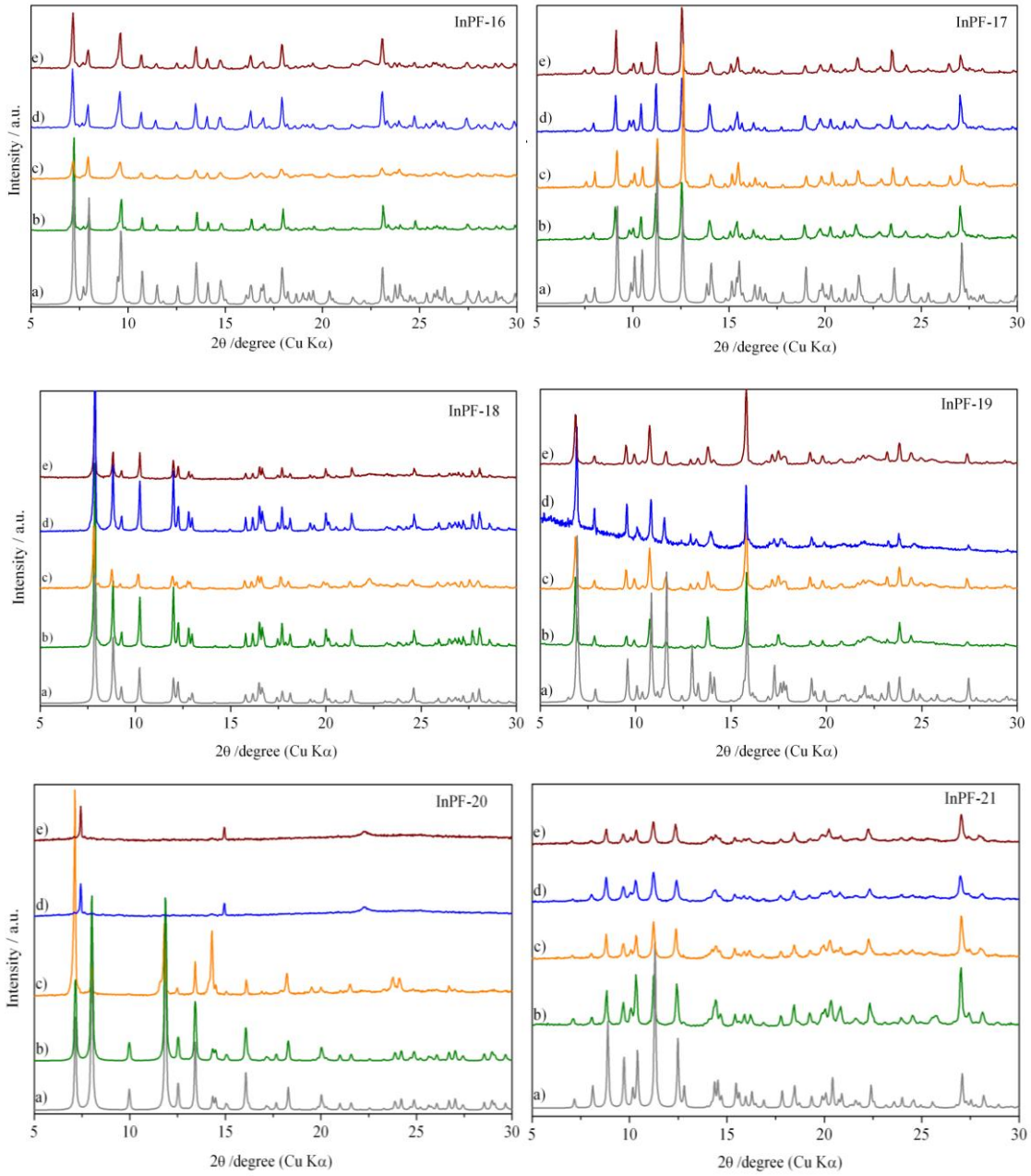

Figure 5.11 Normalized PXRD patterns of **InPF-16** to **InPF-21**: a) simulated, b) Conventional hydrothermal synthesized, c) MW hydrothermal synthesized d) and e) After the first run of catalysis for Conventional and MW-assisted MOFs.

5.2. Multicomponent Reactions (MCR)

Looking for improving of the use of MOFs in heterogeneous catalysis, our efforts were directed towards reactions where the superior tunability of MOFs can be exploited. The heterogeneous catalysts are promising candidates to perform multi-step transformations, especially when different and incompatible active sites (for instance acid–base) are required in each step. The high tunability of MOFs materials and the possibility to own well defined

catalytic active sites at the metallic nodes or at the organic linkers, allow the preparation of multi-functional MOF catalysts.

Those developed MOFs materials containing simultaneously various types of functionalities (acid–base, metal–acid, metal– base or metal–metal), in which the catalytic sites can be used cooperatively to perform one pot multi-component coupling reactions (MCRs), allow process simplification, avoiding costly time and energy consuming isolation and purification of intermediate products. The high added value of fine chemical products on the one hand and the design of new more economic processes on the other hand could largely compensate for the possible higher costs of MOFs as compared to other alternative catalysts.

As described above in section 5.1, several of the developed MOFs materials seem to have in their structure multiple active sites, which could act either in a cooperative way or in different steps of a given catalytic process.

Although until the date, the reports on multifunctional MOF catalysts are still limited and very recent; more are yet to come in the near future. The following sections present the catalytic capacity of the developed MOF materials evaluated using three of the most representative MCRs.

5.2.1. Strecker Three-Component Reaction (S3-CR)

Along the years, it has been found that numerous Lewis acids such as $Yb(OTf)_3$, $Pr(OTf)_3$, $Cu(OTf)_2$, $LiClO_4$, $BiCl_3$, $NiCl_2$, $RuCl_3$, $CeCl_3$, InI_3, RhI_3, $La(NO_3)_3{\cdot}6H_2O$ or $GdCl_3{\cdot}6H_2O$, iodine, and (bromodimethyl)-sulfonium bromide, homogeneously catalyze the Strecker-type reaction (Scheme 5.5). Also, several heterogeneous catalysts, which are more advantageous in terms of catalyst/product separation and continuous production, have been proposed for this reaction, founding among them polymer-supported scandium triflate, montmorillonite, sulfuric acid on silica, heteropoly acid, sulfamic acid, poly(4-vinyl pyridine)–SO_2 complex and aluminum and vanadium salen complexes attached to polystyrene polymers. Only few catalyst-free methods have been explored.[10]

Scheme 5.5 Strecker-3 Component Reaction

However, most of the starting carbonyl compounds are generally limited to aldehydes, being only few examples on the successful 3C-S reaction starting from ketones. Matsumoto and co-workers performed this reaction using ketones under extremely high pressure conditions. Meanwhile, Olah's group used $Ga(OTf)_3$ or TMSOTf as catalysts for the reaction with fluorinated ketones. Khan and co-workers have also reported the efficient $Fe(Cp)_2PF_6$ catalyst for Strecker-type reaction from ketones under solvent-free conditions. However, these last two cases represent homogeneous catalytic systems. Hence, there is still

scope to develop efficient heterogeneous catalysts for preparing a wide range of α-aminonitriles.

In Table 5.8 some examples are shown with different *p*-metal compounds as homogeneous and heterogeneous catalysts in the 3-C Strecker reaction, which show good behavior at high catalyst loadings [5-10mol%] using organic solvents at room temperature.

Table 5.8 Few examples of homogeneous and heterogeneous catalysts for 3C-S reaction [a]

Catalyst	Catalyst loading	Solvent	Time h	Yield %	TON
In	[10 mol%]	H_2O	0.5	98	9
InI_3	[10 mol%]	-	0.17	95	10
$InCl_3$	[10 mol%]	H_2O	0.5	82	8
$Ga(OTf)_3$	[5 mol%]	CH_2Cl_2	3	90	18
Al^{3+} salen complexes	[10 mol%]	MeOH/Toluene	4	82	8
Heterogeneous–Al^{3+} salen complexes	[10 mol%]	MeOH/Toluene	4	24-85	2-9
without	none	Ionic liquid	5-6	87-92	-
without	none	CH_3CN	17.5	97	-

[a] Reaction conditions: 25ºC in most cases, for Al^{3+} complexes the reaction was performed at -40ºC

In our case, considering the good activity displayed before in the cyanosilylation reaction by the **GaPF-1** material using low catalytic loadings [2.5-1mol%] at room temperature (Table 5.x), it was determinate to carry out the initial 3-C catalytic reactions under 1 mol% of catalyst loading, without solvent at room temperature.

As a result, in the following sections are presented the initial tests for the three isostructural MOFs, which showed different catalytic behavior depending on the metal ion nature, and the further investigations leading to develop the first solid solutions MOFs with the combination of gallium and indium cations.

*5.2.1.1. **AlPF-1**, **GaPF-1** and **InPF-11β** isostructural materials.*

Isostructural MOFs, **AlPF-1**, **GaPF-1** and **InPF-11β** showed different catalytic activity behaviour in the S-3C reaction as observed in Table 5.9, which means that the cation nature influences in the activation rate of the organic reactants.

The **GaPF-1** material was employed to study the effect of the temperature rising and catalyst loading on the catalytic reaction (Table 5.10). Results at 25ºC and low catalytic loading showed that the S-3CR does not proceed to the expected α-aminonitrile product.

Consequently, the strong tendency of **GaPF-1** to favor the cyanosilylation product at low temperatures doesn't seem to be affected when the catalyst loading rises, meaning that activation of the carbonyl and silyl groups are faster than the imine intermediary product expected in the Strecker reaction, which is only favored at temperatures above 80ºC.

Table 5.9 Screening of MPF materials as catalysts for 3C-S reaction [a]

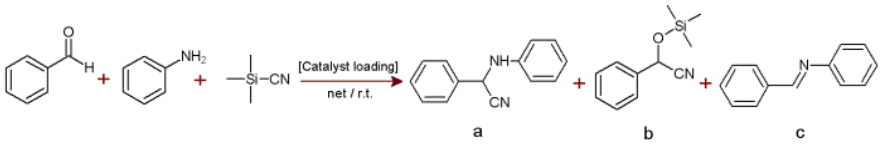

Entry	Catalyst	Time /h	Yield % [b]			TON
			a	b	c	
1	AlPF-1	0.08	99	-	-	99
2	GaPF-1	0.08–8	-	99	-	
3	InPF-11β	0.17-8	-	-	99	
4	[In+Ga]	1	99	-	-	99

[a] Reaction conditions: benzaldehyde (0.001mol), aniline (0.001mol) and TMSCN (0.001mol), 1 mol% catalyst, room temperature (25ºC) without use of solvent. [b] Yields by GC-MS and ^{1}H RMN.

On the other hand, **InPF-11β** material seems to direct the catalytic reaction in a contrary manner, allowing the imine formation at room temperature but with a slow transformation in to the expected α-aminonitrile product, which took 22 hours. This evidences that the Lewis basic site required to activating the silyl group and complete the addition of the cyano group is hindered, probably due to the metal ion size.

Table 5.10 Screening of **GaPF-1** material as catalysts for 3C-S reaction

Catalyst Loading	Temperature ºC	Time h	Yield % [a]		
			a	b	c
[10 mol%]	25	0.08	-	99	-
	60	0.08-8	-	99	-
[5 mol%]	25	0.08-8	-	99	-
	60	0.08-8	-	99	-
	80	0.08	-	5	-
		2	-	5	94
		4	25	5	69
[1 mol%]	25	0.08-8	-	99	-
	80	2	-	<<1	96
		4	50	traces	46

[a] Yields by GC-MS

With the use of **AlPF-1** material as catalyst, the expected α-aminonitrile product is obtained at room temperature. These differences between the catalytic activities of the studied MOFs can be attributed to the possible reaction pathways related to the reactant activation process for each catalyst.

Taking in to account that only **AlPF-1** material acting as catalyst in the 3-C reaction allows reaching the final desired α-aminonitrile product at mild conditions, the possible effect of lowering of this catalyst loading was examined (Table 5.11).

Table 5.11 Strecker 3-CR using different **AlPF-1** loadings. [a]

Catalyst Loading	time h	Yield %	TON	TOF h^{-1}
[1mol%]	0.08	>99	100	1251
[0.1mol%]	0.25	>99	320	4000
[0.01mol%]	0.42	>99	2000	25000

[a] Reaction conditions: benzaldehyde (0.001mol), aniline (0.001mol) and TMSCN (0.001mol),at 25ºC without use of solvent. [b] Yields by ^{1}HRMN

Assuming that the one pot Strecker reaction takes place following a mechanism as the one proposed in Figure 5.12, the formation of the α-aminonitrile requires the activation of both the carbonyl and silyl groups to allow the imine formation, followed by the cleavage of the cyano group and its attack to the imine carbon atom.

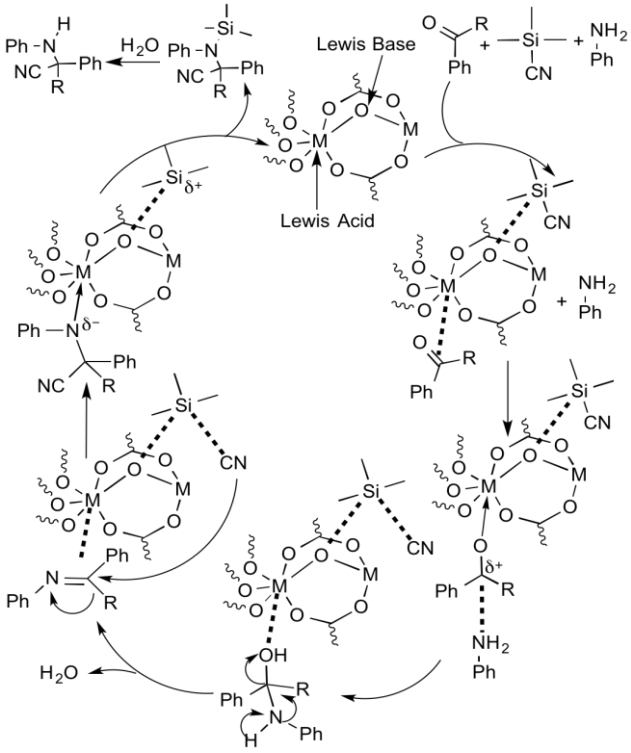

Figure 5.12 Proposed Mechanism for the **MPF** mediated Strecker reaction of carbonyl compounds.

To study the catalytic scope of the **AlPF-1** material, the 3-C Strecker reaction was performed using 0.01 mol% of catalyst loading at room temperature without solvent with different aldehydes as carbonyl source as well as different primary amines as substrates.

The results presented in Table 5.12, showed the preference of **AlPF-1** material to promote the reaction with aromatic aldehydes instead of the linear reactants, where the heptanal (1b) after 72h only reached a low yield (7.4%) of the desired product in a total of 51% conversion. When citral (Table 5.12), an also a lineal reactant, is used, no evolution to the desired product was observed and the reaction only reaches the formation of the imine product, which could be due to the steric hindrance that methyl groups gives to the lineal chain.

Table 5.12 Strecker 3-CR using different aldehyde sources. [a]

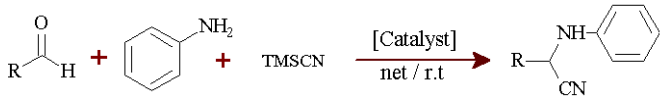

R	Time h	Yield [b] %
-C_6H_5	0.42	>99
-C_5H_{11}	72	7.4
-C_9H_{15}	24	Imine
p-F(C_6H_5)	0.08	>99
p-Cl(C_6H_5)	2	>99
p-CH_3(C_6H_5)	1	90
p-CH_3O(C_6H_5)	1	95
m-O_2N(C_6H_5)	0.5	97
p-O_2N(C_6H_5)	0.25	>99

[a] Reaction conditions: carbonyl compound (0.001mol), aniline (0.001mol) and TMSCN (0.001mol), 0.1mol% catalyst loading at 25ºC, without use of solvent. [b] Yields by GC-MS and ^{1}H RMN.

On the other hand, the **AlPF-1**-catalyzed S-3CR using aromatic aldehydes under the optimized reaction conditions, leads to the corresponding products with good yields (Table 5.12). The effect of different substituent groups in the aromatic ring of the benzaldehyde was studied. It was shown that acceptor groups like fluorine, increases the activation velocity leading to yields of 99% of the desired product in only 8 minutes.

Substituent donor groups like –CH_3 (weak) and –OCH_3 (strong) gave the corresponding products with 90 and 95% yields respectively, and in case of substituent –NO_2 (Table 5.12) the position of the substituent group seems to determinate the reaction velocity, being faster the formation of the product using the carbonyl derivate in *para*, rather than in the *meta* position.

Table 5.13 Strecker 3-CR using different amine sources. [a]

R	Time h	Yield [b] %
-C_6H_5	0.42	>99
-C_5H_{10}	2	87
-C_4H_8	0.5	98
p-(CH_3)(C_6H_5)	0.08	>99
3,4-(CH_3)(C_6H_5)	0.13	>99
p-NO_2(C_6H_5)	0.25	80
n-C_4H_9	0.5	>99

[a] Reaction conditions: benzaldehyde (0.001mol), amine (0.001mol) and TMSCN (0.001mol), 0.1mol% catalyst loading at 25ºC without use of solvent. [b] Yields by GC-MS and ^{1}H RMN.

The effect of the primary amine substituent was tested using different amines. The results (Table 5.13) showed no preference between linear, cyclic or aromatic amines reaching high yields at short times.

The recyclability of **AlPF-1** material was tested; the solid was recovered after centrifugation and washed several times with acetone and ethanol, then dried at 130ºC and reused at least 10 times. This experiment showed that material maintains its crystallinity along all catalytic cycles, with only a small decrease of its catalytic activity after the 9th cycle (Figure 5.13). Hot filtration experiments reveal that **AlPF-1** is a truly heterogeneous catalyst.

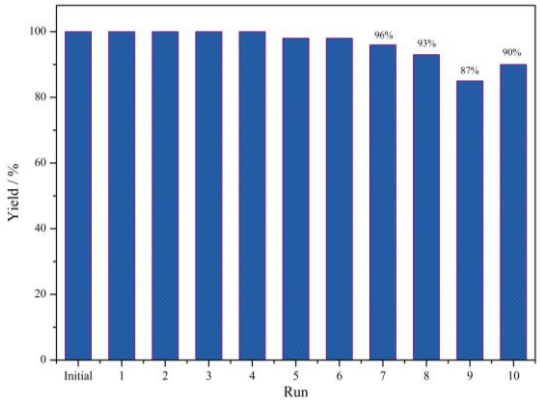

Figure 5.13 Recyclability of the **AlPF-1** catalyst, showing 10 cycles.

*5.2.1.2. **InGaPF** materials: Tuneable catalytic activity of solid solution MOFs*

Taking in to account the different catalytic responses exhibited by **InPF-11β** and **GaPF-1** materials, it was thought that it would be possible to control the rates and selectivity of the different steps involved in the one-pot 3-C Strecker reaction with a combination of Ga and In catalysts. Thus, it was decided to start by using a physical mixture of both **InPF-11β** and **GaPF-1** catalysts and indeed, when using equimolar amounts of both materials (named **[In+Ga]** from now on), the α-aminonitrile product was quantitatively formed (Table 5.14). Encouraged by these results, it was decided to prepare solid solution MOFs with the combinations of gallium and indium cations, which could share the same crystallographic position in the framework.

Therefore, three new MOFs were prepared with general formula $[In_xGa_{1-x}(O_2C_4H_4)_{0.5}(hfipbb)]$, where x = 0.72, 0.55, and 0.28, for **InGaPF-1**, **InGaPF-2**, and **InGaPF-3**, respectively. Note that we formulate these compounds as including ethylene glycoxyde groups instead of OH groups, based on the absence of the typical OH vibration band and the presence of CH_2 bands in their IR spectra (Chapter 7). However, the presence of both hydroxyl and ethylene glycoxyde anions in the structure cannot be completely ruled out.

The metal content was determined with ICP and total X-ray fluorescence (TXRF) spectroscopies. The PXRD patterns of the solid solution MOFs indicate that the three compounds maintain the parent structure. The absence of peak splitting, rules out the possibility of having a mixture of two separate phases. Furthermore, a full pattern profile

refinement carried out for each one of the three compounds demonstrates that their unit cell parameters values are ranging between those of **InPF-11β** and **GaPF-1** (Chapter 4).

The mixed **InGaPF** compounds were subsequently used as catalysts for the 3-C Strecker reaction. **InGaPF-1** leads to the product although at a very slow rate (96 h). This indicates that the cleavage of the cyano group is still hindered in a material with a large percentage of indium in the mixed-metal framework. In the case of **InGaPF-2**, where the metals ratio is close to 1, the Strecker reaction proceeds much faster, reaching a 91% of conversion in 1.33 h. Finally, **InGaPF-3** exhibits a rate of reaction comparable to that of **AlPF-1**, with a 96% of conversion to α-aminonitrile in only 0.33 h, thus indicating that the presence of a small amount of indium is enough to favor the imine formation over the aldehyde cyanosilylation.

Table 5.14 InGaPF catalytic activity in the Strecker-3CR. [a]

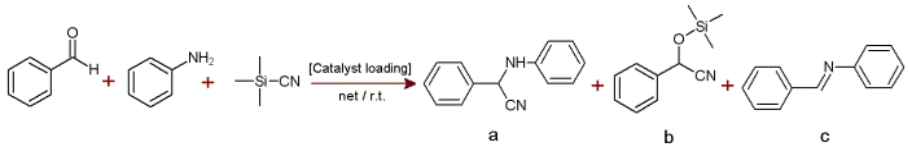

Catalyst	time	Selectivity (%) [b]			TON
	h	a	b	c	
InGaPF-1	96	64	-	-	64
InGaPF-2	1.33	91	-	-	91
InGaPF-3	0.33	96	-	-	96
GaPF-1	0.08–8	-	99	-	
InPF-11β	0.17-8	-	-	99	
[In+Ga]	1	99	-	-	99

[a] Reaction conditions: benzaldehyde (0.001mol), aniline (0.001mol) and TMSCN (0.001mol), 1 mol% catalyst, at 25ºC without solvent. [b] Yields by GC-MS and ^{1}H RMN.

Typically, ketones are more difficult to activate than aldehydes. Thus, there are less than 20 studies reported, where heterogeneous catalysts are used in Strecker reactions with ketones, and in many cases elevated temperatures (50-60 ºC), use of solvents, and/or high catalytic loadings (4-50mol%) are required to obtain the desired aminonitrile product.[11] **AlPF-1**, **InPF-11β** and **GaPF-1** demonstrate excellent activity in the Strecker-3CR using acetophenone as carbonyl compound under neat conditions, low catalyst loading and room temperature with yields between 50-87%. Interestingly, in all cases the Strecker product was obtained, with the highest yield for the cases of **[In+Ga]** (87%) and **InGaPF-3** (80%) materials. The different results between aldehyde- and ketone-based reactions presumably indicate differences in the mechanistic pathway.

The interaction between the organic reactants and all the **InGaPF** materials does not affect their frameworks as can be observed in the PXRD patterns of the recovered materials after the catalytic reactions without having any structural change (Figure 5.14).

Table 5.15 Catalysts performance in the Strecker 3-CR. [a]

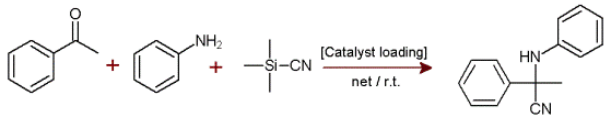

Catalyst	Time h	Yield [b] %	TON
InGaPF-1	0.42	50	50
InGaPF-2	0.75	67	67
InGaPF-3	2	80	80
GaPF-1	0.63	67	67
InPF-11β	0.67	67	67
[In+Ga]	0.5	87	87
AlPF-1	8	75	75

[a] Reaction conditions: acetophenone (0.001mol), aniline (0.001mol) and TMSCN (0.001mol), 1 mol% of catalyst loading at 25ºC, without solvent. [b] Yields by GC-MS and ^{1}H RMN.

Additionally, the recyclability of **InGaPF-3** material was also tested; the solid was recovered after centrifugation and washed several times with acetone and ethanol, then dried at 130ºC and reused at least 10 times. This experiment showed that material maintains its crystallinity along all tested catalytic cycles (Figure 5.15).

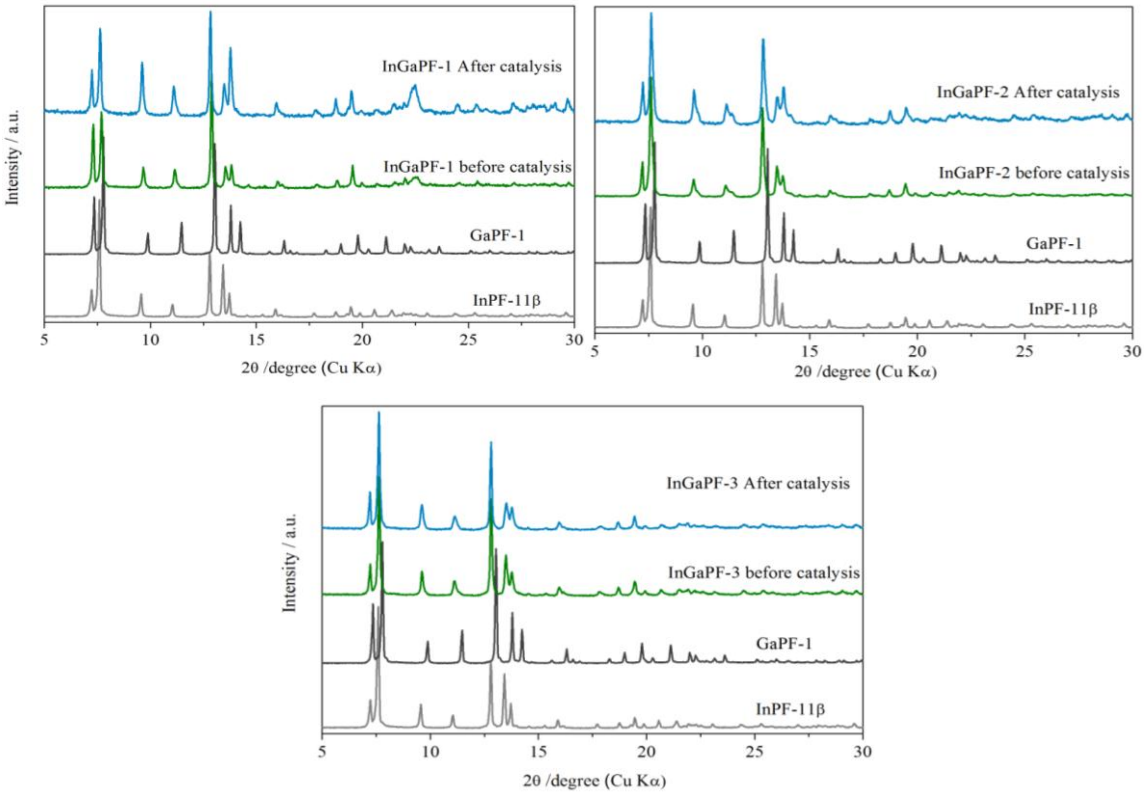

Figure 5.14 PXRD patterns of InGaPF materials before and after first catalytic reaction, Above: **InGaPF-1** (left) and **InGaPF-2** (right), Down: **InGaPF-3**

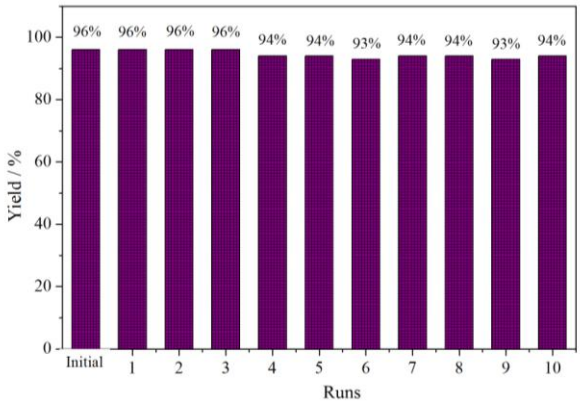

Figure 5.15 Recyclability of the **InGaPF-3** catalyst, showing 10 cycles.

5.2.1.3. Indium MOFs built with the dpmda^{2-} linker

Taking in to account the excellent catalytic response exhibited by **InPF-22** and **InPF-23** materials compared to those **InPF-9** and **InPF-10,** which presented additional nitrogenated ligands in their structure, it was considered that **InPF-22** and **InPF-23** would present good catalytic activity at mild conditions in the one pot Strecker-3C reaction, giving information on the effect of these two different 3D frameworks (**InPF-22** with 2D inorganic supramolecular layers and **InPF-23** with a low metal CN and occupy cavities) in a more complex catalytic reaction. As result, in both cases the α-aminonitrile product was quantitatively formed (Table 5.16 and Figure 5.16) at short times. Lower conversions were observed in case of **InPF-22** material.

Table 5.16 Screening of **InPF** materials as catalysts in the Strecker 3-CR.[a]

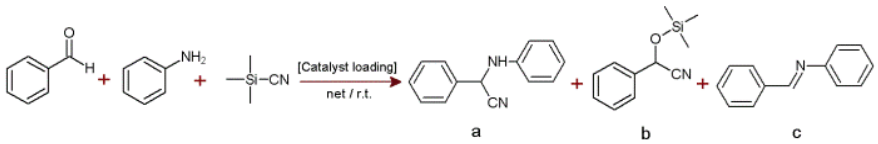

Catalyst	Loading	time h	Yield % [b]			TOF
			a	b	c	
InPF-22	2.5mol%	0.17	93	-	-	444
InPF-23	2.5mol%	0.33	98	-	-	458
InPF-22	1mol%	0.25	88	-	-	
InPF-23	1mol%	0.5	95	-	-	

[a] Reaction conditions: benzaldehyde (0.001mol), aniline (0.001mol) and TMSC (0.001mol), at 25ºC, without use of solvent. [b] Yields by GC-MS and ^{1}H RMN.

The recyclability of **InPF-22** and **InPF-23** materials was also tested; the solids were recovered after centrifugation and washed several times with acetone and ethanol, then dried at 130ºC and reused at least 5 times. maintain their crystallinity along all tested catalytic cycles (Figure 5.17).

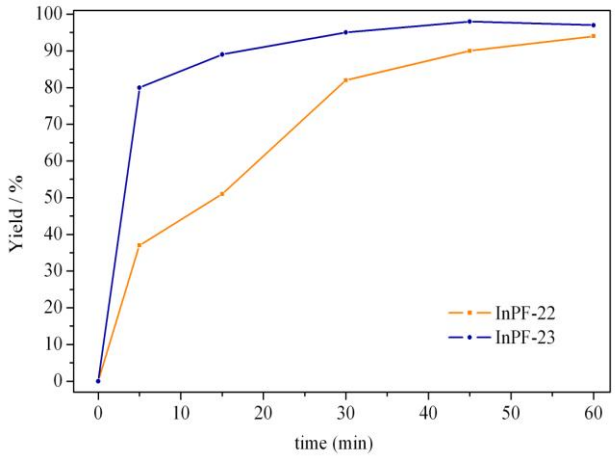

Figure 5.16 Kinetic profiles for the Strecker-3CR

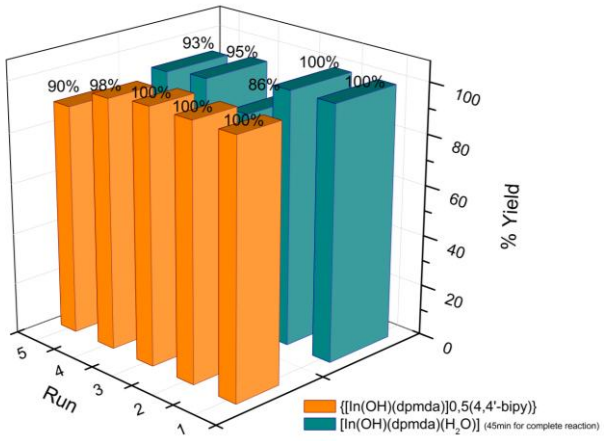

Figure 5.17 Recyclability of the **InPF-22** and **InPF-23** catalysts in the Strecker 3-CR

5.2.2. Passerini Three-Component Reaction (P3-CR)

The Passerini reaction (Scheme 5.4) is one of the isonitrile-based MCR that yields α-acyloxy carboxamides in a one-pot synthesis from an aldehyde, isonitrile, and carboxylic acid. The aldehyde with the carbonyl group is one of the most critical reactants because of the pronounced reactivity with the isonitrile carbon atom towards the sp^2 carbon electrophilic center; this reaction can be time-consuming with low yields if a strong carboxylic acid or an unusually electrophilic carbonyl compound is not used.

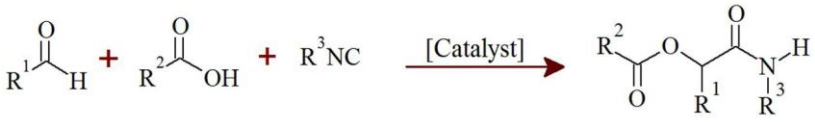

Scheme 5.4 Passerini-3 Component Reaction

5.2.2.1. Indium MOFs built with the popha^{3-} linker

In the present study, Passerini reaction was carried out using the one pot methodology, at room temperature, without any use of solvent and using 1 mol% of catalyst loading.

The **InPF-16**, **InPF-17** and **InPF-18** materials demonstrated good catalytic activities (Table 5.17). Taking into account the dual activation phenomena manifested before by these catalysts, and considering the presence of the basic and acid moieties along their frameworks, the following catalytic mechanism is proposed: i) acid Lewis activation of carbonyl compound and basic Lewis activation of the OH-group of the benzoic acid; ii) attack of the oxygen of OH-group to the isocyanide sp-carbon; iii) subsequent coordination to the sp^3-carbon of the activated carbonyl compound and iv) protonation of the intermediate product and its release from the catalyst. The intermediate product suffers a rearrangement through a 1,4O→O acyl transfer to finally obtain the expected 2-cyclohexylamino-2-oxo-1-phenylethylbenzoate product (Figure 5.18).

Table 5.17 Screening of Indium MOFs as catalysts in the Passerini 3-CR.[a]

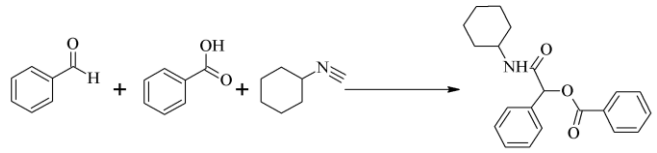

Catalyst	Yield %	time h	TON
InPF-16	89	0.5	89
InPF-17	86	0.7	86
InPF-18	83	0.7	83
InPF-20	66	1	66
Blank	50	24	-

[a] Reaction conditions: benzaldehyde (0.001mol), benzoic acid (0.001mol), cyclohexyl isocyanide (0.001mol) catalyst: 1 mol%, without solvent, N_2 atmosphere at 25ºC. [b] Yields by ^{1}H NMR without further purification.

The TON value of **InPF-17** was unexpectedly found to be similar to those of **InPF-16** and **InPF-18** (indium coordination number is six in the former compounds and seven in the latter one). The activity of **InPF17**, which was the lowest one in the cyanosilylation reaction, becomes similar to the other catalysts in the P-3CR. This indicates that in MCR the metal coordination number is not the only factor to reach a good activity. As several substrates are involved in the reaction, it seems reasonable to think that synchronization in their activation is required to yield the final product with high selectivity.

Finally, the recyclability of **InPF-16** material was tested and compared to the recyclability of the same material in the cyanosilylation reaction; the solid was recovered after centrifugation and washed several times with acetone and ethanol, then dried at 130ºC and reused at least 4 times (Figure 5.19).

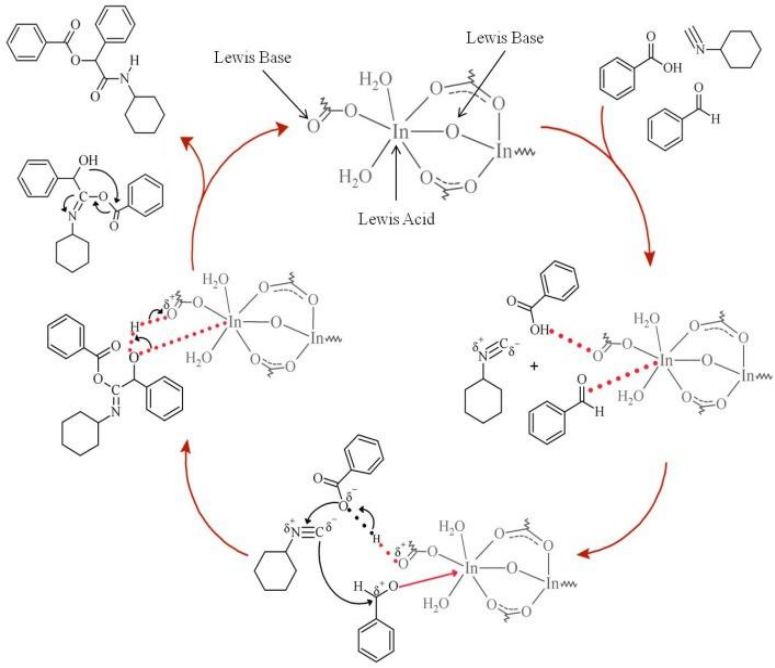

Figure 5.18 Proposed mechanism for **InPF-16**-catalyzed Passerini reaction.

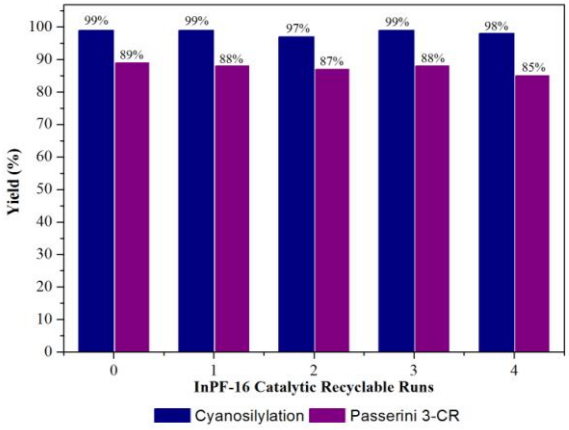

Figure 5.19 Recyclability of the **InPF-16** catalyst

5.2.3. Ugi Four-Component Reaction (U4-CR)

The virtue of the Ugi 4-CR is the construction of two amide bonds (Scheme 5.5). Although a plethora of methods for accessing similar structures is available and countless peptide coupling reagents have been reported, they all suffer from poor atom economy. Thus, Ugi-type chemistry should be considered as a viable green alternative for amide bond formation, an issue of crucial significance to the pharmaceutical industry.

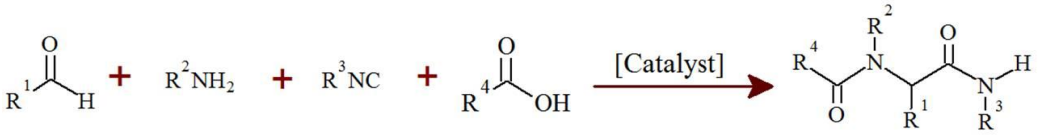

Scheme 5.5 Ugi 4-Component Reaction

5.2.3.1. Indium MOFs built with popha^{3-} linker

The increment in the reactants number, such as in the U4-CR, allows to observe the tendency of catalytic activation processes under indium MOFs catalysts action. The reaction was performed according to a One Pot methodology, at room temperature with a catalyst loading of 1 mol % leading to good yields. Among various solvents screened, ethanol was found to be the best choice as solvent for the reaction. Usually, when this reaction is carried out without catalyst, the condensation of an aldehyde, amine, carboxylic acid, and isocyanide has to be performed via cascade methodology in order to favor the imine transformation to finally obtain the α-aminoacyl amide derivative, yet at lower yields (Table 5.18).

Table 5.18 Screening of Indium MOFs as catalysts in the Ugi 4-CR.[a]

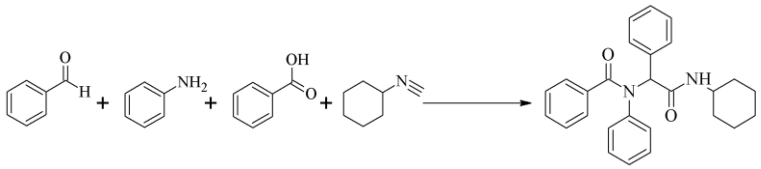

Catalyst	Yield %[b]	TON
InPF-16	traces	-
InPF-17	92	92
InPF-18	67	67
InPF-20	89	89
Blank	40	-

[a] Reaction conditions: benzaldehyde (0.001mol), aniline (0.001mol), benzoic acid (0.001mol), cyclohexyl isocyanide (0.001mol) catalyst: 1 mol%, with EtOH as solvent at 25ºC during 2h. [b] Yields by ^{1}H NMR without further purification.

The proposed catalytic mechanism for the U4-CR using the **InPF** materials also relies on the dual phenomena based on both basic and acid moieties. The acid Lewis activation of carbonyl compound is followed by the imine intermediary product formation and its subsequent activation at the same acid Lewis site. The OH-group from COOH moiety of the benzoic acid activated by the catalyst base component attacks the sp-carbon of the isocyanide derivative, which at the same time coordinates to the sp^2-carbon of the activated imine. This is followed by a protonation of this second intermediary product, and release from the catalyst. Finally, this intermediary product suffers a 1,4O→N acyl transfer known as "mumm rearrangement" resulting in the expected N-(-(cyclohexylaminocarbonyl)(phenyl)methyl)-N-phenylbenzamide product (Figure 5.20).

The Lewis acid centers present in the **InPF** materials frameworks activate of both carbonyl and imine intermediate parts. This seems to occur faster when **InPF-17** catalyst is employed compared to **InPF-18** material.

With the aim of proposing one of the crucial steps of the Ugi mechanism, and checking if the benzoic acid and cyclohexyl isocyanide coupling was possible, the Danishefsky reaction (Scheme 5.5) was carried out.

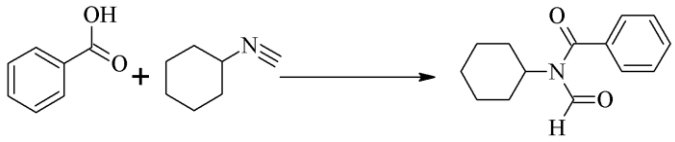

Scheme 5.5 Danishefsky reaction

The reaction was performed under exactly the same conditions that the U4-CR one (RT, ethanol and 1 mol% loading of **InPF-17)**. Following the reaction evolution by GC-MS at different times, **NO** N-formyl amide formation was observed, ruling out thus the presence of this intermediate in the U4-CR. In case of **InPF-16** catalyst, the imine sub product shows no activity after 2h giving only traces of the expected Ugi product.

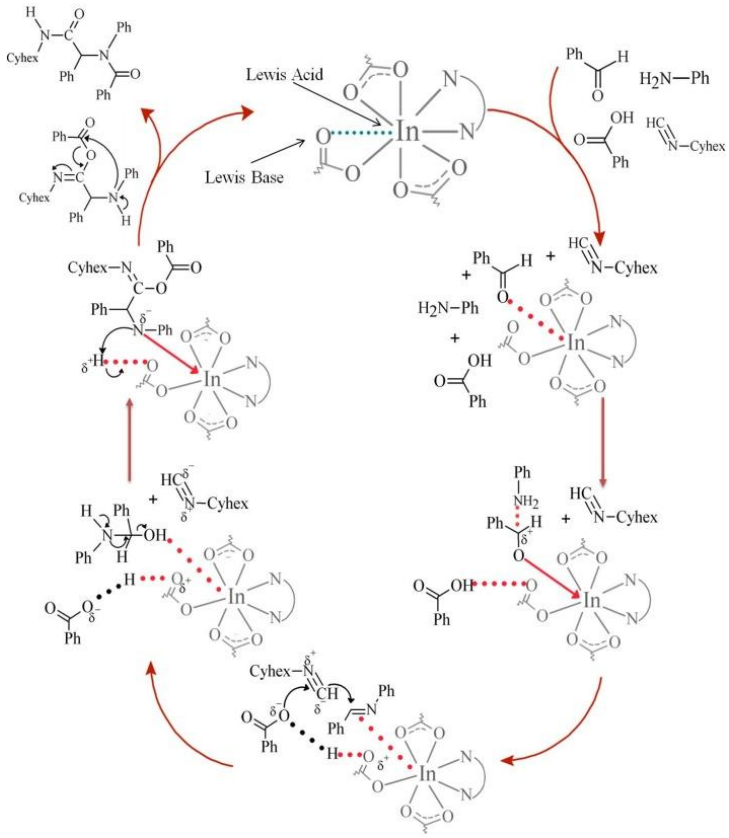

Figure 5.20 Proposal mechanism for Indium mediated U4-CR using the 2D **InPF-17** as catalyst.

At the view of these results and based on the structural features of the catalyst, we have established a parameter **0≤x≤1** based on the base/acid Lewis active site ratio that allow us to explain the differences in the activity in the U4-CR. Considering that the maximum coordination number of indium cations is eight, we define the number of Lewis acid sites (LA) as eight minus the actual coordination number of each indium atom, plus the number of coordinated water ligands (O_L) (easily displaced by the reactants generating additional active sites): $\mathbf{LA = \sum n(8 - CN + O_L)}$, being n the number of In cations per formula. The number of Lewis base sites (LB) is here defined as the number of OH groups plus the number of non-coordinated carboxylate C=O groups per formula. At the view of the **LB/LA** ratio (**x**) for the

catalytically active materials (**InPF-16**, **InPF -17**, **InPF -18**), it seems apparent that the closer is the value to 1, the better the catalytic behavior is. This would support the hypothesis that a synchronization of the substrates' activation rates is required.

Thus, **InPF-17,** in which **x=1**, owns equal amounts of acid and base active sites and shows an excellent catalytic activity, with the higher TON for the studied 4-CR. **InPF-18** with **x=0.8** also presents good activity but the TON value is the second one, and **InPF-16** with **x=0.6** hardly shows catalytic activity. As expected, **InPF-19** and **InPF-21** MOFs with **x=0** do not show any catalytic activity.

The recyclability of **InPF-17** material was also tested; the solid was recovered after centrifugation and washed several times with acetone and ethanol, then dried at 130ºC and reused at least 4 times (Figure 5.21).

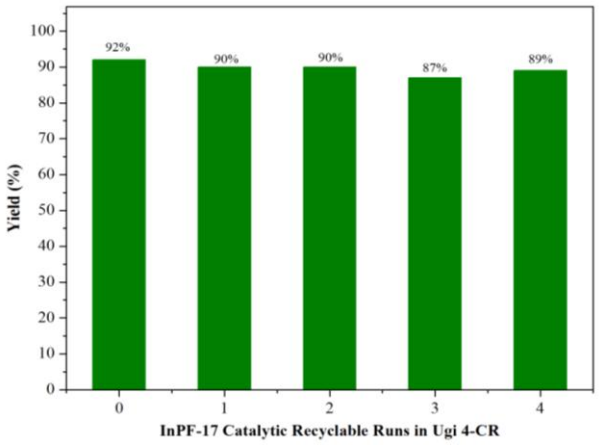

Figure 5.21 Recyclability of the **InPF-17** catalyst, showing 4 cycles.

5.3. References

1. a) T. P. Loh, L. G. Chua, *Chem. Commun.* **2006**, 26, 2739; b) V. Nair, S. Ros, C. N. Jayan, B. S. Pillai, *Tetrahedron.* **2004**, *60*, 1959; c) S. P. Petrosyants and A. B. Ilyukhin, *Russ. J. Inorg. Chem.* **2011**, *26*, 2047; d) P. Cintas. *Synlett.* **1995**, *11*, 1087; e) M. Bandini, P. G. Cozzi, A. Garelli, P. Melchiorre and A. Umani-Ronchi. *Eur. J. Org. Chem.* **2002**, 3243; f) C. Xu, I. Yu and P. Mehrkhodavandi, *Chem. Commun.* **2012**, *48*, 6806; g) A. F. Douglas, B. O. Patrick and P. Mehrkhodavandi, *Angew. Chem., Int. Ed.* **2008**, *47*, 2290.

2. a) J. -Y. Lee, O. K. Farha, J. K. Roberts, A. Scheidt, S. T. Nguyen, J. T. Hupp, *Chem. Soc. Rev*. **2009**, *38*, 1450; b) A. Dhakshinamoorthy, M. Alvaro, H. Garcia, *Chem. Commun.* **2012**, *48*, 11275; c) L. Bromberg, Y. Diao, H. Wu, S. A. Speakman, T. A. Hatton, *Chem. Mater*. **2012**, *24*, 1664.

3. a) A. Dhakshinamoorthy, M. Alvaro and H. Garcia, *Adv. Synth. Catal.* **2009**, *351*, 2271; b) P. Serra-Crespo, E. V. Ramos-Fernandez, J. Gascon and F. Kapteijn, *Chem. Mater.* **2011**, *23*, 2565; c) E. D. Bloch, D. Britt, C. Lee, C. J. Doonan, F. J. Uribe-Romo, H. Furukawa, J. R. Long and O. M. Yaghi, *J. Am. Chem. Soc*. **2010**, *132*, 14382; d) H. Liu, B. Yin, Z. Gao, Y. Li and H. Jiang, *Chem. Commun.* **2012**, *48*, 2033.

4. S. Kozuch, J. M. L. Martin, *ACS Catal.* **2012**, *2*, 2787.

5. S. Kozuch,S. Shaik, *Acc. Chem. Res*. **2011**, *44*, 101.

6. J. A. Dumesic, G. W. Hiber, M. Boudart, *Handbook of Heterogeneous catalysis*; G. Ertl, H. Knözinger, F. Schüth, J. Weitkamp, Eds.; Wiley-VCH: Weinheim, Germany, **2008**, 1445.

7. F. Gándara, B. Gómez-Lor, E. Gutiérrez-Puebla, M. Iglesias, M. A. Monge, D. M. Proserpio, N. Snejko, *Chem. Mater.* **2008**, *20*, 72.

8. a) Y. Hamashima, D. Sawada, M. Kanai and M. Shibasaki, *J. Am. Chem. Soc*. **1999**, *121*, 2641; b) M. Takamura, K. Funabashi, M. Kanai and M. Shibasaki, *J. Am. Chem. Soc.* **2000**, *122*, 6327; c) M. Takamura, K. Funabashi, M. Kanai and M. Shibasaki, *J. Am. Chem. Soc*. **2001**, *123*, 6801; d) K. Funabashi, H. Ratni, M. Kanai and M. Shibasaki, *J. Am. Chem. Soc*. **2001**, *123*, 10784; e) E. Ichikawa, M. Suzuki, K. Yabu, M. Albert, M. Kanai, M. Shibasaki, *J. Am. Chem. Soc*. **2004**, *126*, 11808; f) M. Takamura, Y. Hamashima, H. Usuda,M. Kanai and M. Shibasaki, *Angew. Chem. Int. Ed.* **2000**, *39*, 1650; g) Y. Hamashima, D. Sawada, H. Nogami, M. Kanai and M. Shibasaki, *Tetrahedron* **2001**, *57*, 805.

9. a) D. Rampon, R. Giovenardi, T. L. Silva, R. S. Rambo, A. A. Merlo and P. H. Schneider, *Eur. J. Org. Chem.* **2011**, 7066; b) R. Sarma, N. Rajesh and D. Prajapti, *Chem. Commun.* **2012**, *48*, 4014.

10. a) K. Iwanami, H. Seo, J-C. Choi, T. Sakakura, H.Yasuda. *Tetrahedron.* **2010**, *66*, 1898; b) G. W. Zhang, D.H. Zheng, J. Nie, T. Wang, J. A. Ma. *Org Biomol Chem*. **2010**, *8*, 1399; c) N. H. Khan, S. Agrawal, R. Kureshy, S. H. R. Abdi, S. Singh, E. Suresh, R. V. Jasra, *Tetrahedron*

Lett. **2008**, *49*, 640; d) J. Jarusiewicz, Y. Choe, K. Yoo, C. P. Park, K. W. Jung. *J. Org.Chem.* **2009**, *74*, 2873; e) B. Karimi, A. Maleki, D. Elhamifar, J. H. Clark, A. J. Hunt. *Chem Commun.* **2010**, *46*, 6947; f) B. Karmakar, J. Banerji, *Tetrahedron Lett*. **2010**, *51*, 2748; g) C. Najera and J. M. Sansano, *Chem. Rev.* **2007**, *107*, 4584; h) J. Wang, Y. Masui and M. Onaka, *Eur. J. Org. Chem.*, **2010**, 1763; i) G. K. Surya Prakash, T. Mathew, C. Panja, S. Alconcel, H. Vaghoo, D. Clement and G. A. Olah, *Proc Nat Acad Sci USA*, **2007**, *104*, 3703; j) M. M. Mojtahedi, M. S. Abaee and T. Alishiri, *Tetrahedron lett.* **2009**, *50*, 2322; k) M. Barbero, S. Cadamuro, S. Dughera and G.Ghigo, *Org. Biomol. Chem*. **2012**, *10*, 4058; l) S.K. De, R. A. Gibbs, *Synth. Commun*. **2005**, 35, 951; m) Z.-L. Shen, S.-J. Ji, T.-P. Loh, *Tetrahedron* **2008**, *64*, 8159; n) A. Majhi, S. S. Kim, S. T. Kadam, *Tetrahedron* **2008**, *64*, 5509; o) M. Narasimhulu, T. S. Reddy, K. C. Mahesh, S. M. Reddy, A. V. Reddy, Y. Venkateswarlu, *J. Mol. Catal. A: Chem.* **2007**, *264*, 288; p) B. Das, R. Ramu, B. Ravikanth, K. R. Reddy, *Synthesis* **2006**, 1419; q) H. A. Oskooie, M. M. Heravi, K. Bakhtiari, V. Zadsirjan, F. F. Bamoharram, *Synlett* **2006**, 1768; r) E. Rafiee, S. Rashidzadeh, A. Azad, *J. Mol. Catal. A: Chem.* **2007**, *261*, 49; s) E. Rafiee, S. Rashidzadeh, R. Joshaghani, H. Chalabeh, K. Afza, *Synth. Commun.* **2008**, *38*, 2741; t) A. Heydari, S. Khaksar, M. Pourayoubi, A. R. Mahjoub, *Tetrahedron Lett.* **2007**, *48*, 4059; u) Z. Li, Y. Sun, X. Ren, P. Wei, Y. Shi, P. Ouyang, *Synlett* **2007**, 803; v) G. A. Olah, T. Mathew, C. Panja, K. Smith, G.K.S. Prakash, *Catal. Lett.* **2007**, *114*, 1; w) R. Martínez, D. J. Ramón, M. Yus, *Tetrahedron Lett.* **2005**, *46*, 8471; x) M. A. Esteves, B. Gigante, C. Santos, A. M. Guerreiro, C. Baleizão, *Catalysis Today* **2013**, 65.

11. a) Singh, A. P.; Ali, A.; Gupta, R. *Dalton Trans.* **2010**, *39*, 8135; b) Choi, J.; Yang, Y. Y.; Kim, H. J.; Son, S. U. *Angew. Chem. Int. Ed*. **2010**, *49*, 7718; c) Dekamin, M. G.; Azimoshan, M.; Ramezani, L. *Green Chem.* **2013**, *15*, 811.

CHAPTER 6

CONCLUSIONS AND PERSPECTIVES

6.1. Conclusions

The present work was focused on the obtaining of new MOFs using ***p*-elements** (Aluminium, Gallium and Indium) as metal centers and multicarboxylate bending V-shaped ligands 4,4'-(hexafluoroisopropylidene)*bis*(benzoic acid) (**H_2hfipbb**), diphenylmethane-4,4-dicarboxylic acid (**H_2dpmda**) and 5-(4-carboxy-2-nitrophenoxy)-1,3-benzenedicarboxylic acid (**H_3popha**). As result, twenty new compounds were obtained and studied in detail including their heterogeneous catalytic activities.

The system ***p*-metal element / H_2hfipbb** has been investigated, obtaining six new isostructural materials. Three of them, with only one type of metallic centers were named **MPF** materials: **AlPF-1**, **GaPF-1** and **InPF-11β**. The other three solid-solution MOFs, obtained using different amounts of gallium and indium salts, were named **InGaPF-1**, **InGaPF-2** and **InGaPF-3**. From the exploration of this system, some conclusions can be drawn:

1- MPF materials [M(OR)(hfipbb)], (M = **Al, Ga, In)** were obtained using similar (temperature and time) conditions. The formation of each material depends on the suitable solvent mixture selection. For **InPF-11** two polymorphs are obtained depending on the solvents used: **InPF-11β** polymorph, with an ethyleneglycol/water combination, and **InPF-11α** with different solvents or mixtures. The **MPF** structure consists in rod-shaped SBUs connected through the linker forming a 3D framework that forms a uninodal four connected net with dia topology. Their catalytic activity was tested using the Strecker-3Component Reaction (S-3CR). These three materials showed different behavior in this catalytic reaction affording three different products. In case of **AlPF-1** the expected α-aminonitrile product was obtained; however, when using **GaPF-1** and **InPF-11β**, the cyanohydrin and the imine products were respectively obtained. These differences are attributed to the various possible reaction pathways related to the reactant activation process for each catalyst.

2- In order to probe whether the combination of both paths could reach the desired α-aminonitrile product, we have prepared solid solution MOFs with the combinations of gallium and indium cations. **InGaPF-1**, **InGaPF-2** and **InGaPF-3** with formula **$[In_xGa_{x-1}(O_2C_2H_4)_{0.5}$(hfipbb)]** were designed looking for the control of the rates and selectivity for the different steps involved in the one-pot Strecker-3Component Reaction (S3-CR). The metal content variation in each material case was made in order to appreciate the real effect of the cation nature in the organic transformation. In case of **InGaPF-1**, which possesses more percentage of indium in the framework (x: 0.72), it took 96h to reach the final α-aminonitrile product. However, when **InGaPF-2** with similar percentages of both metals was employed, improving the time of the catalytic reaction (1.3h) and increasing of the product yield was observed. The study of these developed solid-solution MOFs showed how

the reactivity and selectivity of a heterogeneous catalyst can be controlled by modulating the ratio of different metals that occupy the same crystallographic position of the framework.

The system ***p*-metal element / H_2hfipbb / nitrogenated ligand** has been investigated, obtaining five new MOFs materials.

3- Five new **InPF** materials using indium salts with the H_2hfipbb linker and nitrogenated ligands were obtained: **InPF-12**: **[In_2(hfipbb)$_3$(1,10-phen)$_2$]**, **InPF-13**: **[In_2(hfipbb)$_3$(2,2'-bipy)$_2$]**, **InPF-14**: **[In_2(hfipbb)$_3$(4,4'-bipy)]** and **InPF-15: [In_4(OH)$_4$(hfipbb)$_4$(4,4'-bipy)].** Chelating nitrogenated ligands, 1,10-phen and 2,2'-bipy, were employed. In case of **InPF-12** and **InPF-13** an increment of indium coordination number (CN) up to 7 and different coordination modes of the hfipbb^{2-} linker (L_1 and L_2) occurred. The fact that two positions were blocked on the metal ion, gave as a result a 1D polymeric framework with a zigzag ladder topology. When the non-chelate 4,4'-bipy ligand was employed, two different structures were obtained: **InPF-14** and **InPF-15**, which displayed different metal CN (7 and 6) and different hfipbb^{2-} linker coordination modes (L_2 and L_3-L_1). In fact, it was found that after long reaction times **InPF-14** transforms in to **InPF-15,** which means that **InPF-14** was a kinetically stable product and **InPF-15** was a thermodynamically stable one.

The catalytic activity of these materials was tested in the cyanosilylation of carbonyl compounds, showing that i) catalysts without any auxiliary ligands (**InPF-11**α and β) or with a non-chelate second linker (4,4'-bipy) in their structure exhibit excellent catalytic activity, ii) among the latter, the coordination number and μ-OH groups presence seem to be decisive factors to get a better catalytic behavior, and iii) the presence of additional Lewis base moieties (μ-OH and not coordinated to indium cation C=O group), besides the Lewis acid sites, creates a two-component catalytic system, based on the "dual activation" phenomenon that makes **InPF-15** the best catalyst in this type of reactions. It was also found that the use of this highly reactive, recyclable and environmentally benign catalyst allows the synthesis of various trimethylsilyl cyanohydrins from a wide range of cyclic, aliphatic and aromatic ketones.

4- Some observations can be made considering the three different hfipbb^{2-} linker modes. L_1 type gave elongated geometries with high Linker Coordination Angle (LCA) values [119-121º]. In case of the free C-O part of the L_1 linker type present an intramolecular interaction, a different geometrical behavior can be considered for the organic linker. In the MOFs with the L_2-linker mode, distorted geometries with LCA values between [104-113º] are observed. Meanwhile, the L_3-linker mode did not showed alterations in the geometrical parameters with a θ value ~109º (respect to the organic molecule) and LCA values of [112-116º] for those materials built using nitrogenated additional ligands and [104-105º] for materials using only the hfipbb^{2-} linker in their frameworks.

In the system ***p*-metal element / H_2dpmda / nitrogenated ligand**, which includes a less sterically hindered ligand, four new MOFs materials named: **InPF-9, InPF-10, InPF-22** and **InPF-23** were obtained. The conclusions that can be deduced are the following:

5- The use of a less sterically linker as H_2dpmda allowed to increase the framework dimensionality for those materials built using additional chelating nitrogenated ligands such as 1,10-phen and 2,2'-bipy. Contrary to their analogs with the H_2hfipbb linker (**InPF-12** and **InPF-13**, which only formed 1D chains), the use of H_2dpmda gave 2D structures with 8R containing layers in **InPF-9** and **InPF-10** materials, which displayed also L_1 and L_2-linker coordination modes.

InPF-22 [In(OH)(dpmda)(H_2O)] and **InPF-23 [In(OH)(dpmda)].0.5(4,4'-bipy)** materials exhibit 3D frameworks built from sharing-vertex chains (SBU). However, while in the former they are formed by InO_7 polyhedra, in the latter all the polyhedra are InO_6 octahedra. Their frameworks can be simplified as uninodal six-connected nets with **dia** topology for **InPF-22** and with **pcu** topology for **InPF-23**.

6- Concerning the catalytic activity of the four MOFs, these materials exhibit good Lewis acid heterogeneous catalytic activity, whose dimensionality seemed to be directly related with the increment in their catalytically performance. In this matter, **InPF-22** and **InPF-23** both with 3D structures gave higher TOF values than **InPF-9** and **InPF-10** materials, which are built using nitrogenated chelating ancillary ligands and have 2D structure.

From the system ***p*-metal element / H_3popha / nitrogenated ligand**, which employed a tricarboxylate bending V-shaped ligand, six new MOFs materials were obtained: **InPF-16** to **InPF-21**. The conclusions that can be deduced are the following:

7- A series of 6 new Indium MOFs with variation of chemical and structural characteristics (different indium coordination numbers, Lewis active centers, concurrent existence of Lewis bases) have been obtained. Their structures and topological nets were determined.
The MOFs were synthesized via CH and MW hydrothermal synthesis, obtaining the same pure phases with both methods with hardly variation of the synthesis conditions. The advantage of MW procedure, remaining in reduced reaction times and higher yields, facilitates the material manufacture. Structural and topological studies of every compound allowed proposing certain catalytic mechanisms for the tested reactions.

From our catalytic studies on these six new **In-MOFs** we can conclude that:

8- For cyanosilylation reactions, where there only are a couple of reactants, the factor that drives the reaction yield is the Indium coordination number so that catalytic activity decreases in this way: **InPF-16**> **InPF-18 >InPF-17**. **InPF-19** and **InPF-21** do not show any catalytic

activity, since in both of them the indium coordination number is 8, and thus no acid active sites are available.

9- In the Passerini reaction, with three organic substrates, all the three **InPF-16, InPF-18, InPF-17**, which own active sites, show the similar activity. **InPF17** that has the lowest catalytic activity in the cyanosilylation reaction becomes similar to the other catalyst activities in P-3CR, which suggests that reactants activation synchronization would be the reaction driving force. To prove that the larger is the involved substrate number, the more significant their synchronization rates becomes, the catalysts were tested in the U4-CR. Effectively, in this reaction the driving force is the substrate activation rates synchronization, since the order in catalytic activity goes in opposite direction than that in the two-component cyanosilylation: **InPF-16< InPF-18< InPF-17.**

We cautiously propose a parameter **$0 \leq x \leq 1$** based on the base/acid Lewis active site ratio that explains our results in the 4-CR. The closer to 1 the x is, the better is the catalytic behavior of the MOF.

Thus, **InPF-18**, with **x=0.8**, also presents good activity with the second TON value, and **InPF-16**, with **x=0.6**, hardly shows catalytic activity. As expected, **InPF-19** and **InPF-21** MOFs with **x=0** do not show any catalytic activity. In case of **InPF-17**, in which **x=1**, owns equal amounts of acid and base active sites and shows an excellent catalytic activity, with the higher TON for the studied 4-CR.

6.2. Perspectives

The study carried out was essentially experimental and as a result, many ideas have emerged on new developments based on the experimental selectivity control in heterogeneous catalysis processes changing the nature of the metal centers and/or using various combinations of elements. This allows to open new lines of research on multi-metallic MOFs focused on developing materials that could present different properties and be exploited in various applications, including as catalysts in multicomponent reactions.

6.3. Conclusiones

El presente trabajo se centra en la obtención de nuevos materiales tipo MOF empleando aluminio, galio e indio como centros metálicos y ligandos flexibles multicarboxilicos en forma de V como lo son 4,4 '- (hexafluorisopropiliden) bis (ácido benzoico) (H_2hfipbb), difenilmetano ácido 4,4-dicarboxílico (H_2dpmda) y 5- (4-carboxi-2-nitrofenoxi) -1,3-ácido bencenodicarboxílico (H_3popha). Como resultado, se obtuvieron veinte nuevos compuestos y estudiados en detalle, incluyendo el estudio de sus actividades catalíticas heterogéneas.

Se estudió el sistema de *p*-metal / H_2hfipbb, obteniendo seis nuevos materiales isoestructurales. Tres de ellos, empleando un solo tipo de metal los cuales fueron nombrados materiales **MPF**: **AlPF-1**, **GaPF-1** y **InPF-11β**. Las otras tres soluciones sólidas de tipo MOFs, fueron obtenidas mezclando diferentes cantidades de sales de galio e indio, estos materiales fueron nombrados **InGaPF-1**, **InGaPF-2** e **InGaPF-3**, observando:

1- Los materiales **MPF** [M(OR)(hfipbb)], (M = Al, Ga, In) fueron sintetizados bajo condiciones similares de temperatura y tiempo. Sin embargo, la formación de cada material depende de la selección mezcla disolvente adecuada. En el caso del material **InPF-11**, dos polimorfos son obtenidos y estas fases puras son obtenidas dependiendo del tipo de disolventes empleados: Para **InPF-11β**, es necesario una combinación de etilenglicol / agua, mientras que **InPF-11α** puede obtenerse empleando diferentes disolventes o mezclas.

La estructura de **MPF** consiste en cadenas inorgánicas infinitas conectadas a través del ligando orgánico formando una estructura 3D la cual presenta una red uninodal cuatro conectada exhibiendo una topología **dia**. La actividad catalítica de estos tres materiales fue comprobada mediante la reacción de Strecker de tres componentes (S3-CR); mostrando un comportamiento diferente en cada caso, proporcionando tres diferentes productos. Con el material **AlPF-1** se obtuvo el producto α-aminonitrilo esperado; sin embargo, cuando se emplearon **GaPF-1** y **InPF-11β**, se obtuvieron, la cianohidrina y la imina respectivamente. Estas diferencias son atribuidas a las diversas vías de reacción relacionadas con el proceso de activación de los reactantes para cada catalizador.

2- Con el fin de investigar si la combinación de ambos caminos podría alcanzar el producto α-aminonitrilo deseado, se prepararon soluciones sólidas de MOFs empleando combinaciones de sales de galio e indio. **InGaPF-1**, **-2** y **-3** con la fórmula $[M_xM'_{x-1}(O_2C_2H_4)_{0,5}$(hfipbb)] fueron diseñados en busca del control de las velocidades y selectividad de los diferentes pasos implicados en una reacción de tipo Strecker 3-C. La variación en el contenido de metal, en cada caso el material se hizo con el fin de apreciar el efecto real de la naturaleza del catión en la transformación orgánica. En caso de **InGaPF-1**, el cual posee un porcentaje de indio de x: 0,72 en la estructura, tomó 96 horas para alcanzar el producto-α aminonitrilo final, pero cuando se empleó **InGaPF-2** que tenía porcentajes similares de ambos metales, mejorar el tiempo de de la reacción catalítica (1.3h) y el aumento del rendimiento del producto se observó. El desarrollo de estas disoluciones sólidas de tipo MOFs mostró cómo es posible el control de la reactividad y selectividad de un catalizador heterogéneo mediante la modulación

de la relación de los diferentes metales que ocupan la misma posición cristalográfica en la estructura del material.

Del sistema compuesto por *p*-metal / H_2hfipbb / ligando nitrogenado se obtuvieron cinco nuevos materiales de tipo MOFs.

3- Estos cinco nuevos MOFs presentan las siguientes formulas: **InPF-12**: $[In_2(hfipbb)_3(1,10\text{-}phen)_2]$, **InPF-13**: $[In_2(hfipbb)_3(2,2'\text{-}bipy)_2]$, **InPF-14**: $[In_2(hfipbb)_3(4,4'\text{-}bipy)]$ y **InPF-15**: $[In_4(OH)_4(hfipbb)_4(4,4'\text{-}bipy)]$.

En caso de **InPF-12** e **InPF-13**, se emplearon adicionalmente los ligandos nitrogenados de tipo quelato (1,10-phen y 2,2-bipy), se pudo observar el incremento del número de coordinación de indio (CN) hasta 7 con diferentes tipos de coordinación para $hfipbb^{2-}$ (L_1 y L_2). El hecho de que dos posiciones de coordinación del metal fuesen bloqueadas dio como resultados, estructuras poliméricas 1D de topología tipo escalera en zigzag. Al emplearse un ligando auxiliar de tipo no quelato como la 4,4'-bipy, se obtuvieron dos estructuras diferentes: **InPF-14** y **InPF-15**, las cuales presentaron diferentes NC metálico (7 y 6, respectivamente) y diferentes modos de coordinación de $hfipbb^{2-}$ (L_2 y L_3-L_1, respectivamente). De hecho, se encontró que después de largos tiempos de reacción **InPF-14** es transformado en **InPF-15**, lo que significa que el primero era el producto cinéticamente estable, mientras el último era el termodinámicamente estable.

La actividad catalítica de estos materiales de indio fue evaluada mediante la cianosililación de compuestos de carbonilo, mostrando que: i) los catalizadores sin ningún tipo de ligandos auxiliares (**InPF-11α** y **β**) o con un segundo enlazador no quelato (**InPF-14** e **InPF-15**) en su estructura, mostraron una excelente actividad catalítica; ii) el número de coordinación del centro metálico y la presencia de grupos -OH tipo puente, parecen ser factores clave a la hora de conseguir un mejor comportamiento catalítico, y iii) la presencia adicional de sitios catalíticamente activos de tipo base de Lewis (μ-OH y grupo C=O no coordinado al metal), además de los sitios ácidos de Lewis, crea un sistema catalítico dual, basado en el fenómeno de "doble activación" que hace de **InPF-15** el mejor catalizador para este tipo de reacciones. También se encontró que el uso de este catalizador altamente reactivo, reciclable y ambientalmente benigno permite la síntesis de diversas cianohidrinas entre una amplia gama de cetonas cíclicas, alifáticas y aromáticas.

4- Respecto a la geometría del ligando principal $hfipbb^{2-}$, algunas observaciones se pueden hacer teniendo en cuenta las tres modalidades observadas: el modo de coordinación L_1 mostró geometrías alargadas con valores altos de LCA [119-121º]. En el caso de la parte libre del grupo (C=O) del ligando tipo L_1, presenta una interacción intramolecular, y por lo tanto un comportamiento geométrico diferente puede ser considerado para este tipo de ligando. En los MOFs que presentan un ligando de tipo L_2, son observadas geometrías distorsionadas con valores de LCA entre [104-113º]. Mientras, el modo L_3 no mostró alteraciones en los parámetros geométricos con un valor $\theta \sim 109º$ (respecto a la molécula orgánica) y los valores de LCA [112-116º] para los materiales que poseen en su estructura ligandos adicionales nitrogenados y [104-105º] para los materiales que utilizan sólo el ligando $hfipbb^{2-}$.

Al emplear el sistema *p*-metal /H_2dpmda / ligando nitrogenado, se obtuvieron cuatro nuevos materiales de tipo MOF llamados: **InPF-9**, **InPF-10**, **InPF-22** y **InPF-23**. Las conclusiones del estudio de este sistema son:

5- El uso de un ligando menos impedido estéricamente como H_2dpmda permitió aumentar la dimensionalidad de las estructuras obtenidas en el caso de los materiales construidos usando ligandos quelantes nitrogenadas adicionales, tales como 1,10-phen y 2,2'-bipy. Contrariamente a sus análogos con el enlazador H_2hfipbb (**InPF-12** y **InPF-13**, que sólo formaron cadenas 1D), el uso de H_2dpmda por lo tanto, permite obtener estructuras 2D con capas compuestos por anillos de 8 miembros (**InPF-9** e **InPF-10**), que muestran también los modos de coordinación L_1 y L_2 del ligando orgánico principal.

Los materiales **InPF-22** [In(OH)(dpmda)(H_2O)] e **InPF-23** [In(OH)(dpmda)]·0.5(4,4'-bipy) exhiben estructuras 3D construidas a partir de cadenas inorgánicas compartiendo vértices (SBU). Sin embargo, mientras que en el anterior están formados por poliedros de tipo InO_7, este último muestra poliedros octaedros InO_6. Sus estructuras pueden simplificarse entonces como redes uninodales seis-conectadas con topología **dia** para **InPF-22** y topología **pcu** para **InPF-23**.

6- En cuanto a la actividad catalítica de los cuatro MOF, estos materiales presentan una buena actividad catalítica heterogénea ácido de Lewis, cuya dimensionalidad parecía estar directamente relacionado con el incremento en su rendimiento catalítico. En este asunto, los materiales **InPF-22** e **InPF-23** con estructuras 3D mostraron valores de TOF más altos que aquellos materiales **InPF-9** e **InPF-10**, construidos con ligandos nitrogenados tipo quelato y estructura 2D.

El sistema comprendido por *p*-metal / H_3popha / ligando nitrogenado, se obtuvieron seis nuevos materiales MOF: **InPF-16** a **InPF-21**. Las conclusiones que pueden deducirse son las siguientes:

7- Se obtuvieron 6 nuevos MOFs de indio con diversas características químicas y estructurales (diferentes números de coordinación del centro metálico, centros activos de Lewis, la existencia simultánea de bases de Lewis). Para todos sus estructuras y redes topológicas fueron determinadas.

Estos MOFs fueron sintetizaron a través de síntesis hidrotermal convencional y de microondas la obtención de las mismas fases puras con ambos métodos con apenas variación de las condiciones de síntesis. La ventaja de emplear la síntesis por microondas, parece enfocarse únicamente en la reducción de los tiempos de reacción y la obtención de rendimientos más altos, lo que facilita la fabricación material.

8- Los estudios estructurales y topológicos de cada compuesto permitieron proponer ciertos mecanismos catalíticos para las reacciones probadas.

En el caso de la reacción de cianosililación, donde sólo se emplean un par de reactivos, el factor que impulsa el rendimiento de la reacción es el número de coordinación de indio para la cual, la actividad catalítica disminuye de la siguiente manera: **InPF-16> InPF-18> InPF-17**. En el caso de **InPF-19** y **InPF-21** ninguna actividad catalítica es observada, esto se debe a que en ambos materiales el número de coordinación del centro metálico es 8, y por lo tanto no existen sitios catalíticamente activos disponibles.

9- En la reacción de Passerini, que emplea tres sustratos orgánicos, los catalizadores **InPF-16**, **InPF-18**, **InPF-17**, que poseen sitios activos, muestran una actividad similar. Mientras **InPF17** el cual en la anterior cianosililación presentó la actividad catalítica más baja, se comporta en el caso de la Passerini de manera comparable con los tres previamente mencionados, lo que sugiere que la sincronización de la activación de los reactivos sería el motor de reacción.

Para demostrar que cuanto mayor es el número sustrato involucrado, más significativas las tasas de sincronización en la activación son. Se probaron los catalizadores en la reacción Ugi de cuatro componentes. Donde, efectivamente fue demostrado que la fuerza impulsora de la reacción es debido a la tasas de activación de sincronización de sustrato, ya que el orden en la actividad catalítica va en dirección opuesta a la de la cyanosilylation de dos componentes: **InPF-16 <InPF-18 <InPF-17**.

Se propone entonces cautelosamente un parámetro **$0 \leq x \leq 1$** basado en la relación de sitios catalíticamente activos base/ácido de Lewis, que explica los resultados en la U4-CR. Observando la tendencia de mayor actividad catalítica al acercarse a 1 el valor de x.

Por lo tanto, como era de esperar, los materiales **InPF-19** e **InPF-21** con $x = 0$ no muestran ninguna actividad catalítica. Mientras **InPF-16**, con $x = 0.6$ muestra una actividad catalítica pequeña comparado con la buena actividad demostrada por **InPF-18**, con $x = 0.8$. Finalmente es **InPF-17**, con $x = 1$, que posee la misma cantidad de sitios activos de ácidos y bases, quien muestra una excelente actividad catalítica, exhibiendo el mayor TON para la reacción Ugi.

6.4. Perspectivas

El estudio realizado es esencialmente experimental y como consecuencia del mismo han surgido numerosas ideas para realizar nuevos desarrollos experimentales sobre el control de la selectividad en los procesos de catálisis heterogénea modificando la naturaleza de los centros metálicos empleando diversas combinaciones de sales. Todo ello ha permitido abrir nuevas líneas de investigación acerca de las multimetal-MOFs enfocados al desarrollo de materiales que exhiban diferentes propiedades y puedan ser aprovechadas en diversas aplicaciones, entre ellas la selectividad catalítica en reacciones multicomponentes.

APPENDIX

In this part are included the corresponding Infrared spectra, thermogravimetric curves and powder X-ray diffraction patterns of the TG residues, performed to all synthesized materials described in chapter 3. Additionally are presented the SEM images, particle sizes and synthetic conditions of those MOFs materials with popha linker, synthesized through MW and CH hydrothermal assisted synthesis. Finally, the GC-MS, ^{1}H and ^{13}C NMR spectra follow up of the corresponding catalysis reactions, as well as the ESI-MS and IR spectra performed in order to characterize the catalytic products, described in chapter 5.

A. Infrared Spectra for all synthesized materials

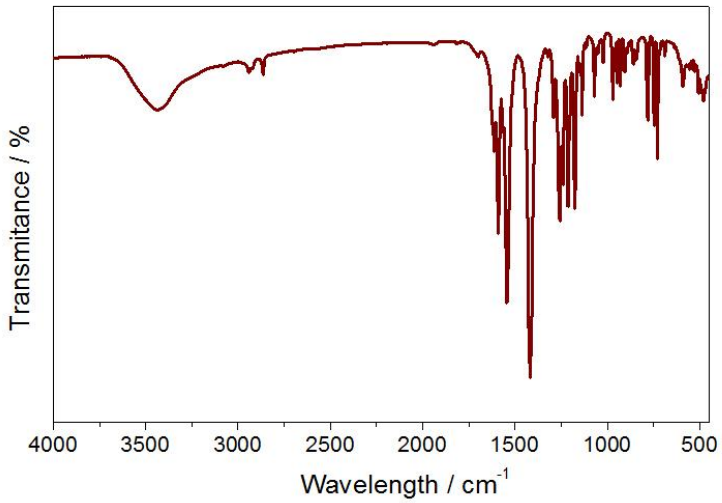

Figure A.1 FT-Infrared spectra of the **InPF-11β**, in the 4000-300 cm^{-1} range.

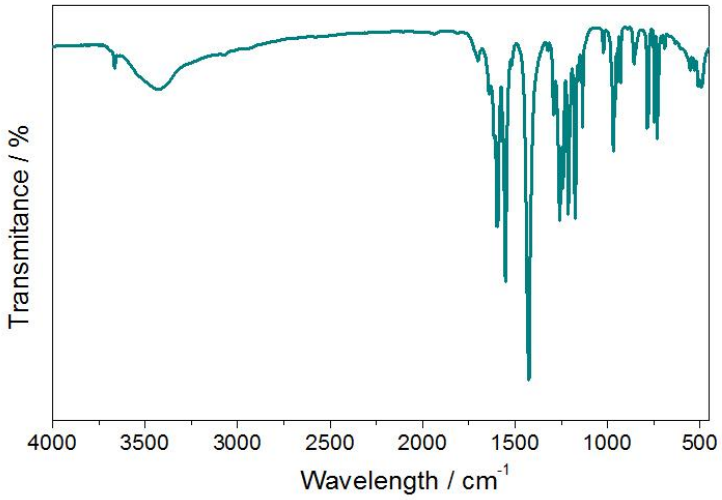

Figure A.2 FT-Infrared spectra of the **GaPF-1**, in the 4000-300 cm^{-1} range.

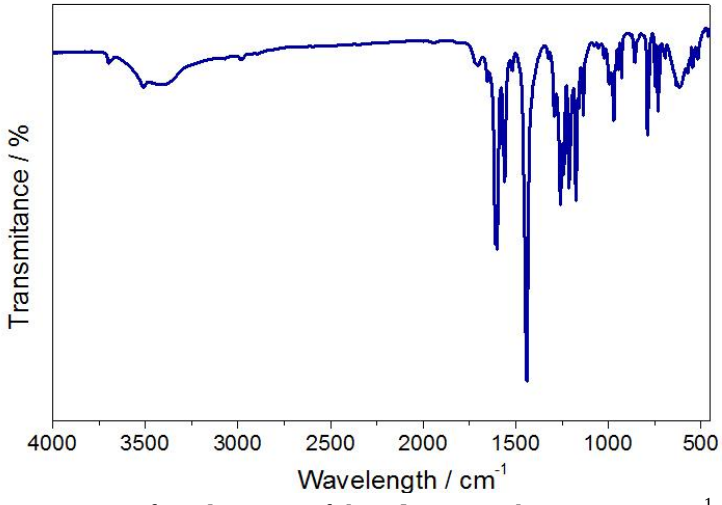

Figure A.3 FT-Infrared spectra of the **AlPF-1**, in the 4000-300 cm^{-1} range.

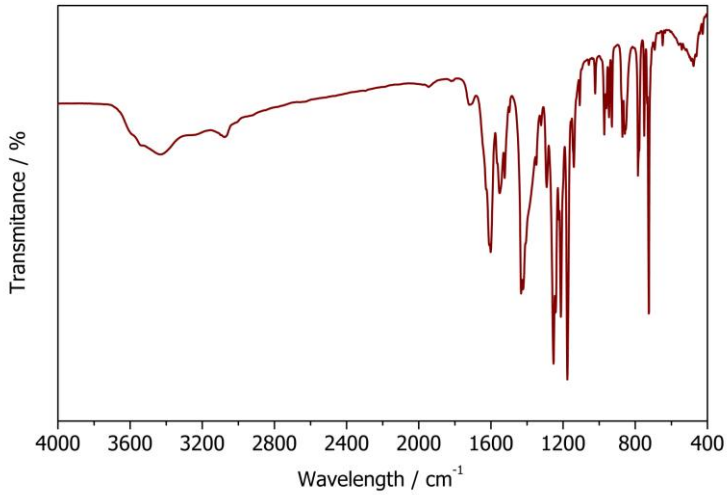

Figure A.4 FT-Infrared spectra of the **InPF-12**, in the 4000-300 cm^{-1} range.

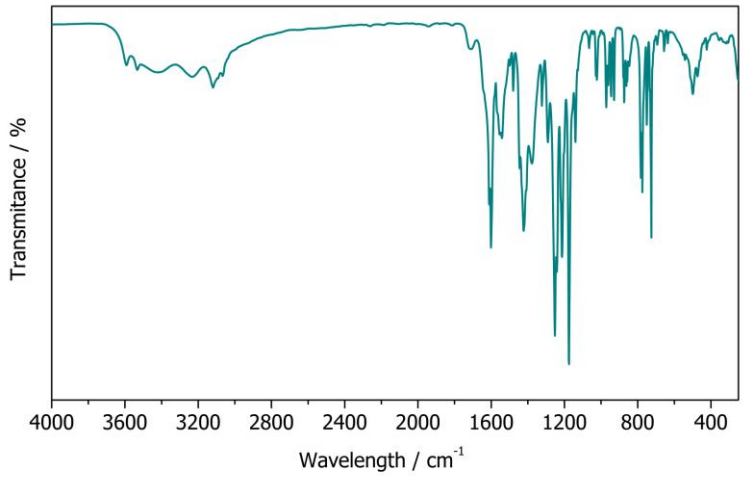

Figure A.5 FT-Infrared spectra of the **InPF-13**, in the 4000-300 cm^{-1} range.

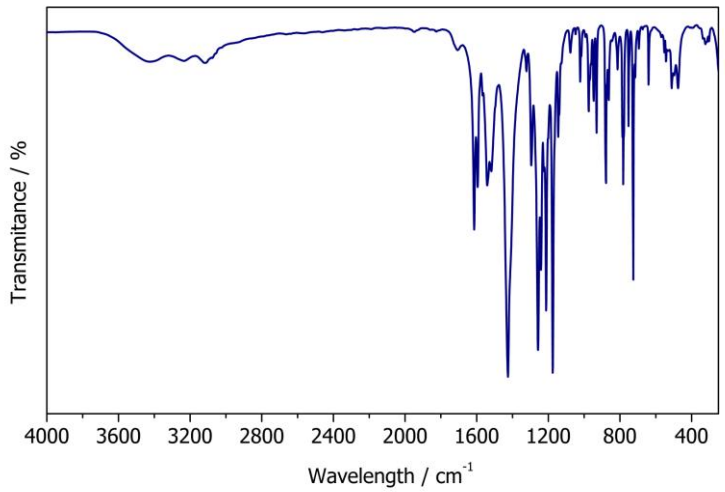

Figure A.6 FT-Infrared spectra of the **InPF-14**, in the 4000-300 cm^{-1} range.

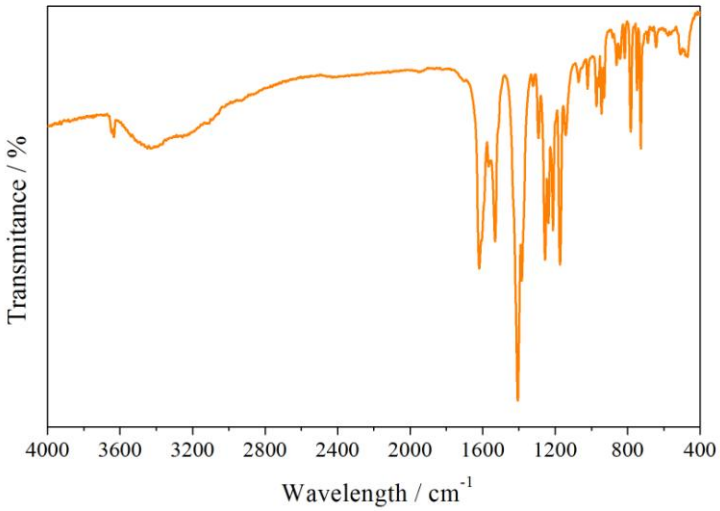

Figure A.7 FT-Infrared spectra of the **InPF-15**, in the 4000-300 cm^{-1} range.

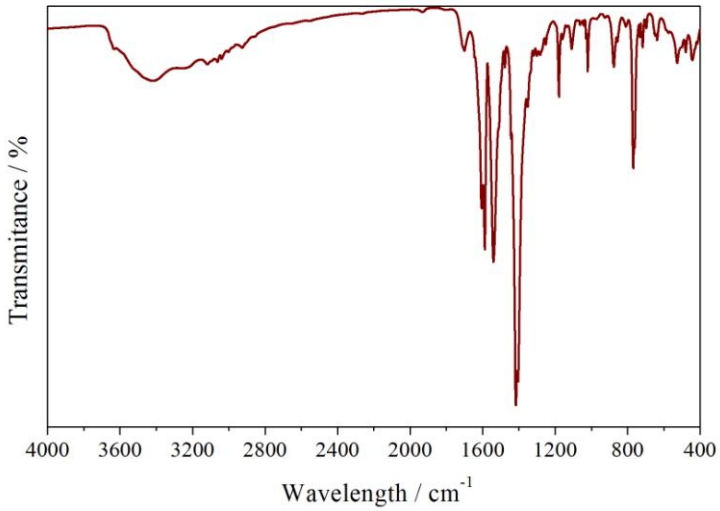

Figure A.8 FT-Infrared spectra of the **InPF-9**, in the 4000-300 cm^{-1} range.

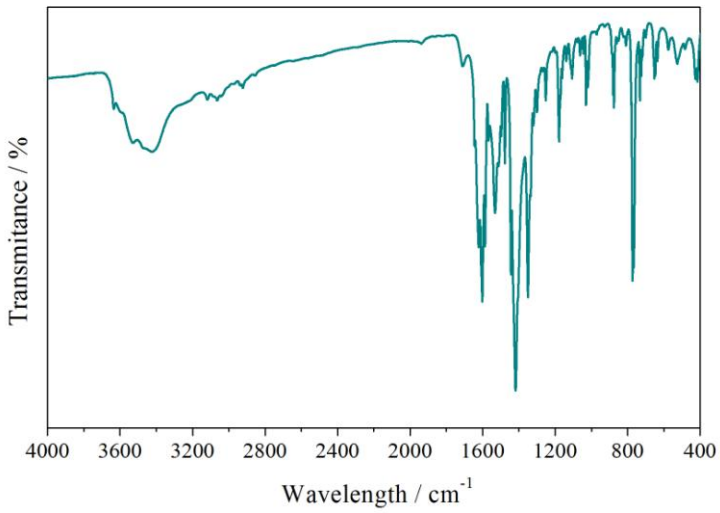

Figure A.9 FT-Infrared spectra of the **InPF-10**, in the 4000-300 cm^{-1} range.

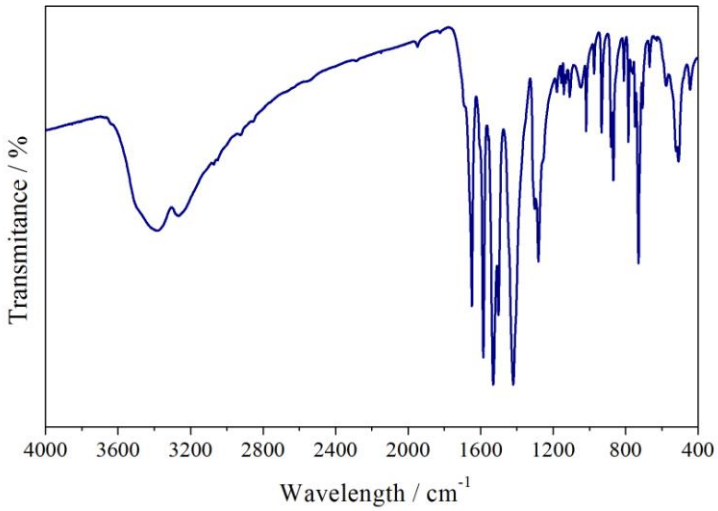

Figure A.10 FT-Infrared spectra of the **InPF-22**, in the 4000-300 cm^{-1} range.

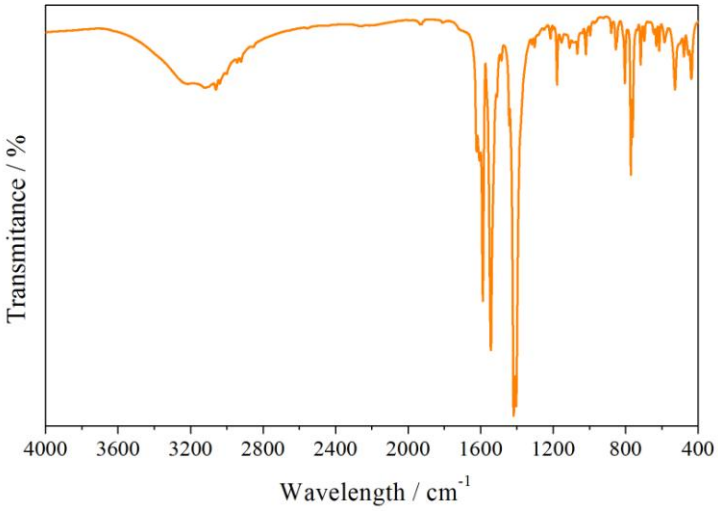

Figure A.11 FT-Infrared spectra of the **InPF-23**, in the 4000-300 cm^{-1} range.

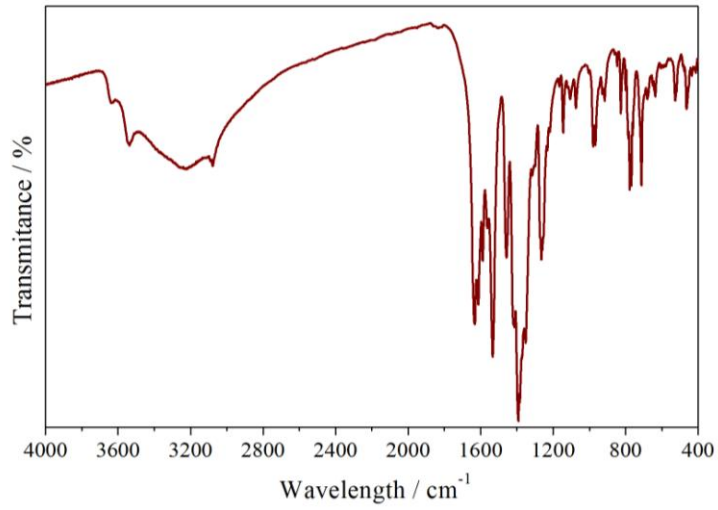

Figure A.12 FT-Infrared spectra of the **InPF-16**, in the 4000-300 cm^{-1} range.

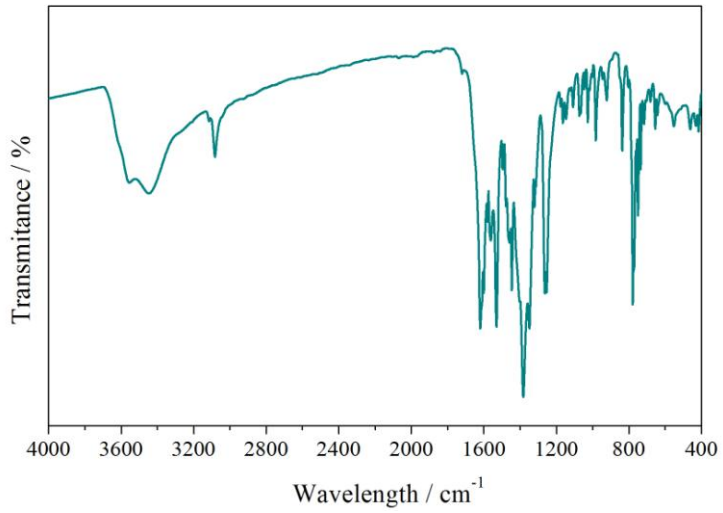

Figure A.13 FT-Infrared spectra of the **InPF-17**, in the 4000-300 cm^{-1} range.

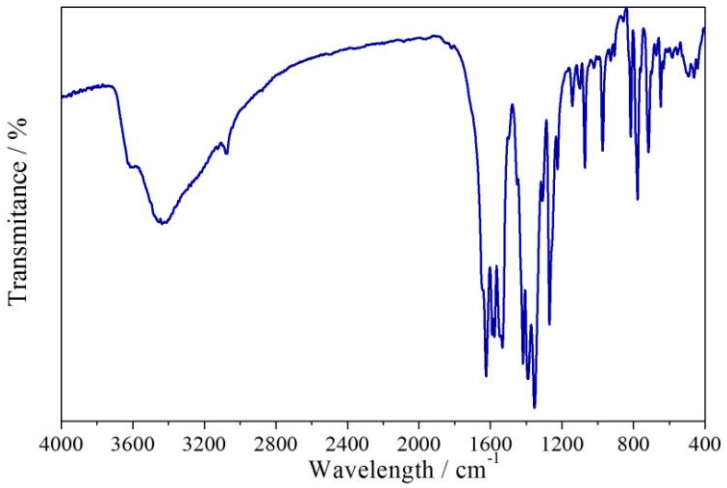

Figure A.14 FT-Infrared spectra of the **InPF-18**, in the 4000-300 cm^{-1} range.

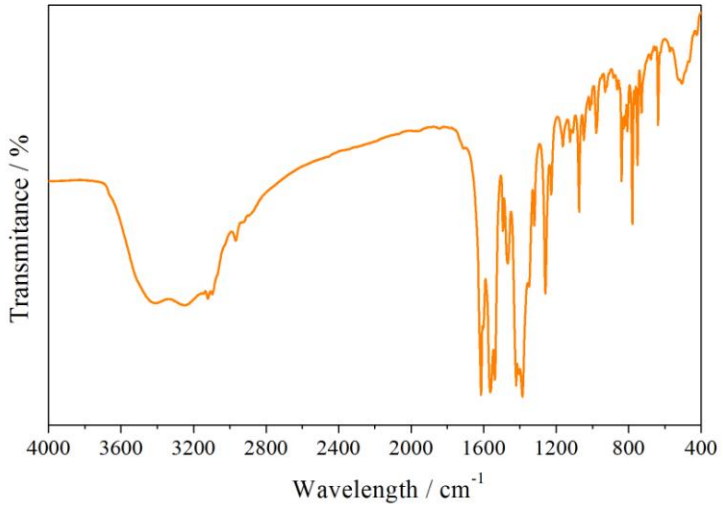

Figure A.15 FT-Infrared spectra of the **InPF-19**, in the 4000-300 cm^{-1} range.

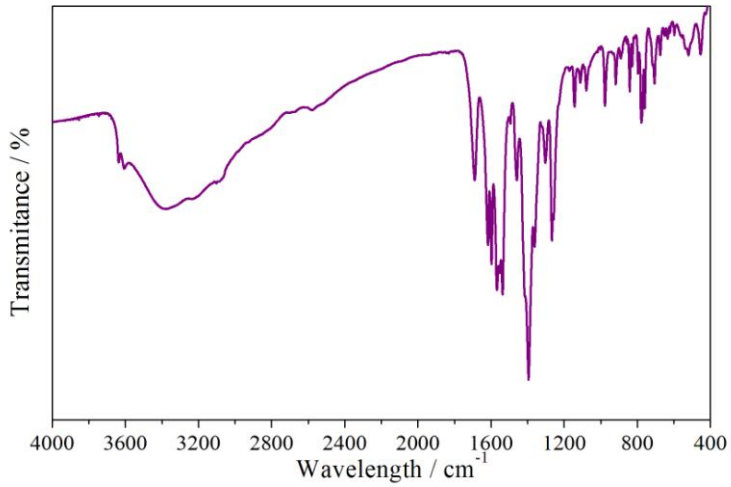

Figure A.16 FT-Infrared spectra of the **InPF-20**, in the 4000-300 cm^{-1} range.

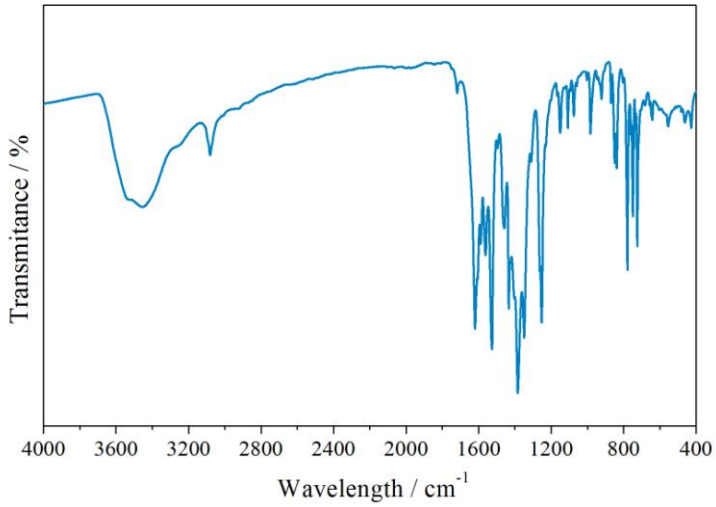

Figure A.17 FT-Infrared spectra of the **InPF-21α**, in the 4000-300 cm^{-1} range.

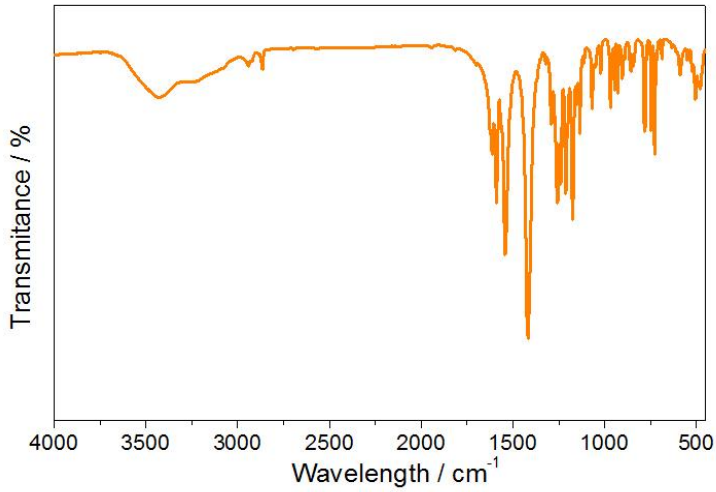

Figure A.18 FT-Infrared spectra of the **InGaPF-1**, in the 4000-300 cm^{-1} range.

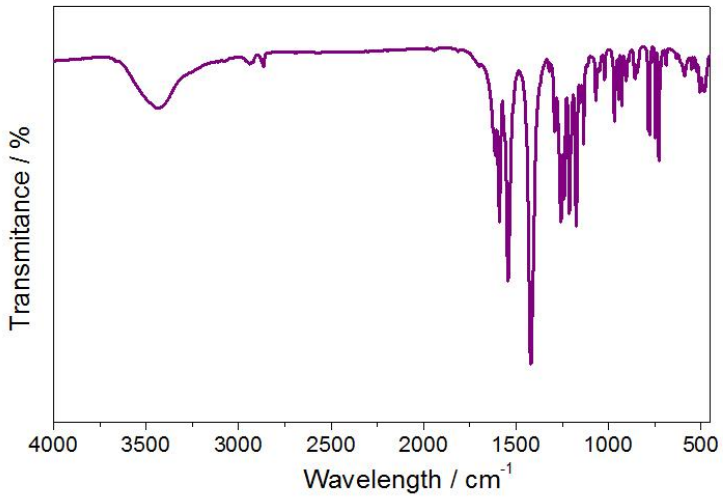

Figure A.19 FT-Infrared spectra of the **InGaPF-2**, in the 4000-300 cm^{-1} range.

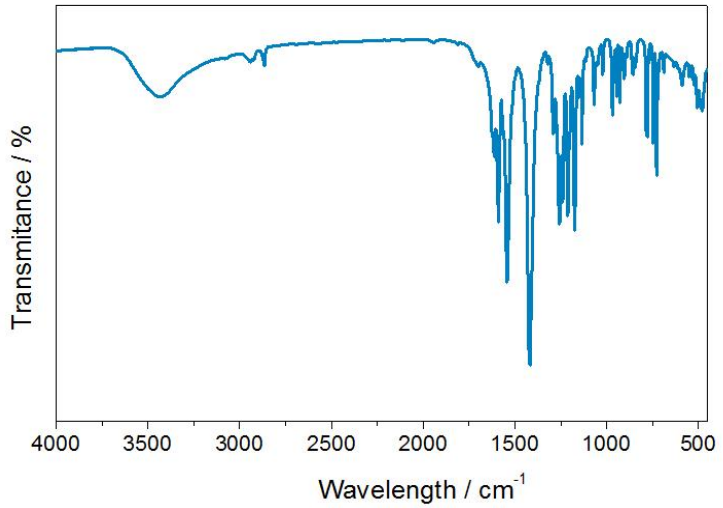

Figure A.20 FT-Infrared spectra of the **InGaPF-3**, in the 4000-300 cm^{-1} range.

B. Thermogravimetric curves for all synthesized materials

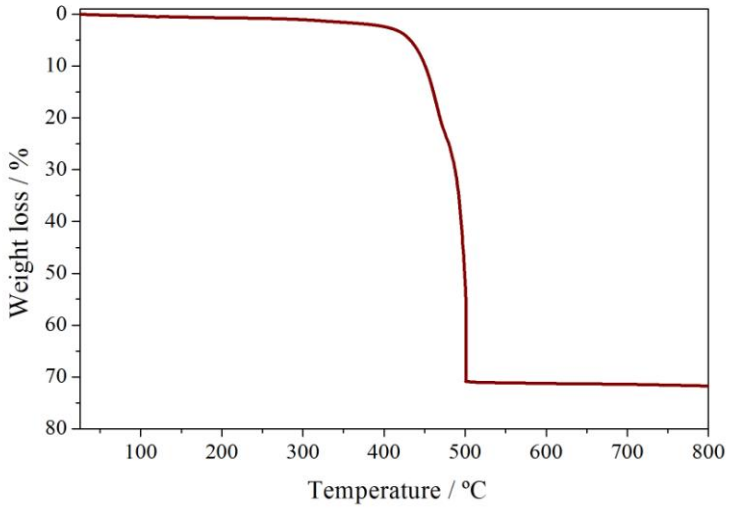

Figure B.1 The **InPF-11β** TG curve

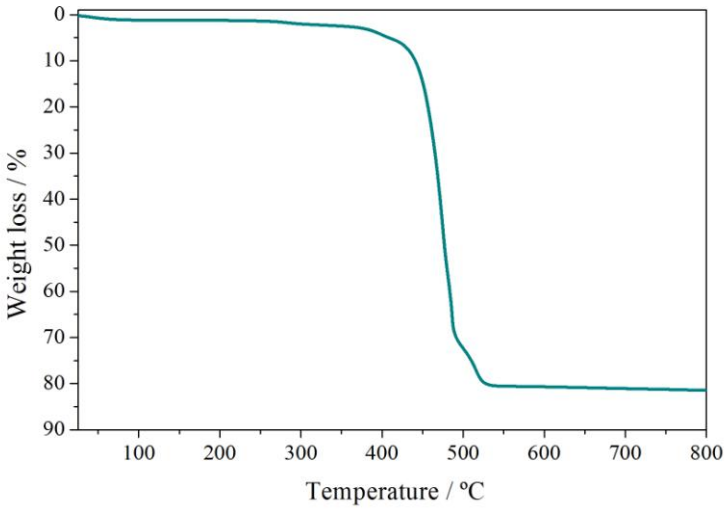

Figure B.2 The **GaPF-1** TG Curve

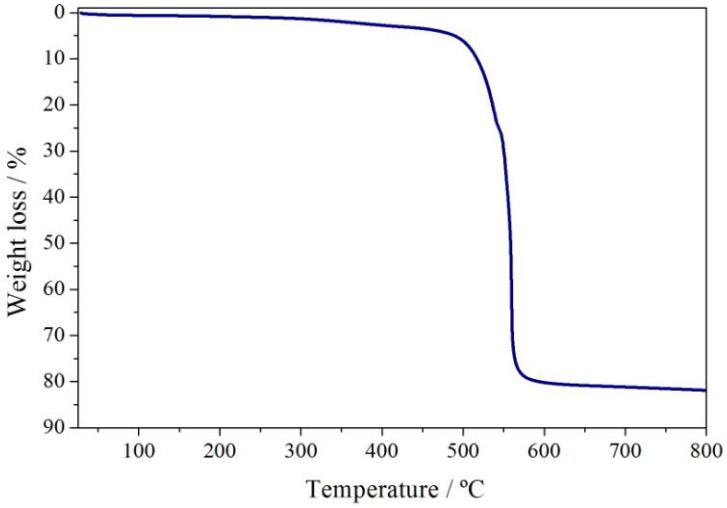

Figure B.3 The **AlPF-1** TG curve

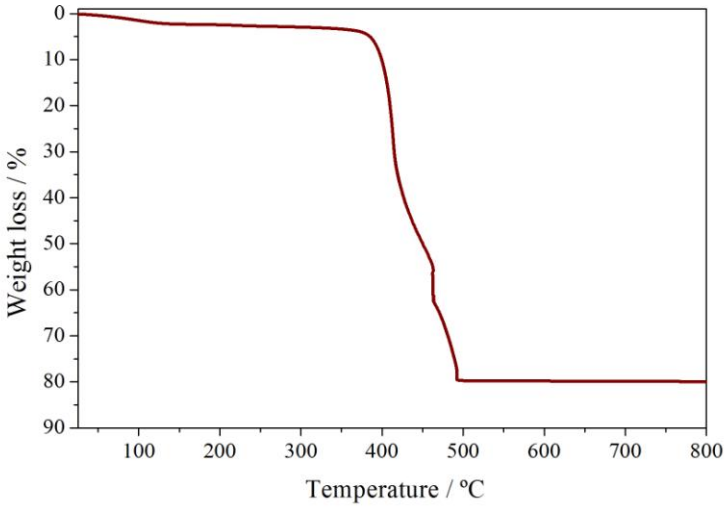

Figure B.4 The **InPF-12** TG curve

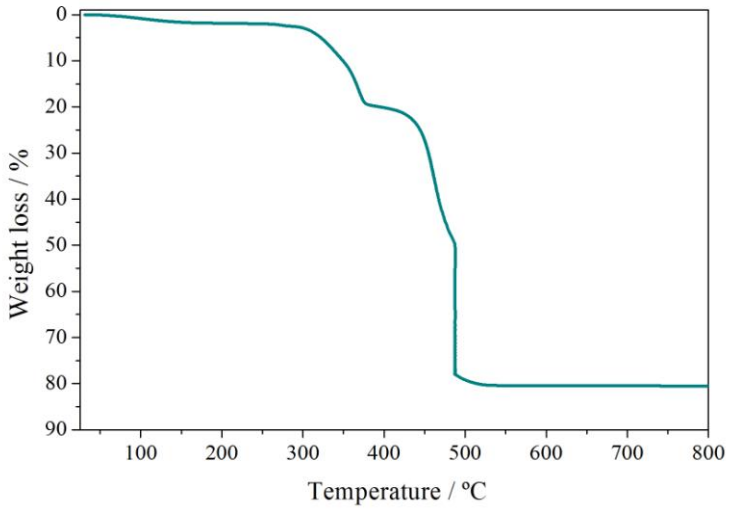

Figure B.5 The **InPF-13** TG curve

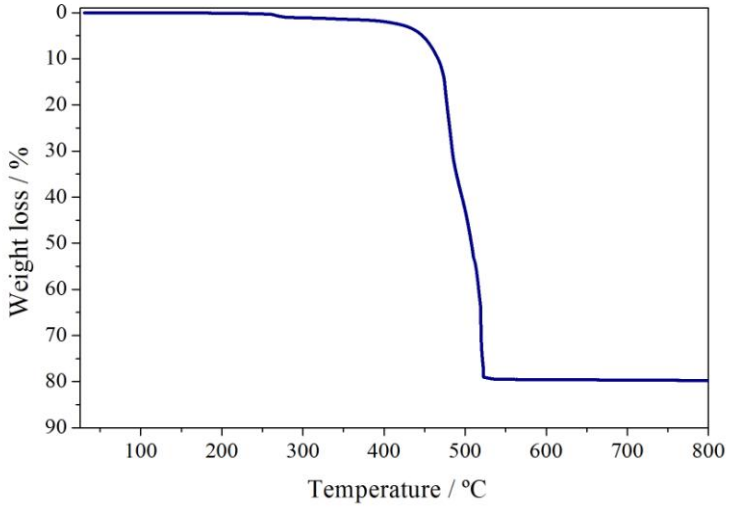

Figure B.6 The **InPF-14** TG curve

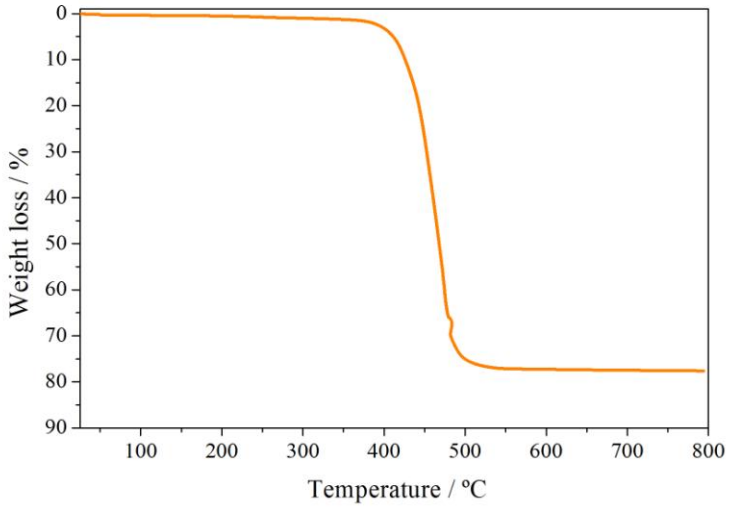

Figure B.7 The **InPF-15** TG curve

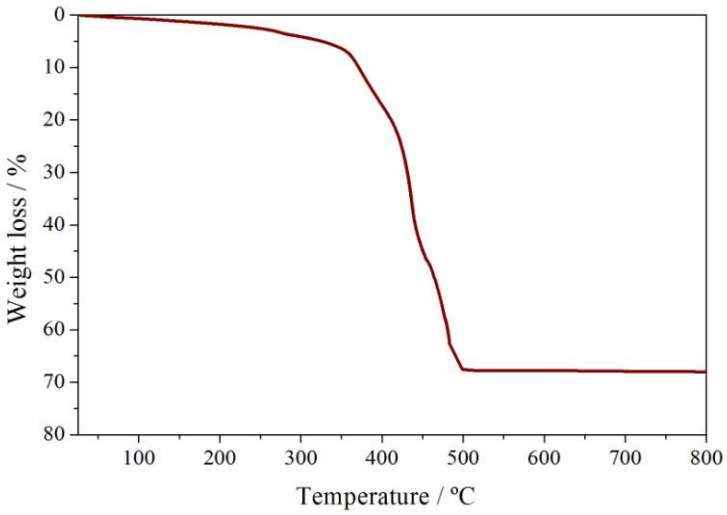

Figure B.8 The **InPF-9** TG curve

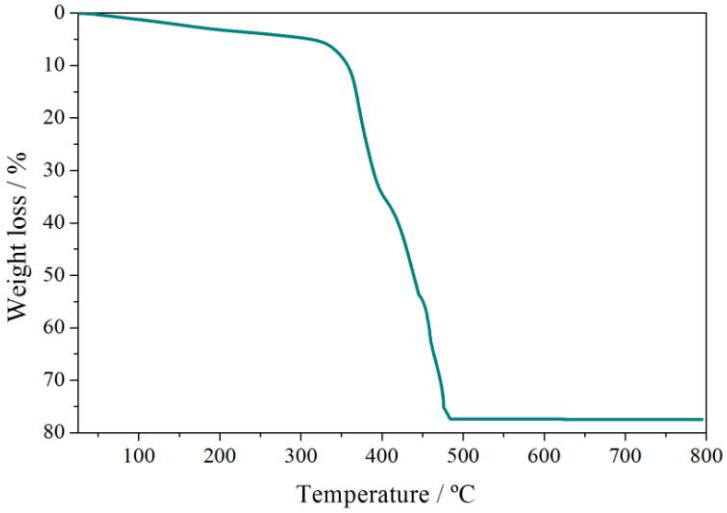

Figure B.9 The **InPF-10** TG curve

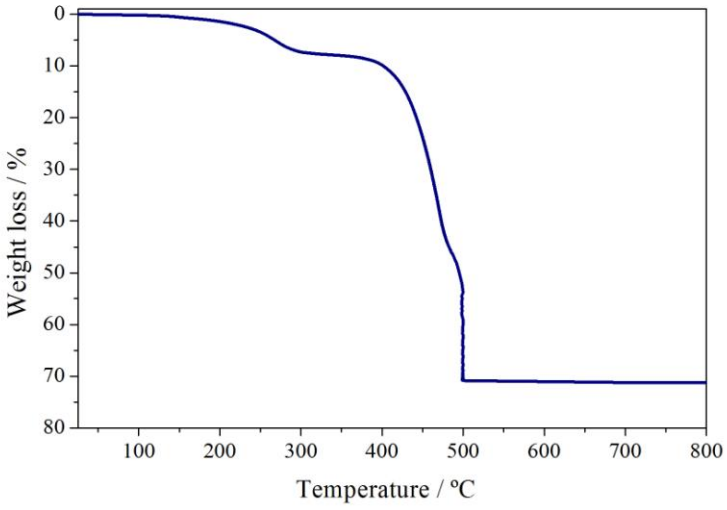

Figure B.10 The **InPF-22** TG curve

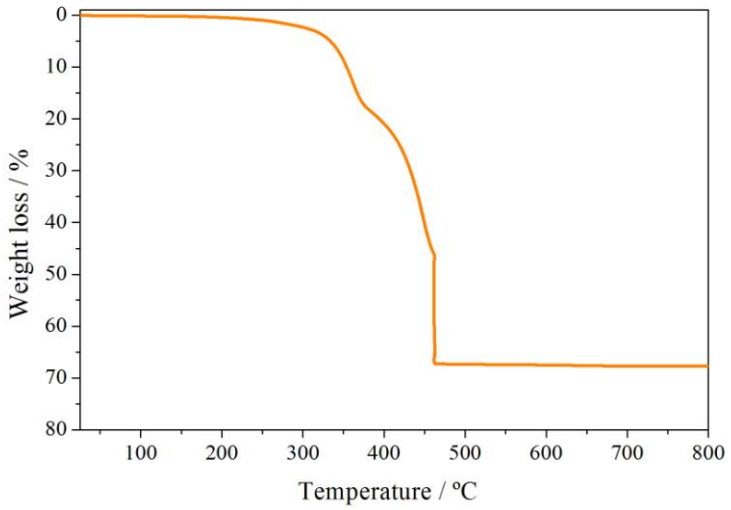

Figure B.11 The **InPF-23** TG curve

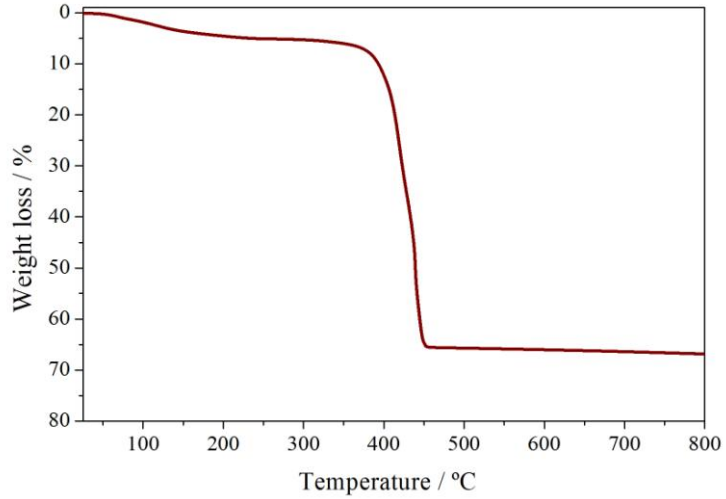

Figure B.12 InPF-16 TG curve

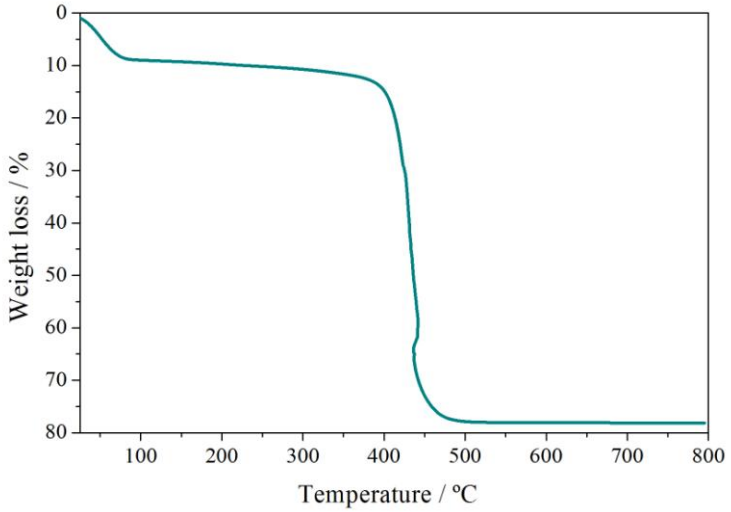

Figure B.13 The **InPF-17** TG Curve

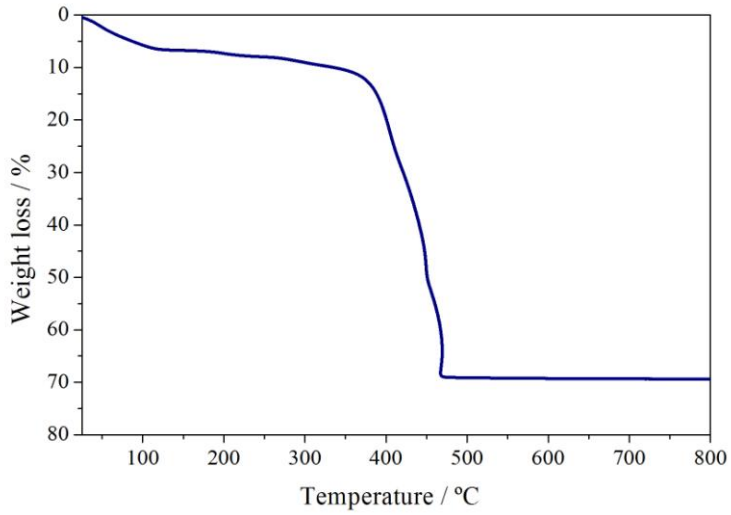

Figure B.14 The **InPF-18** TG curve

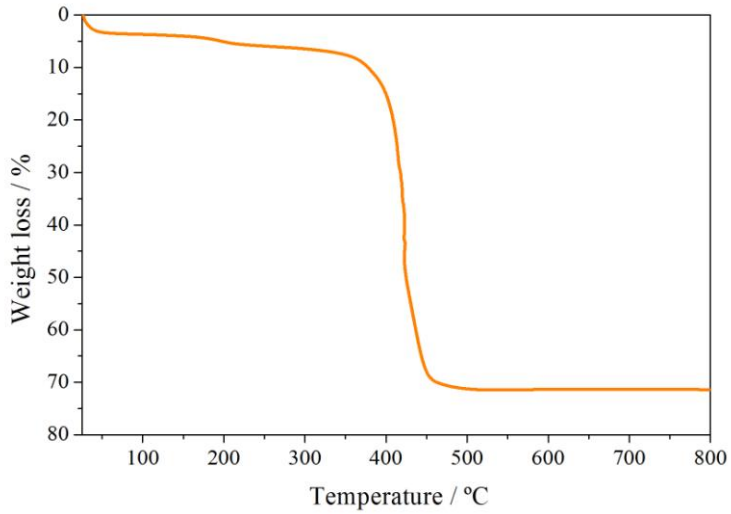

Figure B.15 The **InPF-19** TG curve

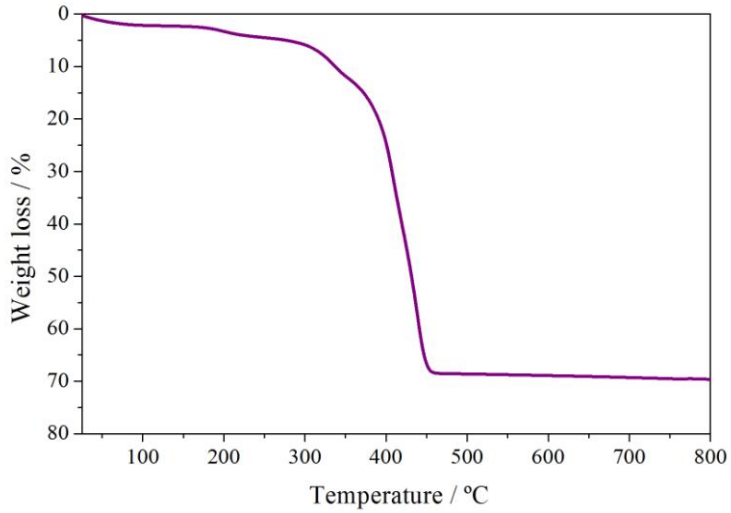

Figure B.16 The **InPF-20** TG Curve

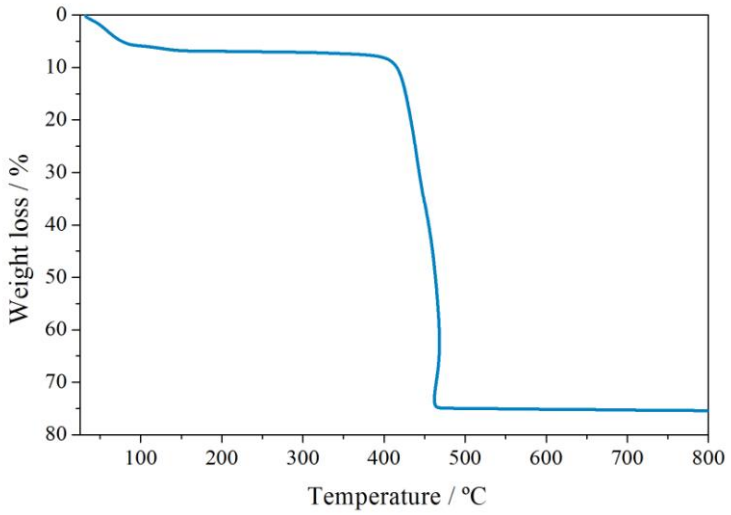

Figure B.17 The **InPF-21α** TG curve

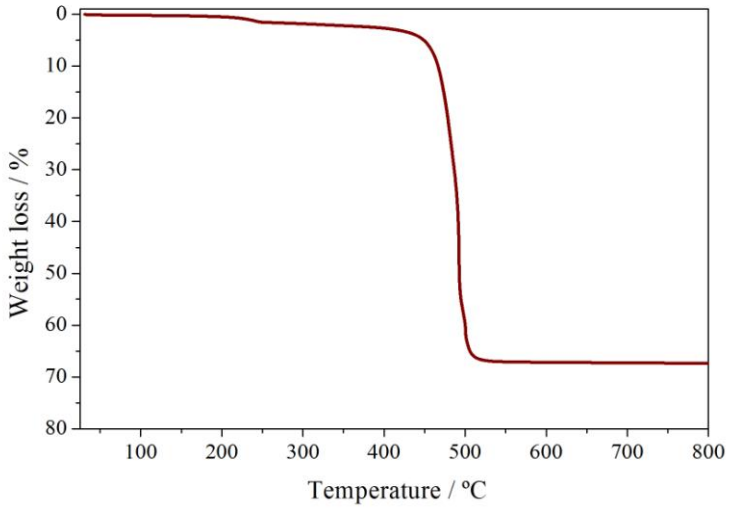

Figure B.18 The **InGaPF-1** TG curve

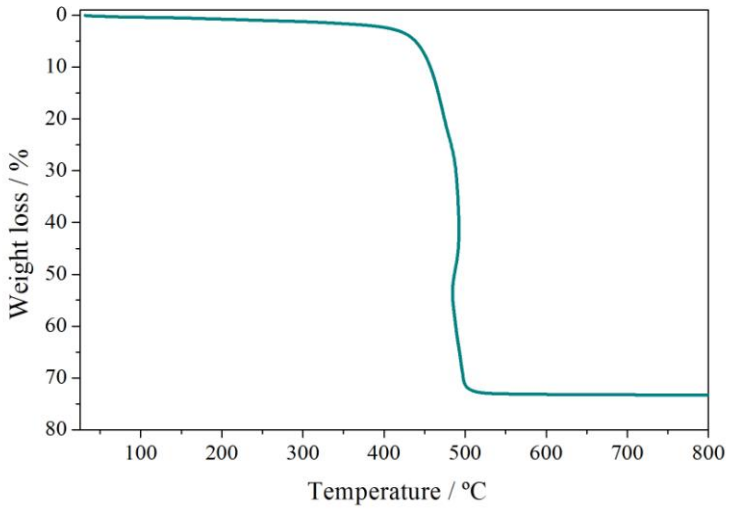

Figure B.19 The **InGaPF-2** TG curve

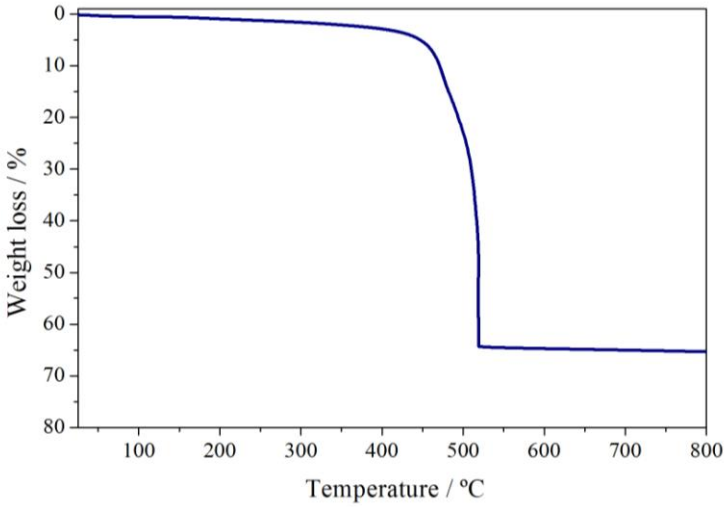

Figure B.20 The **InGaPF-3** TG curve

C. PXRD of all materials TG residues

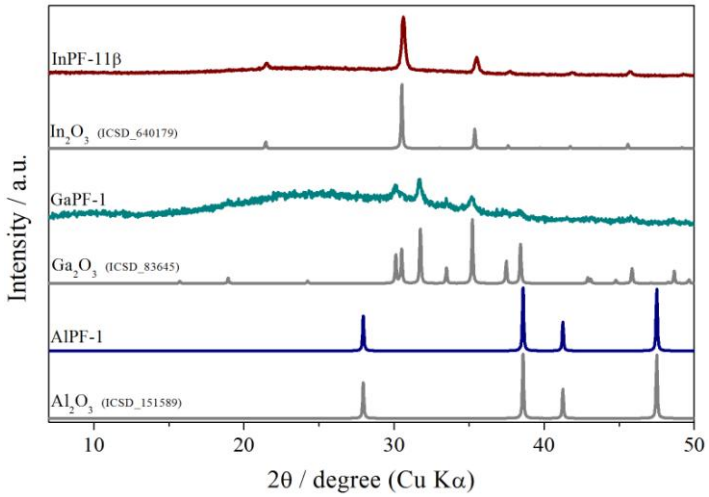

Figure C.1 TG residues of compounds **InPF-11β, GaPF-1** and **AlPF-1**

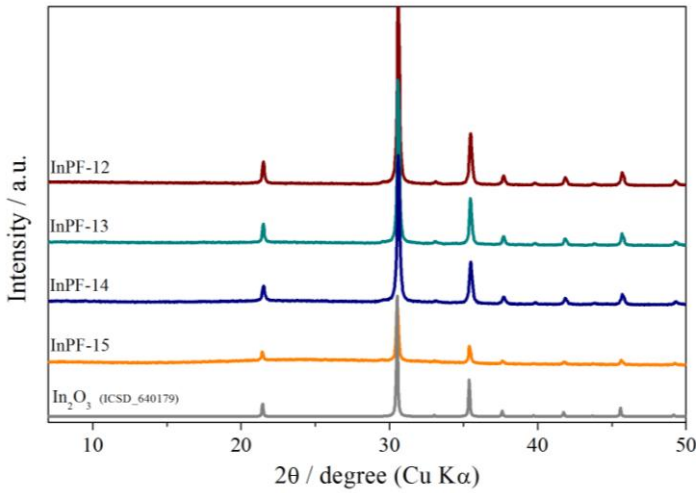

Figure C.2 TG residues of compounds **InPF-12** to **InPF-15** and the In_2O_3

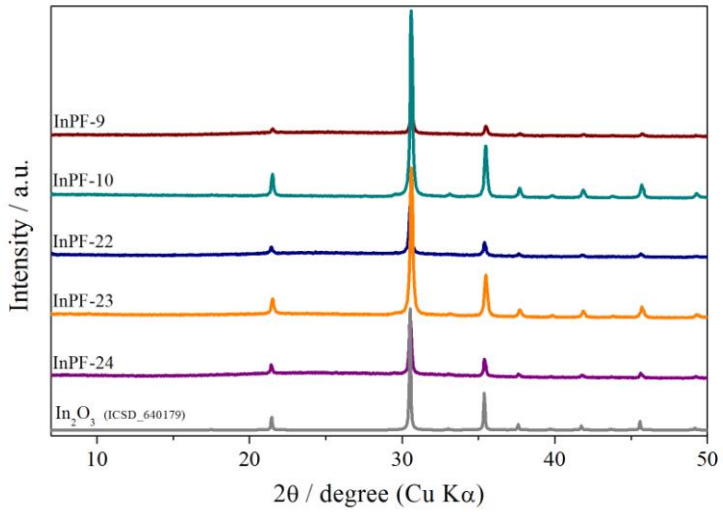

Figure C.3 TG residues of compounds **InPF-9** to **InPF-24** and the In_2O_3

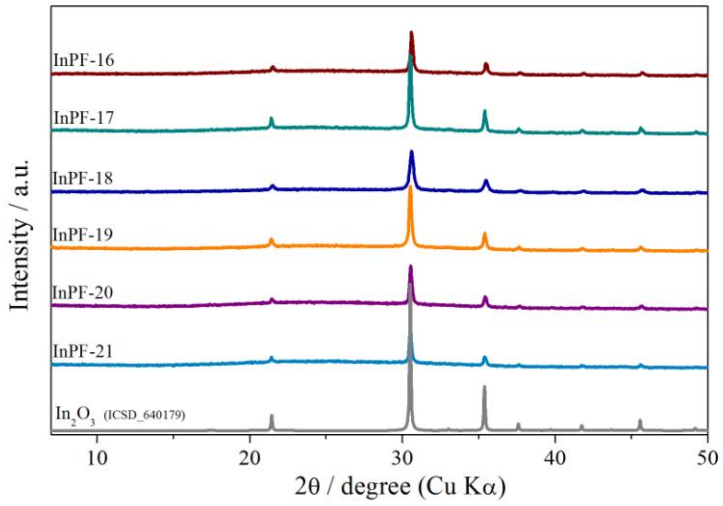

Figure C.4 TG residues of compounds **InPF-16** to **InPF-21** and In_2O_3

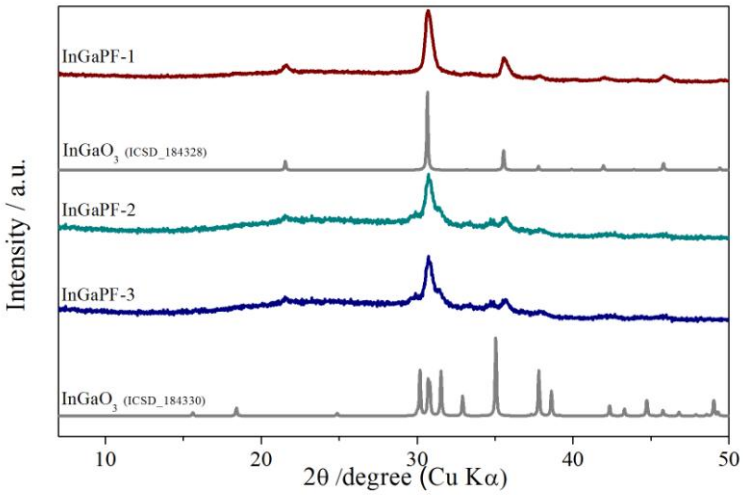

Figure C.5 TG residues of compounds **InGaPF-1** to **InGaPF-3** and In_2O_3

D. InPF materials with popha^{3-} linker synthesized using MW and CH reaction conditions

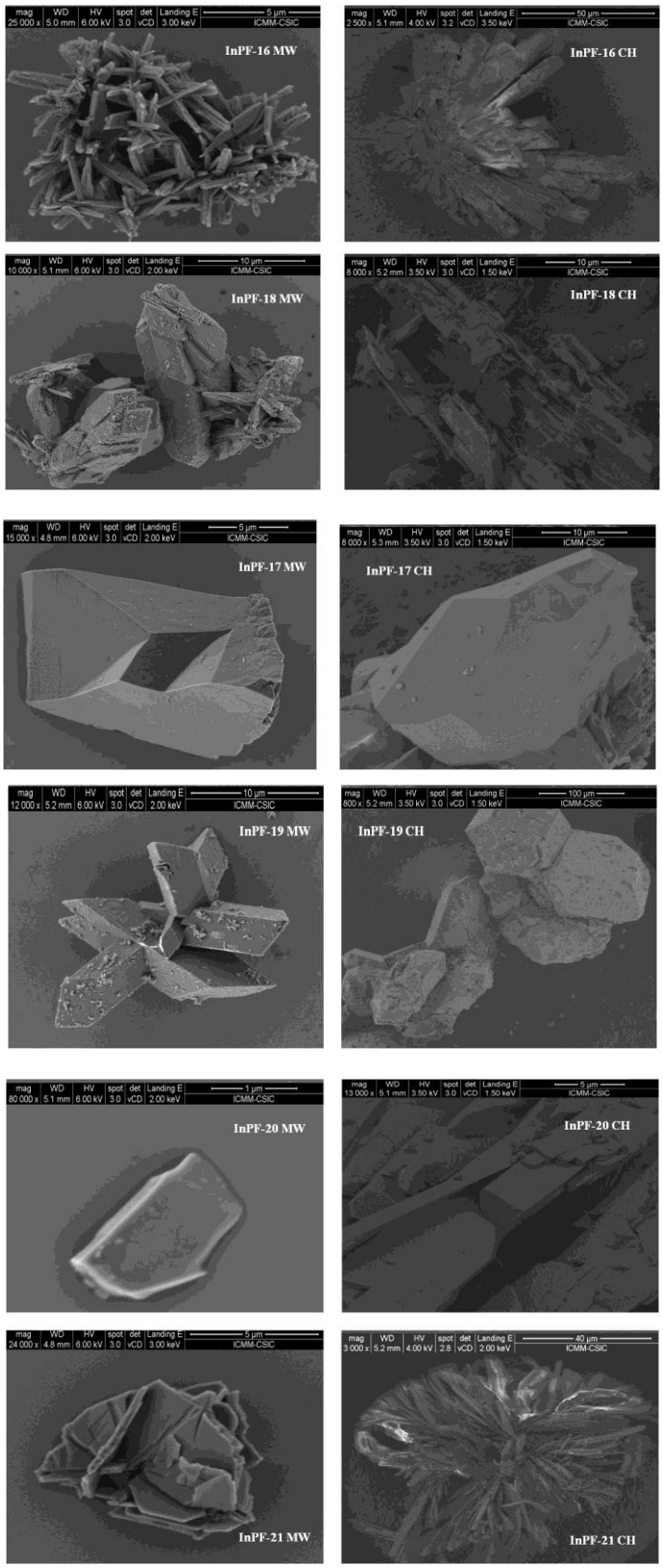

Figure D.1. SEM images of the MW (15000x mag, left) and CH (8000x mag, right) synthesized InPF materials.

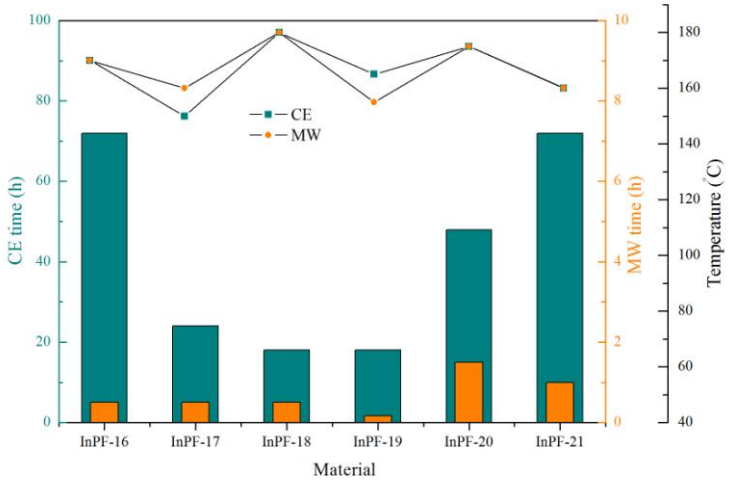

Figure D.2 Comparison between MW and CH reaction conditions to obtain **InPF** materials.

The dynamic light scattering (DLS) analysis, performed using water as a solvent at 25 ºC, showed a broad range of particle sizes for the **InPF** materials. Even though several researches have suggested that using MW well defined particle size materials can be obtained, in our case, for almost all **InPF** materials, the particle average size is around 400nm, and there is a large variation in their size distribution curve. The advantages, remaining in reduced reaction times and higher yields, facilitate the material elaboration.

Table D.1. Average particle size distribution for the I**nPF** materials

Material	No. Particle	Particle size distribution range	% particles in the size range
InPF-16	2037	355-446 nm	78
InPF-17	2817	389-616 nm	98
InPF-18	2518	148-468 nm	68
InPF-19	2982	355-467 nm	41
InPF-20	2537	295-446 nm	74
InPF-21α	3684	389-467 nm	70

E. GC-MS results for catalytic cyanosilylation product characterization

In order to identify the principal product in the cyanosilylation reaction and obtain the conversion yield, small amounts of catalytic sample at different reaction times were analyzed through CG-MS. The yields reported in the document tables were determined by the area under the curve in the reported chromatogram.

(a) 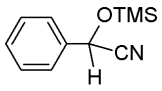

$C_{11}H_{15}NOSi$

205.33g/mol

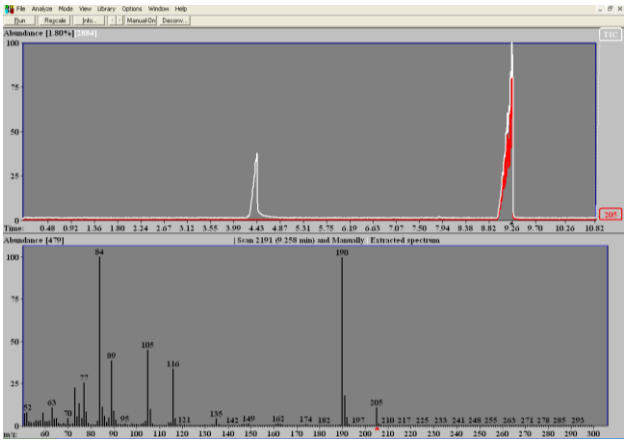

Figure E.1 View of the GC-MS for the cyanohydrin (a)

(b) 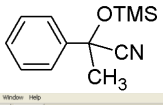

$C_{12}H_{17}NOSi$

219.35g/mol

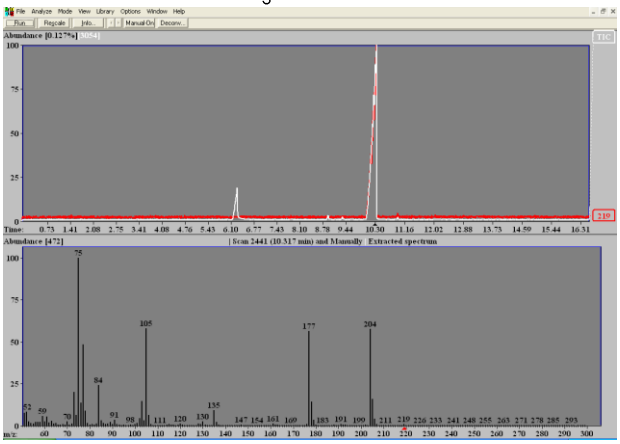

Figure E.2 View of the GC-MS for the cyanohydrin (b)

(c) 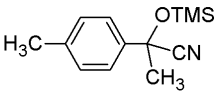

$C_{13}H_{19}NOSi$

233.38g/mol

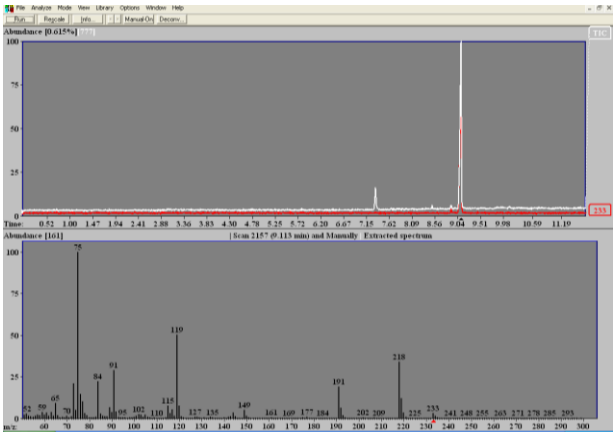

Figure E.3 View of the CG-MS for the cyanohydrin (c)

(d) 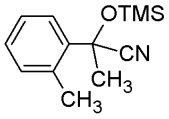

$C_{13}H_{19}NOSi$
233.38g/mol

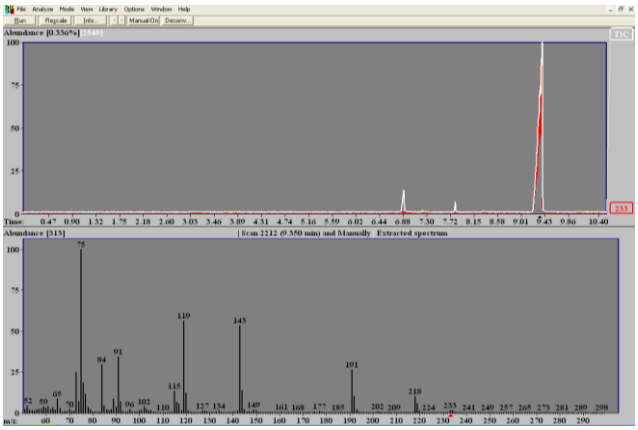

Figure E.4 View of the CG-MS for the cyanohydrin (d)

(e) 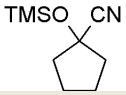

$C_9H_{17}NOSi$
183.32g/mol

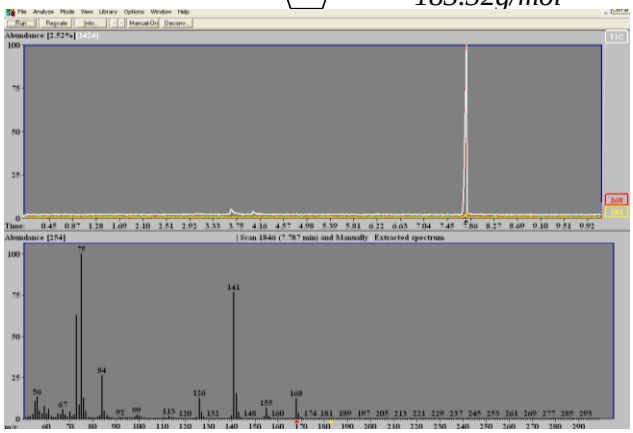

Figure E.5 View of the CG-MS for the cyanohydrin (e)

(f) 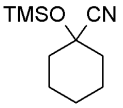

$C_{10}H_{19}NOSi$
197.35g/mol

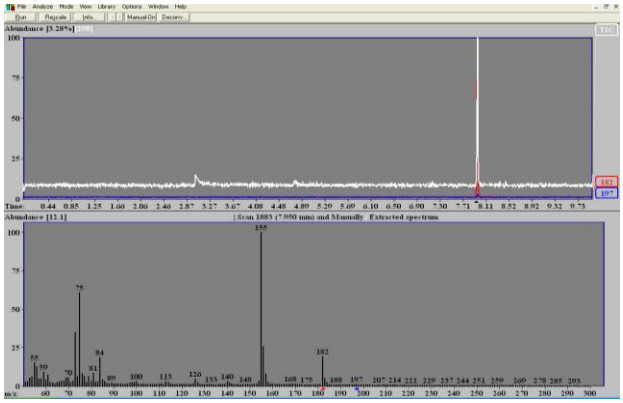

Figure E.6 View of the CG-MS for the cyanohydrin (f)

(g) 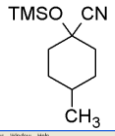

$C_{11}H_{21}NOSi$
211.38g/mol

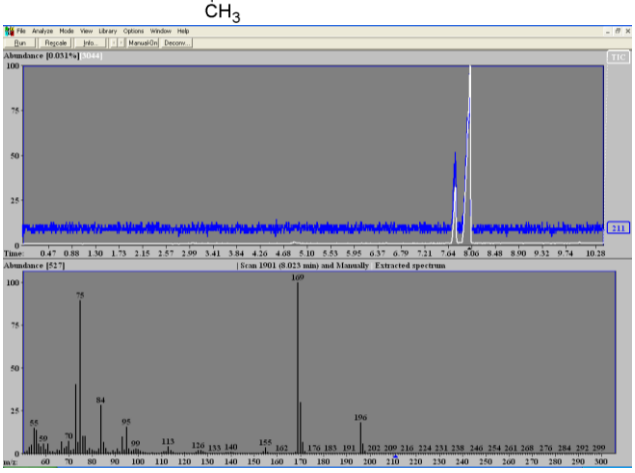

Figure E.7 View of the CG-MS for the cyanohydrin (g)

(h) 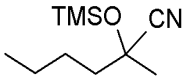

$C_{10}H_{21}NOSi$
199.36g/mol

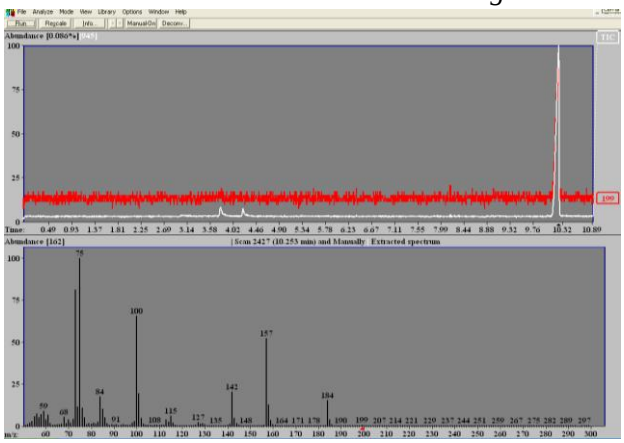

Figure E.8 View of the CG-MS for the cyanohydrin (h)

(i) 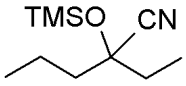

$C_{10}H_{21}NOSi$
199.36g/mol

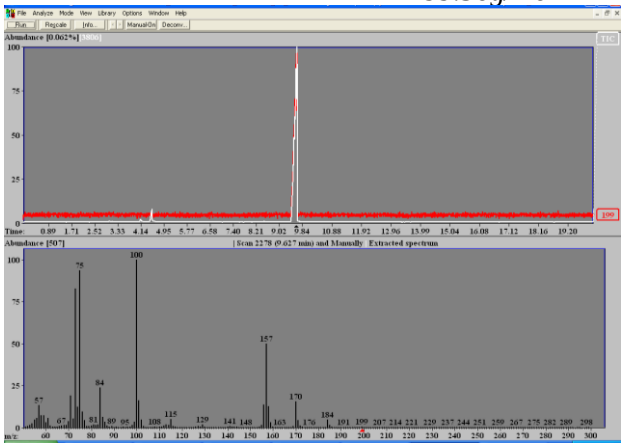

Figure E.9 View of the CG-MS for the cyanohydrin (i)

F. Experimental Follow-up of multicomponent reactions

2-phenyl-2-(phenylamino)acetonitrile (**1**)
White solid: ^{1}H NMR (300 MHz, $CDCl_3$): δ = 4.07 (brs, 1H, NH), 5.45 (s, 1H), 6.76–6.81 (d, 2H), 6.90-6.95 (t, 1H), 7.30–7.61 (m, 7H). ^{13}C NMR ($CDCl_3$): δ = 50.4, 114.4, 118.1, 120.5, 127.3, 129.3, 129.6, 133.7, 144.3. IR (KBr) ν (cm^{-1}): 3339, 3107-2844, 2239, 1600, 1516, 1494, 1448, 1325, 1283, 1240, 1198, 1173, 1114, 1062, 1025, 995, 923, 876, 754, 686, 648, 619, 597, 555, 496, 445, 394 (which corresponds with the spectrum reported for compound with CAS No. 4553-59-7). ESMS: m/z: 209$[M+H]^+$, 182, 149, 116, 93.

2-Phenyl-2-(phenylamino)propanenitrile (**2**)
White solid: ^{1}H NMR ($CDCl_3$): δ = 1.97 (s, 3H), 4.31 (brs, 1H, NH), 6.56-6.58 (d, 2H), 6.80-6.85 (t,1H), 7.12-7.17 (t, 2H), 7.37–7.41 (m, 3H), 7.64–7.67 (m, 2H). ^{13}C NMR ($CDCl_3$): δ 33.2, 57.2, 116.1, 120.2, 120.5, 125.0, 128.7, 129.1, 129.2, 139.4, 143.6. IR (KBr) ν (cm^{-1}): 3386, 3089-2988, 2231, 1600, 1507, 1486, 1448, 1371, 1316, 1257, 1219, 1173, 1101, 1075, 1029, 991, 910, 877, 746, 699, 623, 559, 518, 441, 339. ESMS: m/z: 223 $[M+H]^+$, 218, 196, 149, 130, 103, 94.

2-cyclohexyl-2-oxo-1-phenylethylbenzoate (**3**)
White solid: ^{1}H NMR (300 MHz, $CDCl_3$): δ = 1.14-1.95 (m, 10H, -CH_2 cyclohexyl), 3.82 (d, 1H, -CH cyclohexyl), 6.03 (d, 1H, -NH), 6.30 (s, 1H, -CH), 7.36-7.53 (m, 7H, -HAr), 7.60-7.63 (t, 1H, -HAr), 8.09-8.10 (d, 2H, -HAr). ^{13}C NMR ($CDCl_3$): δ = 24.64, 24.67, 25.40, 32.83, 32.93 and 33.01 (6C, cyclohexyl), 48.21 (1C, quaternary), 127.38, 128.73, 129.74, 130.05, 133.58 and 135.74 (10C, aromatic), 164.89 and 167.32 (2C, C=O). IR (KBr) ν (cm-1): 3304, 3069, 2935, 2918, 2852, 1733, 1658, 1600, 1548, 1497, 1449, 1376, 1363, 1318, 1262, 1247, 1231, 1119, 1094, 1070, 1040, 1028, 1020, 1001, 970, 960, 936, 925, 909, 891, 883, 833, 800, 776, 730, 702, 696, 682, 627, 615, 554, 534 (This corresponds with the spectrum reported for compound with CAS No. 1443685-31-1). ESMS: m/z: 338$[M+H]^+$.

N-((cyclohexylaminocarbonyl)(phenyl)methyl)-N-phenylbenzamide (**4**)
White solid: ^{1}H NMR ($CDCl_3$): ^{1}H NMR (300 MHz, $CDCl_3$): δ = 1.13-1.93 (m, 10H, -CH_2 cyclohexyl), 3.76 (m, 1H, -CH cyclohexyl), 5.82 (broad s, 1H, -NH), 6.02 (s, 1H, -CH aliphatic), 7.01-7.38 (m, 15H, -CH aromatic). ^{13}C NMR ($CDCl_3$): δ = 24.81, 25.54, 32.65, 32.82, 33.16 and 48.73 (6C, cyclohexyl), 66.90 (1C, quaternary), 127.11, 127.61, 128.40, 128.57, 128.80, 129.02, 129.14, 129.31, 129.42, 130.10, 130.27, 134.95, 136.13 and 141.49 (15C, aromatic), 168.58 and 171.29 (2C, C=O). IR (KBr) ν (cm-1): 3427, 3261, 3085, 3059, 2979, 2927, 2850, 1660, 1645, 1595, 1564, 1492, 1448, 1390, 1374, 1272, 1251, 1241, 1194, 1184, 1156, 1107, 1087, 1074, 1035, 1017, 1003, 976, 923, 892, 811, 762, 734, 699. (This corresponds with the spectrum reported for compound with CAS No. 1266385-49-2) ESMS: m/z: 413 $[M+H]^+$

^{1}H and ^{13}C NMR results in case of multicomponent reactions

The ^{1}H-NMR and ^{13}C-NMR experimental spectra of the α-aminonitrile derivatives

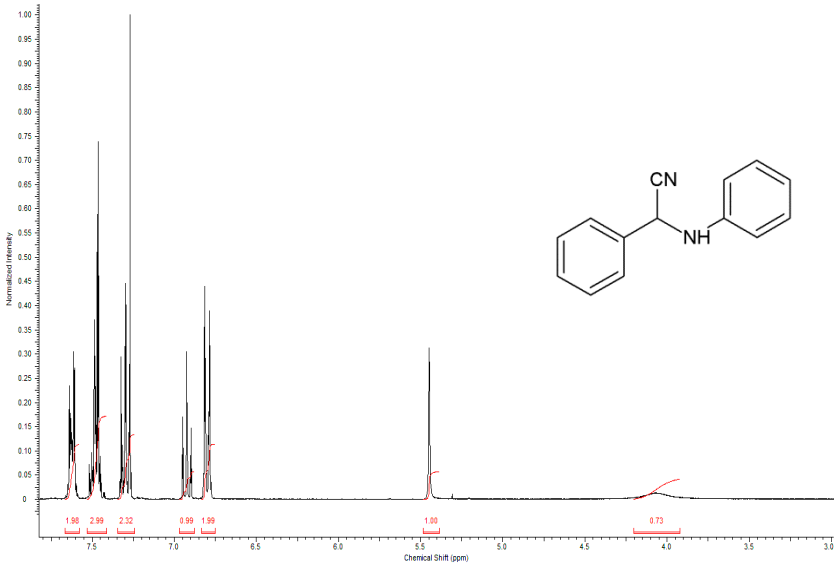

Figure F.1 ^{1}H-NMR experimental spectra for 2-phenyl-2-(phenylamino)acetonitrile.

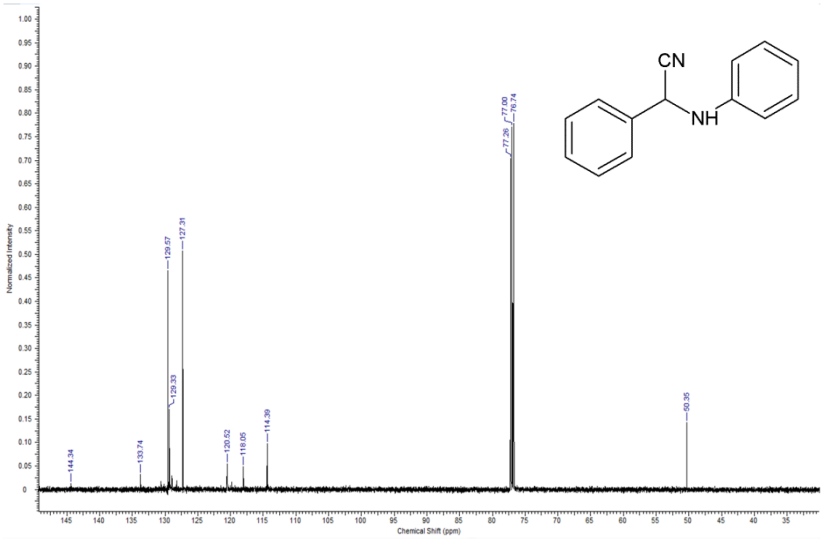

Figure F.2 ^{13}C-NMR experimental spectra for 2-phenyl-2-(phenylamino)acetonitrile.

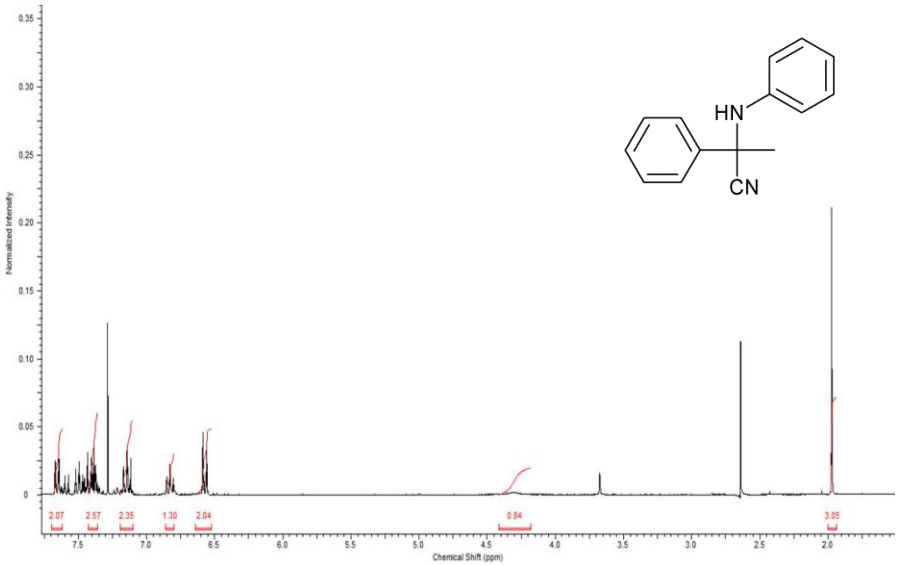

Figure F.3 ^{1}H-NMR experimental spectra for 2-Phenyl-2-(phenylamino)propanenitrile.

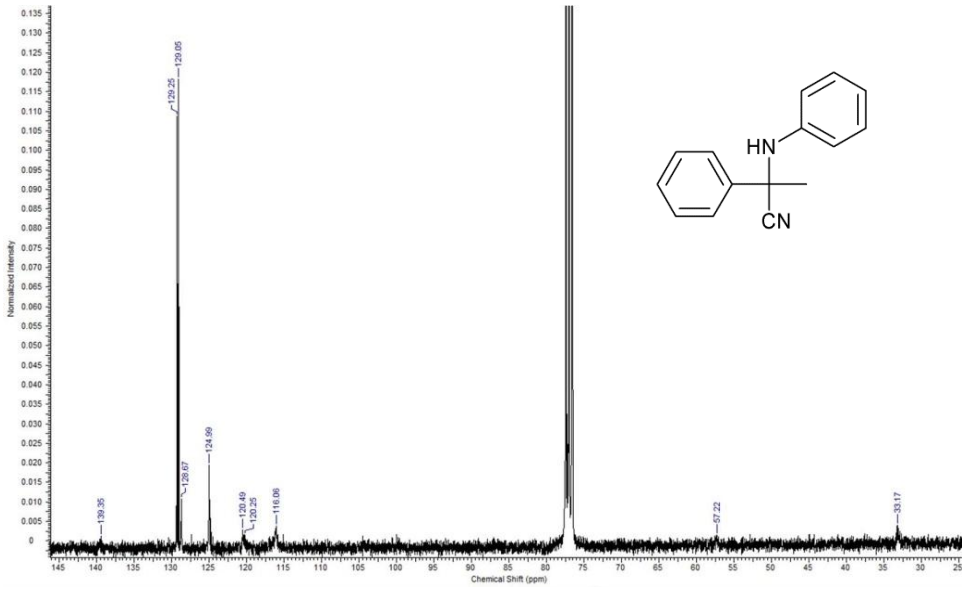

Figure F.4 ^{13}C-NMR experimental spectra for 2-Phenyl-2-(phenylamino)propanenitrile.

The [1]H-NMR and [13]C-NMR experimental spectra of the Passerini reaction product

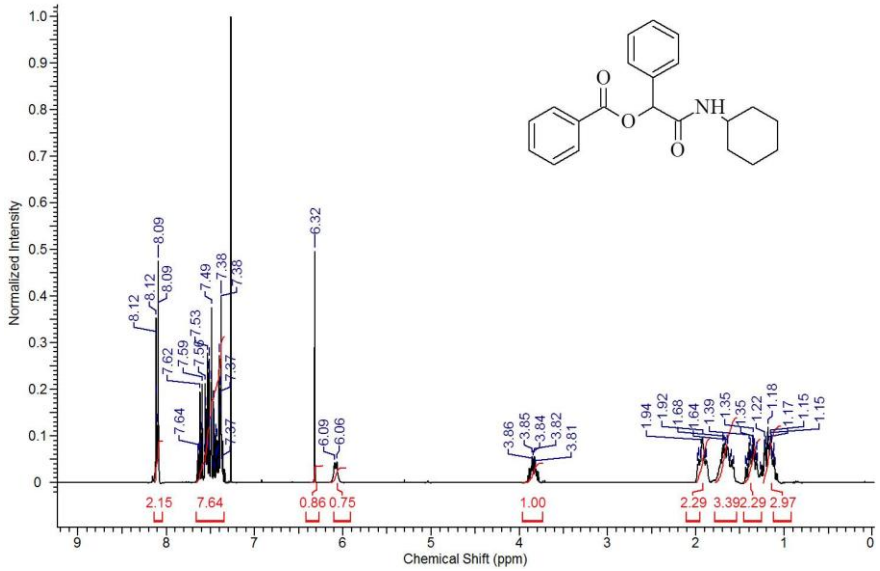

Figure F.5 [1]H-NMR experimental spectra of the 2-cyclohexyl-2-oxo-1-phenylethylbenzoate.

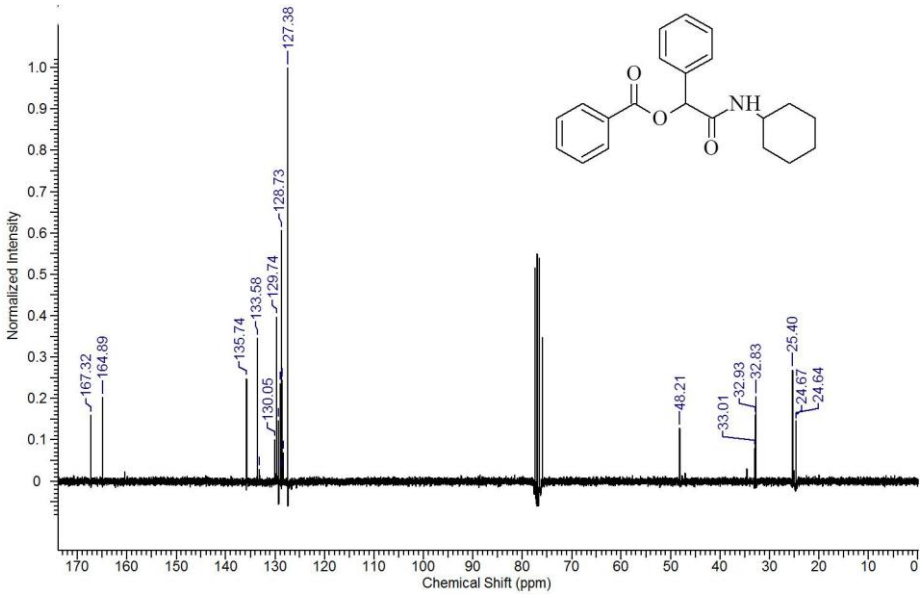

Figure F.6 [13]C-NMR experimental spectra of the 2-cyclohexyl-2-oxo-1-phenylethylbenzoate.

The [1]H-NMR and [13]C-NMR experimental spectra of the Ugi reaction product

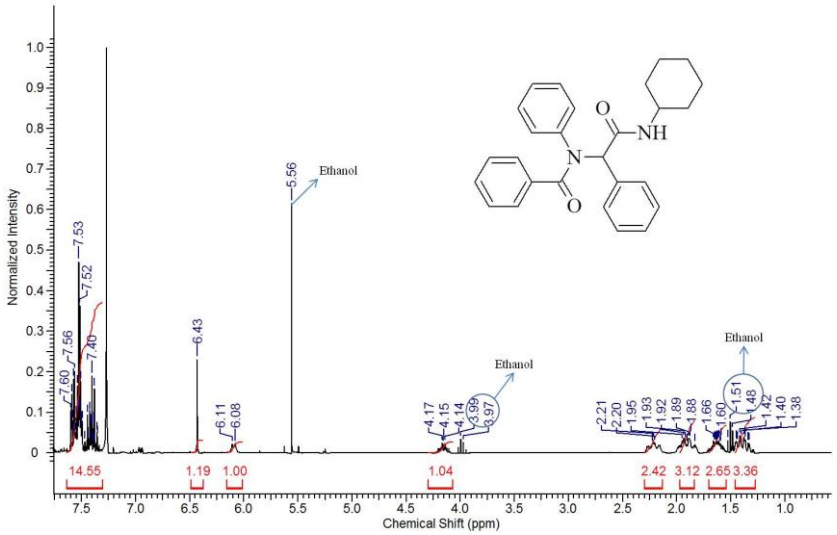

Figure F.7 [1]H-NMR experimental spectra of N-((cyclohexylaminocarbonyl)(phenyl)methyl)-N-phenylbenzamide.

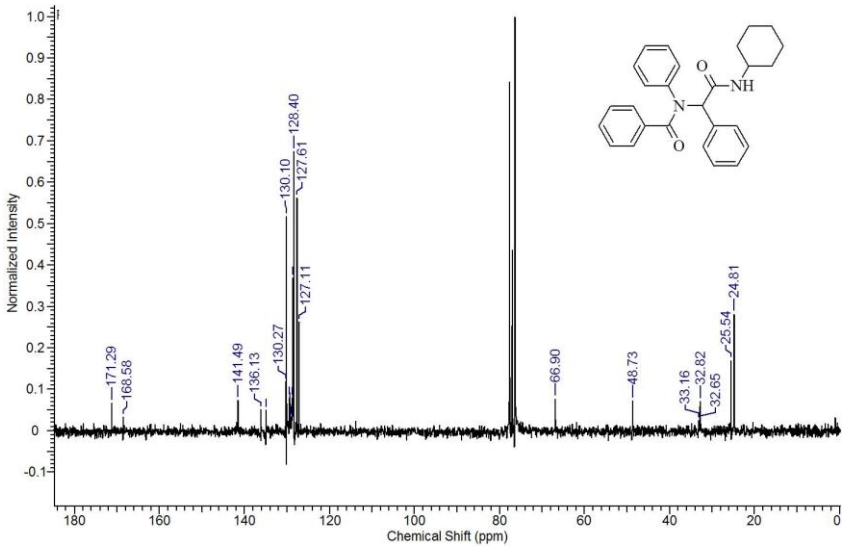

Figure F.8 [13]C-NMR experimental spectra of N-((cyclohexylaminocarbonyl)(phenyl)methyl)-N-phenylbenzamide.

ESI-MS "ESI-MS data: characterization of the multicomponent reaction products"

ESI-MS spectra for the α-aminonitrile derivatives (1 and 2)

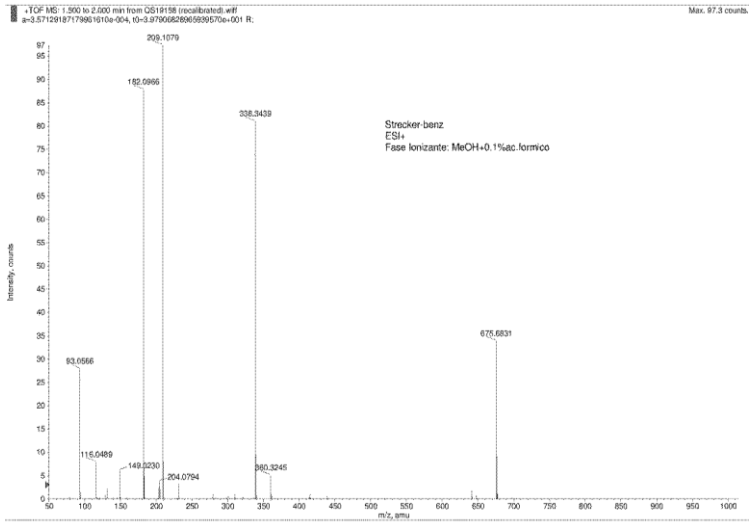

Figure F.9 ESI-MS spectra for 2-phenyl-2-(phenylamino)acetonitrile (**1**). (Signals in 675, 338 and 360 are signals from residues due to the ESI technique employed)

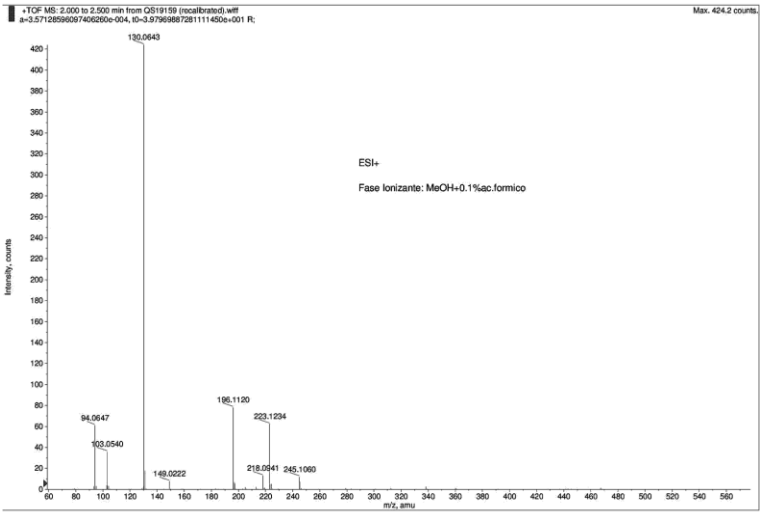

Figure F.10 ESI-MS spectra for 2-Phenyl-2-(phenylamino)propanenitrile (**2**).

Experimental ESI-MS for the 2-cyclohexyl-2-oxo-1-phenylethylbenzoate

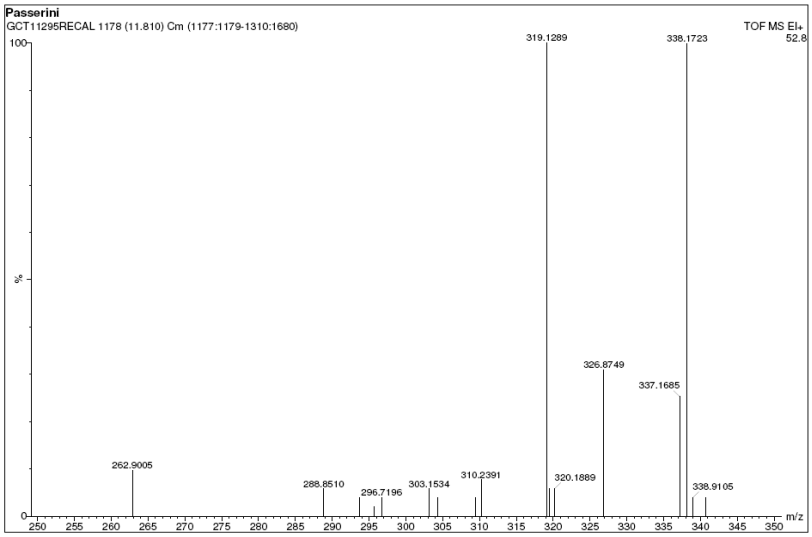

Figure F.11 ESI-MS spectra for 2-cyclohexyl-2-oxo-1-phenylethylbenzoate.

Experimental ESI-MS of the N-((cyclohexylaminocarbonyl)(phenyl)methyl)-N-phenylbenzamide

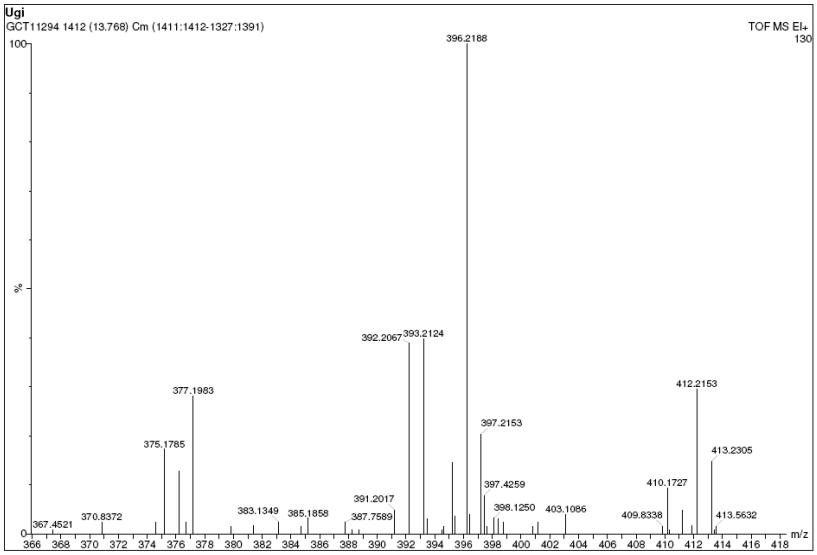

Figure F.12 ESI-MS spectra for N-((cyclohexylaminocarbonyl)(pheny)methyl)-N-phenylbenzamide product.

IR case of multicomponent reactions product characterization

Experimental Infrared spectra of the α-aminonitrile derivatives (1 and 2)

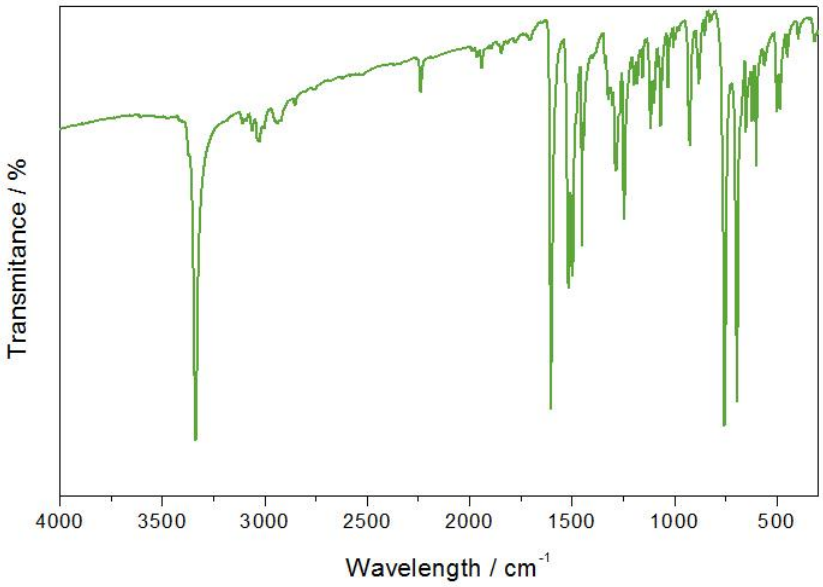

Figure F.13 FT-Infrared spectra for 2-phenyl-2-(phenylamino)acetonitrile, in the 4000-300 cm^{-1} range.

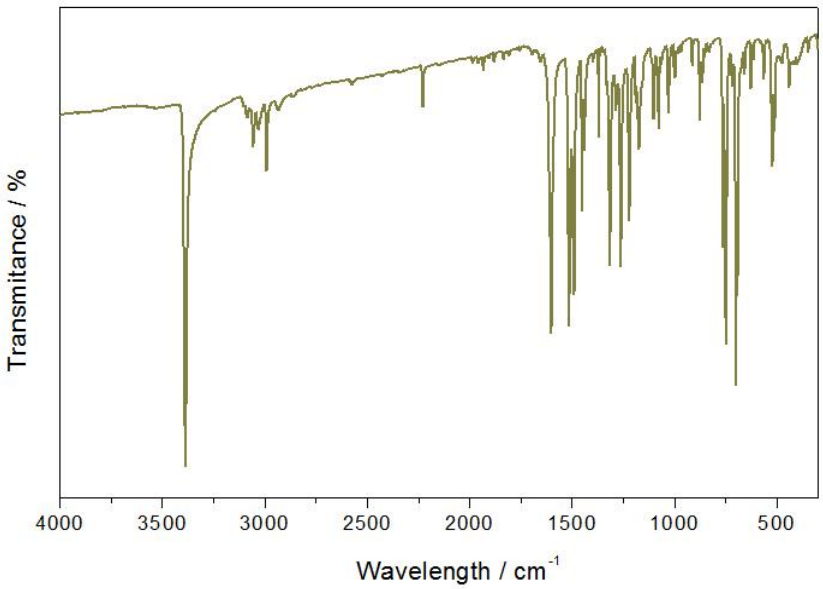

Figure F.14 FT-Infrared spectra for 2-Phenyl-2-(phenylamino)propanenitrile, in the 4000-300 cm^{-1} range.

Experimental Infrared spectra of the 2-cyclohexyl-2-oxo-1-phenylethylbenzoate

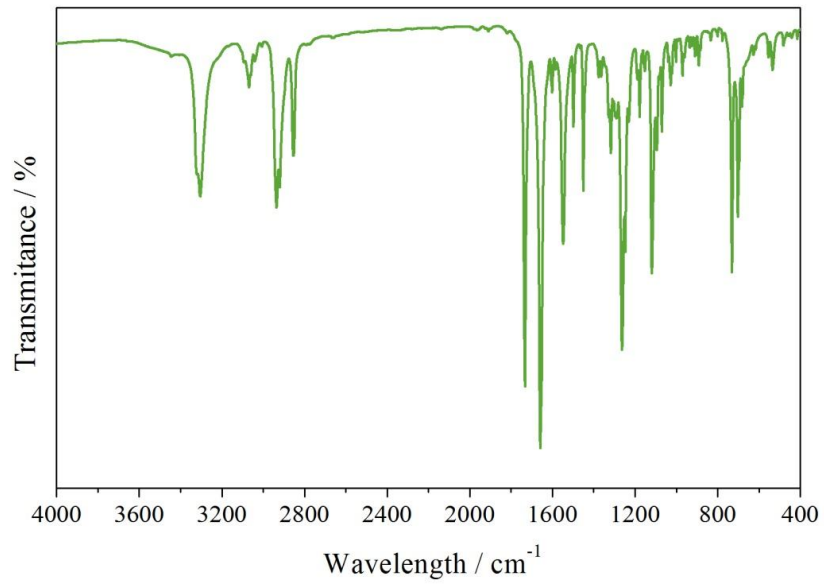

Figure F.15 FT-Infrared spectra of the 2-cyclohexyl-2-oxo-1-phenylethylbenzoate, in the 4000-300 cm^{-1} range.

Experimental Infrared spectra of the N-((cyclohexylaminocarbonyl)(phenyl)methyl)-N-phenylbenzamide,

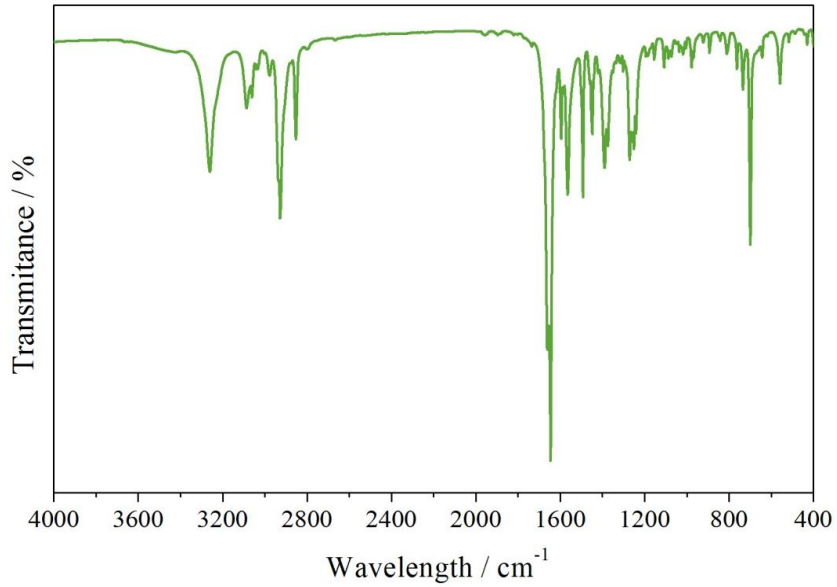

Figure F.16 FT-Infrared spectra of the N-((cyclohexylaminocarbonyl)(phenyl)methyl)-N-phenylbenzamide, in the 4000-300 cm^{-1} range.

PATENT AND PUBLISHED ARTICLES

PATENT

Solicitud internacional PCT/ES2015/070572, referente a "MATERIAL ÓRGANO-INORGÁNICO CRISTALINO BASADO EN CATIONES DEL GRUPO XIII DE LA TABLA PERIÓDICA, PROCEDIMIENTO DE PREPARACIÓN Y USO", a nombre de CONSEJO SUPERIOR DE INVESTIGACIONES CIENTÍFICAS. Autores de la patente: Lina María Aguirre Díaz, Marta Iglesias Hernández, Ángeles Monge Bravo, Natalia Snejko Shalneva, Enrique Gutiérrez Puebla.

PUBLICATIONS

1. Lina María Aguirre-Díaz, Marta Iglesias, Natalia Snejko, Enrique Gutiérrez-Puebla and M. Ángeles Monge. **Synchronising Substrate Activation Rates in Multi-Component Reactions with Metal-Organic Framework Catalysts.** "*Send to Chemistry - European Journal*" **2015**.

2. Lina María Aguirre-Díaz, Felipe Gándara, Marta Iglesias, Natalia Snejko, Enrique Gutiérrez-Puebla and M. Ángeles Monge. **Tunable catalytic activity of solid solution MOFs in One Pot Multicomponent Reaction.** *J. Am. Chem. Soc.* **2015**, *137*, 6132−6135.

3. Lina María Aguirre-Díaz, Marta Iglesias, Natalia Snejko, Enrique Gutiérrez-Puebla and M. Ángeles Monge. **Toward understanding of structure-catalyst activity relationship of new Indium MOFs as catalysts for the solvent-free ketones cyanosilylation.** *RSC Adv.* **2015**, *5*, 7058-7065.

4. Lina María Aguirre-Díaz, Marta Iglesias, Natalia Snejko, Enrique Gutiérrez-Puebla and M. Ángeles Monge. **Indium metal–organic frameworks as catalysts in solvent-free cyanosilylation reaction.** *CrystEngComm*, **2013**, *15*, 9562-9571.

Catalizadores reutilizables de soluciones sólidas de MOFs, In_xGa_{1-x} para reacciones One Pot Strecker Multicomponente

El CSIC ha desarrollado una familia de materiales organo-inorgánicos cristalinos nanoestructurados que contienen cationes del grupo XIII (Al, Ga e In) y se usan como catalizadores heterogéneos reutilizables en reacciones en química orgánica de tipo "One Pot Strecker". Tienen como ventaja entre otras, que podemos sincronizar la velocidad de activación de los sustratos mediante la variación de la proporción metal-metal en la solución sólida del catalizador.

Se buscan empresas del sector químico y farmacéutico para desarrollar y comercializar esta patente

Catalizadores heterogéneos reutilizables

La conocida reacción de Strecker por la que reaccionan acetaldehídos, amoníaco y cianuro de hidrógeno, con la ayuda de un catalizador Lewis, da aminonitrilos, y su posterior hidrólisis proporciona un acceso directo y económicamente viable a varios amino-ácidos, de ahí su relevancia.

Los materiales híbridos órgano-inorgánicos nanoestructurados, también llamados MOFs (del inglés, Metal-Organic Frameworks) han demostrado durante el transcurso de los últimos años su potencial uso como catalizadores heterogéneos multifuncionales en prometedoras aplicaciones. Son sólidos muy cristalinos cuya estructura está formada por la coordinación de cationes metálicos con ligandos polidentados y con una organización espacial porosa, Tienen la capacidad de ser sintonizados química y físicamente para transformaciones químicas específicas.

La familia de materiales órgano-inorgánicos cristalinos desarrollados tiene una composición MaM'1-a(OH)xRy, donde M y M' son dos metales del grupo XIII de la tabla periódica (Al, Ga e In) y/o combinaciones químicas de estos, junto a ligandos orgánicos tipo ácidos policarboxílicos, Estos compuestos, insolubles en la mayoría de los disolventes habituales al ser heterogéneos, son tolerantes al agua, de modo que se pueden llevar a cabo reacciones orgánicas en agua utilizando estos catalizadores insolubles que pueden ser separados fácilmente de los productos del medio de la reacción. Son adecuados en reacciones de química fina y obtención de productos de alto valor añadido, al llevarse a cabo las reacciones en condiciones suaves.

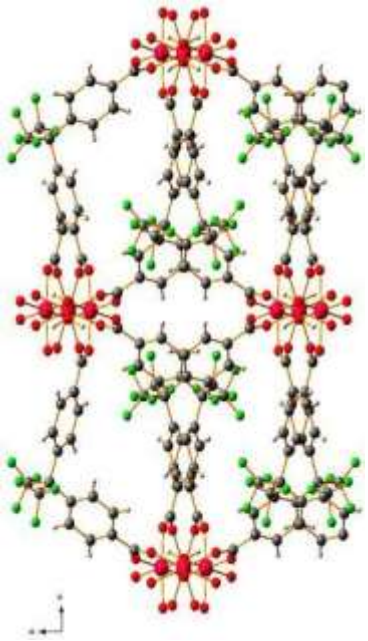

Red covalente Tridimensional de los catalizadores

Aspectos innovadores y ventajas

- Síntesis sencilla de los catalizadores
- Trabaja en ausencia de disolventes orgánicos contaminantes
- Mejor control de la reactividad y selectividad
- Se puede sincronizar la velocidad de activación de los sustratos mediante la variación de la proporción metal-metal en las soluciones sólidas de MOFs,
- Fácil recuperación del catalizador

Estado de la patente

Patente solicitada

Para información adicional, por favor contactar con

Marisa Carrascoso Arranz
Vicepresidencia Adjunta de Transferencia
del Conocimiento (CSIC)
Tel.: + 34 – 91 568 15 33
Fax: + 34 – 91 585 52 87
macarrascoso@orgc.csic.es

May 20, 2015
Volume 137
Number 19
pubs.acs.org/JACS

JACS

JOURNAL OF THE AMERICAN CHEMICAL SOCIETY

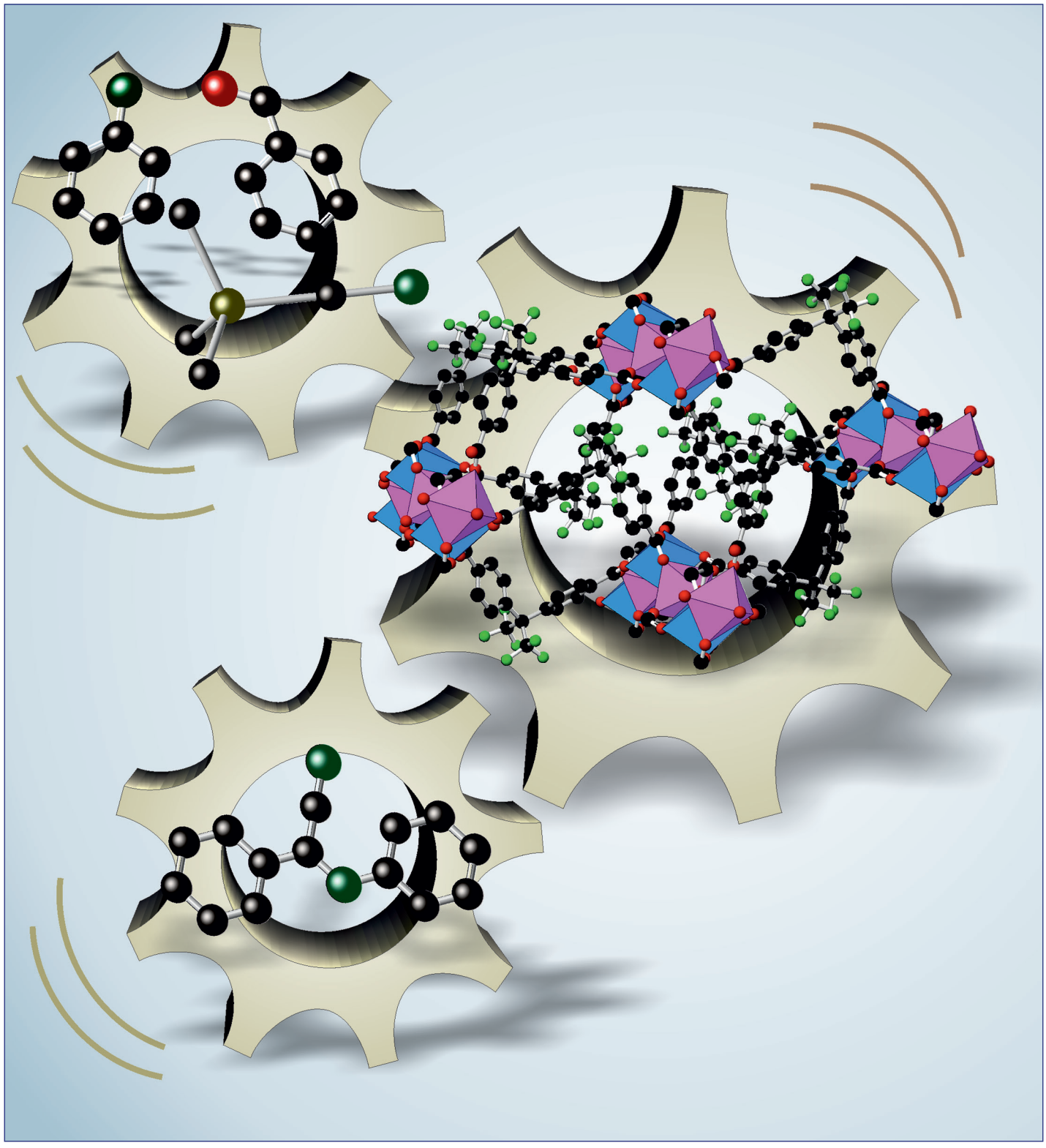

ACS Publications
Most Trusted. Most Cited. Most Read.

www.acs.org

CrystEngComm

RSC Publishing

PAPER

View Article Online
View Journal | View Issue

Published on 29 July 2013. Downloaded by Instituto de Ciencia de Materiales de Madrid (ICMM) on 03/09/2015 14:15:51.

Indium metal–organic frameworks as catalysts in solvent-free cyanosilylation reaction†

Cite this: *CrystEngComm*, 2013, **15**, 9562

Lina María Aguirre-Díaz, Marta Iglesias, Natalia Snejko, Enrique Gutiérrez-Puebla and M. Ángeles Monge*

Received 12th June 2013,
Accepted 26th July 2013

DOI: 10.1039/c3ce41123k

www.rsc.org/crystengcomm

Two new Indium MOFs with the bending multicarboxylate ligand H_2dpmda as a linker and different N-donor ancillary ligands were obtained; the two compounds are isoreticular with 2D-**hcb** uninodal 3-connected nets. Comparison of their activity in cyanosilylation reactions with another eight In-MOFs is also reported. Eight out of the ten resulted in being good catalysts under mild and environmentally friendly conditions. Correlations between indium coordination number (CN), framework topology and catalytic activity are made and discussed, demonstrating that among the studied MOFs, the indium material named **InPF-6** with the formula $[In_2(dpa)_3(1,10\text{-phen})_2]\cdot H_2O$ is the most effective catalyst. A possible catalytic mechanism is discussed.

Introduction

A recyclable catalytic system with high reactivity that furthermore could present economic and environmental sustainability is one of the most pursued issues nowadays. Indium salts ($InCl_3$, $InBr_3$ and $In(OTf)_3$), as well as different indium(III) compounds, have been studied in catalysis because of their low environmental impact. A lack of toxicity and high chemoselectivity allows them to be employed in the performance of chemoselective transformations of polyfunctionalized compounds.[1]

Due to the rich indium(III) coordination capability, developments in coordination chemistry such as the design of Metal–Organic Frameworks (MOFs) and supramolecular indium-containing ensembles have been performed. This is motivated by MOFs potential applications as functional materials in several fields including catalysis, luminescence, magnetism, gas storage and separation, adsorption, conductivity and molecular recognition.[2]

What makes indium compounds particularly useful and attractive in "green chemistry" is their advantage in front of most of the metal compounds in terms of their stability in air or in a humid environment. Combining indium with benzene multicarboxylate ligands, which have been found to be useful building blocks in the construction of organic–inorganic materials, we had obtained indium MOFs with interesting heterogeneous catalytic properties amid the benefits of easy recovery, recycling and operational simplicity.[3–5]

Cyanohydrins are versatile intermediates in chemistry as well as biology, they can be transformed into a wide variety of building blocks such as α-hydroxy acids, α-hydroxy aldehydes, and β-aminoalcohols.[6]

Trimethylsilyl cyanide (TMSCN) is one of the most useful and safe cyanating reagents for nucleophilic addition to carbonyl compounds to give cyanohydrin trimethylsilyl ethers. Hence, the development of efficient catalysts for cyanosilylation of carbonyl compounds with TMSCN is a very important subject in current research, and several efficient catalysts have been developed so far.[7]

Lewis acid catalysts can act as electrophilic catalysts to activate carbonyl compounds, and have been extensively investigated for cyanosilylation. Several nucleophilic catalysts, such as amines, phosphines, phosphazenes, and alkaline earth metal oxides, can activate TMSCN and promote cyanosilylation. In the case of indium salts, previous works studied the use of InF_3, $InCl_3$ and $InBr_3$ to obtain high chemical yields with low catalyst loading with excellent results. This allowed a connection to be established between the desired product yield and Lewis acidity of the metal salts used as catalysts.[1,8] Working with different benzene multicarboxylate ligands, diphenic acid (**H_2dpa**), 1,4-benzenedicarboxylate acid (**H_2bdc**), 1,3,5-benzenetricarboxylate acid (**H_3btc**), 4,4'-(hexafluoroisopropylidene) bis(benzoic acid) (**H_2hfipbb**) and diphenylmethane-4,4'-dicarboxylic acid (**H_2dpmda**), our research group succeeded in obtaining ten indium(III) MOFs with the formulas: $[In_2(OH)_3(bdc)_{1,5}]$, **InPF-1**; $[In(bdc)_{1,5}(2,2'\text{-bipy})]$, **InPF-2**; $[In_2(OH)_2(bdc)_2(1,10\text{-phen})_2]$, **InPF-3**; $[In(btc)(H_2O)(2,2'\text{-bipy})]$, **InPF-4**; $[In(btc)(H_2O)(1,10\text{-phen})]$, **InPF-5**; $[In_2(dpa)_3(1,10\text{-phen})_2]\cdot H_2O$, **InPF-6**;

Department of New Architectures in Material Chemistry, Instituto de Ciencia de Materiales de Madrid (ICMM-CSIC), Sor Juana Ines de la Cruz, 3, Cantoblanco, 28049 Madrid, Spain. E-mail: amonge@icmm.csic.es; Fax: +34 91 372 0623; Tel: +34 91 334 9025

† Electronic supplementary information (ESI) available. CCDC 944511 and 944512. For ESI and crystallographic data in CIF or other electronic format see DOI: 10.1039/c3ce41123k

This journal is © The Royal Society of Chemistry 2013

Published on 19 December 2014. Downloaded by Instituto de Ciencia de Materiales de Madrid (ICMM) on 16/04/2015 17:41:33.

RSC Advances

PAPER

View Article Online
View Journal | View Issue

Cite this: *RSC Adv.*, 2015, **5**, 7058

Toward understanding the structure–catalyst activity relationship of new indium MOFs as catalysts for solvent-free ketone cyanosilylation†

Lina María Aguirre-Díaz,[ab] Marta Iglesias,[a] Natalia Snejko,[a] Enrique Gutiérrez-Puebla[a] and M. Ángeles Monge*[a]

Four new indium metal–organic frameworks, MOFs, namely $[In_2(hfipbb)_3(1,10\text{-phen})_2]\cdot 2H_2O$ (**InPF-12**), $[In_2(hfipbb)_3(2,2'\text{-bipy})_2]\cdot 2H_2O$ (**InPF-13**), $[In_2(hfipbb)_3(4,4'\text{-bipy})]$ (**InPF-14**) and $[In_4(OH)_4(hfipbb)_4(4,4'\text{-bipy})]$ (**InPF-15**), (InPF = indium polymeric framework, hfipbb = hexafluoroisopropylidene bisbenzoate, phen = phenantroline, bipy = bipyridine), have been hydrothermally obtained and result in efficient Lewis acid catalysts in solvent-free cyanosilylation of carbonyl compounds. For acetophenone: (i) the coordination number and μ-OH groups presence seem to be decisive factors to obtain a better catalytic behavior and (ii) the presence of Lewis base moieties (C=O groups not coordinated to indium cation), besides the Lewis acid sites, creates a two-component catalytic system, based on the "dual activation" phenomenon that makes **InPF-15** the best catalyst in this type of reaction. It was also found that the use of this highly reactive, recyclable and environmentally benign catalyst allows the efficient synthesis of various trimethylsilyl cyanohydrins from a wide range of cyclic, aliphatic and aromatic ketones.

Received 5th November 2014
Accepted 19th December 2014

DOI: 10.1039/c4ra13924k

www.rsc.org/advances

Introduction

The development of green materials and processes with easy handling and low cost has become one of the main goals of synthetic chemistry. The manufacture of economic, easily produced and non toxic materials that can then be used as heterogeneous catalysts becomes very important in the development of processes with less environmental impact. These materials will increase efficiency, and could avoid using contaminants – toxic solvents, release agents, *etc.* – and reduce waste.[1] For this purpose, several Metal–Organic Frameworks (MOFs) have attracted great interest during the past years and a large amount of compounds have been designed and synthesized for various energy and environmentally relevant applications, such as heterogeneous catalysis as well as luminescence, magnetism, gas storage and separation, adsorption, conductivity and molecular recognition.[2]

The catalytic interest in MOFs materials arises from the high versatility that they offer. This versatility is due to the wide range of possibilities of combining a variety of polyatomic organic linkers and inorganic units, which act as coordination centers. The control of the bond angles and restricting the number of coordination sites that can be made during the synthesis of MOFs, results in tailored solid robust materials with high thermal and mechanical stability with a wide range of morphologies and geometries, which exhibit particular properties.

Most of the MOFs materials are obtained by slow evaporation method or solvothermal methods. In solvothermal methodology, the use of high-boiling organic solvents (DMF, DEF, acetonitrile, acetone, ethanol, methanol *etc.*) is preferred; however, most of these solvents are toxic and expensive. On the other hand, when water is chosen as solvent (*hydrothermal synthesis*), a cleaner, environmentally friendly and easy to handle methodology for MOF material producing can be used.[3]

Thousands of reported MOF structures contain divalent cations and carboxylate, sulfonate, phosphonate or N donor linkers. MOFs built up from higher valence cations are less abundant (except lanthanide cations). The use of trivalent metals like the p elements in group 13 (Al^{III}, Ga^{III}, In^{III}) for the preparation of MOFs are even less common, in contrast to their use in other inorganic materials, such as aluminosilicates, gallium-phosphates and phosphate zeolites.[4]

However, p elements based MOFs have proved to be very effective in various catalytic processes.[5] Generally, in terms of catalytic applications, MOFs are relatively new materials within the domain of heterogeneous catalysis. Despite the first report on MOF dealing with a catalytic application appeared in 1994, in which a 2D cadmium network was used as heterogeneous catalyst in the cyanosilylation of aldehydes,[6] very few studies

[a]*Department of New Architectures in Material Chemistry, Instituto de Ciencia de Materiales de Madrid (ICMM-CSIC), Sor Juana Ines de la Cruz, 3, Cantoblanco, 28049 Madrid, Spain. E-mail: amonge@icmm.csic.es; Fax: +34 91 372 0623; Tel: +34 91 334 9000*

[b]*Universidad Internacional Menéndez Pelayo, UIMP, 28040 Madrid, Spain*

† Electronic supplementary information (ESI) available. CCDC 1023844–1023846 and 1026919. For ESI and crystallographic data in CIF or other electronic format see DOI: 10.1039/c4ra13924k

This journal is © The Royal Society of Chemistry 2015

JACS
JOURNAL OF THE AMERICAN CHEMICAL SOCIETY
Communication
pubs.acs.org/JACS

Tunable Catalytic Activity of Solid Solution Metal–Organic Frameworks in One-Pot Multicomponent Reactions

Lina María Aguirre-Díaz, Felipe Gándara, Marta Iglesias, Natalia Snejko, Enrique Gutiérrez-Puebla, and M. Ángeles Monge*

Departamento de Nuevas Arquitecturas en Química de Materiales - Instituto de Ciencia de Materiales de Madrid (ICMM-CSIC), Sor Juana Inés de la Cruz 3, Cantoblanco 28049, Madrid, Spain

Supporting Information

ABSTRACT: The aim of this research is to establish how metal–organic frameworks (MOFs) composed of more than one metal in equivalent crystallographic sites (solid solution MOFs) exhibit catalytic activity, which is tunable by virtue of the metal ions ratio. New MOFs with general formula $[In_xGa_{1-x}(O_2C_2H_4)_{0.5}(hfipbb)]$ were prepared by the combination of Ga and In. They are isostructural with their monometal counterparts, synthesized with Al, Ga, and In. Differences in their behavior as heterogeneous catalysts in the three-component, one pot Strecker reaction illustrate the potential of solid solution MOFs to provide the ability to address the various stages involved in the reaction mechanism.

Metal–organic frameworks, MOFs, are a class of crystalline materials formed by the linkage of metal ions or clusters (denoted secondary building units, SBUs) through organic ligands.[1] MOFs have many applications, including gas storage or separation,[2a] luminescence,[2b] drug delivery,[2c] or heterogeneous catalysis.[2d] Compared to traditional heterogeneous catalysts, MOFs exhibit the advantage of offering a wide range of different chemical compositions, as well as topological and structural features. Thus, MOFs can be prepared with different metal ions and in different coordination environments, making them suitable for use as catalytic active sites in organic transformations.[3] In addition, it is possible to use different metal elements to obtain MOFs with the same framework type so that the properties of the materials vary depending on the selected metal atom while keeping the same structural features.[4] More recently, it has also been demonstrated that different metal atoms can be incorporated within the same MOF, occupying equivalent positions in the crystalline framework, which we denote solid solution MOFs.[5] Despite the fact that multimetal systems offer great opportunities in the field of catalysis, thus far the only examples of multimetal MOFs as heterogeneous catalysts are limited to materials where a second metal site is postsynthetically introduced within the framework, typically in the form of metal complexes or as nanoparticles embedded in the MOF pores.[6] Thus, there are no examples yet where the catalytic activity of a MOF is modified with the introduction in the appropriate ratio of various metal atoms in the framework. Herein we report the synthesis and characterization of three new isostructural MOFs, AlPF-1, [Al(OH)(hfipbb)], GaPF-1, [Ga(OH)(hfipbb)], and InPF-11β, $[In(O_2C_2H_4)_{0.5}(hfipbb)]$ (H_2hfipbb = 4,4′-(hexafluoroisopropylidene) bis(benzoic acid)), (Scheme 1), which show catalytic activity in the solvent-free, one-pot Strecker reaction. These three materials showed different behavior in this catalytic reaction affording three different products. In the case of AlPF-1 the expected α-aminonitrile product was obtained; however when using GaPF-1 and InPF-11β, the cyanosilylation and the imine formation products were respectively obtained. These differences are attributed to the various possible reaction pathways related to the reactant activation process for each catalyst. Thus, in order to probe whether the combination of both paths could reach the desired α-aminonitrile product, we have prepared solid solution MOFs with the combinations of gallium and indium cations. Our results demonstrate for the first time that it is possible to control the catalytic activity of the MOFs in a multicomponent reaction by using specifically selected metal ratios.

Scheme 1. Organic Ligand H_2hfipbb Reacts with Aluminum, Gallium, Indium, and Combination of Gallium and Indium To Form a Series of New MOFs

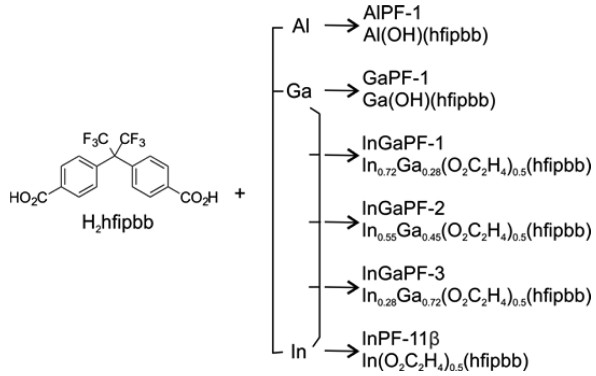

The Strecker reaction is a versatile way of preparing α-aminonitriles through the attack of a nitrile group to an imine group.[7] The resulting α-aminonitriles can be hydrolyzed to obtain α-amino acids or used as intermediates in the preparation of nitrogen-containing heterocycles (such as imidazoles and thiadiazoles) that are significant in organic

Received: March 4, 2015
Published: April 5, 2015

ACS Publications © 2015 American Chemical Society

DOI: 10.1021/jacs.5b02313
J. Am. Chem. Soc. 2015, 137, 6132–6135

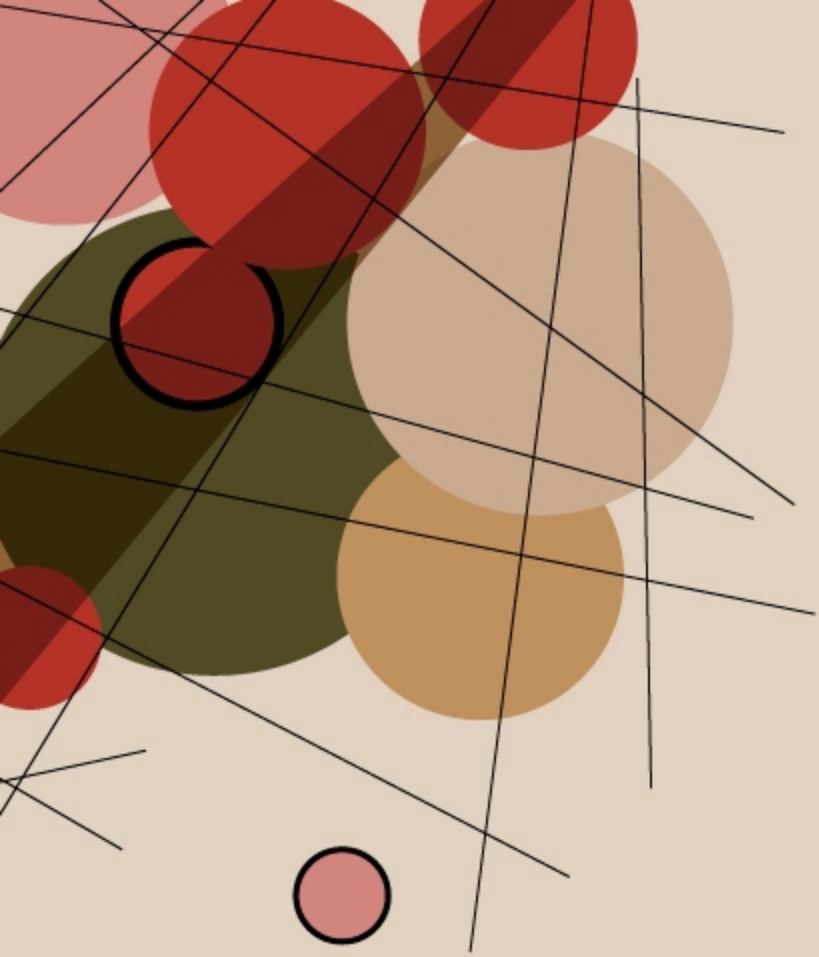

icmm

CSIC

UIMP

Universidad
Internacional
Menéndez Pelayo